UNIVERSITÉ DE GENÈVE
Département de physique théorique

FACULTÉ DES SCIENCES
Professeure Ruth DURRER

Dynamical Casimir Effect: From Photon Creation in Dynamical Cavities to Graviton Production in Braneworlds

THÈSE

présentée à la Faculté des sciences de l'Université de Genève

pour obtenir le grade de Docteur ès sciences, mention physique

par

Marcus RUSER

de

Tornau (Allemagne)

Thèse N° 3903

GENÈVE

Atelier de reproduction de la Section de physique

2007

Meinen Eltern gewidmet

Acknowledgments

First and foremost, I would like to thank my thesis advisor, Ruth Durrer, for her support and patience. Ruth, thank you for having granted me so much freedom. I have learned a lot during the last four years, and your influence will certainly remain.

I am also very grateful to Cyril Cartier for fruitful collaboration during the first three years. I thank David Langlois, Kazuya Koyama and Roy Maartens for discussions.

I would like to thank the members of the Cosmology group, Camille Bonvin, Umberto Cannella, Chiara Caprini, Stefano Foffa, Martin Kunz, Michele Maggiore, Hillary Sanctuary, Domenico Sapone, Riccardo Sturani and Antti Väihkönen, for the very nice atmosphere. Two deserve particular mention. Camille, thanks a lot for the pleasant time in the office, for never having given up to talk in French with me, and for translating the résumé of this thesis from "my French" into French. Martin, thanks for the many nice hikes during the last years and, not to forget, for the many joint lunches during the innumerable weekends in the office.

I also would like to thank the whole department of theoretical physics, and in particular the secretaries Cécile Jaggi, Danièle Chevalier and Francine Gennai-Nicole. Then, of course, I thank Andreas Malaspinas for fixing hardware, software, network and other problems.
I thank as well the Scientific and Parallel Computing Group of the Computer Science Department of the University of Geneva for the use of the Myrinet cluster.

I would like to thank Ralf Schützhold and Günter Plunien from the Technische Universität Dresden, Germany, for valuable discussions and continued collaboration after my move to Geneva.
I am very grateful to Diego Dalvit from the Los Alamos National Laboratory (LANL), New Mexico, for interesting discussions and the possibility to visit him at LANL two times during the last four years.

Also, I appreciate very much that David Langlois and Mikhail Shaposhnikov accepted to join my thesis committee.

I would like to thank all my friends for their support and understanding. One of them, Jan Winter, I would like to mention in particular. Jan, thanks for the nights out here in Geneva during your year at CERN and for the discussions about everything but physics. I wish you all the best for your time at Fermilab.

Finally (hoping that it does not give a too bad impression), I would like to thank the staff of Mulligan's Irish Pub and the Crazy Canadians for some marvelous Thursday nights.

But, without any doubt, my largest debt I owe to my parents, Ralph and Silvia Ruser, without whom this thesis would never have been written. This thesis is dedicated to you.

Publications

Dynamical Casimir effect

- [P1] M. Ruser,
  Vibrating cavities: a numerical approach,
  J. Opt. B: Quantum Semiclass. Opt. **7**, S100 (2005), [arXiv:quant-ph/0408142]
- [P2] M. Ruser,
  Numerical approach to the dynamical Casimir effect,
  J. Phys. A: Math. Gen. **39**, 6711 (2006), [arXiv:quant-ph/0603097]
- [P3] M. Ruser,
  Numerical investigation of photon creation in a three-dimensional resonantly vibrating cavity: Transverse electric modes,
  Phys. Rev. A **73**, 043811 (2006), [arXiv:quant-ph/0509030]

Graviton production in braneworld cosmology

- [P4] C. Cartier, R. Durrer and M. Ruser,
  On graviton production in braneworld cosmology,
  Phys. Rev. D, **72**, 104018 (2005), [arXiv:hep-th/0510155]
- [P5] R. Durrer and M. Ruser,
  Dynamical Casimir Effect in Braneworlds,
  Phys. Rev. Lett. **99**, 071601 (2007), [arXiv:0704.0756]
- [P6] M. Ruser and R. Durrer,
  Dynamical Casimir effect for gravitons in bouncing braneworlds,
  Phys. Rev. D, **76**, 104014 (2007), [arXiv:0704.0790]

Others

- [P7] G. Plunien, M. Ruser, and R. Schützhold,
  A relativistic toy model for back-reaction,
  Class. Quantum Grav. **24**, 4361 (2007), [arXiv:gr-qc/0408028]

Résumé

Introduction

La physique moderne est basée sur deux théories fondamentales: la théorie d'Einstein de la relativité générale, qui est la théorie classique décrivant la géométrie de notre Univers à grande échelle, et la théorie quantique des champs qui forme la trame du modèle standard de la physique des particules.
L'état fondamental de la théorie quantique des champs, *le vide*, présente des propriétés exceptionnelles, bien qu'il ne contienne pas de particules. La raison est l'existence de fluctuations quantiques du vide, appelées *le champ de vide*. La présence de ce champ provoque une variété de phénomènes intéressants et d'effets observables comme l'émission spontanée, le Lamb shift ainsi que beaucoup d'autres effets.
Par exemple, la présence de champs externes, peut modifier les propriétés du vide et induire des réactions intéressantes. Un phénomène particulièrement intéressant est la réaction du champ du vide à des champs de background qui varient avec le temps. Le vide répond à de telles perturbations dépendantes du temps par l'amplification des fluctuations du vide, qui peuvent être interprétées comme la création de particules à partir du vide. Deux exemples sont la production de photons dans un champ électromagnétique fort dépendant du temps ainsi que la création de particules dans l'Univers en expansion.
Un autre exemple est l'expansion rapide de l'Univers après sa création lors du *Big Bang*, appelée *inflation*. L'amplification des fluctuations quantiques pendant cette ère sont responsables des petites anisotropies de densité et de température que nous observons dans le fond de rayonnement cosmique (CMB) avec des expériences de précision élevée comme la *Wilkinson Microwave Anisotropy Probe (WMAP)*. Dans le modèle standard de la cosmologie, qui est soutenu par des observations récentes, les structures que nous observons dans l'Univers aujourd'hui, ont émergé de ces petites fluctuations de densité. Les fluctuations quantiques initiales du vide ont ainsi laissé une impression dans le ciel que nous observons.
Les conditions de bord du système, qui peuvent être considérées comme des champs classiques de background très localisés, ont un impact particulier sur le champ du vide, ils changent la structure de ses modes. Ceci a comme conséquence une force attractive entre deux plaques métalliques appelé l'effet Casimir statique , ainsi que la création de photons par des miroirs en mouvement, appelé l'effet Casimir dynamique .

Tous ces phénomènes sont décrits par ce qui s'appelle l'approche semi-classique. La dynamique des champs quantiques est ainsi étudiée dans le background des champs classiques tels que le champ de gravitation, des champs électromagnétiques forts ou des bornes mobiles.
Néanmains, l'approche semi-classique n'est pas adaptée à la description de l'Univers primordial. Afin de comprendre l'origine de l'Univers, la théorie quantique des champs et la gravitation doivent être unifiés dans ce qui s'appelle la gravitation quantique. De nos jours, la tentative la plus réussie vers une théorie unifiant la théorie de la relativité générale et la théorie quantique des champs est la théorie des cordes. Récemment, la théorie des cordes a motivé l'introduction de modèles de braneworld, dans lesquels notre Univers est décrit comme une hypersurface, appelée *brane*, dans un espace temps à dimensions supplémentaires, appelé *bulk*. Dans ces modèles, le modèle standard de la physique des particules est confiné à cette hypersurface et seule la gravitation peut se propager dans les dimensions supplémentaires. L'expansion de l'Univers que nous observons correspond, dans ces modèles, au mouvement de la brane dans les dimensions supplémentaires. Une brane en mouvement dans le bulk correspond à une borne, ou limite, dépendante du temps pour les perturbations de la gravitation, de la méme manière qu'un miroir mobile est une pour le champ de photons. Par conséquent, une brane mobile engendre la production de gravitons à partir des fluctuations du vide. Ceci constitue l'effet Casimir dynamique pour les gravitons.

Cette thèse étudie l'effet Casimir dynamique pour deux scénarios: premièrement la production de photons dans une cavité dynamique et deuxièmement la production de gravitons par des branes en mouvement.

L'effet Casimir statique

L'effet Casimir a été prédit par le physicien hollandais Hendrik Casimir en 1948. Sous sa forme la plus simple, l'effet Casimir statique correspond à l'attraction d'une paire de plaques conductrices parallèles engendrée par les perturbations du vide du champ électromagnétique. Puisqu'il n'existe aucune force entre des plaques neutres dans l'électrodynamique classique, cet effet est purement quantique. Dans une situation idéale, á température nulle par exemple, il n'y a aucun photons réels entre les plaques. Par conséquent, c'est seulement l'état fondamental de l'électrodynamique quantique, le vide, qui fait s'attirer les plaques macroscopiques. Pour cela, l'effet Casimir est souvent cité comme preuve de l'existence des fluctuations du vide du champ électromagnétique, et du vide quantique en général. Non seulement cet effet a été mesuré en laboratoire avec une grande précision, mais on doit de plus en tenir compte dans la nanotechnologie.
La force Casimir entre deux plaques parallèles est donnée par

$$F(d) = -\frac{\pi^2}{240}\frac{\hbar\, c}{d^4}\, S \ .$$

Ice, d est la séparation entre les deux plaques et S leur surface. La force Casimir est une conséquence exclusive des conditions aux limites, imposées par les plaques. Celles-ci modifient la structure des modes des fluctuations du vide et, par conséquent, l'énergie du point zéro du champ par rapport à celle dans l'espace libre [cf. Fig. 1].

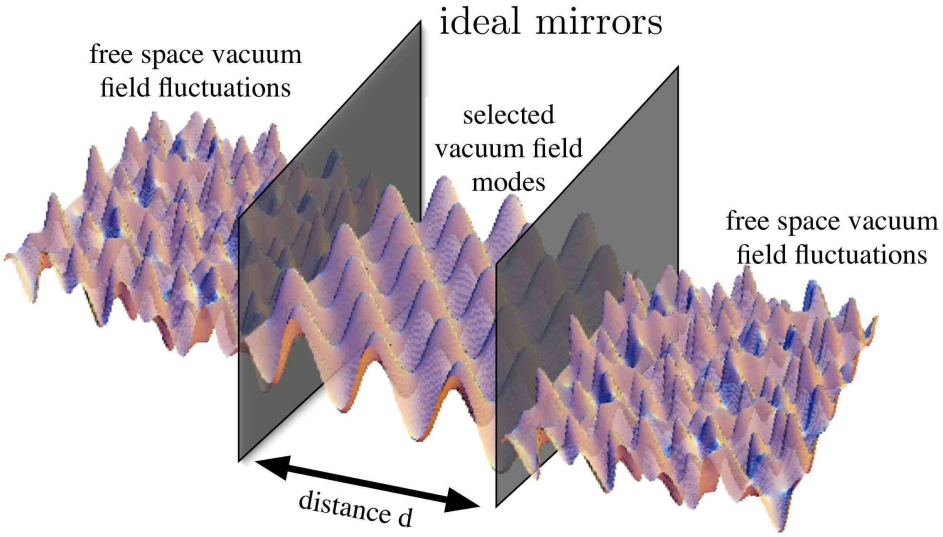

Figure 1: Représentation imagée de l'effet Casimir. Les miroirs idéaux changent la structure des modes du champ du vide. Alors que toutes les fréquences sont permises dans l'espace libre, les conditions aux limites de Dirichlet pour le champ du vide imposées par les miroirs, limitent l'éventail des modes du champ à certaines fréquences particulières dans le volume entre les deux plaques. Cette différence dans la structure des modes du champ du vide crée la force Casimir [cf. Section 2.2].

L'effet Casimir dynamique

La contre-partie dynamique de l'effet Casimir statique, l'effet Casimir dynamique, semble encore plus frappante. Quand les plaques sont mises en mouvement, le vide quantique répond aux conditions aux limites dépendantes du temps induites par la création de photons réels provenant de fluctuations du vide quantique. Cet effet est également appelé *motion induced radiation*.

Cet effet de création de particules à partir des fluctuations du vide dues aux conditions aux limites dépendantes du temps se produit pour n'importe quel champ quantique. Il est possible de prouver que différents scénarios peuvent être réduits à un problème $1+1$–dimensionnel d'un champ réel scalaire et massif $\Phi(t,x)$ sur un intervalle dépendant du temps $x \in [0, l(t)] \equiv I(t)$. La borne $l(t)$ suit une trajectoire classique définie. L'action décrivant le champ $\Phi(t,x)$ sur $I(t)$ est

$$\mathcal{S} = \frac{1}{2}\int dt \int_{I(t)} dx \left[(\partial_t \Phi)^2 - (\partial_x \Phi)^2 - \mathfrak{m}^2 \Phi^2\right] \ ,$$

où $\mathfrak{m}$ est la masse du champ. Pour poser le problme adéquatement, on doit exiger des conditions aux limites pour $\Phi(t,x)$ $x = 0$ et à $x = l(t)$. La forme spécifique des conditions aux limites est donnée par le problème physique particulier étudié, mais également contrainte par le principe variationnel. Afin de préparer le terrain pour la quantification canonique, on doit présenter un ensemble approprié de fonctions permettant l'expansion du champ $\Phi(t,x)$ dans des variables canoniques. Plus précisément, on a besoin d'un ensemble complet et orthonormal de fonctions propres $\phi_n(t,x)$ de l'opérateur laplacien unidimensionnel ∂_x^2. L'existence d'un tel ensemble dépend des conditions aux limites et est assurée si le problème est de type de Sturm-Liouville. Puisque les fonctions propres $\phi_n(t,x)$ doivent satisfaire des conditions aux limites dépendantes du temps à $x = l(t)$, elles dépendent explicitement du temps. Les valeurs propres correspondantes $\omega_n(t)$ sont également dépendantes du temps. Avec un ensemble des fonctions propres appropriées, on peut faire une expansion en série du champ:

$$\Phi(t,x) = \sum_n q_n(t)\phi_n(t,x) \ .$$

Les nouvelles variables $q_n(t)$ sont les variables canoniques du champ décrivant son évolution temporelle. Elles satisfont un système infini d'équations couplées de second ordre de la forme

$$\ddot{q}_n + \Omega_n^2(t) q_n + \sum_m \left[M_{mn}(t) - M_{nm}(t)\right] \dot{q}_m + \sum_m \left[\dot{M}_{mn}(t) - N_{nm}(t)\right] q_m = 0$$

où le point dénote la dérivé temporelle. Ici

$$\Omega_n(t) = \sqrt{\omega_n^2(t) + \mathfrak{m}^2}$$

est la fréquence dépendante du temps d'un mode du champ et $M_{nm}(t)$ et $N_{nm}(t)$ sont les matrices de couplage dépendantes du temps avec $N_{nm} = \sum_k M_{nk} M_{mk}$. La matrice de couplage $M_{nm}(t)$ d'accouplement contient la condition aux limites dynamique. Pour le cas particulier des conditions aux limites de Dirichlet $\Phi(t, x=0) = \Phi(t, l(t)) = 0$, on a:

$$\begin{aligned} \omega_n(t) &= \frac{n\,\pi}{l(t)} \text{ with } n = 1, 2, \ldots \ , \\ M_{nm}(t) &= \begin{cases} \dfrac{\dot{l}(t)}{l(t)}(-1)^{n+m}\dfrac{2\,n\,m}{m^2 - n^2} & \text{si} \quad n \neq m \\ 0 & \text{si} \quad n = m \ . \end{cases} \end{aligned}$$

Après la quantification, les deux dépendances temporelles dans les équations du mouvement, la fréquence $\Omega_n(t)$ et le couplage $M_{nm}(t)$, correspondent à deux sources de création de particules à partir des fluctuations du vide. Dans la littérature sur l'effet Casimir dynamique, l'apparition du couplage des modes dépendants du temps est parfois désigné *effet d'accélération*. C'est une conséquence exclusive des conditions aux limites. La dépendence temporelle de la fréquence $\Omega_n(t)$, due à la variation temporelle du volume de quantification, c'est-à-dire du "squeezing " du vide, est habituellement appelée *squeezing effect*.
L'apparition de l'effet d'accélération reflète la différence principale entre l'effet Casimir dynamique et d'autres

phénomènes établis de production de particules comme la création de particules dans un Univers en expansion homogène et isotrope, et de photons dans un champ électromagnétique classique dépendant du temps. Dans tous ces cas, l'évolution temporelle est décrite par des équations non-couplées d'oscillateurs avec une fréquence dépendante du temps comme seule source de création de particules, ce qui pose un problème beaucoup plus simple. Les couplages intermodaux empêchent de trouver des expressions analytiques pour des observables physiques comme le nombre de photons créés ou leur spectre d'énergie. Les exceptions sont des situations où des approximations peuvent être employées pour simplifier les équations, comme dans le cas de résonance. Il est donc nécessaire d'appliquer des méthodes numériques afin d'étudier l'effet Casimir dynamique pour des situations générales. Dans cette thèse, j'ai développé un tel formalisme permettant des simulations numériques efficaces de l'effet Casimir dynamique.

Le concept de particule n'est pas sans ambiguïté, et en général problématique dans la théorie quantique des champs sous l'influence de conditions externes. J'ai soigneusement abordé ces questions importantes dans le texte principal de la thèse.
Afin de présenter un concept canonique de particules pour des systèmes avec un bord mobile, j'exige que le problème dynamique soit tel qu'il est possible de trouver deux temps $t_{\rm in}$ et $t_{\rm out}$, tels que le bord $l(t)$ soit au repos pour $t < t_{\rm in}$ et $t > t_{\rm out}$. Les configurations initiales (in) et finales (out) du système sont caractérisées par les conditions

$$\begin{aligned} &\text{configuration initiale du système :} \quad \Omega_n^{\rm in} = \Omega_n(t < t_{\rm in}) = \text{const} \neq 0, \qquad M_{nm}(t < t_{\rm in}) = 0 \\ &\text{configuration finale du système :} \quad \Omega_n^{\rm out} = \Omega_n(t > t_{\rm out}) = \text{const} \neq 0, \quad M_{nm}(t > t_{\rm out}) = 0 \end{aligned}$$

pour tout n, m. Ceci permet l'introduction des états du vide initiaux $|0, \text{in}\rangle$ et finaux $|0, \text{out}\rangle$, associés avec des opérateurs d'annihilation et de création, $\{\hat{a}_n^{\rm in}, \hat{a}_n^{\rm in\dagger}\}$ et $\{\hat{a}_n^{\rm out}, \hat{a}_n^{\rm out\dagger}\}$ respectivement, par

$$\hat{a}_n^{\rm in} \, |0, \text{in}\rangle = 0 \;\text{ and }\; \hat{a}_n^{\rm out} \, |0, \text{out}\rangle = 0 \;\; \forall \; n \; .$$

Des particules définies par rapport aux états initiaux et finaux du vide, c'est-à-dire les quanta d'énergies $\Omega_n^{\rm in}$ et $\Omega_n^{\rm out}$ respectivement, sont comptées par les opérateurs de nombre de particules

$$\hat{N}_n^{\rm in} = \hat{a}_n^{\rm in\dagger} \hat{a}_n^{\rm in} \;\text{ et }\; \hat{N}_n^{\rm out} = \hat{a}_n^{\rm out\dagger} \hat{a}_n^{\rm out}.$$

Durant la dynamique du bord, pour des temps $t \in [t_{\rm in}, t_{\rm out}]$, les modes du champ évoluent temporellement tels que, en général, $\hat{a}_n^{\rm out} \neq \hat{a}_n^{\rm in}$. Cette différence peut même persister si le système est revenu à sa position initiale, c'est-à-dire si $\Omega_n^{\rm in} = \Omega_n^{\rm out} \; \forall \; n$.
Des opérateurs d'état initiaux et finaux sont liés par une transformation de Bogoliubov

$$\hat{a}_n^{\rm out} = \sum_m \left[\mathcal{A}_{mn}(t_{\rm out}) \, \hat{a}_m^{\rm in} + \mathcal{B}_{mn}^*(t_{\rm out}) \, \hat{a}_m^{\rm in\dagger} \right] .$$

Si $\mathcal{B}_{nm}(t_{\rm out}) \neq 0$, le vide $|0, \text{in}\rangle$ contient des particules définies par rapport à l'état final du vide $|0, \text{out}\rangle$ et vice versa. Ce mélange des opérateurs d'annihilation et de création est interprété comme une conversion des fluctuations virtuelles du vide quantique en particules réelles, c'est-à-dire production de particules à partir du vide. Le nombre de quanta d'énergie $\Omega_n^{\rm out}$ qui pour $t > t_{\rm out}$ sont présents dans le vide initial est donné par

$$\mathcal{N}_n^{\rm out} = \langle 0, \text{in} | \hat{N}_n^{\rm out} | 0, \text{in} \rangle = \sum_m |\mathcal{B}_{mn}(t_{\rm out})|^2.$$

De cette valeur d'expectation, des quantités comme le nombre total de particules et l'énergie associée peuvent être déduites. Pour ceci, le coefficient $\mathcal{B}_{mn}(t_{\rm out})$ de Bogoliubov doit être calculé.

Dans cette thèse, j'ai présenté et j'ai testé un formalisme qui permet la recherche numérique efficace de l'effet Casimir dynamique. De ce fait, le coefficient $\mathcal{B}_{mn}(t_{\rm out})$ de Bogoliubov est directement lié aux solutions d'un système couplé des équations de premier ordre de la forme

$$\dot{\mathbf{X}}(t) = \mathbf{W}(t)\mathbf{X}(t)$$

où la matrice $\mathbf{W}(t)$ contient la fréquence $\Omega_n(t)$ et la matrice de couplage $M_{nm}(t)$. La mise en œuvre numérique d'un tel système est évident et les résultats numériques obtenus pour différents scénarios sont en accord parfait avec les résultats analytiques connus. C'est le "proof of concept" de la méthode présentée. Les résultats correspondants sont publiés dans [P1,P2].

La production de photons dans une cavité dynamique

Une installation expérimentale particulièrement intéressante est une cavité dynamique comme représenté dans Fig. 5.1 où un des miroirs oscille avec une fréquence égale à la fréquence d'un mode du champ électromagnétique à l'intérieur de la cavité. Dans ce cas, des effets de résonance entre le mouvement mécanique du miroir et les modes du champ se produisent. Ceci engendre la production "explosive" de particules à partir du vide, c'est-à-dire le nombre de photon dans la cavité augmente exponentiellement, ce qui fait ce scénario le candidat le plus prometteur pour une vérification expérimentale de l'effet Casimir dynamique. La difficulté principale pour concevoir cette expérience est que les fréquences typiques de résonance des cavités micro-onde sont de l'ordre du gigahertz. Du point de vue expérimental il est très difficile de construire un dispositif mécanique macroscopique (le miroir) oscillant à une fréquence si élevée. Cependant, des progrès sont accomplis dans cette direction et des expériences concrètes ont été proposées.

Dans le chapitre 5 de cette thèse, j'étudie la production des photons dans une cavité résonnante tridimensionnelle idéale. Le miroir dynamique vibre de façon sinusoïdale à une fréquence qui est exactement deux fois la fréquence d'un mode du champ à l'intérieur de la cavité. C'est un cas idéal de résonance. Ces études numériques confirment les résultats analytiques connus qui sont basés sur des approximations mais ont également indiqué leurs limitations. Les effets de couplage intermodaux ont été étudiés en détail, ce qui est possible uniquement par des simulations numériques. Les simulations numériques ont indiqué que l'efficacité de la production de photon dans une cavité vibrante peut être controle en accordant la taille de cavité. Par conséquent, l'efficacité de production de photons peut être maximisé si on construit la cavité telle que les dimensions non-dynamiques de cavité sont suffisamment supérieures aux dimension dynamique. Ce résultat important et nouveau, qui pourrait être très utile pour l'optimisation des expériences dynamiques proposées d'effet Casimir dynamique, est publiés dans [P3].

Le modèle standard de la cosmologie

Le modèle standard de la cosmologie s'appuie sur trois piliers: l'isotropie de l'expansion cosmique, l'isotropie du fond de rayonnement diffus (le CMB) ainsi que la synthèse des éléments légers.
La géometrie d'un univsers isotrope autour de chaque point est donnée par la métrique de Friedmann-Lemaître-Robertson-Walker (FLRW)

$$ds^2 = g_{\mu\nu} dx^\mu dx^\nu = -d\tau^2 + a^2(\tau) \left[\frac{dr^2}{1 - K\, r^2} + r^2 \left(d\theta^2 + \sin^2\theta d\varphi^2 \right) \right]$$

où a est le facteur d'échelle, τ le temps cosmique et K la courbure des surfaces $\tau = \text{const.}$. La dynamique du champ gravifique, la métrique $g_{\mu\nu}$, est régie par les équations d'Einstein

$$G_{\mu\nu} + \Lambda_4 g_{\mu\nu} = \kappa_4 T_{\mu\nu} \ .$$

$G_{\mu\nu}$ est le tenseur d'Einstein qui contient le champ métrique $g_{\mu\nu}$ et $T_{\mu\nu}$ est le tenseur énergie-impulsion décrivant la matière contenue dans l'Univers. Λ_4 est la constante cosmologique et κ_4 la constante du couplage gravifique qui est liée à la masse de Planck m_{Pl} par

$$\kappa_4 = \frac{8\pi}{m_{\text{Pl}}^2} \ .$$

La forme la plus générale de $T_{\mu\nu}$ compatible avec l'homogénéité et l'isotropie, c'est-à-dire compatible avec la métrique FLRW, est un tenseur énergie-impulsion qui a la forme d'un fluide parfait

$$T^\mu{}_\nu = \text{diag}\left(-\rho, P, P, P\right).$$

Ici ρ est la densité d'énergie et P la pression de la matière contenue dans l'Univers. Les deux quantités peuvent dépendre du temps seulement.

L'insertion du tenseur énergie-impulsion dans les équations d'Einstein mène aux équations décrivant l'évolution du facteur d'échelle $a(\tau)$. On obtient la première

$$H^2 + \frac{K}{a^2} = \frac{\kappa_4}{3}\rho + \frac{\Lambda_4}{3}$$

et le deuxième

$$\frac{1}{a}\frac{d^2\,a}{d\tau^2} = -\frac{\kappa_4}{6}\,(\rho + 3\,P) + \frac{\Lambda_4}{3}$$

équation de Friedmann qui décrivent la dynamique du facteur d'échelle de l'Univers selon le contenu en énergie, la courbure et la constante cosmologique. H est le paramètre de Hubble

$$H = \frac{1}{a(\tau)}\frac{da(\tau)}{d\tau}\ .$$

Le tenseur d'Einstein satisfait les identités de Bianchi $G^{\mu\nu}{}_{||\nu} = 0$ selon la loi locale de conservation pour le tenseur énergie-impulsion $T^{\mu\nu}{}_{||\nu} = 0$. Pour un fluide parfait, cette relation implique l'équation de continuité

$$\frac{d\,\rho}{d\tau} = -3\,H\,(\rho + P)\ ,$$

qui décrit (localement) le changement de la densité d'énergie dans un Univers FLRW. Les deux équations de Friedmann et l'équation de continuité ne sont pas indépendantes, mais seulement deux d'entre elles.
La densité ρ d'énergie et la pression P sont souvent reliés par une équation d'état

$$P = w\,\rho$$

où w est constant. Dans ce cas, l'équation de continuité peut facilement être intégrée

$$\rho = \rho_0 a^{-3(1+w)}\ ,$$

où ρ_0 est une constante d'intégration. Pour un Univers plat, la première équation de Friedmann peut alors être résolue facilement. Par exemple, si l'Univers est dominé par de la matière ultra-relativiste (rayonnement) on a $w = 1/3$, et par conséquent $a \propto \tau^{1/2}$.

Les ondes gravitationnelles

Les ondes gravitationnelles, ou perturbations tensorielles, c'est-à-dire les petites perturbations de la géométrie de l'espace-temps se manifestent comme "des ondes se propageant sur la courbure de l'espace-temps ". L'amplitude d'une onde gravitationnelle libre dans un Univers FLRW plat, rempli d'un fluide parfait est décrite par l'équation

$$\frac{\partial^2}{\partial\eta^2}h(\eta,\mathbf{k}) + 2\mathcal{H}\frac{\partial}{\partial\eta}h(\eta;\mathbf{k}) + k^2 h(\eta;\mathbf{k}) = 0\ .$$

Ici $\mathcal{H} = Ha$ est le paramètre de Hubble. Il est fonction du temps conforme η, qui est lié au temps cosmique τ par $d\tau = a d\eta$. $k = |\mathbf{k}|$ est le nombre d'onde. La dynamique du facteur d'échelle entre dans cette équation au travers du terme de friction $\propto \mathcal{H}$. Par conséquent, en fonction de l'évolution de a, l'amplification des ondes gravitationnelles peut avoir lieu. Après la quantification, et à condition qu'une définition du vide et des particules soit possible, ceci correspond à la création de gravitons, c'est-à-dire de particules de spin 2 sans masse. Un exemple important est l'amplification des ondes gravitationnelles durant l'inflation. L'inflation est une époque d'accélération de l'Univers primordial, qui résout les imperfections du scénario standard du Big Bang. Durant l'inflation de-Sitter, par exemple, le facteur d'échelle est

$$a(\tau) = e^{H\,\tau} \ \text{ with } \ H = \text{const.}\ .$$

Dans ce cas, le spectre de puissance des ondes gravitationnelles [voir Eq. (6.54)] produites sur de grandes échelles est

$$\mathcal{P}_h(k) = \frac{\kappa_4\,H^2}{(2\pi)^3}\ .$$

Il ne dépend pas du nombre d'onde k, il est donc invariant d'échelles. L'invariance d'échelles du spectre de puissance est une prévision saisissante de l'inflation, et est de nos jours confirmée par les observations du CMB avec une précision impressionnante. Ces problèmes sont discutés en détail dans le section 6.5 de la thèse.

La partie restante de la thèse étudie la production d'ondes gravitationnelles dans le contexte de la cosmologie de braneworld.

Dimensions supplémentaires et branes

L'idée que notre Univers a plus de trois dimensions spatiales germa dans les années 1920. Afin d'essayer d'unifier la gravitation et l'électromagnétisme Theodor Kaluza et Oscar Klein ont découvert que les champs gravitationnels et électromagnétiques quadridimensionnels peuvent être compris comme composants du tenseur métrique dans une théorie avec une cinquième dimension compacte.

De nos jours, la recherche pour un théorie de gravitation quantique a mené à des théories et des modèles qui contiennent de nouvelles dimensions spatiales supplémentaires. Le candidat le plus abouti pour une théorie d'unification est la théorie des cordes dont les constituants fondamentaux ne sont plus des particules ponctuelles, mais des objets unidimensionnels, les cordes. La théorie des (super)cordes peut être formulée de manière consistente seulement dans un espace-temps avec dix dimensions. Ainsi des dimensions supplémentaires sont un ingrédient habituel de théorie des cordes. Les excitations des cordes génèrent des états représentant diverses particules aussi biens sans masse que massives, y compris un état de spin 2 sans masse, le graviton. Les champs du modéle standard, comme les bosons et les fermions, sont décrits par des cordes ouvertes tandis que les gravitons correspondent aux excitations de cordes fermées.

La découverte de *D-branes* (D représente Dirichlet) par Polchisnki en 1995 a mené à l'idée de braneworld où le modèle standard de la physique des particules est confiné à une hypersurface, une *brane*. D'après Polchinski: " Les D-branes sont des objets étendu, des défauts topologiques dans un certain sens, définis par la propriété que les cordes peuvent se terminer sur eux ". Par conséquent, les particules du modèles standard qui correspondent aux cordes ouvertes, sont naturellement confinées sur une hypersurface puisque leurs points finaux sont attachés au D-brane. D'autre part, les gravitons qui correspondent aux cordes fermées, se propagent dans les dimensions supplémentaires, voir Figure 2. Ceci a des conséquences étonnantes, par exemple pour le problème de la hiérarchie. Ces sujets sont discutés en détail dans le chapitre 7.

Randall-Sundrum braneworld et cosmologie d'une brane

Les scénarios de braneworld de Randall-Sundrum (RS) I et II présenté en 1999 ont attiré énormément d'attention durant ces récentes années. Dans ces modèles avec une dimension spatiale supplémentaire, l'univers, supposé plat, est décrit comme une 3−brane (une hypersurface) de tension $\mathcal{T}$ plangée dans un espace-temps Anti-de-Sitter (AdS) à cinq dimensions. La métrique de l'AdS est

$$ds^2 = \frac{L^2}{y^2}\left[-dt^2 + \delta_{ij}dx^i dx^j + dy^2\right].$$

Ici δ_{ij} est le Kronecker-delta (Univers plat $K = 0$), t est le temps conforme du bulk, et y dénote la coordonnée de la cinquième dimension. Le facteur L^2/y^2 s'appelle le *warp-factor* où L est le rayon de courbure d'ADS qui est lié à la constante cosmologique en cinq dimension négative Λ_5 par

$$-\Lambda_5 = \frac{6}{L^2} = \frac{\kappa_5^2\mathcal{T}^2}{6}\ .$$

κ_5 est de ce fait la constante de couplage de la gravitation en cinq dimensions.

$$\kappa_5 = 6\pi^2 G_5 = \frac{1}{M_5^3}\ .$$

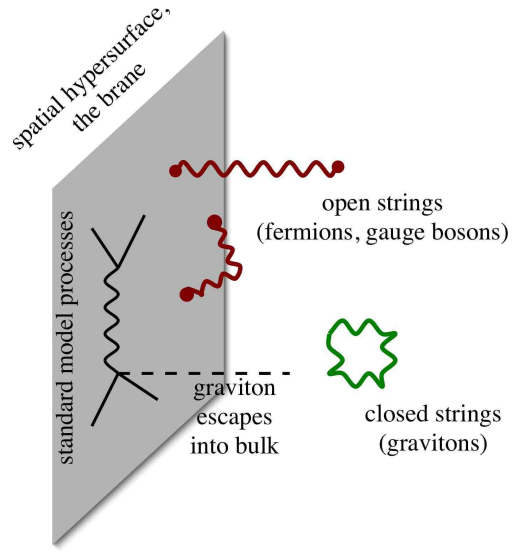

Figure 2: Représentation imagée de l'idée de braneworld: une brane dans un espace-temps à dimensions supplémentaires. Alor que les champs du modèle standard (cordes ouvertes) sont confinés sur la brane, les gravitons (cordes fermées) se propagent dans le volume total.

M_5 et G_5 sont respectivement la masse réduite de Planck et la constante (fondamentale) de Newton en cinq dimensions.
Le modèle de RS II contient une brane, habituellement appelée *visible brane*, représentant notre Univers tandis que le modèle de RS I contient une brane additionnelle (*hidden brane*). En raison de la courbure de AdS, le modèle de RS I peut résoudre le problème de hiérarchie d'une façon élégante, alors que le modèle de RS II a la propriété intéressante de localiser la gravitation quadridimensionnelle sur la brane. Une introduction détaillée aux modèles de RS est donnée dans le chapitre 8.

La situation cosmologique d'un Univers en expansion dans le modèle de RS est obtenue par une brane se déplaçant dans le espace-temps à cinq dimensions d'ADS. Dénotant par η le temps conforme d'un observateur sur la brane, et la position de la brane dans la cinquième dimension par y_b, la métrique de brane induite par la métrique d'AdS est

$$ds^2 = a^2(\eta)\left[-d\eta^2 + \delta_{ij}dx^i dx^j\right] \ ,$$

c'est-à-dire une métrique FLRW plate. Le facteur d'échelle $a(\eta)$ est lié à la position de la brane $y_b(t)$ par

$$a(\eta) = \frac{L}{y_b(t)} \ ,$$

et

$$d\eta = \sqrt{1 - \left(\frac{dy_b}{dt}\right)^2}\, dt \ .$$

Quand la brane se déplace vers des valeurs décroissantes de y, l'Univers est en expansion, alors qu'il contracte dans le cas opposé.

La dynamique du facteur d'échelle est régie par l'équation de Friedmann modifiée

$$H^2 = \frac{\kappa_4 \rho}{3}\left(1 + \frac{\rho}{2\mathcal{T}}\right) .$$

A grand temps, tels que $\rho \ll \mathcal{T}$, la dynamique de l'Univers dans la cosmologie de la brane n'est pas modifiée. Cependant, elle est modifiée dans l'Univers primordial (à haute énergie) car $H^2 \propto \rho^2$. Les observations cosmologiques imposent une limite inférieure à la tension $\mathcal{T}$ de la brane. Ceci est discuté en détail dans la section 8.4.

Perturbations tensorielles dans une braneworld de Randall-Sundrum

Puisque la gravitation, à la différence des champs du modèle standard, se propage dans l'espace-temps entier, les perturbations de la gravitation peuvent être employées pour étudier les effets liés à la cinquième dimension. Du point de vue (quadridimensionnel) de la brane, indépendamment du graviton quadridimensionnel standard, les braneworlds contiennent une tour de Kaluza-Klein de gravitons massifs. Les perturbations quadridimensionnelles tensorielles, c'est-à-dire les ondes gravitationelles de notre Univers, sont ainsi une superposition du graviton quadridimensionnel standard et des gravitons massifs de Kaluza-Klein qui sont des traces de la nature cinq-dimensionnelle de la gravitation. Des signatures de la dimension supplémentaire, provenant de l'époque primordiale de l'Univers ont pu être gravées dans le fond d'ondes gravitationelles et dans les anisotropies du CMB.
Dans la section 8.5 on montre en détail que des ondes gravitationelles dans une braneworld de RS sont décrites par une équation d'ondes dans l'espace-temps à cinq dimensions d'AdS. L'amplitude de chaque polarisation satisfait

$$\left[\partial_t^2 + k^2 - \partial_y^2 + \frac{3}{y}\partial_y\right] h_\bullet(t, y; \mathbf{k}) = 0 \ .$$

De plus, une brane se déplaçant dans le bulk impose des conditions aux limites dépendantes du temps pour les perturbations, les *conditions de jonction*,

$$(v\partial_t + \partial_y)\, h_\bullet(t, y; \mathbf{k})|_{y_b(t)} \ = 0 \ ,$$

où v est la vitesse de la brane. L'évolution des ondes gravitationnelles dans la cosmologie de braneworld est ainsi décrite par une équation d'ondes soumise à une condition aux limites dépendante du temps. Par conséquent, par le même mécanisme qu'un miroir mobile crée des photons à partir du vide électromagnétique, une brane mobile mène à la production de gravitons à partir des fluctuations du vide. C'est l'effet Casimir dynamique pour des gravitons. Si la production des gravitons, en particulier des particules massives de Kaluza-Klein, est suffisamment importante, ils pourraient par la suite dominer la densité d'énergie de l'Univers et corrompre la phénoménologie. Il est donc important d'étudier l'évolution des ondes gravitationelles dans la cosmologie de braneworld afin de confronter des modèles de braneworld avec des contraintes observationnelles.

L'effet Casimir dynamique pour les gravitons et la localisation de la gravitation sur une brane en mouvement

Dans le chapitre 9, je décris la production de gravitons par une brane mobile en utilisant les méthodes pour l'effet Casimir dynamique développées dans la première partie de la thèse. Il s'avérera que le formalisme employé pour décrire l'effet Casimir dynamique pour le champ électromagnétique est très approprié à l'étude des perturbations tensorielles dans la cosmologie de braneworld. Ceci se fonde en particulier sur sa capacité à traiter les couplages entre les modes de Kaluza-Klein provoqués par les conditions de bord dépendantes du temps d'une manière claire en employant des matrices de couplage. Cette approche a certains avantages par rapport à d'autres formulations employées dans la littérature, et apporte une nouvelle perception du problème. Les résultats de la deuxième partie de la thèse sont publiés dans [P3, P4, P5].

Des quantités observables peuvent être reliées au nombre de gravitons produits $\mathcal{N}^{\rm out}_{\alpha,k}$ à la fréquence $\Omega_{\alpha,k}$. Ici α est le nombre quantique de l'impulsion concernant la dimension supplémentaire et $k = |\mathbf{k}|$ est l'impulsion du graviton parallèle à la brane. Le cas $\alpha = 0$ décrit le mode zéro qui n'a aucune impulsion dans la dimension supplémentaire, c'est-à-dire le graviton quadridimensionnel standard. Les nombres quantiques $\alpha = n \geq 1$ correspondent aux gravitons de Kaluza-Klein de masses m_n, représentant l'impulsion quantifiée dans la dimension supplémentaire. $\mathcal{N}^{\rm out}_{\alpha,k}$ peut être obtenu à partir de simulations numériques du système d'équations

pour les coefficients de Bogoliubov. En termes de nombre de gravitons, le spectre de puissance du graviton quadridimensionnel standard à de temps retardé (après que la production de gravitons a cessé) est

$$\mathcal{P}_0(k) = \frac{\kappa_4}{a^2}\frac{k^2}{(2\pi)^3}\mathcal{N}^{\rm out}_{0,k}.$$

tandis que pour les modes de Kaluza-Klein il est

$$\mathcal{P}_{\rm KK}(k) = \frac{k^3}{a^4}\frac{\kappa_4 L^2}{32\pi}\sum_n \mathcal{N}^{\rm out}_{n,k}\,\frac{m_n^2}{\Omega^{\rm out}_{\rm n,k}}Y_1^2(m_n y_s)\ ,$$

où Y_1 est une fonction de Bessel. Comme prévu, pour les gravitons quadridimensionnels standards, le spectre de puissance décroît avec l'expansion de l'Univers comme $1/a^2$. Par contre, le spectre de puissance de Kaluza-Klein décroît comme $1/a^4$, c'est-à-dire avec un facteur $1/a^2$ plus rapide que $\mathcal{P}_0$. Le spectre de puissance à grand temps est donc dominé par le spectre de puissance du mode zéro et semble quadridimensionnel.

Pour la densité d'énergie du mode zéro on obtient

$$\rho_0 = \frac{1}{a^4}\int \frac{d^3k}{(2\pi)^3}\,k\,\mathcal{N}^{\rm out}_{0,k}\ .$$

C'est le comportement prévu. La densité d'énergie des gravitons du mode zéro se comporte comme celle du rayonnement.
Par contre, pour la densité d'énergie des modes de Kaluza-Klein on trouve

$$\rho_{\rm KK} = \frac{L^2}{a^6}\frac{\pi^2}{4}\sum_n\int\frac{d^3k}{(2\pi)^3}\Omega^{\rm out}_{n,k}\,\mathcal{N}^{\rm out}_{n,k}\,m_n^2 Y_1^2(m_n y_s)\ ,$$

qui se comporte comme $1/a^6$. Par conséquent, durant l'expansion de l'Univers, la densité d'énergie des gravitons massifs sur la brane est rapidement diluée. Une conséquence immédiate de ce comportement est que les gravitons de Kaluza-Klein ne peuvent pas jouer le rôle de la matière sombre dans une braneworld de Randall-Sundrum. Je discute en détail dans la section 9.5.4, que ce comportement particulier pour $\mathcal{P}_{\rm KK}$ et $\rho_{\rm KK}$ découle de la localisation de la gravitation standard sur la brane. Ceci implique que les gravitons de Kaluza-Klein, qui sont des traces de la nature à cinq dimensions de la gravitation, se évadent rapidement de la brane dans la cinquième dimension.

La production des gravitons dans un bouncing model

Comme exemple explicite, j'étudie la production de graviton dans un modèle ekpyrotic constitué de deux branes rebondissant à de basses énergies dans le chapitre 10. Je constate que pour les longues longueurs d'onde $kL \ll 1$, le mode zéro évolue pratiquement indépendamment des modes de Kaluza Klein. Des gravitons de mode zéro sont produits par le couplage du mode zéro au brane mobile. Pour le nombre de gravitons sans masse produits, j'ai trouvé l'expression analytique simple $2v_b/(kL)$, òu v_b est la vitesse de rebond du brane. Ces modes de grande longueur d'onde sont intéressants pour le spectre de puissance du mode zéro. En accord avec qu'un scènario ekpyrotic prévoit, je constate que le spectre de puissance du mode zéro est bleu sur des échelles plus grand. Par conséquent, l'éventail des gravitons de Casimir a une puissance beaucoup trop faible sur de grandes échelles pour affecter les fluctuations du CMB.
La situation est complètement differente pour les longueurs d'onde courtes $kL \gg 1$. Des effets nouveaux et intéressants apparaissent qui sont discutés en détail. Une des conclusions principales de cette partie finale de la thèse est que la backreaction des gravitons massifs doit être prise en considération pour un rebond réaliste.

Contents

Chapter 1

Introduction

Boundary conditions, which can be considered as very localized classical fields, change the mode structure of the electromagnetic quantum vacuum leading to an attractive force between two uncharged, perfectly conducting parallel plates (ideal mirrors). The prediction of this effect by the Dutch physicist Hendrik Casimir in 1948 and its experimental verification during the last ten years, have impressively demonstrated the non-trivial nature of the quantum vacuum, the ground state of quantum field theory (QFT). This so-called *Casimir effect* reveals that changes in the infinite zero-point energy of the electromagnetic vacuum can be finite, observable and even affect macroscopic bodies. It is therefore often considered as proof for the reality of quantum vacuum fluctuations.
The dynamical counterpart of this effect - the *dynamical Casimir effect* - appears to be even more striking. When the boundaries are set in motion, the quantum vacuum responds to the induced time-dependent boundary conditions by the creation of real particles out of quantum vacuum fluctuations. As a consequence, a mirror moving through the vacuum of the electromagnetic field produces real photons "out of nothing". Sometimes, this effect is also referred to as *motion induced radiation*. A particular interesting setup is a dynamical cavity with one wall (mirror) oscillating at a frequency which is twice the frequency of a field mode inside the cavity. In this case, resonance effects between the mechanical motion of the wall and the quantum vacuum occur, leading to "explosive" photon production. After all, the Casimir effect, static and dynamical, is only one out of the many fascinating manifestations of the non-trivial nature of the quantum vacuum within the broad field of quantum field theory under the influence of external conditions. [1] .

In cosmology, which at first sight has nothing in common with the dynamical Casimir effect, we are currently experiencing exciting times. The precise measurements of the anisotropies in the cosmic microwave background (CMB) with experiments like the Wilkinson Microwave Anisotropy Probe (WMAP) and its predecessor COBE (COsmic Background Explorer) have impressively confirmed the cosmological standard model and have transformed cosmology into a precise science. However, despite its great success, the standard cosmological model contains building blocks whose fundamental theoretical understanding is still lacking. Just to name a few of the puzzles cosmologists are facing: What is the inflaton, or more precisely, the underlying physics of the inflationary paradigm whose predictions are so impressively in agreement with recent observations? What is the nature of dark energy and dark matter? And, how can the initial singularity problem (Big Bang), inherent in general relativity, be resolved?
It is widely accepted that a theory of quantum gravity which unifies gauge interactions and gravity is needed in order to address (at least) some of these questions. Their unification represents maybe the biggest challenge theoretical physics has ever seen. An early attempt for a unifying theory, a prototype, so to speak, goes back to Nordström, Kaluza and Klein who tried to unify gravity and electromagnetism already in the 1920's. Even though their model was phenomenologically not feasible, they were the first to introduce the concept of *extra dimensions*, which had its revival in the 1970's when the 11-dimensional theory of supergravity was constructed. Nowadays, the most successful attempt towards a unified theory is *String theory*, which can be formulated consistently in a higher-dimensional spacetime only; ten-dimensional for *Superstring theory* and 11-dimensional for *M-theory*. String theory also predicts the existence of *branes*, i.e. hypersurfaces in the higher-dimensional

[1] Since it took place for the first time in 1989 in Leipzig, Germany , with the intention of being "an East-West bring-together", the series of workshops on *QUANTUM FIELD THEORY UNDER THE INFLUENCE OF EXTERNAL CONDITIONS* has developed into one of the most prominent international meetings in this field. For more information on the current workshop to be held again in Leipzig, please visit http://www.physik.uni-leipzig.de/~ bordag/QFEXT07 .

spacetime on which the standard model of particle physics (e.g., gauge particles and fermions) is confined. Then, gravity is the only fundamental force propagating in the whole spacetime. This has motivated the consideration of braneworld models, where our Universe is described as such a hypersurface (a 3-brane) in a higher-dimensional spacetime (*the bulk*) onto which the standard model of particle physics is confined. The difference between gravitation and standard model fields with respect to their possibility to probe the extra dimensions in these models, allows to address the hierarchy problem, i.e. the unnatural vast disparity between the electroweak and Planck scale. After the initial proposal by Arkani-Hamed, Dimopoulos and Dvali in 1998, the Randall-Sundrum (RS) braneworld models introduced in 1999 have attracted most of the attention.
In the RS II model, our Universe is described as a 3-brane, usually called the *visible brane*, in a five-dimensional anti-de Sitter spacetime. The RS I model contains an additional *hidden brane*. Due to the curvature of anti-de Sitter, the RS I model is able to address the hierarchy problem in an elegant manner, while the RS II model has the appealing feature of localizing four-dimensional gravity on the brane.

The cosmological situation of an expanding Universe within the RS setup is obtained by a brane moving through the five-dimensional anti-de Sitter spacetime. Thereby, the scale factor of the Universe and the position of the brane in the bulk are directly related. The dynamics of the scale factor is governed by a modified Friedmann equation which changes the standard cosmological evolution in the early Universe, but does not affect its evolution at low energies.
Since gravity, unlike standard model fields, probes the whole spacetime, gravitational perturbations can be used to explore effects related to the extra dimension. From the brane (four-dimensional) point of view, apart from the standard four-dimensional graviton, braneworlds allow for a tower of massive Kaluza-Klein gravitons. Four-dimensional tensor perturbations, i.e. gravity waves in our Universe, are thus a superposition of the standard four-dimensional graviton and massive Kaluza-Klein gravitons which are traces of the five-dimensional nature of gravity. Signatures of the extra dimension stemming from the very early epoch of the Universe could be engraved in the gravitational wave background and in the anisotropies of the CMB.
Gravitational perturbations in RS braneworld cosmology are described by a wave equation in the five-dimensional anti-de Sitter bulk. In addition, a brane moving through the bulk enforces time-dependent boundary conditions for the perturbations. This is the point where the dynamical Casimir effect enters the stage: A brane moving through the extra dimension acts as a time-dependent boundary for five-dimensional gravitational perturbations in the same way, as a moving mirror acts as a time-dependent boundary for the electromagnetic field. Consequently, by the same mechanism a moving mirror creates photons out of the electromagnetic vacuum, a moving brane leads to the production of gravitons from vacuum fluctuations. If the production of gravitons, in particular of the massive Kaluza-Klein particles, is sufficiently copious, they could eventually dominate the energy density of the Universe and spoil phenomenology. It is therefore an important task to study the evolution of gravity waves in braneworld cosmology in order to confront braneworld models with observational constraints.

The study of particle creation by moving mirrors and branes is the subject of this thesis. It will turn out that the formalism used to describe the dynamical Casimir effect for the electromagnetic field is very suitable for the study of tensor perturbations in braneworld cosmology. This relies in particular on its power to deal with the couplings between the Kaluza-Klein modes caused by the time-dependent boundary conditions in a clear way by using coupling matrices. This approach has certain advantages compared to other formulations which are being used in the literature, and admits a new perception to the problem.

The thesis is organized as follows. In Chapter 2 I give a very brief introduction to the static Casimir effect. Chapter 3 represents the first main technical part in which I introduce the canonical formulation of the dynamical Casimir effect. Thereby I shall set great store on the discussion of issues regarding particle definition in external field problems as well as on the difference to other quantum vacuum radiation effects like the Unruh effect. With a particular parameterization for the time evolution of the field modes, I derive a relatively simple system of coupled differential equations determining the Bogoliubov transformations between initial and final vacuum states. Its solutions can be obtained from numerical simulations. In Chapter 4 I show and discuss results of numerical simulations for the dynamical Casimir effect in two dimensions and compare them with analytical predictions. This will show the applicability and reliability of the numerical formalism. The material presented in Chapters 3 and 4 is published in [P1,P2]. In chapter 5 I apply the formalism to study the realistic scenario of photon production in a three-dimensional vibrating cavity. Thereby, new results regarding the interplay between the geometry of the cavity and the strength of the intermode coupling are presented. I show in particular that the rate of photon production in a vibrating cavity can be enhanced by tuning its size. This

may be important for the optimization of future experiments aiming to verify the dynamical Casimir effect in the laboratory. These results are published in [P3]. After this more "down to earth" physics, I discuss the production of gravitons by moving branes in the second part of the thesis.
After a description of the standard model of cosmology in Chapter 6, I introduce the concept of extra dimensions and braneworlds in Chapter 7. Chapter 8 is entirely devoted to the discussion of the Randall Sundrum models, braneworld cosmology and tensor perturbations within this context. The more technical Chapter 9 deals with the generalization of the dynamical Casimir effect formulation of Chapter 3 to tensor perturbations in braneworld cosmology. The connection between observable quantities, like the power spectrum and energy density, and quantum mechanical expectation values is established in detail. I shall show that, very generically, massive Kaluza-Klein gravitons cannot play the role of dark matter since their energy density in our Universe scales like stiff matter. A comprehensive discussion on the underlying physics of this new and very important result is provided. It is a consequence of the localization of four-dimensional gravity on the brane, implying that massive Kaluza-Klein gravitons escape from the moving brane into the bulk. Finally, motivated by the ekpyrotic Universe and similar ideas, I study graviton production in a model of two bouncing branes in Chapter 10. The numerical results are discussed in detail and bounds on the parameters of the model are derived. I show that such a model is not constrained by the standard four-dimensional graviton, but that for a realistic model of bouncing universes, the back reaction of the massive Kaluza-Klein gravitons cannot be neglected. The second part is based on the publications [P4,P5,P6]. I conclude the thesis by summarizing the main results and providing an outlook for future work in Chapter 11.
Two appendices provide some details of technical nature (A) and on the numerical simulations (B), whose implementation, code writing and testing engulfed most of the time during the last four years.

Some notations and conventions

In the following I summarize some basic notations and conventions which I shall use throughout this thesis. Other notations which are not used so frequently are explained upon their first appearance.

- D denotes the total number of spacetime dimensions, while d the number of spatial dimensions and n the number of extra spatial dimensions. With n extra dimension in our Universe it is $D = 1 + d = 1 + 3 + n$.
- Without extra dimensions $n = 0$, indices $\mu, \nu, \rho, ...$ label the coordinates of the D-dimensional spacetime while i, j denote the d spatial dimensions.
- With extra dimensions, indices A, B, C, D label coordinates of the full spacetime. Coordinates are split as $x^A = (x^\mu, z) = (t, x^i, z)$ in case of one extra dimension $(D = 1 + 3 + 1)$ denoted here by z.
- In the first part of the thesis dealing with quantum field theory, I shall use the metric signature $(+, -, ..., -)$ while in the second part on braneworld cosmology I switch to $(-, +, ..., +)$.
- $\Box_{(D)}$ denotes the Klein-Gordon (wave) operator which is defined as $\Box_{(D)} = \frac{1}{\sqrt{g}}\partial_\mu(\sqrt{g}g^{\mu\nu}\partial_\nu)$, where $g_{\mu\nu}$ is the spacetime metric and $g = (-1)^d \det(g_{\mu\nu})$ (first part) and $g = -\det(g_{\mu\nu})$ (second part), respectively. ∂_μ is the partial derivative.
- Lowercase boldface quantities denote d-dimensional spatial vectors like the wave vector $\mathbf{k}$, and uppercase boldface quantities denote vectors and matrices for linear systems of equations like $\mathbf{Y} = \mathbf{WX}$.
- Quantum operators are denoted by an over-hat, e.g. $\hat{a}$ and $\hat{a}^\dagger$ for particle annihilation and creation operators, respectively, where $\dagger$ denotes the adjoint.
- $[\hat{a}, \hat{b}] = \hat{a}\hat{b} - \hat{b}\hat{a}$ defines the commutator between quantum operators.
- c^* is the complex conjugate of the quantity c.
- h.c. is hermitian conjugate

In addition, I work in units $\hbar = c = k_\mathrm{B} = 1$, such that there is only one dimension, energy, which is usually measured in GeV. Then,

$$[\text{energy}] = [\text{mass}] = [\text{temperature}] = [\text{length}]^{-1} = [\text{time}]^{-1}.$$

An exception is Chapter 2 where I discuss the static Casimir effect.

Part I

Dynamical Casimir effect

Chapter 2

The Casimir effect

I mentioned my results to Niels Bohr, during a walk. That is nice, he said, that is something new. I told him that I was puzzled by the extremely simple form of the expression for the interaction at very large distances and he mumbled something about zero-point energy. That was all, but it put me on a new track. (H. B. G. Casimir to P. W. Milonni, March 1992 [158].)

2.1 The Casimir force

In this section I shall give a short introduction to the Casimir effect. Excellent reviews on which the presented material is partly based are [19, 175, 160, 135, 158, 164].
In its simplest form, the Casimir effect is the interaction of a pair of neutral, parallel conducting planes due to the disturbance of the vacuum of the electromagnetic field. Since there is no force between neutral plates in electrodynamics, it is a pure quantum effect. In an ideal situation, at zero temperature for instance, there are no real photons between the plates. Hence it is only the ground state of quantum electrodynamics, the vacuum, which causes the plates to attract each other. Therefore it is often cited as the proof for the reality of the vacuum electromagnetic field and quantum vacuum fluctuations in general. There are of course more observable consequences of the vacuum field like spontaneous emission, the Lamb shift and many others [158]. But the fascination in the Casimir effect relies on the fact that it is a pure quantum effect which acts on macroscopic scales. It has not only been experimentally verified in the laboratory with high precision (see section below) but is nowadays even important for nanotechnology [19].
In his famous paper [33] Casimir found (with a nudge from Bohr [160, 35] - see above) that the force between two parallel plates caused by the vacuum fluctuations is given by [1]

$$F(d) = -\frac{\pi^2}{240}\frac{\hbar c}{d^4} S \ . \tag{2.1}$$

Thereby, d is the separation between the two plates and S their area. I shall derive an analogous expression for a simple two-dimensional example in the next section to illustrate the way of its occurrence. Note, that apart from the two geometric quantities d and S, only fundamental constants enter the force. Also the electron charge is absent. This demonstrates the above statement that the electromagnetic field is not coupling to matter in the usual sense. The Casimir force is purely a consequence of the boundary conditions imposed by the plates which modify the mode structure of the vacuum fluctuations and thus the zero-point energy of the field compared with free space [cf. Fig. 2.1]. In the ideal case, i.e. in the limit of perfect conductivity, the microscopic properties of the plates are not important. The Casimir energy, in particular its sign, depends strongly on the geometry. While the force is attractive for two parallel plates, it is repulsive for a sphere which was first shown by Boyer in 1968 [21], who calculated the Casimir self-energy for a perfectly conducting shell. This represented the demise of Casimir's proposal [34] that a classical electron could be stabilized by zero-point attraction [160].
Nowadays, the Casimir effect has become a very active field of research, with attention focusing on finite-temperature and roughness corrections as well the treatment of realistic boundary conditions. See the above cited reviews for details.

[1] Only in this section I shall keep units $\hbar$ and c. Later on I use $\hbar = c = 1$ throughout.

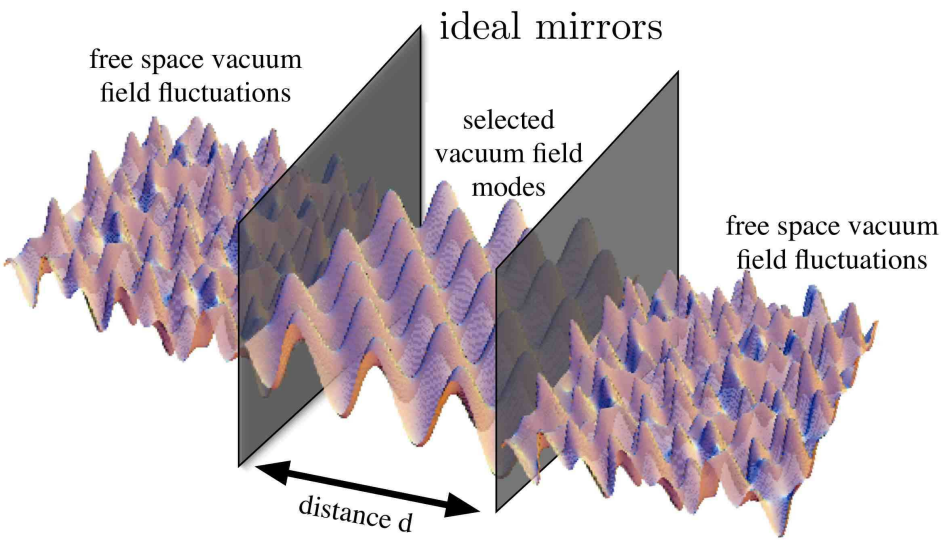

Figure 2.1: Pictorial representation of the Casimir effect. The ideal mirrors change the mode structure of the vacuum field. While arbitrary frequencies are allowed in free space, Dirichlet boundary conditions for the vacuum field at the ideal mirrors restrict the spectrum of field modes to particular (quantized) frequencies in the intervening volume. This difference in the mode structure of the vacuum field leads to the Casimir force [cf. section 2.2].

After the first attempt by Sparnaay in 1958 [203] whose experimental data "do not contradict Casimir's theoretical prediction", the Casimir force has been measured with high accuracy only during the last decade. First, in 1996/97, Lamoreaux [133, 134] clearly demonstrated the presence of the Casimir force using a torsion pendulum. Only one year later, Mohideen and Roy measured the Casimir force with a statistical precision of 1% [162] for the configuration of a metallic sphere above a plate for separations from 0.1 to 0.9 μm using an atomic force microscope. This method has been improved since then [187, 188]. But it took until the year 2002 to demonstrate the Casimir force for Casimir's original configuration of two parallel plates [24].
As an representative example, I show in Figure 2.2 the experimental results obtained with the sphere-plate configuration [162, 19], which impressively demonstrates the existence of the Casimir force. For a detailed discussion see Section 6.4 of [19].

2.2 A simple example

As an illustration, let me discuss the simple example of a real massless scalar field $\Phi(t,x)$ on an interval $[0,l_0]$. Ideal, perfectly reflecting, boundary conditions imply that the field vanishes at the edges of the interval, i.e. $\Phi(t,0)=\Phi(t,l_0)=0$. The ground state energy of the field is the sum of the ground state energies (frequencies) of all field modes (harmonic oscillators) [cf. Chapter 3]

$$E_0(l_0) = \frac{\hbar}{2}\sum_{n=1}^{\infty}\frac{c\,\pi n}{l_0}\ . \tag{2.2}$$

This divergent expression can be regularized by introducing an exponential damping function

$$E_0(l_0,\delta) = \frac{\hbar}{2}\sum_{n=1}^{\infty}\frac{c\,\pi n}{l_0}\exp\left(-\delta\frac{c\pi n}{l_0}\right) \tag{2.3}$$

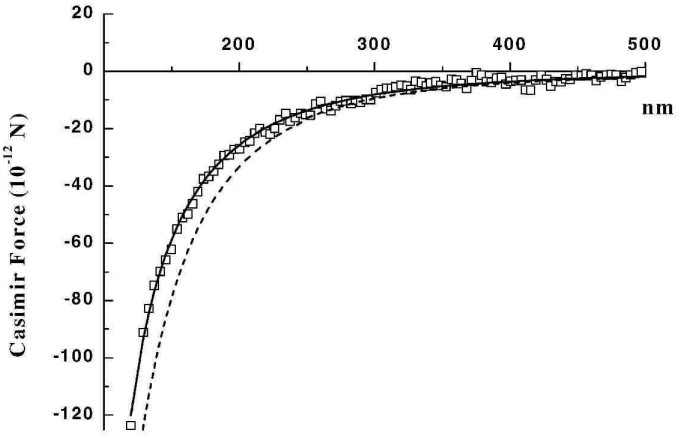

Figure 2.2: Measured Casimir force as a function of the plate-sphere separation shown as squares. The solid line is the theoretical prediction for the Casimir force including corrections due to surface roughness and finite conductivity while the dashed line is the prediction without any corrections. Picture taken from [19].

with $\delta \geq 0$. The regularization is removed in the limit $\delta \to 0$. With this trick, the summation can be performed, leading to

$$E_0(l_0, \delta) = \frac{\pi\hbar c}{8\, l_0} \sinh^{-2} \frac{\delta c \pi}{l_0} = \frac{\hbar\, l_0}{2\pi c \delta^2} + E(l_0) + \mathcal{O}(\delta^2) \tag{2.4}$$

with

$$E(l_0) = -\frac{\pi\hbar c}{24\, l_0}. \tag{2.5}$$

Consequently, the vacuum energy is given as a sum of a singular term and a finite contribution.
The singular term can be removed by subtracting the regularized vacuum energy without the presence of the boundary. Without the boundary, the total vacuum energy on the axis is

$$E_{0,\mathrm{M}}(-\infty, +\infty) = L\, \frac{\hbar\, c}{2\pi} \int_0^\infty dk\, k \tag{2.6}$$

where $L \to \infty$ is the normalization length and M stands for Minkowski. Separating the whole axis into intervals of size l_0 yields for the vacuum energy corresponding to such an interval

$$E_{0,M}(l_0) = \frac{E_{0,\mathrm{M}}(-\infty, +\infty)\, l_0}{L} = \frac{\hbar\, c\, l_0}{2\pi} \int_0^\infty dk\, k\ . \tag{2.7}$$

Regularizing it by again using an exponential damping function $\exp(-\delta c k)$ leads to

$$E_{0,M}(l_0, \delta) = \frac{\hbar\, c\, l_0}{2\pi} \int_0^\infty dk\, k e^{-\delta c k} = \frac{\hbar\, l_0}{2\pi c \delta^2}\ , \tag{2.8}$$

i.e. the same singular term as in (2.4). The renormalized vacuum energy on the interval $[0, l_0]$ is then defined as

$$E_0^{\mathrm{ren}}(l_0) = \lim_{\delta \to 0} \left[E_0(l_0, \delta) - E_{0,M}(l_0, \delta)\right] = E(l_0) = -\frac{\pi\hbar c}{24\, l_0}. \tag{2.9}$$

The force exerted on the endpoints is

$$F(l_0) = -\frac{\partial E(l_0)}{\partial l_0} = -\frac{\pi\hbar c}{24\, l_0^2}\ . \tag{2.10}$$

This attractive force is the two-dimensional analog of the Casimir force (2.1) in four dimensions.
Note that (2.9) can also be directly obtained from (2.2) using the powerful technique of *Zeta-function* regularization, since

$$\sum_{n=1}^{\infty} n = \zeta(-1) = -\frac{1}{12} \tag{2.11}$$

where $\zeta(s)$ is the Riemannian Zeta-function. For a detailed discussion see [71].

Chapter 3

Dynamical Casimir effect

3.1 Prelude: Wave equation on a time-dependent interval

In order to familiarize with the mathematical problem, I begin with the simple example of a real massless scalar field $\Phi(t,x)$ on a time-dependent interval $x \in [0, l(t)] \equiv I(t)$ subject to Dirichlet boundary conditions. The dynamics of the field is described by the equations

$$\left[\partial_t^2 - \partial_x^2\right] \Phi(t,x) = 0 \;\text{ with }\; \Phi(t,0) = \Phi[t, l(t)] = 0 \; . \tag{3.1}$$

To arrive at a formulation of the field dynamics in terms of field modes and eventually pave the way for canonical quantization, a complete and orthonormal set of eigenfunctions $\{\phi_n\}$ of the one-dimensional Laplacian $-\partial_x^2$ has to be introduced. On a static interval $[0, l_0 = \text{const.}]$ such a set of eigenfunctions satisfying the Dirichlet boundary conditions is simply given by $\left\{\sqrt{\frac{2}{l_0}} \sin\left(\frac{n\pi}{l_0} x\right)\right\}$ with $n = 1, 2, \ldots$. The corresponding eigenvalues are $(n\pi/l_0)^2$. When the boundary is in motion, a suitable set of eigenfunctions has to satisfy both, the eigenvalue equation and the boundary conditions at any time t. This forces the eigenfunctions to be explicitly time dependent, and consequently, so are the eigenvalues. Such a set of instantaneous eigenfunctions can be obtained from the eigenfunctions on a static interval through replacing l_0 with $l(t)$:

$$\phi_n(t,x) = \sqrt{\frac{2}{l(t)}} \sin\left[\omega_n(t)\, x\right] \;\text{ with frequency }\; \omega_n(t) = \frac{n\pi}{l(t)}. \tag{3.2}$$

It is readily checked that the set $\{\phi_n(t,x)\}_{n=1}^{\infty}$ is complete and orthonormal with respect to the inner product on $I(t)$, $\int_0^{l(t)} dx \phi_n(t,x)\phi_m(t,x)$, i.e. it forms an instantaneous basis. This allows me to expand the field Φ in these eigenfunctions and canonical variables $q_n(t)$:

$$\Phi(t,x) = \sum_{n=1}^{\infty} q_n(t)\phi_n(t,x). \tag{3.3}$$

Inserting the expansion into the wave equation (3.1), multiplying it by $\phi_m(t,x)$ and integrating over $I(t)$ leads to the equations of motion for the q_n's

$$\ddot{q}_n + \omega_n^2(t) q_n - 2\sum_m M_{nm}(t)\dot{q}_m + \sum_m \left[\dot{M}_{mn}(t) - N_{nm}(t)\right] q_m = 0. \tag{3.4}$$

The dot denotes the derivative with respect to time t and $M_{nm}(t)$ and $N_{nm}(t)$ are coupling matrices defined by

$$M_{nm}(t) \;=\; \int_{I(t)} dx\, \dot{\phi}_n(t,x)\phi_m(t,x) = \begin{cases} \dfrac{\dot{l}(t)}{l(t)}(-1)^{n+m}\dfrac{2\,n\,m}{m^2-n^2} & \text{if} \quad n \neq m \\ 0 & \text{if} \quad n = m \; , \end{cases} \tag{3.5}$$

$$N_{nm}(t) \;=\; \int_{I(t)} dx\, \dot{\phi}_n(t,x)\dot{\phi}_m(t,x) = \sum_k M_{nk}M_{mk}. \tag{3.6}$$

Using the completeness and orthonormality of the eigenfunctions ϕ_n, the relation between N_{nm} and M_{nm} is easily demonstrated.

Even if the problem of a massless scalar field in two dimensions might seem to be relatively simple at first glance, the time-evolution of the field modes is described by a coupled system of infinitely many differential equations, each of which containing an infinite number of time-dependent terms. The mode couplings are a direct consequence of the time-dependence of the boundary and their specific form depends on the particular boundary condition the field is subject to. Hence, in general, no analytical solutions to the equations can be found even for simple motions $l(t)$.
Of course, exploiting conformal invariance of a massless scalar field in two dimensions one would expect that the equations can be simplified. The first works on the dynamical Casimir effect were indeed based on conformal invariance, but still, "closed form" solutions could be found only for particular wall motions. This will be briefly discussed in the next section.
In higher dimensions, for different geometries of the time-dependent region and massive fields, the corresponding time evolution of the field modes is always described by a system of coupled differential equations of the form of Eq. (3.4). For very special cases like the scenario of vibrating cavities which I discuss later, approximations can be used to simplify the equations. But in general, if one wishes to study more complicated models, the problem has to be attacked by means of numerical methods.

3.2 Remarks

As I shall show below, after quantization the two time dependencies in the equations of motion, the frequency $\omega_n(t)$ and the coupling $M_{nm}(t)$, correspond to two sources of particle creation from vacuum fluctuations. In the dynamical Casimir effect literature, the appearance of the time-dependent mode coupling is sometimes referred to as *acceleration effect*. The time-dependence of the frequency $\omega_n(t)$, as consequence of the time-dependent quantization volume, i.e. the "squeezing" of the vacuum, is usually called *squeezing effect* [195].
The occurrence of the acceleration effect reflects the main difference between the dynamical Casimir effect and other established particle production phenomena like particle creation in an isotropic and homogeneous expanding Universe [15], particle production in reheating and preheating in inflationary models [127, 202, 128, 20, 73] or photon creation in a time-dependent classical electromagnetic field [87]. In all these cases, the time-evolution is described by uncoupled oscillator equations with time-dependent frequency as the only source of particle creation, which poses a much simpler problem.

In 1970 G. Moore published his paper entitled *"Quantum Theory of the Electromagnetic Field in a Variable-Length One-Dimensional Cavity"* [163] which was the first paper dealing with the quantum aspects of the problem, including particle creation from vacuum. Exploiting the conformal invariance of equation (3.1), he showed that the problem can be mapped onto a stationary problem, and that the mode functions $\phi_n(t,x)$ inside a one-dimensional dynamical cavity $I(t)$ satisfying the initial value problem (3.1) can be written (up to a normalization) as

$$\phi_n(t,x) = \exp\{-ik\pi R(t+x)\} - \exp\{-in\pi R(t-x)\} \tag{3.7}$$

provided that $R(z)$ satisfies the equation

$$R[t+l(t)] - R[t-l(t)] = 2. \tag{3.8}$$

This equation has entered the literature as *Moore's equation*. It can be solved and $R(z)$ evaluated exactly only for a very restricted class of mirror trajectories [163, 36]. Among them is the simple example of a uniform motion (cf. Section 4.2). It serves also as starting point for perturbative and numerical studies of particle production in one-dimensional cavities [56, 140, 39, 47, 40].

By again exploiting the conformal invariance of a massless scalar field in two dimensions Fulling and Davis calculated the total energy radiated by a *single* moving mirror [78] and pointed out the close analogy to the Hawking radiation (see also [195]). A few years, later Ford and Vilenkin developed a method for the calculation of the radiation emitted by a moving mirror in higher dimensions [75]. Let the trajectory of the moving mirror be $l(t)$, then the radiated energy is (using certain approximations, e.g., $\dot{l} \ll 1$, see [195])

$$\mathcal{E} \propto \int dt\, \ddot{l}^{\,2}(t)\ . \tag{3.9}$$

The creation of quantum radiation, i.e. the production of particles from vacuum, is related to the acceleration of the mirror. This is analogous to classical electrodynamics where acceleration of charges gives rise to radiation. Hence, the mirror does not emit quantum radiation, i.e. no particles are produced from vacuum fluctuations, when it undergoes a uniform motion.
Other early papers devoted to field theory with moving boundaries are by Razavy [183] and by Razavy and Terning [184].

3.3 Canonical formulation

3.3.1 Expanding the action and equations of motion

I restrict myself in the following to the consideration of a real massive scalar field in two dimensions $\Phi(t,x)$, described by the Lagrange density

$$\mathcal{L} = \frac{1}{2}\left[(\partial_t\Phi)^2 - (\partial_x\Phi)^2 - \mathfrak{m}^2\Phi^2\right], \tag{3.10}$$

where $\mathfrak{m}$ is the mass of the field. The corresponding action of the field on a time-dependent interval $I(t) = [0, l(t)]$ then reads

$$\mathcal{S} = \int d^2x\,\mathcal{L} = \frac{1}{2}\int dt \int_{I(t)} dx\left[(\partial_t\Phi)^2 - (\partial_x\Phi)^2 - \mathfrak{m}^2\Phi^2\right]. \tag{3.11}$$

In addition I impose time-dependent boundary conditions (BC's) for the field at the end points of the interval. Their particular form depends on the physical system under consideration. Examples are

- *Dirichlet BC's* : $\Phi(t,0) = \Phi[t,l(t)] = 0$
- *Neumann BC's* : $\partial_x\Phi(t,0) = \partial_x\Phi[t,l(t)] = 0$
- *Mixed BC's* : $\Phi(t,0) = \partial_x\Phi[t,l(t)] = 0$ or $\partial_x\Phi(t,0) = \Phi[t,l(t)] = 0$.

In order to achieve a canonical formulation, I introduce a set of real time-dependent eigenfunctions $\{\phi_n(t,x)\}$ of the Laplace operator $-\partial_x^2$ which (i) obey the eigenvalue relation

$$-\partial_x^2\phi_n(t,x) = \omega_n^2(t)\phi_n(t,x) \tag{3.12}$$

on $I(t)$ with time-dependent eigenvalues $\omega_n^2(t)$, and (ii) are subject to the boundary conditions of the field Φ for all times t. The spectrum $\{\omega_n^2(t)\}$ is discrete due to the finite volume of $I(t)$. In addition, orthonormality

$$\int_0^{l(t)} dx\,\phi_n(t,x)\phi_m(t,x) = \delta_{nm} \tag{3.13}$$

and completeness

$$\sum_n \phi_n(t,x)\phi_n(t,x') = \delta(x-x')\ , \tag{3.14}$$

at any t is postulated. The existence of such a set of instantaneous eigenfunctions does of course depend on the particular type of BC's one is confronted with. It is ensured if the BC's are such that equation (3.12) forms a regular Sturm-Liouville problem (see, e.g., [174]). All examples given above belong to this class. However, as I shall show in a short while, not all of these BC's are actually compatible with a wave equation on a time-dependent interval.

Given such a complete set of eigenfunctions compatible with the BC's, the real scalar field can be expanded in these eigenfunctions by introducing mode functions $q_n(t)$:

$$\Phi(t,x) = \sum_n q_n(t)\phi_n(t,x). \tag{3.15}$$

Inserting this expansion into the action (3.11) and making use of (3.13) and (3.14) one obtains the Lagrangian for the mode functions $q_n(t)$

$$L(q_n, \dot{q}_n, t) = \frac{1}{2}\sum_n \left[\dot{q}_n^2 - \Omega_n^2(t) q_n^2\right] + \sum_{n\,m}\left[q_n M_{nm}(t)\dot{q}_m + \frac{1}{2} q_n N_{nm}(t) q_m\right] \tag{3.16}$$

where

$$\Omega_n^2(t) = \omega_n^2(t) + \mathfrak{m}^2 \tag{3.17}$$

is the time-dependent frequency of a massive field mode and M_{nm} and N_{nm} are the coupling matrices already introduced in Eq. (3.5):

$$M_{nm}(t) = \int_{I(t)} dx\, \dot{\phi}_n(t,x)\phi_m(t,x)\,, \tag{3.18}$$

$$N_{nm}(t) = \int_{I(t)} dx\, \dot{\phi}_n(t,x)\dot{\phi}_m(t,x) = \sum_k M_{nk}(t) M_{mk}(t). \tag{3.19}$$

The relation between M_{nm} and N_{nm} follows from the orthonormality and completeness relations (3.13) and (3.14), respectively. Employing the Euler-Lagrange equations

$$\frac{d}{dt}\frac{dL}{d\dot{q}_n} - \frac{dL}{dq_n} = 0 \tag{3.20}$$

leads to the equations of motion for the mode functions $q_n(t)$

$$\ddot{q}_n + \Omega_n^2(t) q_n + \sum_m \left[M_{mn}(t) - M_{nm}(t)\right]\dot{q}_m + \sum_m \left[\dot{M}_{mn}(t) - N_{nm}(t)\right] q_m = 0. \tag{3.21}$$

As already seen in the introductionary example given in 3.1, the time evolution of the field modes inside a dynamical cavity is described by infinitely many coupled second-order differential equations. The structure of the inter-mode coupling mediated by the coupling matrix $M_{nm}(t)$ depends on the particular kind of boundary conditions which decide on the specific form of the instantaneous eigenfunctions $\phi_n(t,x)$. Note that Eq. (3.21) contains the combination $M_{mn} - M_{nm}$ instead of $2M_{nm}$ in Eq. (3.4), because I have not restricted myself to a particular boundary condition for the field. Considering Dirichlet boundary conditions as done in Section 3.1, M_{nm} is anti-symmetric [see Eq. (3.5)] and therefore $M_{mn} - M_{nm} = -2M_{nm}$.

The canonical conjugated momentum p_n of a field mode is given by

$$p_n = \frac{\partial L}{\partial \dot{q}_n} = \dot{q}_n + \sum_m q_m M_{mn}(t), \tag{3.22}$$

i.e. it is coupled to all other "positions" q_n through the coupling matrix M_{nm}. The Hamiltonian obtained via a Legendre-transformation

$$H(t) = \sum_n \dot{q}_n(t) p_n(t) - L(t) \tag{3.23}$$

takes the form

$$H[q_n, p_n, t] = H_{\rm osc}[q_n, p_n, t] + H_{\rm int}[q_n, p_n, t] \tag{3.24}$$

where

$$H_{\rm osc}[q_n, p_n, t] = \frac{1}{2}\sum_n \left[p_n^2 + \Omega_n^2(t) q_n^2\right] \tag{3.25}$$

corresponds to a collection of vacuum field modes with time-dependent frequency (squeezing effect) and the interaction part

$$H_{\rm int}[q_n, p_n, t] = -\sum_{nm} M_{nm}(t) q_n p_m \tag{3.26}$$

describes their coupling due to the boundary motion (acceleration effect).
The Hamilton equations equivalent to the Lagrange equations (3.21) are given by

$$\dot{q}_n = \frac{\partial H}{\partial p_n} = p_n - \sum_m M_{mn} q_m, \tag{3.27}$$

$$\dot{p}_n = -\frac{\partial H}{\partial q_n} = -\left[\Omega_n^2 q_n - \sum_m M_{nm} p_m\right]. \tag{3.28}$$

So far, the discussion has been based on the expansion of the action into instantaneous eigenfunctions subject to given boundary conditions. This allows me to write down the Hamiltonian (3.24) associated with the dynamics of the field modes on the interval $I(t)$ described by Eq. (3.21). Taking this as a starting point, a well defined quantum theory including a meaningful particle definition can be constructed as I shall show later. However, Equation (3.21) does not describe the dynamics of field modes corresponding to a field Φ satisfying a free wave equation on $I(t)$ for all boundary conditions for which the set of eigenfunctions $\{\phi_n(t,x)\}$ can be introduced. The possible boundary conditions compatible with a free wave equation in a time-dependent domain are rather constraint.

3.3.2 Variation of the action, wave equation and compatible boundary conditions

In order to see what kind of boundary conditions are compatible with a free wave equation, I shall investigate the variation of the action (3.11) with respect to Φ. Note that similar considerations arise very generally in the theory of radiation boundary conditions for wave equations [25, 45].
Varying the action (3.11) with respect to Φ leads to

$$\delta\mathcal{S} = -\int_T dt \int_{I(t)} dx \left(\Box_{(2)}\Phi + \mathfrak{m}^2\Phi\right)\delta\Phi - \int_T dt \left\{\left[\left(v\partial_t + \partial_x\right)\Phi\right]\delta\Phi|_{l(t)} - \left(\partial_x\Phi\right)\delta\Phi|_0\right\} \tag{3.29}$$

where I have assumed that $\delta\Phi$ vanishes at the boundaries of the time interval T and $v = \dot{l}(t)$ denotes the velocity of the boundary motion. In order for Φ to satisfy the wave equation $\left[\Box_{(2)} + \mathfrak{m}^2\right]\Phi = 0$ on the interval, the choice of boundary conditions and their possible combinations is very restricted. It is given by the requirement that the integrand of the second integral vanishes

$$\left[\Box_{(2)} + \mathfrak{m}^2\right]\Phi = 0 \quad \Leftrightarrow \quad \left[\left(v\partial_t + \partial_x\right)\Phi\right]\delta\Phi|_{l(t)} - \left(\partial_x\Phi\right)\delta\Phi|_0 = 0. \tag{3.30}$$

One can either require that the field is of constant value at one or both boundaries, i.e. Dirichlet BC's such that $\delta\Phi$ vanishes at the boundary, or the field has to be subject to a Neumann BC at the mirror at rest and to satisfy $(v\partial_t + \partial_x)\Phi = 0$ at the moving boundary. In the literature this boundary condition linking time and spatial derivative of the field at the boundary is sometimes called *generalized Neumann* BC. Physically it means that the scalar field satisfies a Neumann BC in the instantaneous rest frame of the moving mirror. In Chapter 5 I shall explicitely derive this BC from the requirement that BC's for the electromagnetic field have to be imposed in the instantaneous rest frame. Thereby, the operator $v\partial_t + \partial_x$ is (up to a γ-factor) related to a Lorentz transformation from the rest frame to the laboratory frame.

Not all the possible combinations of BC's which I have considered in 3.3.1 are therefore consistent with the variational principle. For example a Dirichlet BC at $x = l(t)$ and a Neumann BC at $x = 0$ is consistent with (3.30) but the opposite choice is not. The generalized Neumann BC does not at all fall into the class of BC's for which (in the (t,x)-coordinates) a set of instantaneous eigenfunctions $\{\phi_n(t,x)\}$ can be introduced.

Inserting the expansion (3.15) which, on the level of the action, has lead to Eq. (3.21), into the wave equation $\left[\Box_{(2)} + \mathfrak{m}^2\right]\Phi = 0$, multiplying it with an eigenfunction $\phi_n(t)$ and integrating over $I(t)$ yields

$$\ddot{q}_n + \Omega_n^2(t)q_n(t) + 2\sum_m M_{mn}(t)\dot{q}_m + \sum_m \dot{M}_{mn}(t)q_m + \sum_{mk} M_{mk}(t)M_{kn}(t)q_m = 0. \tag{3.31}$$

This equation following from the expansion of the wave equation does in general not agree with Eq. (3.21) resulting from the expansion of the action. It turns out that both equations differ by a boundary term

$$\sum_k \left(M_{nk} + M_{kn}\right)\left[\dot{q}_k + \sum_m M_{mk}q_m\right] \tag{3.32}$$

which, since

$$M_{nk} + M_{kn} = -v\,\phi_n[t, l(t)]\phi_k[t, l(t)] \ , \quad v = \dot{l}(t) \ , \tag{3.33}$$

vanishes only if the BC's at the moving mirror are of Dirichlet type leading to an anti-symmetric coupling matrix. This is certainly not surprising since (in the (t, x)-coordinates) eigenfunctions $\phi_n(t, x)$ can be introduced for Dirichlet BC's at the moving mirror, but not for the generalized Neumann BC's. As expected, both Equations (3.21) and (3.31) are identical whenever the action is expanded in eigenfunctions which are consistent with BC's determined by (3.30). This implies in particular, that if the action is expanded under the assumption of BC's which do not comply with (3.30), the resulting system of differential equations (3.21) does not describe the dynamics of a free scalar field on $I(t)$ even though the Hamiltonian etc. is well defined. I shall come back to this issue below.

3.3.3 Energy vs Hamiltonian

It is important to emphasize that the dynamical Casimir effect does not belong to the class of problems where the Hamiltonian $H[q_n, p_n, t]$ corresponds to the energy of the system [195].
The total energy of the Φ-field is given by the integral over the 00-component of the "canonical" energy momentum tensor for a massive scalar field in Minkowski space [80] [1]

$$T_{00} = \frac{1}{2}\left[\dot{\Phi}^2 + (\partial_x\Phi)^2 + \mathfrak{m}^2\Phi^2\right] \ . \tag{3.34}$$

Introducing the conjugated field [80]

$$\Pi(t, x) = \frac{\partial\mathcal{L}}{\partial\dot{\Phi}} = \dot{\Phi} \ , \tag{3.35}$$

T_{00} is identical to the Hamilton density $\mathcal{H}$ obtained via Legendre transformation

$$\mathcal{H} = \dot{\Phi}\Pi - \mathcal{L} = \frac{1}{2}\left[\Pi^2 + (\partial_x\Phi)^2 + m^2\Phi^2\right] . \tag{3.36}$$

Given a set of suitable eigenfunctions $\{\phi_n(t, x)\}$, the field Π can be expanded as

$$\Pi(t, x) = \sum_n p_n(t)\phi_n(t, x) \tag{3.37}$$

with p_n defined in Eq. (3.22). Then, the total energy of the Φ-field reads

$$E[q_n, p_n, t] = \int_{I(t)} dx T_{00} = \int_{I(t)} dx\mathcal{H} = \frac{1}{2}\sum_n \left[p_n^2 + \Omega_n^2(t)q_n^2\right] = H_{\rm osc}[q_n, p_n, t] \neq H[q_n, p_n, t]. \tag{3.38}$$

$E[q_n, p_n, t]$ does not agree with the full Hamiltonian $H[q_n, p_n, t]$ for the canonical variables defined via the Legendre transformation (3.23). Hence, $H[q_n, p_n, t]$ determines the dynamics of the canonical variables q_n and p_n but is not identical to the energy of the field to which the coupling part $H_{\rm int}$ does not contribute. This difference is a result of the time-dependent transformation $\Phi(t, x) \to q_n(t)$ through introducing eigenfunctions which satisfy the time-dependent boundary condition [195].

It is also useful to consider the time-dependence of the energy of the field. Taking the time derivative of (3.38) one finds

$$\frac{dE}{dt} = \int_0^{l(t)} dx(\partial_t\Phi)\left[\Box_{(2)} + \mathfrak{m}^2\right]\Phi + (\partial_x\Phi)(\partial_t\Phi)\big|_0^{l(t)} + v\,T_{00}[t, l(t)] \ , \quad v = \dot{l}(t). \tag{3.39}$$

Hence, when Φ satisfies the wave equation, the change of the energy is given by

$$\frac{dE}{dt} = T_{01}[t, l(t)] + v\,T_{00}[t, l(t)] \tag{3.40}$$

where I have assumed that the field satisfies Dirichlet or Neumann BC's at $x = 0$ as required by Eq. (3.30).

[1] A more general consideration on the definition of energy is given in 3.6.3.

3.4 Quantization, vacuum and particle definition

3.4.1 Canonical quantization

In the following I shall quantize the real scalar field on a time-dependent interval based on the expansion of the action (3.11) in canonical variables (3.15). The starting point for the following considerations is therefore the Hamiltonian (3.24).
Canonical quantization is promoted by replacing the classical field variables $\Phi(t,x)$ and $\Pi(t,x)$ with the corresponding operators $\hat{\Phi}(t,x)$, $\hat{\Pi}(t,x)$, and imposing the equal-time commutation relations [80]

$$\left[\hat{\Phi}(t,x),\hat{\Phi}(t,x')\right] = \left[\hat{\Pi}(t,x),\hat{\Pi}(t,x')\right] = 0\ , \quad \left[\hat{\Phi}(t,x),\hat{\Pi}(t,x')\right] = i\delta(x-x'). \tag{3.41}$$

The canonical variables q_n, p_n are replaced by operators $\hat{q}_n$ and $\hat{p}_n$. They are subject to the equal-time commutation relations

$$[\hat{q}_n(t),\hat{q}_m(t)] = [\hat{p}_n(t),\hat{p}_m(t)] = 0\ , \quad [\hat{q}_n(t),\hat{p}_m(t)] = i\delta_{nm}\ , \tag{3.42}$$

in accordance with (3.41).

The Hamilton operator follows from the replacement $H[q_n,p_n,t] \to \hat{H}[\hat{q}_n,\hat{p}_n,t]$. But now, when going from the classical Hamiltonian to the Hamilton operator, one has to keep in mind that $\hat{q}_n$ and $\hat{p}_n$ do not commute. To make $\hat{H}[\hat{q}_n,\hat{p}_n,t]$ hermitian, one has to symmetrize the coupling term $q_n p_m$ in (3.26) when quantizing the Hamiltonian:

$$\begin{aligned}\hat{H}[\hat{q}_n,\hat{p}_n,t] &= \hat{H}_{\rm osc}[\hat{q}_n,\hat{p}_n,t] + \hat{H}_{\rm in}[\hat{q}_n,\hat{p}_n,t] &(3.43)\\ &= \frac{1}{2}\sum_n \left[\hat{p}_n^2 + \Omega_n^2(t)\hat{q}_n^2\right] - \frac{1}{2}\sum_{nm} M_{nm}(t)\left[\hat{q}_n\hat{p}_m + \hat{p}_m\hat{q}_n\right]. &(3.44)\end{aligned}$$

The time evolution of a quantum mechanical system can be described in different pictures. In this thesis I shall work exclusively in the Heisenberg picture which is very convenient for studying particle production, in particular numerically. In the Heisenberg picture the time evolution of an operator $\hat{O}$ is governed by the equation

$$\dot{\hat{O}} = i\left[\hat{H},\hat{O}\right] + \left(\frac{\partial\hat{O}}{\partial t}\right)_{\rm expl.}. \tag{3.45}$$

Here "expl" denotes the derivative with respect to an explicit time dependence. States $|\Psi(t)\rangle$ in the associated Hilbert space of the quantum system do not evolve in time; i.e. $|\Psi(t)\rangle = |\Psi(t_0)\rangle\ \forall\ t \geq t_0$ where t_0 is some initial time.
Using (3.45) it is readily shown that the time evolution of the not explicitly time-dependent operator $\hat{q}_n$ is described by the differential equation (3.21) which determines the time evolution of the corresponding classical variable q_n. This similarity of the equations of motion for the classical variables and operators is what the Heisenberg picture stands out for.

3.4.2 The particle concept

Our common notion of particles in a free field theory in Minkowski space relies on the existence of a preferred set of solutions: plane wave solutions describing the time evolution of the field modes. With their aid the Hamiltonian, which coincides with the energy of the field, can be diagonalized leading to an expression familiar from the treatment of the quantum mechanical oscillator. A canonically quantized field is identical to a superposition of infinitely many Hamilton operators describing *independent* harmonic oscillators. Each of those harmonic oscillators corresponds to a field mode to which a certain amount of quantized energy is associated. The field modes can then be interpreted as particles when the occupation numbers of the harmonic oscillators are identified with the number of field quanta. In that sense our notion of particles is that those are "objects", which exhibit the following properties: They are (i) countable, (ii) independent and (iii) carry a certain energy [197]. These conditions are automatically satisfied when it is possible to diagonalize a Hamiltonian which *coincides* with the energy of the field.
The definition of energy and the selection of a preferred set of solutions associated with the time evolution

of the field modes is therefore crucial if one wishes to work with a particle concept in field theory. But this is not without ambiguity, and in general problematic in quantum field theory under the influence of external conditions, in particular in curved spacetimes [79, 80, 15, 197, 218].
The scenarios considered in this work allow to introduce an unambiguous particle concept based on Hamiltonian diagonalization for well defined initial and final states. For an extensive and mathematically founded discussion of particle definition in field theory under the influence of external conditions, I would like to refer the interested reader to [197]. I shall also come back to this issue below in more detail when discussing the important difference between the dynamical Casimir effect and the so-called Unruh effect.

3.4.3 Vacuum and particle definition

In order to introduce a canonical particle concept for systems described by the Hamiltonian (3.44), I require that the dynamical problems under consideration are such that it is possible to introduce two times $t_{\rm in}$ and $t_{\rm out}$, such that the boundary $l(t)$ is at rest for $t < t_{\rm in}$ and $t > t_{\rm out}$. This includes asymptotic times, e.g., $t_{\rm in} \to -\infty$ and $t_{\rm out} \to +\infty$, as well as finite times at which the motion of the boundary is (smoothly) turned on and off, respectively [2].
The initial (in) and final (out) configuration of the system is characterized by the conditions

$$\begin{array}{ll} \text{initial system configuration :} & \Omega_n^{\rm in} = \Omega_n(t < t_{\rm in}) = \text{const} \neq 0, \qquad M_{nm}(t < t_{\rm in}) = 0 \\ \text{final system configuration :} & \Omega_n^{\rm out} = \Omega_n(t > t_{\rm out}) = \text{const} \neq 0, \quad M_{nm}(t > t_{\rm out}) = 0 \end{array}$$

for all n, m. I do not require that $\Omega_n^{\rm in} = \Omega_n^{\rm out}$; i.e. the final configuration of the system does not have to be equal to the initial one. Under these assumptions, the Hamiltonian does coincide with the energy for times $t < t_{\rm in}$ and $t > t_{\rm out}$ and corresponds to a superposition of independent harmonic oscillators. It can therefore be diagonalized in the usual way by introducing time-independent annihilation and creation operators associated with the initial and final system configuration, through [3]

$$\hat{q}_n(t) = \begin{cases} \dfrac{\hat{a}_n^{\rm in}}{\sqrt{2\Omega_n^{\rm in}}} e^{-i\Omega_n^{\rm in} t} + \text{h.c.} & \text{for } t < t_{\rm in} \\ \dfrac{\hat{a}_n^{\rm out}}{\sqrt{2\Omega_n^{\rm out}}} e^{-i\Omega_n^{\rm out} t} + \text{h.c.} & \text{for } t > t_{\rm out} \end{cases} \tag{3.46}$$

and

$$\hat{p}_n(t) = \begin{cases} i\sqrt{\dfrac{\Omega_n^{\rm in}}{2}} \hat{a}_n^{\rm in\dagger}\, e^{i\Omega_n^{\rm in} t} + \text{h.c.} & \text{for } t < t_{\rm in} \\ i\sqrt{\dfrac{\Omega_n^{\rm out}}{2}} \hat{a}_n^{\rm out\dagger}\, e^{i\Omega_n^{\rm out} t} + \text{h.c.} & \text{for } t > t_{\rm out} \end{cases} \tag{3.47}$$

where h.c. stands for hermitian conjugated. Both sets of operators $\{\hat{a}_n^{\rm in}, \hat{a}_n^{\rm in\dagger}\}$ and $\{\hat{a}_n^{\rm out}, \hat{a}_n^{\rm out\dagger}\}$ satisfy the usual commutation relations for annihilation ($\hat{a}_n$) and creation ($\hat{a}_n^\dagger$) operators:

$$[\hat{a}_n, \hat{a}_m] = \left[\hat{a}_n^\dagger, \hat{a}_m^\dagger\right] = 0 \ , \ \left[\hat{a}_n, \hat{a}_m^\dagger\right] = \delta_{nm}. \tag{3.48}$$

Initial $|0, \text{in}\rangle \equiv |0, t < t_{\rm in}\rangle$ and final $|0, \text{out}\rangle \equiv |0, t > t_{\rm out}\rangle$ vacuum states can now be introduced as the states which are annihilated by $\hat{a}_n^{\rm in}$ and $\hat{a}_n^{\rm out}$, respectively:

$$\hat{a}_n^{\rm in} |0, \text{in}\rangle = 0 \ \text{ and } \ \hat{a}_n^{\rm out} |0, \text{out}\rangle = 0 \ \ \forall\, n. \tag{3.49}$$

[2] If the motion is turned on in a non-smooth way but rather with a non-zero velocity (instantaneously), spurious effects might contribute to the particle creation process. This will be discussed later on more detailed.

[3] The quantization procedure assumes that in the initial and final frequency spectra $\Omega_n^{\rm in} \neq 0$ and $\Omega_n^{\rm out} \neq 0 \ \forall\, n$. For Neumann boundary conditions $\partial_x \Phi = 0$ at both walls $x = 0$ and $x = l(t)$, a zero-mode $\phi_0(t)$ of equation (3.12) with $\omega_0(t) = 0 \ \forall\, t$ appears. The normalized eigenfunctions are

$$\left\{\phi_0(t) = 1/\sqrt{l(t)}, \phi_n(t, x) = \sqrt{2/l(t)} \cos(n\pi x/l(t)\right\} \ .$$

If the field is massless, i.e. $\Omega_0^{\rm in} = \Omega_0^{\rm out} = 0$, the quantization of the zero-mode goes then along the lines of the quantization of the bosonic string [48]. But if the field is massive, $\Omega_0^{\rm in} = \Omega_0^{\rm out} \neq 0$, the above quantization scheme can be used. Actually, for a massless field Φ in two dimensions, a complete set of solutions satisfying the generalized Neumann boundary condition $(\partial_x + v\partial_t)\Phi = 0$ at $l(t)$ is given by solutions of Moore's equation (3.8) of the form (up to normalization) [48]

$$\phi_0(t, z) = R(t + z) + R(t - z) \ , \quad \phi_n(t, z) = \exp\{-in\pi R(t + z)\} + \exp\{-in\pi R(t - z)\} \ .$$

The associated Hilbert spaces $\mathcal{H}_{\rm in}$, $\mathcal{H}_{\rm out}$ of the quantum system are introduced as the Fock-spaces build up through successive application of the creation operators onto the vacuum states. The basis of $\mathcal{H}_{\rm in}$ and $\mathcal{H}_{\rm out}$ is then given by the vectors

$$\left\{|0,{\rm in}\rangle, \hat{a}_n^{\rm in\dagger}|0,{\rm in}\rangle, \hat{a}_n^{\rm in\dagger}\hat{a}_m^{\rm in\dagger}|0,{\rm in}\rangle, ...\right\} \quad \text{and} \quad \left\{|0,{\rm out}\rangle, \hat{a}_n^{\rm out\dagger}|0,{\rm out}\rangle, \hat{a}_n^{\rm out\dagger}\hat{a}_m^{\rm out\dagger}|0,{\rm out}\rangle, ...\right\}, \tag{3.50}$$

respectively. Thereby the vacuum states are normalized according to

$$\langle 0,{\rm in}|0,{\rm in}\rangle_{\mathcal{H}_{\rm in}} = \langle 0,{\rm out}|0,{\rm out}\rangle_{\mathcal{H}_{\rm out}} = 1. \tag{3.51}$$

Here $\langle|\rangle_{\mathcal{H}_{\rm in}}$ ($\langle|\rangle_{\mathcal{H}_{\rm out}}$) denotes the scalar product in $\mathcal{H}_{\rm in}$ ($\mathcal{H}_{\rm out}$).
Particles defined with respect to the initial and final vacuum states, i.e. quanta of energies $\Omega_n^{\rm in}$ and $\Omega_n^{\rm out}$, respectively, are counted through the particle number operators

$$\hat{N}_n^{\rm in} = \hat{a}_n^{\rm in\dagger}\hat{a}_n^{\rm in} \quad \text{and} \quad \hat{N}_n^{\rm out} = \hat{a}_n^{\rm out\dagger}\hat{a}_n^{\rm out}. \tag{3.52}$$

In the above Fock basis, initial and final Hamilton operators are diagonal

$$\hat{H}^{\rm in} = \sum_n \Omega_n^{\rm in}\left[\hat{N}_n^{\rm in} + 1/2\right] \quad \text{and} \quad \hat{H}^{\rm out} = \sum_n \Omega_n^{\rm out}\left[\hat{N}_n^{\rm out} + 1/2\right], \tag{3.53}$$

and correspond to the energy of the field quanta. The ground states, i.e. the vacua, have zero-point energy

$$E_0^{\rm in} = \langle 0,{\rm in}|\hat{H}^{\rm in}|0,{\rm in}\rangle_{\mathcal{H}_{\rm in}} = \frac{1}{2}\sum_n \Omega_n^{\rm in} \quad \text{and} \quad E_0^{\rm out} = \langle 0,{\rm out}|\hat{H}^{\rm out}|0,{\rm out}\rangle_{\mathcal{H}_{\rm out}} = \frac{1}{2}\sum_n \Omega_n^{\rm out}, \tag{3.54}$$

respectively. As demonstrated in Section 2.2, these formally divergent quantities lead after renormalization to finite Casimir energies, which cause the attraction of macroscopic bodies (parallel plates).

Introduced by means of diagonalization of a Hamiltonian which corresponds to the energy of the field, this definition of particles before and after the motion is without ambiguity and physically meaningful.

During the dynamics of the system for times $t \in [t_{\rm in}, t_{\rm out}]$ the field modes evolve in time such that, in general, $\hat{a}_n^{\rm out} \neq \hat{a}_n^{\rm in}$. The final state operator $\hat{a}_n^{\rm out}$ will rather be a combination of initial annihilation and creation operators. In other words, the vacuum states of the initial and final Hamiltonians (3.53) do not coincide. This discrepancy can even persist if the system has returned to its initial position, i.e. if $\Omega_n^{\rm in} = \Omega_n^{\rm out}\ \forall\ n$.
Initial and final state operators are linked through a Bogoliubov transformation [15]

$$\hat{a}_n^{\rm out} = \sum_m \left[\mathcal{A}_{mn}(t_{\rm out})\,\hat{a}_m^{\rm in} + \mathcal{B}_{mn}^*(t_{\rm out})\,\hat{a}_m^{\rm in\dagger}\right]. \tag{3.55}$$

This mixture of annihilation and creation operators is interpreted as the conversion of virtual quantum vacuum fluctuations into real particles, i.e. particle production from vacuum. It implies that, if $\mathcal{B}_{nm}(t_{\rm out}) \neq 0$, the vacuum $|0,{\rm in}\rangle$ contains particles defined with respect to the final vacuum state $|0,{\rm out}\rangle$ and vice versa. Notice that, due to the intermode couplings, the Bogoliubov transformation (3.55) is not diagonal. The number of quanta of energy $\Omega_n^{\rm out}$ which for times $t > t_{\rm out}$ are present in the initial vacuum is given by

$$\mathcal{N}_n^{\rm out} = \langle 0,{\rm in}|\hat{N}_n^{\rm out}|0,{\rm in}\rangle = \sum_m |\mathcal{B}_{mn}(t_{\rm out})|^2. \tag{3.56}$$

It may happen that the initial vacuum state contains an infinite number of final state particles. In that case, the two Fock spaces cannot be related by a unitary transformation [220].
By virtue of the commutation relations (3.48) the Bogoliubov coefficients $\mathcal{A}_{mn}(t_{\rm out})$ and $\mathcal{B}_{mn}(t_{\rm out})$ satisfy the relations

$$\sum_m \left[\mathcal{A}_{mn}(t_{\rm out})\mathcal{A}_{mk}^*(t_{\rm out}) - \mathcal{B}_{mn}^*(t_{\rm out})\mathcal{B}_{mk}(t_{\rm out})\right] = \delta_{nk}, \tag{3.57}$$

$$\sum_m \left[\mathcal{A}_{mn}(t_{\rm out})\mathcal{B}_{mk}^*(t_{\rm out}) - \mathcal{B}_{mn}^*(t_{\rm out})\mathcal{A}_{mk}(t_{\rm out})\right] = 0. \tag{3.58}$$

In the next paragraph the Bogoliubov coefficients $\mathcal{A}_{mn}(t_{\rm out})$, $\mathcal{B}_{mn}(t_{\rm out})$ will be constructed explicitely as solutions of an infinite system of coupled differential equations.

From (3.56) quantities like the total particle number $\mathcal{N}^{\rm out}$ and associated energy $\mathcal{E}^{\rm out}$ given by

$$\mathcal{N}^{\rm out} = \sum_n \mathcal{N}_n^{\rm out} \quad \text{and} \quad \mathcal{E}^{\rm out} = \sum_n \Omega_n^{\rm out} \mathcal{N}_n^{\rm out}, \tag{3.59}$$

respectively, can be deduced. When applying the formalism to tensor perturbations in braneworld cosmology in the second part of the thesis it will turn out that observable quantities, like power spectrum and energy density of gravitons, can be expressed entirely through the particle number and energy.

The quantities (3.59) are, under certain circumstances, ill defined and require appropriate regularization. For example, if the boundary motion $l(t)$ is not sufficiently smooth, the discontinuities in its velocity cause the excitation of modes of arbitrary high frequencies. Hence the summations in (3.59) do not converge. This can be avoided most easily by introducing a frequency cutoff which effectively smoothes the dynamics $l(t)$. Introducing an explicit frequency cutoff is in many cases physically well motivated since, for instance, it accounts for imperfect (non-ideal) boundary conditions for high frequency modes [195]. As a matter of fact one has to make use of such a frequency cutoff in the numerical simulations in any case. These issues will be discussed below in more detail.

3.5 Time evolution

3.5.1 Bogoliubov transformations

Allowing for mode mixing during the motion of the boundary, the operators $\hat{q}_n$ and $\hat{p}_n$ may be expanded in initial state operators $\hat{a}_n^{\rm in}$, $\hat{a}_n^{\rm in\dagger}$ and complex functions $\epsilon_n^{(m)}(t)$:

$$\hat{q}_n(t > t_{\rm in}) = \sum_m \frac{\hat{a}_m^{\rm in}}{\sqrt{2\Omega_m^{\rm in}}}\, \epsilon_n^{(m)}(t) + \text{h.c.}, \tag{3.60}$$

$$\hat{p}_n(t > t_{\rm in}) = \sum_m \frac{\hat{a}_m^{\rm in}}{\sqrt{2\Omega_m^{\rm in}}}\, f_n^{(m)}(t) + \text{h.c.} \tag{3.61}$$

with

$$f_n^{(m)}(t) = \dot{\epsilon}_n^{(m)}(t) + \sum_k M_{kn}(t)\epsilon_k^{(m)}(t). \tag{3.62}$$

The complex functions $\epsilon_n^{(m)}(t)$ satisfy

$$\ddot{\epsilon}_n^{(m)} + \Omega_n^2(t)\epsilon_n^{(m)} + \sum_k \left[M_{kn}(t) - M_{nk}(t)\right]\dot{\epsilon}_k^{(m)} + \sum_k \left[\dot{M}_{kn}(t) - N_{nk}(t)\right]\epsilon_k^{(m)} = 0, \tag{3.63}$$

i.e. the same system of differential equations as the canonical variables q_n [cf. Eq. (3.21)].
The system of second order differential equations is equivalent to the system of first order differential equations for $\epsilon_n^{(m)}$ and $f_n^{(m)}$

$$\dot{\epsilon}_n^{(m)}(t) = f_n^{(m)}(t) - \sum_k M_{kn}(t)\epsilon_k^{(m)}(t), \tag{3.64}$$

$$\dot{f}_n^{(m)}(t) = -\Omega_n^2(t)\epsilon_n^{(m)}(t) + \sum_k M_{nk}(t) f_k^{(m)}(t)\ , \tag{3.65}$$

corresponding to the Hamilton equations (3.27) and (3.28).

Through the formal expansion (3.60) I have reduced the problem of finding the time evolution for the operator $\hat{q}_n(t)$ to the problem of solving the system of coupled second-order differential equations (3.63). This requires initial conditions for $\epsilon_n^{(m)}(t)$. Demanding that Eqs. (3.60) and (3.61) have to match with the corresponding expressions (3.46) and (3.47) for $t = t_{\rm in}$ leads to the initial conditions:

$$\epsilon_n^{(m)}(t_{\rm in}) = \delta_{nm}\Theta_\alpha^{\rm in}\,, \quad \dot{\epsilon}_n^{(m)}(t_{\rm in}) = \left[-i\Omega_n^{\rm in}\,\delta_{nm} - M_{mn}(t_{\rm in})\right]\Theta_m^{\rm in} \quad \text{with} \quad \Theta_n^{\rm in} = e^{-i\Omega_n^{\rm in}\,t_{\rm in}}\ . \tag{3.66}$$

I have decided to keep the, in principle arbitrary, phase $\Theta_n^{\rm in}$, since it is especially useful for the numerical work later on [cf. Section 10.2]. With $M_{mn}(t_{\rm in})$ vanishing only if $\dot{l}(t_{\rm in}) = 0$, the initial condition $\dot{\epsilon}_n^{(m)}(t_{\rm in})$ is not simply $-i\Omega_n^{\rm in}\,\delta_{nm}$ when dealing with boundary motions $l(t)$ which have an initial discontinuity in the velocity. This subtle point is sometimes disregarded in the literature, but it is needed for consistency.

The Bogoliubov coefficients $\mathcal{A}_{mn}(t_{\rm out})$ and $\mathcal{B}_{mn}(t_{\rm out})$ introduced in Eq. (3.55) are obtained by matching (3.60) and (3.61) at the end of the dynamics $t = t_{\rm out}$ with the corresponding expressions (3.46) and (3.47). One finds

$$\mathcal{A}_{mn}(t_{\rm out}) = \frac{\Theta_n^{\rm out^*}}{2}\sqrt{\frac{\Omega_n^{\rm out}}{\Omega_m^{\rm in}}}\left\{\epsilon_n^{(m)}(t_{\rm out}) + \frac{i}{\Omega_n^{\rm out}}\left[\dot{\epsilon}_n^{(m)}(t_{\rm out}) + \sum_k M_{kn}(t_{\rm out})\epsilon_k^{(m)}(t_{\rm out})\right]\right\} \tag{3.67}$$

$$\mathcal{B}_{mn}(t_{\rm out}) = \frac{\Theta_n^{\rm out}}{2}\sqrt{\frac{\Omega_n^{\rm out}}{\Omega_m^{\rm in}}}\left\{\epsilon_n^{(m)}(t_{\rm out}) - \frac{i}{\Omega_n^{\rm out}}\left[\dot{\epsilon}_n^{(m)}(t_{\rm out}) + \sum_k M_{kn}(t_{\rm out})\epsilon_k^{(m)}(t_{\rm out})\right]\right\} \tag{3.68}$$

with phase $\Theta_n^{\rm out}$ defined as in (3.66). Starting in the initial vacuum state $|0, {\rm in}\rangle$, the Bogoliubov transformation (3.55) has to become trivial for $t_{\rm out} = t_{\rm in}$, i.e. $\hat{a}_n^{\rm out} = \hat{a}_n^{\rm in}$. This implies the vacuum initial conditions

$$\mathcal{A}_{mn}(t_{\rm in}) = \delta_{mn} \quad \text{and} \quad \mathcal{B}_{mn}(t_{\rm in}) = 0 \tag{3.69}$$

which are consistent with the initial conditions (3.66). The emergence of $M_{mn}(t_{\rm in})$ in the initial conditions (3.66) therefore guarantees to meet the vacuum initial conditions even for the unphysical situation that the motion of the boundary starts instantaneously with a non-zero velocity. To take this into account consistently is of particular importance for the numerical simulations. For the same reason $M_{nm}(t_{\rm out})$ is kept explicitely though I have required that $M_{nm}(t > t_{\rm out}) = 0$.

3.5.2 First-order system

From the solutions of the system of differential equations (3.63) or from the system of first-order differential equations (3.64) and (3.65) the Bogoliubov coefficient $\mathcal{B}_{mn}(t_{\rm out})$ and hence the number of created final state particles (3.56) can now be calculated. It is however useful to introduce another set of complex (auxiliary) functions $\xi_n^{(m)}$ and $\eta_n^{(m)}$:

$$\xi_n^{(m)}(t) = \epsilon_n^{(m)}(t) + \frac{i}{\Omega_n^{\rm in}}\left[\dot{\epsilon}_n^{(m)}(t) + \sum_k M_{kn}(t)\,\epsilon_k^{(m)}(t)\right] = \epsilon_n^{(m)}(t) + \frac{i}{\Omega_n^{\rm in}} f_n^{(m)}(t), \tag{3.70}$$

$$\eta_n^{(m)}(t) = \epsilon_n^{(m)}(t) - \frac{i}{\Omega_n^{\rm in}}\left[\dot{\epsilon}_n^{(m)}(t) + \sum_k M_{kn}(t)\,\epsilon_k^{(m)}(t)\right] = \epsilon_n^{(m)}(t) - \frac{i}{\Omega_n^{\rm in}} f_n^{(m)}(t). \tag{3.71}$$

With their aid, the Bogoliubov coefficients (3.67) and (3.68) can be cast into the form

$$\mathcal{A}_{mn}(t_{\rm out}) = \frac{\Theta_n^{\rm out^*}}{2}\sqrt{\frac{\Omega_n^{\rm out}}{\Omega_m^{\rm in}}}\left[\Delta_n^+(t_{\rm out})\,\xi_n^{(m)}(t_{\rm out}) + \Delta_n^-(t_{\rm out})\,\eta_n^{(m)}(t_{\rm out})\right], \tag{3.72}$$

$$\mathcal{B}_{mn}(t_{\rm out}) = \frac{\Theta_n^{\rm out}}{2}\sqrt{\frac{\Omega_n^{\rm out}}{\Omega_m^{\rm in}}}\left[\Delta_n^-(t_{\rm out})\,\xi_n^{(m)}(t_{\rm out}) + \Delta_n^+(t_{\rm out})\,\eta_n^{(m)}(t_{\rm out})\right]. \tag{3.73}$$

$\Delta_n^{\pm}(t_{\rm out})$, defined by

$$\Delta_n^{\pm}(t) = \frac{1}{2}\left[1 \pm \frac{\Omega_n^{\rm in}}{\Omega_n(t)}\right] \quad , \tag{3.74}$$

is a measure for the deviation of the final system configuration (e.g., cavity size), characterized by $l(t_{\rm out})$, with respect to its initial configuration $l(t_{\rm in})$.

In the important case that at time $t_{\rm out}$ the system has returned to its initial position, for example in an asymptotic scenario where the motion of the boundary ceases for $|t| \to \infty$, it is

$$\mathcal{N}_n^{\rm out} = \frac{1}{4}\sum_m \frac{\Omega_n^{\rm in}}{\Omega_m^{\rm in}}|\eta_n^{(m)}(t_{\rm out})|^2. \tag{3.75}$$

The advantage of introducing the functions $\xi_n^{(m)}$ and $\eta_n^{(m)}$ is due to the fact that they satisfy the following "symmetric" system of first-order differential equations:

$$\dot{\xi}_n^{(m)}(t) = -i\left[a_{nn}^{+}(t)\xi_n^{(m)}(t) - a_{nn}^{-}(t)\eta_n^{(m)}(t)\right] - \sum_k \left[c_{nk}^{-}(t)\xi_k^{(m)}(t) + c_{nk}^{+}(t)\eta_k^{(m)}(t)\right], \tag{3.76}$$

$$\dot{\eta}_n^{(m)}(t) = -i\left[a_{nn}^{-}(t)\xi_n^{(m)} - (t)a_{nn}^{+}(t)\eta_n^{(m)}(t)\right] - \sum_k \left[c_{nk}^{+}(t)\xi_k^{(m)}(t) + c_{nk}^{-}(t)\eta_k^{(m)}(t)\right] \tag{3.77}$$

with the vacuum squeezing contribution

$$a_{nn}^{\pm}(t) = \frac{\Omega_n^{\rm in}}{2}\left\{1 \pm \left[\frac{\Omega_n(t)}{\Omega_n^{\rm in}}\right]^2\right\} \tag{3.78}$$

and the time-dependent mode coupling term (acceleration effect)

$$c_{nk}^{\pm}(t) = \frac{1}{2}\left[M_{kn}(t) \pm \frac{\Omega_k^{\rm in}}{\Omega_n^{\rm in}}M_{nk}(t)\right]. \tag{3.79}$$

By "symmetric" I mean the behavior of the system under the exchange of the superscripts $+ \leftrightarrow -$. Into this system of coupled differential equations, besides the time-dependent frequency $\Omega_n(t)$, only the coupling matrix $M_{kn}(t)$ enters but neither its square $N_{nk}(t)$ nor its time derivative $\dot{M}_{kn}(t)$.

The vacuum initial conditions (3.69) entail the initial conditions for the functions $\xi_n^{(m)}$ and $\eta_n^{(m)}$ to be

$$\xi_n^{(m)}(t_{\rm in}) = 2\delta_{mn}\ , \quad \eta_n^{(m)}(t_{\rm in}) = 0. \tag{3.80}$$

Let me emphasize that all derivations and equations shown so far, do not rely on particular symmetry properties of the coupling matrix.

By means of Eq. (3.73), the number of particles created during the dynamics of the system may now be calculated from the solutions $\xi_n^{(m)}$ and $\eta_n^{(m)}$ of the system of coupled first-order differential equations formed by Eqs. (3.76) and (3.77) [4] . Being of the form $\dot{\mathbf{x}} = \mathbf{W}\mathbf{x}$, the numerical implementation of the system of differential equations is straight forward. A cutoff parameter $n_{\rm max}$ is introduced to make the system of differential equations finite and suitable for a numerical treatment. The system is then evolved numerically from $t_{\rm in}$ up to final time $t_{\rm out}$ where the final particle spectrum $\mathcal{N}_n^{\rm out}$ is calculated. The stability of the numerical solutions with respect to the cut-off $n_{\rm max}$, i.e. the independence of $\mathcal{N}_n^{\rm out}$ on the value of $n_{\rm max}$, has to be ensured. $n_{\rm max}$ will be chosen such that the numerical result for $\mathcal{N}_n^{\rm out}$ is stable for a given range of quantum numbers. In addition, the quality of the numerical results can be assessed by testing the relations (3.57), (3.58). Details on the numerical simulations can be found in Appendix B.

In the course of the thesis I shall encounter the situation where the velocity of the mirror has discontinuities. As it is clear from Eq. (3.9), any discontinuity in the velocity will lead to an infinite particle number since the acceleration of the mirror diverges there. Arbitrary high frequency modes are excited and it is expected that the convergence of the numerics is very slow. Explicit examples are discussed in the next Chapter. Note, however, that the initial conditions are such that the particle number is zero at $t_{\rm in}$ by construction, even with

[4] The occurrence of the mode coupling due to the moving boundary represents the main difficulty of the dynamical Casimir effect compared to, e.g., cosmological particle creation [15] or reheating [127, 202, 128]. In those scenarios, the time evolution of the mode functions is just described by an oscillator equation

$$\ddot{\epsilon}_n(t) + \Omega_n^2(t)\epsilon_n(t) = 0$$

where the time-dependent frequency $\Omega_n(t)$ reflects the dynamics of the external (classical) field which couples to the quantum fluctuations. The number of produced final state quanta is then simply given by

$$\mathcal{N}_n^{\rm out} = \frac{1}{4}\frac{\Omega_n^{\rm out}}{\Omega_n^{\rm in}}\left[|\epsilon_n(t_{\rm out})|^2 + \frac{|\dot{\epsilon}_n(t_{\rm out})|^2}{(\Omega_n^{\rm out})^2}\right] - \frac{1}{2}\ ,$$

which can be immediately obtained from the above equations by setting $M_{nm} \equiv 0$.

an initial discontinuity in the velocity [cf. Eq. (3.66)].
Any well behaved, i.e. physical, motion does of course not have discontinuities in its velocity. But as a matter of fact, discontinuities are sometimes unavoidable in the numerical simulations. If, for example, a mirror following a smooth trajectory is only asymptotically at rest, i.e. $M_{nm} \to 0$ for $|t| \to \infty$, the physical velocity does not exhibit any discontinuity. The numerical simulation on the other hand has to be started and stopped at finite times leading to discontinuities in the velocity. Of course, the motion could be turned on and off smoothly with an artificial function avoiding discontinuities. However, unless not done adiabatically slow which is a disadvantage for the numerics because of the additional very long integration times, any such artificial function will also contribute to the particle production because of its non-vanishing acceleration [cf. Eq. (3.9)]. Consequently, the influence of discontinuities (or of an artificial "smoothing" - function) on the numerical results has to be examined case by case. If for special situations analytical results can be derived with which the numerical results can be compared, provides certainly the best way to detect how numerical results are contaminated by discontinuities.
In the simulations the expectation value (3.56) is also calculated for several times steps in between of $[t_{\rm in}, t_{\rm out}]$. By doing so, $t_{\rm out}$ is interpreted as a continuous variable such that Eq. (3.56) becomes a continuous function of time; i.e. $\mathcal{N}_n^{\rm out} \to \mathcal{N}_n(t)$. Such a procedure corresponds to the use of an instantaneous particle concept.

3.5.3 Instantaneous vacuum

When interpreting $t_{\rm out}$ as continuous time variable, I can write the Bogoliubov transformation Eq. (3.55) as

$$\hat{a}_n(t) = \sum_m \left[\mathcal{A}_{mn}(t)\hat{a}_m^{\rm in} + \mathcal{B}^*_{mn}(t)\hat{a}_m^{\rm in\,\dagger}\right] \quad , \tag{3.81}$$

where at any time t I have introduced a set of operators $\{\hat{a}_n(t), \hat{a}_n^\dagger(t)\}$. Vacuum states defined at any time t can be associated with these operators via

$$\hat{a}_n(t)|0,t\rangle = 0 \ \ \forall\, n. \tag{3.82}$$

Similar to Eq. (3.56) a "particle number" can be introduced through

$$\mathcal{N}_n(t) = \langle 0,{\rm in}|\hat{a}_n^\dagger(t)\hat{a}_n(t)|0,{\rm in}\rangle = \sum_m |\mathcal{B}_{mn}(t)|^2 \quad . \tag{3.83}$$

I shall denote $|0,t\rangle$ as the *instantaneous vacuum* state and the quantity $\mathcal{N}_n(t)$ as *instantaneous particle* number. It could be interpreted as the number of particles which would have been created if the motion of the boundary stops at time t. (Recall that my notation $|0,t\rangle$ does not imply that the state of the system is time dependent!) However, even if I call it "particle number" and shall plot it for illustrative reasons, I consider only the particle definitions for the initial and final states (asymptotic regions) as physically meaningful particles. When interpreting $t_{\rm out}$ as a continuous variable t, one can of course derive a corresponding system of coupled differential equations for $\mathcal{A}_{mn}(t)$ and $\mathcal{B}_{mn}(t)$ simply by differentiating Eq. (3.67) and (3.68) with respect to t and using the equations of motion for $\epsilon_n^{(m)}$.

More formally, this can be achieved as follows: Introduce non-hermitian and explicitely time-dependent operators $\hat{a}_n(t)$ and $\hat{a}_n^\dagger(t)$ via

$$\hat{q}_n(t) = \frac{1}{\sqrt{2\Omega_n(t)}}\left[\hat{a}_n(t) + \hat{a}_n^\dagger(t)\right] \ , \ \ \hat{p}_n(t) = i\sqrt{\frac{\Omega_n(t)}{2}}\left[\hat{a}_n^\dagger(t) - \hat{a}_n(t)\right]. \tag{3.84}$$

With their aid, the oscillator part of the Hamiltonian (3.44) which corresponds to the energy of the field can be diagonalized for all times

$$\hat{H}_{\rm osc.}(t) = \sum_k \Omega_k(t)\left[\hat{a}_k^\dagger(t)\hat{a}_k(t) + \frac{1}{2}\right]. \tag{3.85}$$

The coupling Hamiltonian $\hat{H}_{\rm int}$ on the other hand reads

$$\hat{H}_{\rm int}(t) = -\frac{i}{2}\sum_{km}\sqrt{\frac{\Omega_m(t)}{\Omega_k(t)}}M_{km}(t)\left[\hat{a}_m^\dagger(t)\hat{a}_k(t) - \hat{a}_k^\dagger(t)\hat{a}_m(t) - \hat{a}_k(t)\hat{a}_m(t) + \hat{a}_k^\dagger(t)\hat{a}_m^\dagger(t)\right]. \tag{3.86}$$

Introducing the instantaneous vacuum state (3.82), then $\langle 0,t|\hat{H}_{\rm int}(t)|0,t\rangle = 0$. Thus the expectation value of $\hat{H}(t)$ in the state $|0,t\rangle$ is just what one would identify as *instantaneous* vacuum energy $(1/2)\sum_n \Omega_n(t)$. As for the classical field, the interaction part does not contribute to the energy.
From the Heisenberg equation (3.45) one obtains the equation of motion for $\hat{a}_n(t)$

$$\dot{\hat{a}}_n(t) = -i\Omega_n(t)\hat{a}_n(t) + \frac{1}{2}\frac{\dot{\Omega}_n(t)}{\Omega_n(t)}\hat{a}_n^\dagger(t) - \frac{1}{2}\sum_m \left[A^-_{mn}(t)\hat{a}_m(t) + A^+_{mn}(t)\hat{a}_m^\dagger(t)\right] \tag{3.87}$$

where I have defined

$$A^\pm_{mn}(t) = \sqrt{\frac{\Omega_n(t)}{\Omega_m(t)}}M_{mn}(t) \pm \sqrt{\frac{\Omega_m(t)}{\Omega_n(t)}}M_{nm}(t). \tag{3.88}$$

The term $\propto \dot{\Omega}_n(t)/\Omega_n(t)$ comes from the explicit time derivative in the Heisenberg equation. Inserting the Bogoliubov transformation (3.81) into Equation (3.87) leads to the differential equations for $\mathcal{A}_{mn}(t)$ and $\mathcal{B}_{mn}(t)$ which one obtains by formally replacing $t_{\rm out} \to t$ and differentiating Eq. (3.67) and (3.68) with respect to t.

3.6 A more formal point of view

In this section I shall discuss the dynamical Casimir effect from a more formal point of view to stress the difference to other quantum vacuum radiation effects like the Unruh effect. I first review the formulation of field quantization in Minkowski spacetime in the way it is usually presented in textbooks and courses on quantum field theory in curved spacetime, e.g., [15, 103, 76, 220] (see also [197]). Then, I introduce the concept of Killing vectors, discuss quantum fields in static spacetimes, describe the Unruh effect and eventually reformulate the dynamical Casimir effect in this more formal language.

3.6.1 QFT in Minkowski spacetime

For a real free scalar field in $D = 1 + d$ – dimensional Minkowski spacetime a natural set of solutions to the Klein-Gordon equation

$$\left[\Box_{(D)} + \mathfrak{m}^2\right]\Phi = 0 \tag{3.89}$$

is given by

$$u_{\mathbf{k}}(t,\mathbf{x}) = \frac{1}{\sqrt{2\Omega_{\mathbf{k}}(2\pi)^d}}e^{i\mathbf{k}\mathbf{x}-i\Omega_k t} \;\text{ with }\; \Omega_{\mathbf{k}} = \sqrt{\mathbf{k}^2+\mathfrak{m}^2}. \tag{3.90}$$

These solutions are eigenfunctions of ∂_t, i.e.

$$\partial_t u_{\mathbf{k}} = -i\Omega_{\mathbf{k}} u_{\mathbf{k}} \tag{3.91}$$

and define so-called *positive frequency solutions*. The corresponding complex conjugated solutions $u^*_{\mathbf{k}}$ are called *negative frequency solutions*. With respect to the inner product of two arbitrary solutions u_1, u_2 of the Klein Gordon equation

$$(u_1,u_2) = -i\int dx^d \left[u_1\,\partial_t u_2^* - (\partial_t\, u_1)\; u_2^*\right]\;, \tag{3.92}$$

the positive and negative frequency solutions satisfy [5]

$$(u_{\mathbf{k}},u_{\mathbf{k}'}) = \delta_{\mathbf{k}\mathbf{k}'}\;,\;\; (u^*_{\mathbf{k}},u^*_{\mathbf{k}'}) = -\delta_{\mathbf{k}\mathbf{k}'}\;,\;\; (u_{\mathbf{k}},u^*_{\mathbf{k}'}) = 0. \tag{3.93}$$

Thereby the integration is performed over a spacelike hyperplane at constant t. Quantization is achieved by promoting the field Φ to a field operator $\hat{\Phi}$ and expanding it in positive and negative frequency solutions and operator valued coefficients, the annihilation and creation operators $\hat{a}_{\mathbf{k}}$, $\hat{a}^\dagger_{\mathbf{k}}$:

$$\hat{\Phi} = \sum_{\mathbf{k}} \hat{a}_{\mathbf{k}}\, u_{\mathbf{k}} + \text{h.c.}\;. \tag{3.94}$$

[5] Here $\delta_{\mathbf{k}\mathbf{k}'}$ is understood as a d-dimensional delta function if the entire Minkowski spacetime is considered, or as a Kronecker-delta corresponding to quantized wave numbers when the field is, for example, restricted to a torus. Furthermore I shall use the symbol $\sum_{\mathbf{k}}$ for both, the summation in the discrete case and for integration if $\mathbf{k}$ is continuous.

The corresponding vacuum state $|0\rangle$ is defined as

$$\hat{a}_{\mathbf{k}}|0\rangle = 0 \ \forall \ \mathbf{k} \ , \tag{3.95}$$

and the Fock space is constructed like in 3.4. Hamilton and momentum operators associated with the classical conserved energy and momentum of the field are given by the corresponding densities of the energy momentum tensor integrated over the spatial dimensions

$$\hat{H} = \int \hat{T}_{00}\, d^d x = \frac{1}{2}\sum_{\mathbf{k}} \Omega_{\mathbf{k}} \left(\hat{a}^\dagger_{\mathbf{k}} \hat{a}_{\mathbf{k}} + \frac{1}{2} \right) \tag{3.96}$$

$$\hat{P}_i = \int \hat{T}_{0i}\, d^d x = \sum_{\mathbf{k}} k_i\, \hat{a}^\dagger_{\mathbf{k}} \hat{a}_{\mathbf{k}}. \tag{3.97}$$

This quantization procedure relies on the existence of the set of modes $u_{\mathbf{k}}, u^*_{\mathbf{k}}$ which are closely related to the symmetry properties of Minkowski spacetime. The special property of Minkowski spacetime is that the vacuum state as defined in (3.95) is the vacuum state for all inertial observers, i.e. all inertial observers agree on the same vacuum state. It is invariant under the action of the Poincaré or inhomogeneous Lorentz group (application of which leave the Minkowski line element invariant) and so are the inertial observers in Minkowski spacetime [15].

3.6.2 Killing vectors

Equation (3.91) shows that the mode-functions (3.90) are eigenfunctions of ∂_t. This has been used to define the notion of *positive frequency* solutions and the vacuum state. Strictly speaking, ∂_t is the time-like Killing vector $\xi = \xi^\nu \partial_\nu = \partial_t$ of Minkowski spacetime.
Killing vectors are deeply connected with symmetry properties of a spacetime metric $g_{\mu\nu}$ and are defined by $\mathcal{L}_\xi g_{\mu\nu} = \xi_{\mu\|\nu} + \xi_{\nu\|\mu} = 0$ where $\mathcal{L}_\xi$ is the Lie-derivative and "$\|$" denotes the covariant derivative [206]. The above condition is equivalent to $g_{\mu\nu|\rho}\xi^\rho + g_{\rho\nu}\xi^\rho_{|\mu} + g_{\mu\rho}\xi^\rho_{|\nu} = 0$ where "$|$" denotes the partial derivative. If $\xi^\mu(x^\nu)$ is a solution to the above equations at every point x^ν of the spacetime, then the metric $g_{\mu\nu}$ does not change under a flux along the direction of ξ^μ [206, 217]. Killing vectors therefore express the symmetries of a spacetime. Ten Killing vectors exist in four-dimensional Minkowski space, given by $\xi_\mu = c_\mu + \epsilon_{\mu\nu}x^\nu$ with $\epsilon_{\mu\nu} = -\epsilon_{\nu\mu}$. The four constants c_μ describe four translations and $\epsilon_{\mu\nu}$ three spatial rotations and three boosts [206].
Such transformations in the direction of a Killing vector, which map the space onto itself without altering the metric, form a group (Lie-group). Thereby, the linearly independent Killing vectors form a basis for generating the group [206].
In particular, the Killing vector ∂_t mediates the Minkowski time translation symmetry. It corresponds to usual observes at rest and generates the time evolution with respect to them.
Since the definition of vacuum states is associated with modes that are of positive frequency, it inherently depends on the existence of time-like Killing vectors [212]. If, for example, a spacetime has different time-like Killing vectors, each of which generating the time evolution with respect to different observers, the particle interpretation will be observer dependent. A spacetime might not have any Killing vectors in which case one probably has to give up the particle concept all together [220].

3.6.3 QFT in curved spacetimes

In a general curved spacetime the Poincaré group is no longer a symmetry group and no Killing vectors exist with which positive frequency modes can be defined. A particular exception where a meaningful particle definition can be accomplished is the case of static spacetimes. In a static spacetime $\mathcal{M}$ of dimension $D = d+1$, using appropriate coordinates with $t \equiv x^0$ timelike, all metric components $g_{\mu\nu}$ are independent of t and $g_{0j} = 0$ for $j = 1, ..., d$ [80]. This is equivalent to the existence of a time-like Killing vector field $\xi = \xi^\mu \partial_\mu$ and of a family of space-like hypersurfaces orthogonal to the time-like Killing vector everywhere [80]. The space-like hypersurfaces are Cauchy surfaces, i.e. space-like hypersurfaces which are intersected by every inextensible causal curve (a curve whose tangent vector is everywhere time- or light-like) exactly once. I shall denote those surfaces by Σ. One can scale ξ such that the Killing time t is the proper time measured by at least one co-moving clock [220] and $\xi = \partial_t$. Positive frequency can then be defined via modes which are eigenfunctions of this time-like Killing vector. In this situation a preferred foliation of spacetime and hence a meaningful

notion of positive frequency modes does exist, making it possible to introduce a unique concept of particles. The spacetime $\mathcal{M}$ can be factorized as $\mathcal{M} = \mathbb{R} \times \Sigma$ with metric

$$ds^2 = g_{00}dt^2 - g^{\Sigma}_{ij}dx^i dx^j \tag{3.98}$$

where g^{Σ}_{ij} is the metric of the Cauchy surface Σ. The metric is called *ultrastatic* if $g_{00} = 1$ [80].

I restrict my considerations in the following to a real non-interacting massive minimally coupled scalar field Φ. Its action is given by

$$\mathcal{S} = \int_{\mathcal{M}} dx^D \mathcal{L} = \int_{\mathcal{M}} dx^D \frac{\sqrt{g}}{2} \left[(\partial_\mu \Phi)(\partial^\mu \Phi) - \mathfrak{m}^2 \Phi^2\right] \tag{3.99}$$

with $g = (-1)^d \det(g_{\mu\nu})$. Variation of the action with respect to the field leads to the Klein-Gordon equation

$$\left[\Box_{(D)} + \mathfrak{m}^2\right] \Phi = 0 \;\text{ with }\; \Box_{(D)} = \frac{1}{\sqrt{g}} \partial_\mu \left(\sqrt{g} g^{\mu\nu} \partial_\nu\right). \tag{3.100}$$

I have made the assumption that the spatial surface terms appearing when varying the action vanish. As I have shown in Section 3.3.2, this implies particular boundary conditions in case that the field is confined inside a time-dependent domain.
The foliation of the spacetime implies that the Klein-Gordon operator can be written as

$$\Box_{(D)} = g^{00}\partial_t^2 + \frac{1}{\sqrt{g}} \partial_i \left(\sqrt{g} g^{ij} \partial_j\right). \tag{3.101}$$

Introducing an operator $\mathcal{K} = g_{00}\left[\frac{1}{\sqrt{g}}\partial_i\left(\sqrt{g}g^{ij}\partial_j\right) + \mathfrak{m}^2\right]$ the Klein-Gordon equation can be cast into the form $-\partial_t^2\Phi = \mathcal{K}\Phi$. The operator $\mathcal{K}$ is formally self adjoint with respect to the inner product in $\mathcal{L}^2_\rho$ with $\rho = g^{00}\sqrt{g}$ [80]. In the case that the metric is ultrastatic it is $\mathcal{K} = -\triangle_\Sigma + \mathfrak{m}^2$ where $\triangle_\Sigma$ the Laplacian on the Cauchy hypersurface; i.e. $\triangle_\Sigma = \frac{1}{\sqrt{g^\Sigma}}\partial_i\left(\sqrt{g^\Sigma} g^{\Sigma\, ij}\partial_j\right)$.

Quantization can be performed by expanding the field in eigenfunction of $\triangle_\Sigma$ (or $\mathcal{K}$) similar to the Minkowski case. Since positive frequency solutions can be defined with respect to the time-like Killing vector ∂_t, a physically meaningful vacuum state can be introduced. The generalization of the inner product (3.92) of two solutions of the Klein-Gordon equation reads [15]

$$(u_1, u_2) = -i \int_\Sigma \left[u_1\, \partial_\mu u_2^* - (\partial_\mu\, u_1)\; u_2^*\right] \sqrt{g^\Sigma} d\Sigma^\mu, \tag{3.102}$$

with $d\Sigma^\mu = n^\mu d\Sigma$. Thereby n^μ is the future directed unit normal vector to Σ and $d\Sigma = dx^d$ is the volume element on Σ. Using Gauss' theorem it follows that this product is independent of Σ [15].
Since for the static metric $n^\mu = \left(1/\sqrt{g_{00}}, \mathbf{0}\right)$ one has $\sqrt{g^\Sigma} n^0 = \sqrt{g^\Sigma g^{00}} = \rho$, i.e. it is exactly the integration measure for which the operator $\mathcal{K}$ is self-adjoint.

The energy momentum tensor obtained from the variation of the action with respect to the metric reads

$$T_{\mu\nu} = \frac{2}{\sqrt{g}} \frac{\delta \mathcal{S}}{\delta g^{\mu\nu}} = \partial_\mu\Phi\partial_\nu\Phi - \frac{1}{2} g_{\mu\nu}\partial_\rho\Phi\partial^\rho\Phi + \frac{1}{2}\mathfrak{m}^2 g_{\mu\nu}\Phi^2. \tag{3.103}$$

In a general spacetime no conserved quantity can be constructed from the local conservation law $T^\mu{}_{\nu||\mu} = 0$:

$$T^\mu{}_{\nu\|\mu} = \frac{1}{\sqrt{g}}\partial_\mu\left(\sqrt{g} T^\mu_\nu\right) - \frac{1}{2} T^{\rho\kappa}\partial_\nu g_{\rho\kappa} = 0. \tag{3.104}$$

The second term leads to an exchange of energy and momentum between the gravitational and scalar field. If, however, the spacetime possesses Killing vectors, i.e. in particular if $\partial_0 g_{\mu\nu} = 0$, a conservation law can be associated with every Killing vector field [206, 218, 197]. In particular, a conserved energy can be introduced if spacetime admits a time-like Killing vector ξ (like in the static case) [206, 197]:

$$E = \int_\Sigma d\Sigma_\mu T^{\mu\nu}\xi_\nu. \tag{3.105}$$

The formalism presented for the dynamical Casimir effect on a time-dependent interval can immediately be extended to the case of a static curved spacetime. This will allow me to study the dynamical Casimir effect for gravitons in braneworld cosmology with the same formalism which is the subject of the second part of this thesis.

3.6.4 Bogoliubov transformations

In the spirit of general covariance of general relativity there is, in general, no preferred coordinate system (no preferred foliation of spacetime). In this case, there exist not only one but rather many (even infinitely many) valid sets of basis functions, i.e. solutions of the Klein-Gordon equation (3.100), belonging to particular coordinate systems. Each expansion of the field associated with such a set corresponds to a different particle definition which makes the particle concept ambiguous. On the other hand, spacetime might possess different time-like Killing vectors which then can be used by different observers to define positive frequency solutions. What is the consequence of this?

Let the decomposition of the field with respect to two of such sets be

$$\Phi(x) = \sum_n \left[\hat{a}_n u_n(x) + \text{h.c.}\right] = \sum_m \left[\hat{\tilde{a}}_m \tilde{u}_m(x) + \text{h.c.}\right]. \tag{3.106}$$

Each decomposition defines an own vacuum state via

$$\hat{a}_n|0\rangle = 0\ , \quad \hat{\tilde{a}}_m|\tilde{0}\rangle = 0 \ \ \forall\ n,\ m\ , \tag{3.107}$$

and therefore an own Fock space $\mathcal{H}$ and $\tilde{\mathcal{H}}$, respectively. The completeness (separately) of these sets of functions allows to expand functions of one set into functions of the other set

$$\tilde{u}_m = \sum_n \left[\alpha_{mn} u_n + \beta_{mn} u_n^*\right]\ , \quad u_n = \sum_m \left[\alpha^*_{mn} \tilde{u}_m - \beta_{mn} \tilde{u}^*_m\right]. \tag{3.108}$$

It follows immediately that the operators $\hat{a}_n, \hat{a}_n^\dagger$ and $\hat{\tilde{a}}_m, \hat{\tilde{a}}_m^\dagger$ are related via a Bogoliubov transformation

$$\hat{a}_n = \sum_m \left[\alpha_{mn} \hat{\tilde{a}}_m + \beta^*_{mn} \tilde{\hat{a}}^\dagger_m\right]\ , \quad \hat{\tilde{a}}_m = \sum_n \left[\alpha^*_{mn} \hat{a}_n - \beta^*_{mn} \hat{a}^\dagger_n\right]. \tag{3.109}$$

If $\beta_{nm} \neq 0$, the Fock spaces associated with both sets of modes are not equal. While $\hat{a}_n$ annihilates $|0\rangle$, the operator $\hat{\tilde{a}}_m$ associated with the second mode decomposition does not:

$$\hat{\tilde{a}}_m|0\rangle = -\sum_n \beta^*_{mn} \hat{a}^\dagger_n|0\rangle \neq 0. \tag{3.110}$$

Consequently, calculating the expectation value of the particle number operator $\hat{\tilde{a}}^\dagger_m \hat{\tilde{a}}_m$ counting the number of particles defined with respect to the $\tilde{u}_m$-modes, leads to

$$\tilde{\mathcal{N}}_m = \langle 0|\hat{\tilde{a}}^\dagger_m \hat{\tilde{a}}_m|0\rangle_{\mathcal{H}} = \sum_n |\beta_{mn}|^2. \tag{3.111}$$

Ergo, the vacuum $|0\rangle$ of the u_n-modes contains $\tilde{\mathcal{N}}_m$ particles of the $\tilde{u}_m$-modes. Hence what one observer considers as a vacuum state might be a many particle state for a different observer. Two main origins of the presence of this *quantum vacuum radiation* have to be distinguished:

1. quantum vacuum radiation caused by the dynamics of some (time-dependent) background field and
2. the presence of particles due to observers using different particle definitions .

For the former case, imagine a situation in which asymptotically ($t \to \pm\infty$) the spacetime is Minkowskian. Thus, asymptotically, Lorentz invariant initial and final vacuum states can be introduced which all inertial observers agree on. If gravity is switched on for intermediate times (expanding Universe, for example) the field will in general depart from its initial vacuum state. Then, a field mode which was of positive frequency

for $t \to -\infty$ may evolve into a field mode which is a mixture of positive and negative frequency solutions for $t \to +\infty$. Hence, $\beta_{nm} \neq 0$, i.e. particles have been created by the gravitational field. The scenario of cosmological particle production, discussed in e.g., [15], belongs to this class.
Another example is the scenario discussed in this thesis: the motion of boundaries which can be viewed as very localized classical background fields. For example it is discussed in [15] (see also [78, 51]) that for a particular non-uniformly accelerating trajectory of a mirror an *inertial* detector will detect a thermal flux of radiation.
To the latter class of the above mentioned origins of quantum vacuum radiation belongs the Unruh effect [212], i.e. the detection of a thermal spectrum of particles by an uniformly accelerated detector. Note that both effects, the Unruh effect and the creation of particles (detected via an inertial detector) by moving mirrors are rather distinct (see [15, 212, 213, 197]).

3.6.5 Unruh effect

It is enlightening to briefly discuss the Unruh effect. I shall just sketch the basic ideas following [220] and refer the interested reader to the original literature for the quite involved calculations.
Consider a massless scalar field Φ in a two-dimensional Minkowski space $ds^2 = dt^2 - dx^2$. Positive frequency solutions $\frac{1}{\sqrt{4\pi\Omega_k}} e^{-i\Omega_k t + ikx}$ which are eigenfunctions of the time-like Killing vector $\xi = \partial_t$ mediating Minkowski time translation symmetry can be used to define a vacuum state via $\hat{a}^{\mathrm{M}}_k |0\rangle_{\mathrm{M}} = 0 \ \forall \ k$. In this section I use explicitly sub- and super-scripts to denote the vacuum states, here "M" for Minkowski. If one introduces so-called Rindler coordinates (τ, ρ) via $t = \rho \sinh(\kappa\tau)$ and $x = \rho\cosh(\kappa\tau)$, the metric takes the form $ds^2 = \kappa^2\rho^2 d\tau^2 - d\rho^2$. Thereby κ is called *surface gravity* [220] and the range of the new coordinates is $0 < \rho < \infty$, $-\infty < \tau < \infty$ covering only a quarter of Minkowski space. This so-called Rindler wedge $x > |t|$ is globally hyperbolic and may be viewed as a spacetime in its own right [220]. The Rindler metric is obviously static, hence a quantum field theory can be constructed along the lines described above. In particular $\eta = \partial_\tau$ is a time-like future directed Killing vector for the Rindler metric. In Rindler coordinates positive frequency solutions (with respect to η) are given by $\frac{1}{\sqrt{4\pi\Omega_{k'}}} \rho^{ik'/\kappa} e^{-i\Omega_{k'}\tau}$ which can be used to define the Rindler vacuum via $\hat{a}^R_{k'} |0\rangle_{\mathrm{R}} = 0 \ \forall \ k'$. For the stationary observes in the Rindler wedge, i.e. for observers following orbits of η, the states of the Fock space have a natural particle interpretation. Since the Killing vector ∂_τ can be written as $\partial_\tau = \kappa(x\partial_t + t\partial_x)$, it represents the Killing field which generates the group of Lorentz boost isometries [218, 220]. Hence those observers all undergo uniform acceleration varying from orbit to orbit. In Rindler coordinates one has $\eta^\mu\eta_\mu = (\kappa\rho)^2 = g_{00}$. Since for the orbit with $\eta^\mu\eta_\mu = 1$, i.e. $\rho = 1/\kappa$, the proper acceleration is κ, it is conventional to view the orbits of η as corresponding to a family of observers naturally associated with an observer who accelerates uniformly with acceleration κ [220, 218]. Following Wald [218], "the notion of 'particles' obtained from this quantum field construction are referred to as the 'particles seen by an observer who undergoes uniform acceleration κ' ". The relation between $|0\rangle_{\mathrm{M}}$ and $|0\rangle_{\mathrm{R}}$ is given by the corresponding Bogoliubov transformation. The calculation of the Bogoliubov coefficients is rather lengthy and technically involved so I just state the results. Detailed calculations can be found in, e.g., [15, 197, 212, 208, 220]. Calculating the expectation value of the number operator for Rindler particles in the Minkowski vacuum one finds ${}_{\mathrm{M}}\langle 0|\hat{a}^{\mathrm{R}\dagger}_{k'}\hat{a}^{\mathrm{R}}_{k'}|0\rangle_{\mathrm{M}} \propto 1/(e^{2\pi\Omega_{k'}/\kappa} - 1)$ where I have dropped a volume factor. Thus one is led to the surprising conclusion that an accelerated observer experiences the Minkowski vacuum as a thermal bath of particles of temperature $T = \kappa/(2\pi)$. This result was first discovered by Unruh [212].

3.6.6 Dynamical Casimir effect

I now come back to the situation of a scalar field Φ confined on a time-dependent interval $I(t)$. In the following I shall discuss the dynamical Casimir effect along the lines of the formal considerations on quantization and particle definition discussed above. As already discussed in section 3.4, a meaningful particle definition can be accomplished for times $t < t_{\mathrm{in}}$ and $t > t_{\mathrm{out}}$ where the couplings M_{nm} vanish. By virtue of the expansion of the field (3.15) and the definition of initial and final states [cf. Eqs. (3.46) and (3.47)] the field can asymptotically be written as

$$\hat{\Phi}^{\mathrm{in}}(t,x) = \hat{\Phi}(t < t_{\mathrm{in}}, x) = \sum_n \hat{a}^{\mathrm{in}}_n u^{\mathrm{in}}_n(t,x) + \mathrm{h.c.}\,, \quad u^{\mathrm{in}}_n(t,x) = \frac{e^{-i\Omega^{\mathrm{in}}_n t}}{\sqrt{2\Omega^{\mathrm{in}}_n}} \phi^{\mathrm{in}}_n(x)\,, \tag{3.112}$$

$$\hat{\Phi}^{\mathrm{out}}(t,x) = \hat{\Phi}(t > t_{\mathrm{out}}, x) = \sum_n \hat{a}^{\mathrm{out}}_n u^{\mathrm{out}}_n(t,x) + \mathrm{h.c.}\,, \; u^{\mathrm{out}}_n(t,x) = \frac{e^{-i\Omega^{\mathrm{out}}_n t}}{\sqrt{2\Omega^{\mathrm{out}}_n}} \phi^{\mathrm{out}}_n(x). \tag{3.113}$$

Thereby $\phi_n^{\rm in}(x) \equiv \phi_n(t < t_{\rm in}, x)$ and $\phi_n^{\rm out}(x) \equiv \phi_n(t > t_{\rm out}, x)$ do not depend on time. The complex functions $u_n^{\rm in}$ and $u_n^{\rm out}$ are solutions of the Klein-Gordon equation and correspond to the positive frequency solutions defining the initial $|0, {\rm in}\rangle$ and final $|0, {\rm out}\rangle$ vacuum state, respectively [cf. Eq. (3.49)].
During the motion of the boundary the field can be expanded as [cf. Eqs. (3.15) and (3.60)]

$$\hat{\Phi}(t,x) = \sum_n \hat{a}_n^{\rm in} u_n(t,x) + {\rm h.c.}\ , \quad u_n(t,x) = \frac{1}{\sqrt{2\Omega_n^{\rm in}}} \sum_m \epsilon_m^{(n)} \phi_m(t,x). \tag{3.114}$$

The functions $u_n(t,x)$ are not only solutions to the Klein Gordon equation while the mirror is in motion, but also satisfy the boundary conditions at all times. Furthermore, the $u_n(t,x)$'s are positive frequency solutions $u_n^{\rm in}$ for $t < t_{\rm in}$ associated with the initial vacuum state. Being solutions of the Klein-Gordon equation the complex solutions $u_n^{\rm in}$, $u_n^{\rm in*}$, $u_n^{\rm out}$, $u_n^{\rm out*}$ and u_n, u_n^* obey the relations (3.93) with respect to the inner product (3.92) with $d = 1$ and the integration is performed over the time-dependent interval only.

The completeness of the sets $\{u_n^{\rm in}, u_n^{\rm in*}\}$ $\{u_n^{\rm out}, u_n^{\rm out*}\}$ and $\{u_n, u_n^*\}$ (separately) allows to expand every function of each set with respect to the other set (for appropriate times). In particular at $t = t_{\rm out}$, one may expand $u_n(t_{\rm out}, x)$ as a linear combination of $u_n^{\rm out}(t_{\rm out}, x)$ and $u_n^{\rm out*}(t_{\rm out}, x)$ or vice versa:

$$u_n(t_{\rm out}, x) = \sum_m \left[\mathcal{A}_{nm}(t_{\rm out}) u_m^{\rm out}(t_{\rm out}, x) + \mathcal{B}_{nm}(t_{\rm out}) u_m^{\rm out*}(t_{\rm out}, x)\right], \tag{3.115}$$

$$u_m^{\rm out}(t_{\rm out}, x) = \sum_n \left[\mathcal{A}_{nm}^*(t_{\rm out}) u_n(t_{\rm out}, x) - \mathcal{B}_{nm}(t_{\rm out}) u_n^*(t_{\rm out}, x)\right]\ , \tag{3.116}$$

which corresponds to the expansions (3.108) and hence represents a Bogoliubov transformation. The coefficients $\mathcal{A}_{nm}$ and $\mathcal{B}_{nm}$ are the same Bogoliubov coefficients already introduced in Eq. (3.55) which follows from (3.112) and (3.113) jointly with (3.115) and (3.116). The $\mathcal{B}_{nm}(t_{\rm out})$ coefficient leading to the particle number can be obtained by using the inner product (3.92) and the relations (3.93) [6]

$$\mathcal{B}_{nm}(t_{\rm out}) = (u_m^{\rm out}(t_{\rm out}, x), u_n^*(t_{\rm out}, x)). \tag{3.117}$$

Evaluating this expression yields (3.68).

The solutions of the Klein-Gordon equation u_n which are at $t = t_{\rm in}$ positive frequency solutions $u_n^{\rm in}$ with respect to the initial observer are, in general, for $t = t_{\rm out}$ a mixture of positive *and* negative frequency solutions $u_n^{\rm out}$, $u_n^{\rm out*}$ with respect to the out-observer, i.e. $\mathcal{B}_{nm}(t_{\rm out}) \neq 0$. Unlike in the Unruh effect, the two observers (here inertial in- and out-observers) use the same Killing vector mediating the time translation symmetry of Minkowski spacetime to define positive frequency solutions

$$\partial_t u_n^{\rm in/out} = -i\Omega_n^{\rm in/out} u_n^{\rm in/out}\ , \tag{3.118}$$

and the associated Lorentz invariant vacuum states $|0, {\rm in}\rangle$ and $|0, {\rm out}\rangle$, respectively. Nevertheless, after the dynamical period, both vacuum states will, in general, be different, even if the moving wall has returned to its initial position; i.e., if $\Omega_n^{\rm in} = \Omega_n^{\rm out}\ \forall n$. Consequently, the out-observer detects the presence of out-particles $\mathcal{N}_n^{\rm out}$ in the vacuum $|0, {\rm in}\rangle$ of the initial observer. Thereby, the complete amount of particles has been created entirely during the dynamics of the boundary (the mirror) and does not arise due to the comparison of different observers, or the use of an ambiguous particle definition, cf. Fig. 3.1.

[6] Note that this formulation is equivalent to the so-called *Wronskian formulation* of particle production employed in [4] for the dynamical Casimir effect, and in [121, 122] for graviton production in braneworld cosmology.

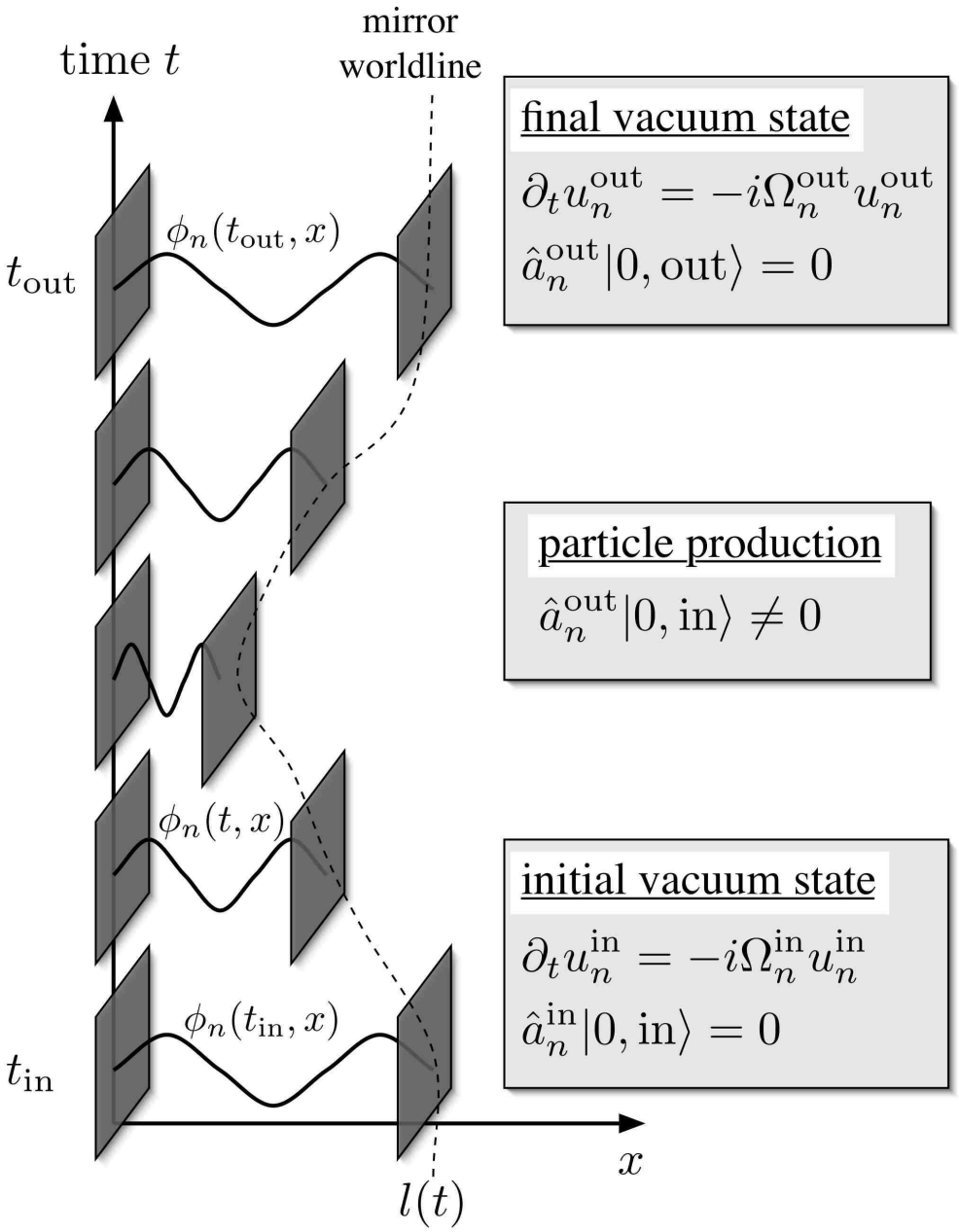

Figure 3.1: Pictorial demonstration of the dynamical Casimir effect and the used particle and vacuum definitions. Shown is the worldline of the moving mirror and snapshots of particular mirror positions together with the evolution of the instantaneous eigenfunction $\phi_n(t, x)$ for the particular case $n = 3$ as representative example. The motion of the mirror squeezes and stretches the mode functions leading, together with the mode coupling, to particle creation from vacuum. Initial and final particles and vacuum states are defined using the mode functions $u_n^{\rm in}$ [Eq. (3.112)] and $u_n^{\rm out}$ [Eq. (3.113)], respectively, which are of positive frequency with respect to the Killing vector ∂_t.

Chapter 4

Dynamical Casimir effect for a massless scalar field in a one-dimensional cavity

The example of the electromagnetic field in a one-dimensional cavity $[0, l(t)]$ represents the most simple scenario of the dynamical Casimir effect and has extensively been studied in the literature. Its dynamics is completely determined in terms of the corresponding vector potential $A(t, x)$ which, in this case, is a scalar function. In Coulomb gauge it obeys the two-dimensional wave equation [163]

$$\partial_t^2 A(t, x) - \partial_x^2 A(t, x) = 0. \tag{4.1}$$

The continuity requirement on the electric field at the ideal "mirrors" $x = 0$ and $x = l(t)$ implies Dirichlet boundary conditions

$$A(t, x = 0) = A[t, x = l(t)] = 0. \tag{4.2}$$

The example of the electromagnetic field in a one-dimensional dynamical cavity is therefore equivalent to the problem of a massless scalar field introduced in Section 3.1. After summarizing known results and phenomena I shall compare available analytical predictions with the results obtained by solving the system of differential equations (3.76,3.77) numerically.

4.1 Preliminary remarks on numerics

In order to solve the system of coupled differential equations formed by Eqs. (3.76) and (3.77) numerically a cutoff $n_{\max}$ is introduced at which the summations are truncated. I shall call numerical results stable when the final particle spectrum $\mathcal{N}_n^{\text{out}}$ does not change for all quantum numbers n smaller than a particular value n_s when increasing $n_{\max}$ further. The simulations are started at $t_{\text{in}} = 0$. Sometimes the particle number is plotted for various time steps, i.e. the notion of instantaneous particles is adapted here for purely illustrative reasons [cf. Section 3.5.3]. All physical quantities carrying dimensions are measured with respect to the initial cavity length l_0, the only scale in the problem. Dimensionless quantities are used throughout without introducing additional notations.

4.2 Moore's original example: A uniformly moving mirror and the role of discontinuities

The first scenario which has been studied analytically is the one of a mirror moving uniformly with velocity v [163, 78]

$$l(t) = l_0 + vt \ . \tag{4.3}$$

For this particular case Moore's equation (3.8) [cf. Section 3.2] can be solved exactly, leading to [163, 4]

$$R(z) = \frac{1}{\text{arctanh} v} \ln\left(z + \frac{l_0}{v}\right). \tag{4.4}$$

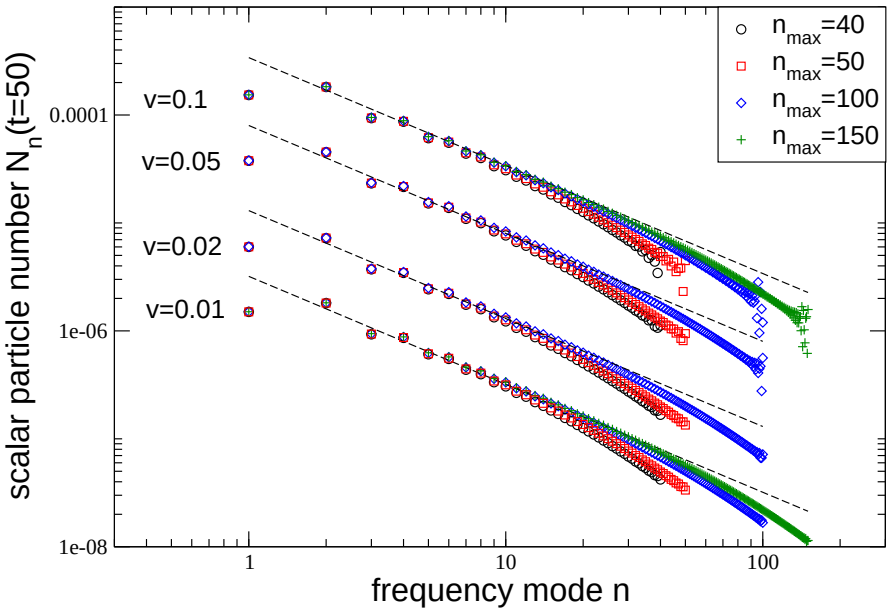

Figure 4.1: Final particle spectrum $\mathcal{N}_n^{\text{out}}$ for the motion (4.3) with initial cavity size $l_0 = 50$ and final integration time $t_{\text{out}} = 50$. Numerical results for different velocities v and cutoff parameters $n_{\max}$ are shown. The dashed lines indicate $\mathcal{N}_n^{\text{out}} = 0.035v^2/n$.

The mode functions (3.7) read

$$\phi_n(t,x) = \exp\left[-i\frac{n\pi}{\operatorname{arctanh} v}\ln\left(t+x+\frac{l_0}{v}\right)\right] - \exp\left[-i\frac{n\pi}{\operatorname{arctanh} v}\ln\left(t-x+\frac{l_0}{v}\right)\right] \tag{4.5}$$

with $n = 1, 2, ..., \infty$.

As already noted by Moore [163], the total particle number diverges logarithmically due to the discontinuities in the velocity at the beginning and end of the motion. Castagnino and Ferraro [36] calculated the Bogoliubov coefficients explicitely and found for the particle spectrum

$$\mathcal{N}_n^{\text{out}} \propto \frac{v^2}{n} \quad \text{for} \quad n > 6 \text{ and } v \ll 1 \ . \tag{4.6}$$

They also conclude that particle creation in this scenario is entirely due to the discontinuities, and no particle creation takes place during periods of uniform motion, i.e. when the acceleration of the mirror is zero. That a discontinuity in the mirror velocity does create infinitely many particles has already been discussed at the end of section 3.5.2. Since particle production from vacuum is related to the mirrors acceleration [see Eq. (3.9)], any sudden change in the velocity will give rise to a divergent radiated energy.

The numerical simulations are, in general, sensitive to discontinuities in the velocity. Since modes of arbitrary high frequency are excited by a discontinuity and the modes are coupled to each other due to the time-dependent boundary condition, one has to expect that the convergence of the numerical results is not very good for cases like the uniform motion (4.3) where discontinuities in the velocity are the only source of particle production.
In Figure 4.1 I show the final particle spectrum $\mathcal{N}_n^{\text{out}}$ obtained from numerical simulations for the motion (4.3) with an initial cavity size $l_0 = 50$. The final integration time is $t_{\text{out}} = 50$, and results for different velocities and cutoff parameters are displayed. As expected, the convergence of the numerical results with respect to $n_{\max}$ is very slow. Only for $n_{\max} \geq 100$, the spectrum $\mathcal{N}_n^{\text{out}}$ is stable for the first field modes $n \leq 10$. But it is nevertheless evident that the spectra converge towards a linear decrease $\propto 1/n$ when increasing the cutoff. The spectra towards which the numerical results converge are indeed all very well fitted by $\mathcal{N}_n^{\text{out}} = 0.035v^2/n$ (dashed lines), as predicted by Eq. (4.6). In the simulation, particles are entirely created at t_{in} and t_{out}. At these points, the initial and final plane wave solutions [cf. Eqs. (3.46),(3.47)] are matched to the intermediate

solutions (3.60),(3.60) even though the coupling, which is proportional to the velocity, does not vanish. These are the discontinuities which lead to the $1/n$ behavior of the final particle spectrum in accordance with the analytical prediction (4.6).
Particle production related to discontinuities is proportional to the square of the corresponding velocity for non-relativistic velocities $\mathcal{N}_n \propto v^2$, $v \leq 0.1$. (Recall that in the above discussed example the maximal number is $\simeq 10^{-4}$ for $v = 0.1$.) Therefore, when dealing with non-relativistic cavity motions where other effects like resonances are the primary source of particle production, contributions from the discontinuity to the particle production are expected to be small. Nevertheless, when summing over the entire spectrum the total particle number does diverge. In the simulations this is automatically avoided by the cutoff $n_{\max}$ such that the total particle number and energy is practically only given by the "truly" excited modes, i.e. modes which are excited due to primary effects (resonances). Such examples are discussed in the next section for vibrating cavities. Note that, as already mentioned before, the cutoff $n_{\max}$ has indeed a physical meaning since it accounts for the non-ideality of the boundary conditions for high frequency modes.

4.3 Particle creation in a vibrating cavity - An overview

The scenario which has attracted most of the attention in recent years are so-called vibrating cavities [132]. In these systems, the distance between two parallel mirrors changes periodically in time leading to resonance effects between the mechanical motion of the mirror and the quantum vacuum. Under certain conditions, this results in an exponential growth of the total energy inside the cavity, making it the most prominent candidate for an experimental verification of the dynamical Casimir effect.

Particle creation in a one-dimensional vibrating cavity has been studied in numerous works, e.g., [56, 57, 58, 104, 195, 59, 120, 77, 37, 219]. Thereby the oscillations of the cavity are considered to be of the particular form

$$l(t) = l_0 \left[1 + \epsilon \sin(\omega_{\rm cav}\, t)\right] \ , \tag{4.7}$$

and small amplitude oscillations $\epsilon \ll 1$ are assumed. For such a *trembling cavity*, approximations can be made and perturbative methods can be used to simplifying the system of coupled second-order differential equations (3.1). Other work is based on approximate solutions to Moore's equation [56, 140, 39, 47, 40], again valid for small amplitudes only.

In the so-called *main resonance* case where the frequency of the cavity vibrations is twice the frequency of the first quantized eigenmode inside the cavity,

$$\omega_{\rm cav} = 2\Omega_1^{\rm in}, \tag{4.8}$$

the total particle number increases quadratically in the short as well as long time limit [57]. Higher cavity frequencies have been considered in [104, 59]. Particle creation due to off-resonant wall motions, i.e. the frequency of the wall oscillations does not exactly match the resonance condition, called *detuning*, has been studied in, e.g., [59]. In an off-resonantly vibrating cavity the number of created particles may still increase eternally, or, if the detuning effect is too strong, the particle number oscillates with a period much larger than the period of the cavity vibrations. Furthermore, it was shown in [46], that the creation of motion induced radiation is enhanced in a cavity with two moving boundaries (see also [105]).

The evolution of the energy density in a one-dimensional cavity with one vibrating wall has been studied by numerous authors [140, 39, 157, 47, 186, 2, 147]. In a resonant one-dimensional cavity the energy density consists mainly of pulses (traveling wave packets) whose number depends on the mechanical frequency of the cavity vibration. The height of the pulses increases exponentially and their width decreases exponentially with time while moving inside the cavity and becoming reflected at the boundaries. This proceeds in such a way, that the total area beneath each peak grows exponentially in time. Consequently, the total energy inside a resonantly vibrating cavity grows exponentially in time as well [47], although the total number of particles increases only with a power law [57]. Thus, a pumping of energy into higher frequency modes takes place and particles of frequencies exceeding the mechanical frequency of the oscillating mirror are created. The energy for this process is provided by the energy which has to be given to the system from outside to maintain the motion of the mirror against the radiation reaction force [75, 9, 155, 169].

Turning the motion (4.7) on at $t = 0$ leads to a discontinuity in the velocity of the mirror. It has been shown in [47] that due to such an initial discontinuity a δ-function singularity develops in the energy density inside the cavity which is reflected back and forth between the mirrors. This $\delta-$function singularity is related to the artificial excitation of modes of arbitrary high frequency as discussed before. Since it represents an unphysical process which does not appear in a realistic setup it is usually disregarded in the calculations.

An important result which reveals the coupling structure between the field modes for an arbitrary cavity frequency $\omega_{\rm cav}$ is derived in [41] by means of multiple scale analysis: Two field modes l and k inside an oscillating cavity are resonantly coupled whenever one of the conditions

$$\omega_{\rm cav} = |\Omega_l^{\rm in} \pm \Omega_k^{\rm in}| \tag{4.9}$$

is satisfied. This result holds for all cavity dimensions and reveals that the structure of the mode coupling does depend on the spectrum of frequencies $\{\Omega_n^{\rm in}\}$. In the one-dimensional case under consideration, the frequency spectrum $\{\Omega_n^{\rm in} = n\pi/l_0\}$ is equidistant and therefore infinitely many modes are coupled. For the main resonance case $\omega_{\rm cav} = 2\pi/l_0$, for example, Eq. (4.9) predicts that only odd modes are coupled, while even modes are not excited. The numerical simulations will confirm this statement.
It is therefore clear that the scenario of a massless scalar field with its equidistant frequency spectrum in a one-dimensional cavity represents a special case with strong intermode coupling. Adding a mass or going to higher cavity dimensions breaks the equidistance of the spectrum and yields a different coupling behavior where only a few or even no modes are coupled. I shall discuss this in more detail in Chapter 5 where I study the realistic case of the electromagnetic field in a three-dimensional cavity.

4.4 Particle creation in a vibrating cavity - Numerical results

4.4.1 Main resonance $\omega_{\rm cav} = 2\Omega_1^{\rm in}$

Analytical expressions for the number of particles created in the resonant mode $n = 1$ and for the total particle number valid for all times have been obtained in [57]

$$\mathcal{N}_1(t) = \frac{2}{\pi^2} E(\kappa) K(\kappa) - \frac{1}{2}, \tag{4.10}$$

$$\mathcal{N}(t) = \frac{1}{\pi^2}\left[\left(1 - \frac{1}{2}\kappa^2\right) K^2(\kappa) - E(\kappa)K(\kappa)\right]. \tag{4.11}$$

Thereby

$$\kappa = \sqrt{1 - \exp\{-8\tau\}} \tag{4.12}$$

and τ is the so-called *slow time*

$$\tau = \frac{1}{2}\epsilon\,\Omega_1^{\rm in}\, t = \frac{\pi}{2}\frac{\epsilon}{l_0}\, t. \tag{4.13}$$

$E(\kappa)$ and $K(\kappa)$ are the complete elliptic integrals [86]. For $\tau \ll 1$ these expressions yield $N(\tau) = N_1(\tau) = \tau^2$ while they lead to the asymptotic behavior $N_1(\tau) = \tau$ and $N(\tau) = \tau^2$ for $\tau \gg 1$.

In Figure 4.2 (a) I show the numerical results for a cavity of initial length $l_0 = 0.1$ and $\epsilon = 10^{-5}$ obtained for an integration time $t_{\rm out} = 3500$ and compare them to the analytical expressions (4.10) and (4.11). The numerical results perfectly agree with the analytical expressions of [57] for all times predicting that the initial quadratic increase of both, the total particle number and the number of particles created in the resonance mode $n = 1$, devolves in a quadratic increase of the total particle number and a linear behavior for the number of resonance mode particles. The particle spectrum at the end of the integration shown in panel (b) for the two cutoff parameters $n_{\rm max} = 10$ and 15 indicates the stability of the numerical results. As one infers from the spectrum, only odd modes are created as predicted by Eq. (4.9). From the particle spectrum shown for short times $\mathcal{N}_n(t = 250)$ one reads off the value $\mathcal{N}_1(t = 250) = 1.5419 \times 10^{-3}$ which agrees perfectly with the analytical prediction $\mathcal{N}_1(\tau) = \tau^2|_{t=250} = 1.5421 \times 10^{-3}$.

In Fig. 4.2 I further show results of numerical simulations for a cavity with initial size $l_0 = 1$ and $\epsilon = 0.001$ [Panels (c) and (d)] and 0.01 [Panels (e) and (f)]. Also for these parameters the analytical predictions (4.10)

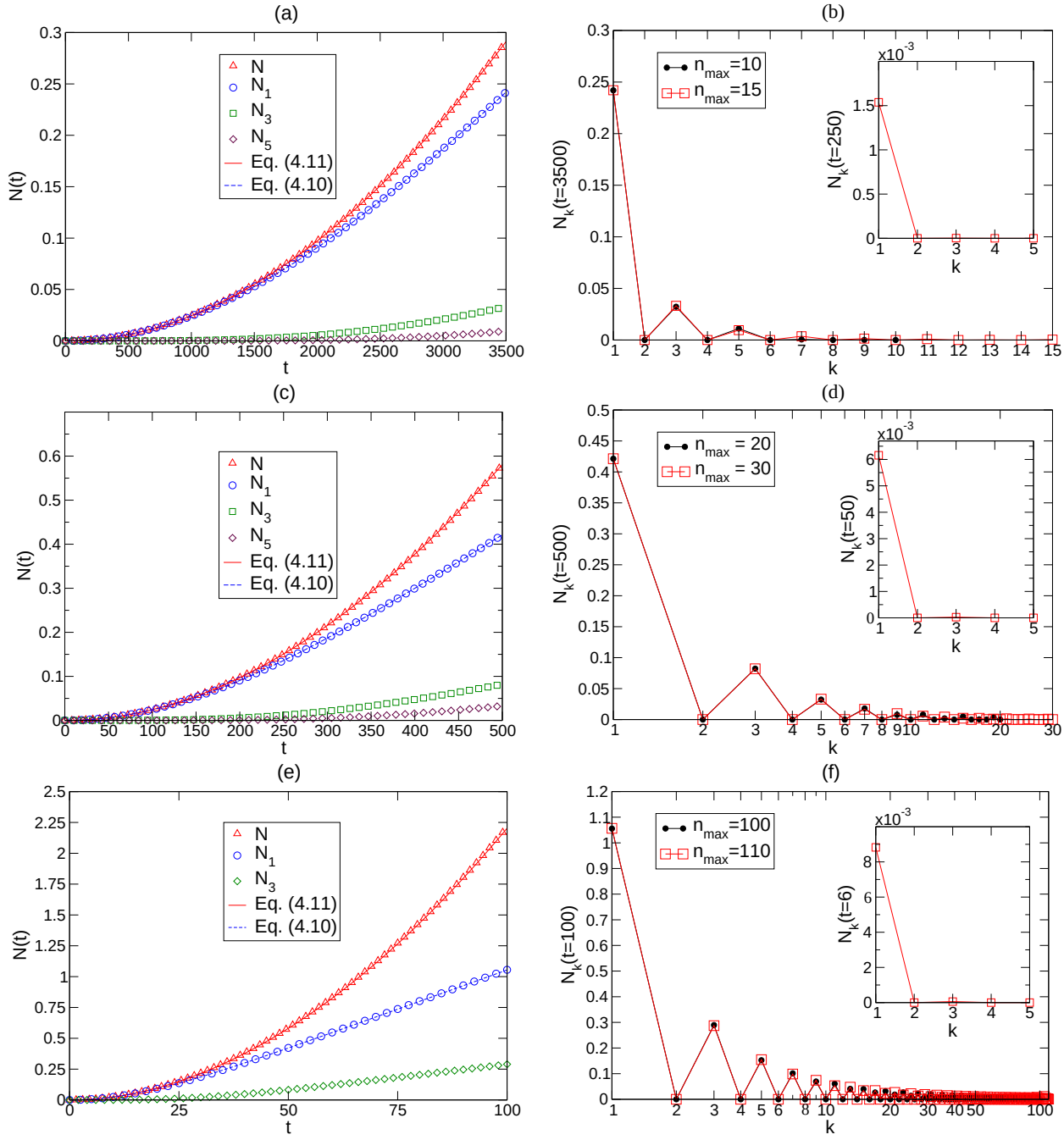

Figure 4.2: Particle numbers $\mathcal{N}_n(t)$ and final particle spectra $\mathcal{N}_n^{\rm out} = \mathcal{N}_n(t_{\rm out})$ of particles produced in a cavity vibrating with (4.7) in the main resonance $\omega_{\rm cav} = 2\Omega_1^{\rm in}$ for parameters: (a) and (b) $l_0 = 0.1$, $\epsilon = 0.00001$; (c) and (d) $l_0 = 1$, $\epsilon = 0.001$ and (e) and (f) $l_0 = 1$, $\epsilon = 0.01$. The numerical results are compared to the predictions (4.10) and (4.11) and the spectra are shown for two cutoff parameters $n_{\rm max}$ to indicate numerical stability.

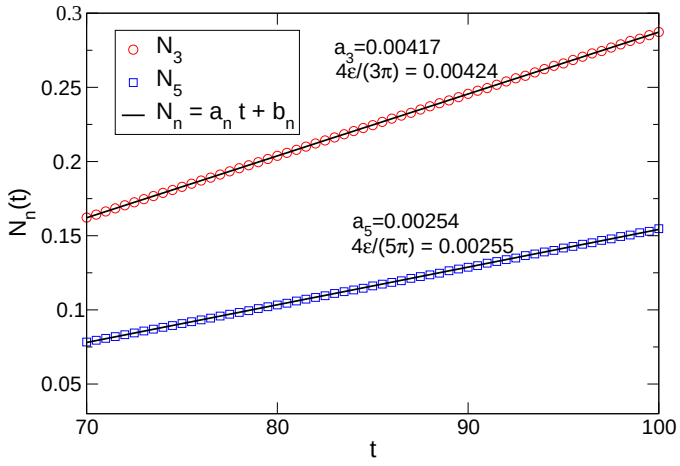

Figure 4.3: Number of particles created in the modes $n = 3$ and $n = 5$ for $\tau > 1$ and parameters $l_0 = 1$ and $\epsilon = 0.01$ corresponding to Fig. 4.2 (e) and (f). The data is fitted to the linear law $\mathcal{N}_n(t) = a_n\, t + b_n$.

and (4.11) reproduce the numerical solutions very well for all time scales under consideration. For the amplitude $\epsilon = 0.01$ the number of excited field modes inside the cavity increases drastically. This is reflected by the value for the cutoff parameter $n_{\max}$ which has to be chosen in order to obtain numerically stable solutions for the field modes. Whereas for $\epsilon = 0.001$ the value $n_{\max} = 30$ guarantees stability of the numerical solutions up to $t = 500$ it has to be increased to $n_{\max} = 110$ to provide stable solutions for $\epsilon = 0.01$ up to $t = 100$.

Already three years before their paper [57] the same authors found in [56] that in the main resonance case, the rate of particle creation for a mode of frequency $\Omega_n^{\rm in}$ (n odd) is given by

$$\frac{d\mathcal{N}_n(t)}{dt} = \frac{4\,\epsilon}{\pi\, n} \tag{4.14}$$

if $\epsilon\, t \gg 1$, i.e. $\tau \gg 1$. Thus, the number of particles created in the excited modes increases linearly for large times [1]. By expanding Eq. (4.10) one easily recovers Eq. (4.14) for the particular case $n = 1$. As mentioned in [57], this asymptotic formula works quite well even for $\tau \approx \frac{1}{2}$.
In Figure 4.3 I show the results for the number of particles created in the modes $n = 3$ and $n = 5$ for $l_0 = 1$ and $\epsilon = 0.01$ [cf. Fig. 4.2 (e), (f)] for $\tau > 1$. The rate of particle creation obtained by fitting the data to $\mathcal{N}_n(t) = a_n t + b_n$ agrees very well with the values predicted by Eq. (4.14). The numerical calculations lead to $a_3 = 0.00417$ and $a_5 = 0.00254$ which are in very good agreement with the values $a_3 = 4\,\epsilon/(3\,\pi) = 0.00424$ and $a_5 = 4\,\epsilon/(5\,\pi) = 0.00255$ predicted by Eq. (4.14). The numerical simulations show that the rate of particle creation for higher frequency modes is very well described by the analytical expression (4.14) beginning at $\tau \approx 1$. It was noted in [56] that Eq. (4.14) is valid only for not very large numbers n due to limitations of the used approximations. For $\epsilon = 0.01$ I have found that Eq. (4.14) perfectly describes the rate of particle creation for $n = 7$ and $n = 9$ as well.

As mentioned before, a particular feature of a resonantly vibrating cavity is the exponential growth of the total energy associated with the produced quantum vacuum radiation. For the main resonance case it is shown in [57] that the total energy is described by

$$E(\tau) = \frac{1}{4}\Omega_1^{\rm in} \sinh^2(2\,\tau). \tag{4.15}$$

That the energy of the created quantum radiation grows much faster than the total particle number reflects the excitation of the high frequency modes visible in the spectra shown in Fig. 4.2. Those modes of frequencies higher than the mechanical frequency of the cavity vibration significantly contribute to the total energy. Much of the energy is transfered from the resonant mode to the high frequency modes due to the mode coupling.
In Fig. 4.4 (a) I have arranged the numerical results for the particle numbers $\mathcal{N}(t)$ and $\mathcal{N}_1(t)$ and show the

[1] Note that in [56] a factor 2 was missed which has been corrected in [57].

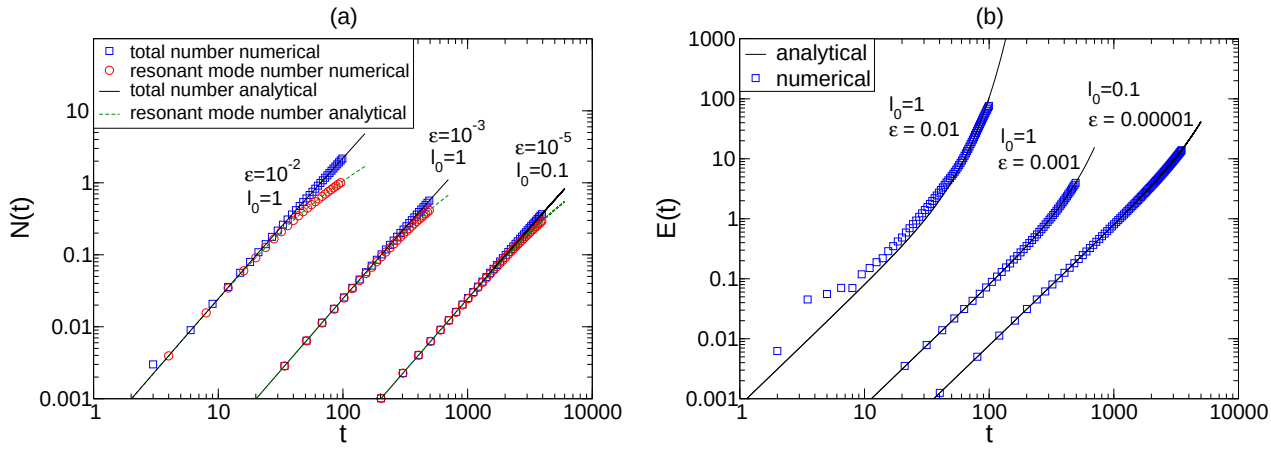

Figure 4.4: (a) Summary of numerical results obtained for the particle production in a cavity oscillating with (4.7) in the main resonance. The total particle number as well as the number of particles created in the resonance mode is shown for amplitudes $l_0\,\epsilon = 10^{-6}, 10^{-3}$ and 10^{-2} corresponding to Fig. 4.2. (b) Comparison of the numerical results obtained for the energy associated with the created quantum radiation for the parameters shown in part (a) with the analytical expression (4.15).

corresponding total energy $\mathcal{E}(t)$ in panel (b) in comparison with Eq. (4.15). Figure 4.4 (a) again demonstrates that the analytical expressions (4.10) and (4.11) describe the numerical results very well for values of ϵ up to 0.01. Comparing the numerical results for the energy with the analytical prediction shows, that for small amplitudes $\epsilon = 0.00001$ and $\epsilon = 0.001$ the numerical results agree perfectly with the analytical prediction (4.15). In the case of $\epsilon = 0.01$ the numerically calculated energy deviates slightly from the analytical prediction in particular for small times where the total particle number is still in very good agreement with the analytical expression. This can be attributed to spurious effects caused by the initial discontinuity in the mirror velocity. The discontinuity artificially excites modes up to very high frequencies right at the very beginning of the dynamics. Since the energy of the created quantum radiation is much more sensitive to contributions from higher frequency modes than the total particle number, those modes dominate the total energy for short times. In addition, once excited, these higher frequency modes damp the evolution of the resonant mode. That the influence of the discontinuity becomes visible for larger values of ϵ is expected, since the initial velocity is proportional to ϵ [2].
The perfect agreement of the numerics for $l_0\,\epsilon = 0.001$ with the analytical prediction Eq. (4.15) proves that the initial discontinuity is of no relevance for such small amplitudes. I shall therefore consider exclusively this case in the course of the following discussion.

4.4.2 Higher resonances $\omega_{\rm cav} = 2\Omega_n^{\rm in}, n > 1$

The scenario in which the cavity oscillates at a higher frequency $\omega_{\rm cav} = 2\Omega_n^{\rm in} = 2n\pi$ ($l_0 = 1$) is studied, for instance, in [104, 59]. Provided that the slow time (4.13) is small, $\tau \ll 1$, the number of particles produced in a mode k is given by [104]

$$\mathcal{N}_k(\tau) = (2\,n - k)\,k\,\tau^2 \quad , \quad k < 2n \; , \tag{4.16}$$

and $\mathcal{N}_k = 0$ for $k \geq 2n$. Here n characterizes the frequency $\omega_{\rm cav} = 2\Omega_n^{\rm in}$ of the cavity vibrations and can take the values $n = 1, 1.5, 2, \ldots$. Consequently, in the short-time limit, the total particle number is given by

$$\mathcal{N}(\tau) = \sum_{k=1}^{2n-1} (2\,n - k)\,k\,\tau^2 = \frac{n}{3}(4n^2 - 1)\tau^2 \;\; \text{if} \;\; \tau \ll 1. \tag{4.17}$$

This expression is also derived in [59] by means of a different method. In [59] it was found that for long times the particle number grows quadratically, too,

$$\mathcal{N}(\tau) = \frac{8n^3}{\pi^2}\tau^2 \;\; \text{if} \;\; \tau \gg 1 \; , \tag{4.18}$$

[2] This is discussed in more detail in the publications cited in the introduction.

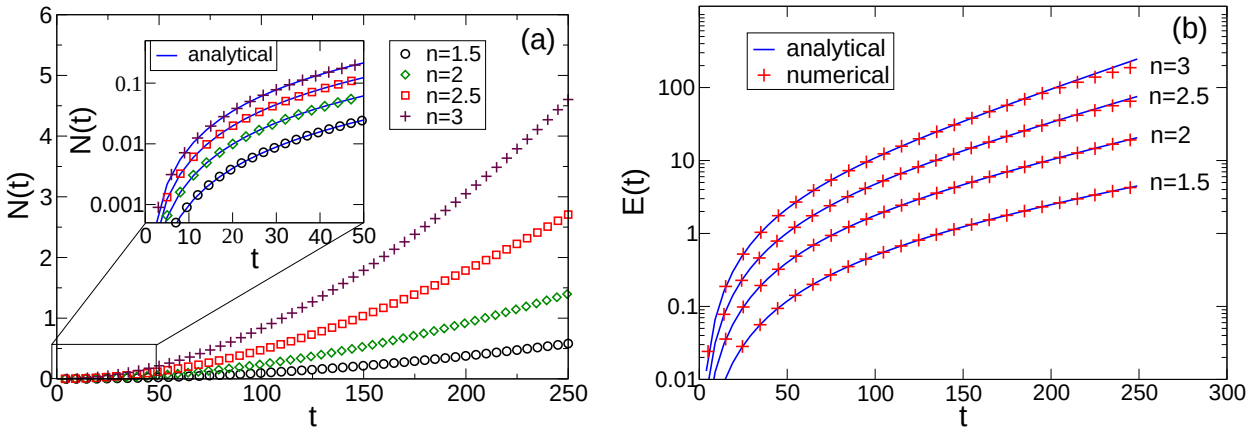

Figure 4.5: (a) Total number of particles produced in a cavity vibrating with (4.7) and $\omega_{\rm cav} = 2n\pi$ with $n = 1.5, 2, 2.5$ and 3. The small plot shows the results in the time range $[0, 50]$ together with the analytical prediction (4.17) (solid line). (b) Energy $\mathcal{E}(t)$ corresponding to the results shown in (a) together with the analytical prediction (4.19) (solid line). The results correspond to the largest cut-off parameters as given in Fig. 4.6.

and that the energy associated with the motion induced radiation grows, as in the main resonance case, exponentially in time

$$\mathcal{E}(\tau) = \frac{4n^2 - 1}{12}\,\pi\,\sinh^2(2n\tau). \tag{4.19}$$

In Fig. 4.5 (a) I show the numerical results for the total particle number in the time range $[0, 250]$ for resonant cavity frequencies $\omega_{\rm cav} = 2n\pi$ for $n = 1.5, 2, 2.5$ and 3. The associated energy of the created quantum radiation is depicted in Fig. 4.5 (b) and the corresponding particle spectra are shown in Fig. 4.6 for different cutoff parameters $n_{\rm max}$ to demonstrate numerical stability of the results. The spectra confirm that no modes $k = 2np$ with $p = 1, 2, 3, ...$ are coupled (and therefore excited) as predicted by the coupling condition (4.9).

One observes, that by going to higher cavity frequencies the number $n_{\rm max}$ of modes taken into account in the system of coupled differential equations has to be increased in order to ensure stability of the numerical solutions in the given range of integration. While for $n = 1.5$ the value $n_{\rm max} = 30$ guarantees stability, one has to increase the cut-off to $n_{\rm max} \approx 100$ in the case of $n = 3$ to obtain stable solutions for the first few modes. This is due to the fact that for higher cavity frequencies, modes of higher frequencies become excited faster. Furthermore, for higher cavity frequencies also modes close to the resonant mode become excited due to the particular structure of the mode coupling.

For short times $\epsilon\,\pi\,t = 10^{-3}\,\pi\,t \ll 1$, the numerical results are well described by the analytical predictions of [104, 59]. The numerically calculated spectra for times $t = 25$ shown in Fig. 4.6 are well fitted by the analytical expression (4.16), predicting a parabolic shape of the particle spectrum. More quantitatively, for $n = 2$, for instance, the predicted values $\mathcal{N}_1(t = 25) = \mathcal{N}_3(t = 25) = 4.63 \times 10^{-3}$, $\mathcal{N}_2(t = 25) = 6.17 \times 10^{-3}$ agree well with the values $\mathcal{N}_1(t = 25) = 4.62 \times 10^{-3}$, $\mathcal{N}_2(t = 25) = 6.14 \times 10^{-3}$ and $\mathcal{N}_3(t = 25) = 4.59 \times 10^{-3}$ obtained from the numerical simulations with $n_{\rm max} = 50$. The total number of created particles is perfectly described by the expression (4.17) as it is demonstrated in the small plot in Fig. 4.5 (a).

An interesting observation in the final particle spectrum for $\omega_{\rm cav} = 2\Omega_3^{\rm in}$ [cf. Fig. 4.6 (d)] is that the number of particles produced in the resonant mode $k = 3$ is slightly less than the number of particles produced in the mode $k = 2$. I find that up to $t \approx 200$ the number of resonant mode particles $\mathcal{N}_3$ is larger than $\mathcal{N}_2$ but then $\mathcal{N}_2$ grows faster and finally overtakes $\mathcal{N}_3$. Even though the numerically calculated spectrum is not stable for higher modes, it is perfectly stable for small k. To demonstrate this, the results for three cut-off parameters $n_{\rm max} = 90, 100$ and 110 are shown in Fig. 4.6 (d). The values of $\mathcal{N}_k(t = 250)$ do not change for

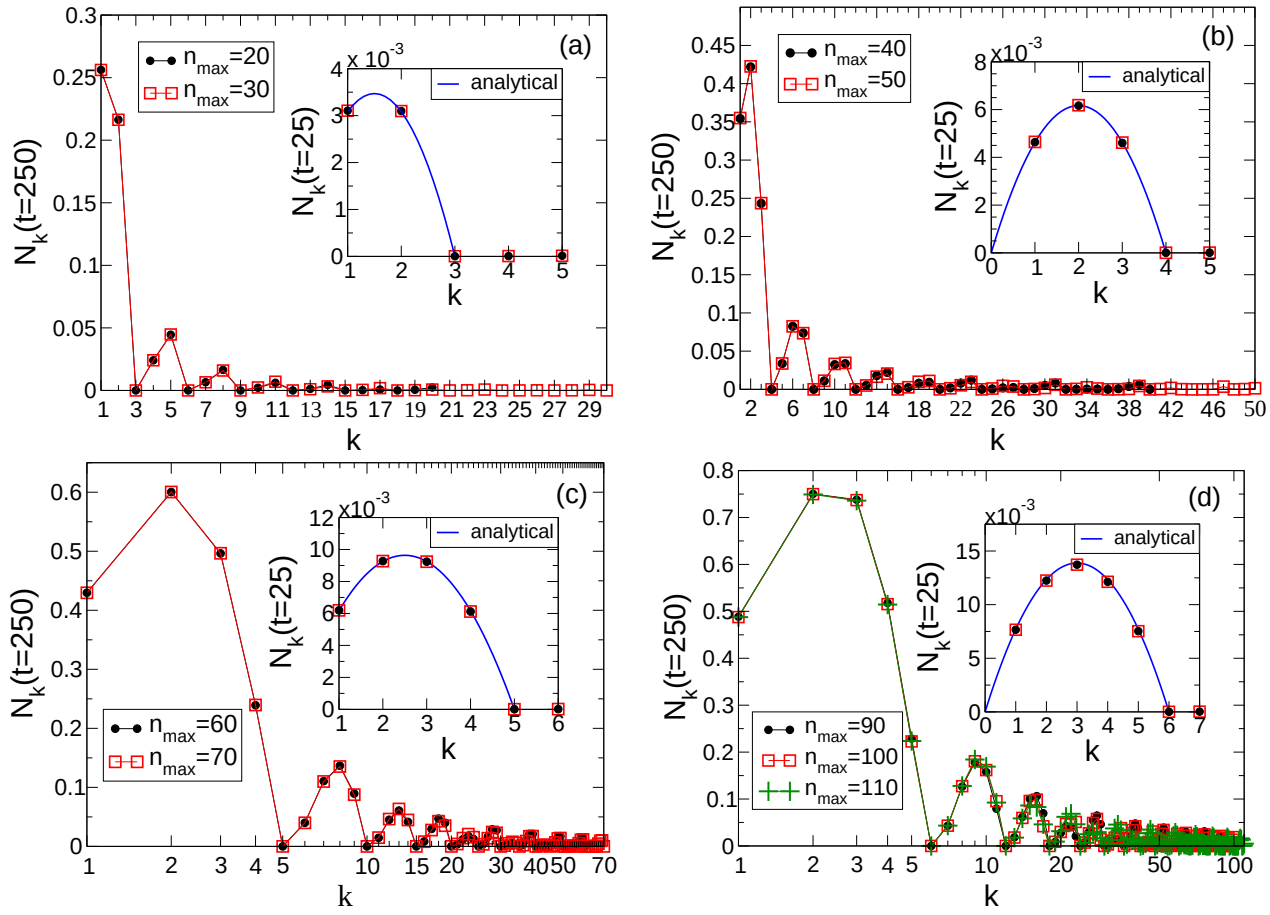

Figure 4.6: Particle spectra for (a) $\omega_{\rm cav} = 3\pi$, (b) $\omega_{\rm cav} = 4\pi$, (c) $\omega_{\rm cav} = 5\pi$ and (d) $\omega_{\rm cav} = 6\pi$ corresponding to the results shown in Fig. 4.5. The small plots compare the numerical results for $\mathcal{N}_k(t = 25)$ with the analytical prediction (4.16) plotted for continuous values of k (solid line).

$k = 1, 2$ and 3 at all when varying $n_{\rm max}$ form 90 to 110 [3]. Also the results for higher frequency modes up to $k \simeq 10$ are very stable when changing $n_{\rm max}$ from 100 to 110. For that reason the fact that the number of particles created in the resonant mode $k = 3$ is slightly smaller than the number of particles produced in the less energetic close-by mode $k = 2$ is not an artefact of numerical instability of the solutions but rather a real feature.

For the energy, the numerical values and the analytical prediction agree very well for $n = 1.5$ and 2. In the case of $n = 2.5$ and 3 we observe slight deviations towards the end of the integration range. This is due to the numerical instabilities in the corresponding particle spectra [cf Figs. 4.6 (c) and (d)]. The numerical values for $\mathcal{N}_k$ with k larger than some value ($k > 10$ for $n = 3$, for instance) do not remain unchanged when varying $n_{\rm max}$. Even $\mathcal{N}_k$ is small for the higher frequencies compared to the values of $\mathcal{N}_k$ for the excited lowest modes, their contribution to the total energy is significant because of their high frequency. Hence relatively small instabilities in $\mathcal{N}_k$ for larger k give rise to a non-stable (with respect to $n_{\rm max}$) result for the energy. In order to gain better agreement of the numerical results for the energy for $n = 2.5$ and 3 with the analytical prediction a further increase of $n_{\rm max}$ is necessary.

[3] The values, rounded to the third digit, are $(0.489, 0.750, 0.738)$ for $n_{\rm max} = 90$, $(0.488, 0.750, 0.737)$ for $n_{\rm max} = 100$ and $(0.488, 0.749, 0.736)$ for $n_{\rm max} = 110$ where we use the notation $(\mathcal{N}_1, \mathcal{N}_2, \mathcal{N}_3)$. For comparison, regarding the numerical accuracy, the largest deviation in the Bogoliubov test is $\approx 4 \times 10^{-4}$ for $n_{\rm max} = 100$ (see Appendix B).

4.4.3 Detuning

As I have demonstrated, the energy inside a vibrating one-dimensional cavity increases exponentially under the perfect resonance condition $\omega_{\rm cav} = 2\Omega_n^{\rm in}$. The same phenomenon occurs also in three-dimensional cavities which has led to the hope that it might actually be possible to observe the dynamical Casimir effect in the laboratory. I will comment on proposals for experiments at the end of Chapter 5 in which I shall discuss the electromagnetic field. In a realistic experimental setup it will not be possible to operate a (macroscopic) mechanical device like a moving mirror at exactly the resonance frequency. It is therefore important to study how particle production is affected if the frequency of the cavity vibration does not exactly match the resonance condition, i.e. if it is detuned.

The detuned frequency may be parameterized by

$$\omega_{\rm cav} = \omega_{\rm res} + \Delta \tag{4.20}$$

with exact resonance frequency $\omega_{\rm res}$ and detuning parameter Δ.

Detuning for a massless scalar field in a one-dimensional cavity subject to sinusoidal oscillations of the form (4.7) has been investigated analytically in [59, 186]. The exact resonance frequency is again $\omega_{\rm res} = 2\Omega_n^{\rm in}$. Let me rewrite the detuning parameter Δ introduced in Eq. (4.20) as

$$\Delta = \frac{2\pi\,\delta n}{l_0} \tag{4.21}$$

with δn controlling the deviation of the cavity frequency from the exact resonance condition. Introducing the new parameter

$$\gamma = \frac{\delta n}{n\epsilon}\ , \tag{4.22}$$

it has been shown in [59] that there exist three different possibilities for the time evolution of the energy inside an off-resonantly vibrating cavity depending on γ. If $\gamma < 1$ the energy increases exponentially in time

$$\mathcal{E}(\tau) = \frac{4n^2-1}{12}\pi\frac{\sinh^2(2na\tau)}{a^2} \ \text{ with } \ a = \sqrt{1-\gamma^2}. \tag{4.23}$$

This is an important threshold. As long as it is possible to adjust the cavity frequency with such an accuracy that $\gamma < 1$, the energy inside the cavity still increases exponentially. For $\gamma = 1$ the energy still increases in time, but only quadratically

$$\mathcal{E}(\tau) = \frac{\pi}{3}(4n^2-1)(n\tau)^2. \tag{4.24}$$

If finally $\gamma > 1$, detuning is too large and the cavity motion does not support a continuous increase of the energy inside the cavity anymore. It oscillates instead according to

$$\mathcal{E}(\tau) = \frac{4n^2-1}{12\tilde{a}^2}\,\pi\,\sin^2(2n\tilde{a}\tau) \ \text{ with } \ \tilde{a} = \sqrt{\gamma^2-1} \tag{4.25}$$

and period

$$T_n(\delta n, \epsilon) = \frac{1}{n\,\epsilon\,\tilde{a}}. \tag{4.26}$$

An oscillating energy corresponds to an oscillating particle number. Hence, for strong detuning, particles are created and annihilated by the off-resonant motion of the cavity. Processes leading to oscillating occupation numbers can be found in many other scenarios dealing with quantum fields under the influence of time-dependent external fields [87].

In Figure 4.7 (a) I show the numerical results for the total energy for different off-resonant frequencies covering all three different possibilities for γ and compare them with the analytical predictions. As before, the parameters $l_0 = 1$ and $\epsilon = 0.001$ have been used. For $n = 2$, $\delta n = 0.001$ and hence $\gamma = 0.5$ the energy still increases exponentially in time. The case $\gamma = 1$ is realized by the parameter combination $n = 1$ and $\delta n = 0.001$ yielding quadratic growth of the energy inside the cavity. Furthermore, three examples for $\gamma > 1$ leading to oscillations of the energy are shown. In all three cases, the results of the numerical simulations coincide with

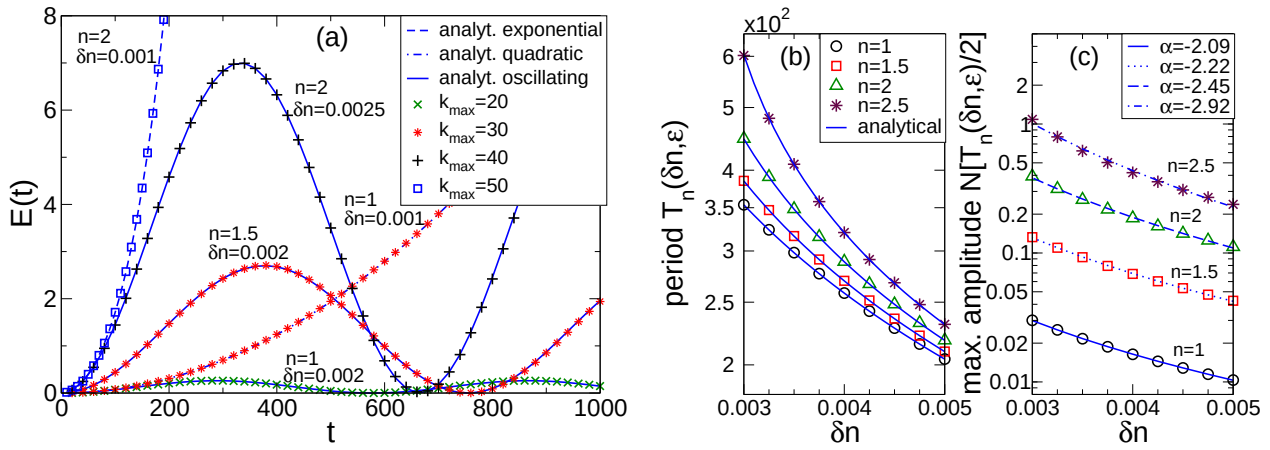

Figure 4.7: (a) Total energy associated with the particles produced in an off-resonantly vibrating cavity. The numerical results are compared with the analytical predictions (4.23) - (4.25). The given values for the cut-off ensure numerical stability. (b) Period and (c) maximal amplitude of the particle number oscillations caused by detuning. The numerically obtained periods are compared with Eq. (4.26).

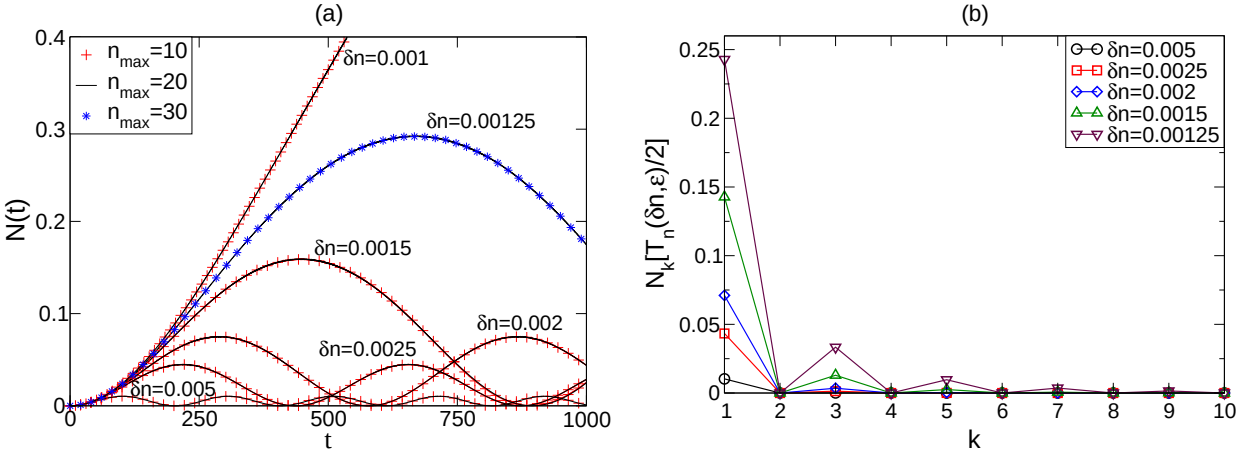

Figure 4.8: (a) Time evolution $\mathcal{N}(t)$ and (b) spectra $\mathcal{N}_k[T_1(\delta n, \epsilon)/2]$ of the occupation numbers in a cavity oscillating with detuned frequency $2(1+\delta n)\pi$. The spectra are shown for the oscillating occupation numbers only and correspond to times where the amplitude is maximal, i.e. $T_1(\delta n, \epsilon)/2$.

the analytical predictions. Figure 4.7 (b) depicts the periods of the energy (and particle number) oscillations as obtained from the simulations with $n = 1, 1.5, 2$ and 2.5 and δn ranging from 0.003 to 0.005. Comparison with the analytical prediction Eq. (4.26) shows that they are in excellent agreement. The numerical values for the maximal amplitudes $\mathcal{N}[T_n(\delta n, \epsilon)/2]$ of the corresponding particle number oscillations are shown in Fig. 4.7 (c) and fitted to the power law $\mathcal{N}[T_n(\delta n, \epsilon)/2] \propto (\delta n)^\alpha$ with values of α as indicated in the figure.

Let me discuss the $n = 1$ case in more detail. Figure 4.8 (a) depicts the numerical results for the total particle number $\mathcal{N}$ for the detuned case $\omega_{\rm cav} = 2\pi(1+\delta n)$ for different δn. Panel (b) shows the corresponding particle spectra for values of δn such that $\gamma > 1$ taken at half the period $T_n(\delta n, \epsilon)/2$ of the oscillations, i.e. when $\mathcal{N}(t)$ has its maximal amplitude. In each case the total particle number $\mathcal{N}(t)$ is shown for two cutoff parameters $n_{\rm max}$ to underline numerical stability of the results.

One observes, that for decreasing δn the shape of the spectra converges towards the spectra obtained for the resonance case, cf. Fig. 4.2 (d). For the largest considered value $\delta n = 0.005$, i.e. strongest detuning, the shape of the particle spectra equals the parabolic short time spectra of the exact resonance case, i.e. only the resonant mode itself becomes excited, cf. small plot in Fig. 4.2 (d). The turning point in the time evolution of the number of particles created in the "resonant" mode $n = 1$ is already reached when higher modes are still

not excited. The excitation of the next coupled mode $n = 3$ is sufficiently strong from $t \approx 150$ on only since $\mathcal{N}_3$ does not contribute to the total particle number for times $t < 150$ as visible in Fig. 4.2 (c). For times $t > 150$, the coupling to the resonance mode excites the $n = 3$-mode and creation of particles in this mode sets in. From Fig. 4.8 (a) one infers that the first maximum of the oscillating particle number is at $t \approx 100$, i.e. it is reached before the $n = 3$-mode is excited. Thus, with $\mathcal{N}_1$ decreasing afterwards due to detuning, there is no time left to excite the $n = 3$-mode. For smaller values of the detuning parameter the maximum of the oscillating particle number is shifted towards larger times. Hence the excitation of higher modes can set in before detuning leads to damping, and thus the shapes of the particle spectra equal more and more the one of the exact resonant case.

Next, I compare the results for particle production obtained for the sinusoidal motion (4.7) with the following cavity dynamics

$$l(t) = l_0 \left[1 + \epsilon \left(1 - \cos(\omega_{\rm cav} t)\right)\right] = l_0 \left[1 + 2\epsilon \sin^2\left(\frac{\omega_{\rm cav}}{2} t\right)\right] \quad \text{with} \quad \omega_{\rm cavity} = 2\Omega_n^{\rm in}. \tag{4.27}$$

Note that for this motion $\ddot{l}$ jumps at $t = 0$, but not $\dot{l}$.
Studying particle creation for this motion reveals an important effect related to detuning which, as it seems, has not been emphasized in the literature so far. It is frequently assumed (e.g., [4, 57]) that the behavior of the occupation number in an oscillating cavity is the same for both motions (4.7) and (4.27). However, as I will show now, this is not the case. Let me restrict my discussion to the main resonance case $\omega_{\rm cav} = 2\pi$ ($l_0 = 1$). In Fig. 4.9 (a) the numerical results for the number of created particles for the same parameters as in Fig. 4.2 (c) and (d) [$l_0 = 1, \epsilon = 0.001$] are shown and compared to the analytical predictions (4.10) and (4.11). The final particle spectra are depicted in panel (b). One observes that the numerical results do not match the analytical predictions, except for short times. Consequently, particle production behaves indeed differently for the two motions.
Comparing $\mathcal{N}(t)$ obtained for the motion (4.27) [cf. Fig. 4.9 (a)] with $\mathcal{N}(t)$ for the detuned sinusoidal motion with detuning strength $\delta n = 0.001$ [cf. Fig. 4.8 (a)], reveals that both are identical, not only qualitatively but also quantitatively. Recall that the detuned case $\delta n = 0.001$ corresponds to $\gamma = 1$, i.e. the total energy inside the cavity increases quadratically with time [cf. Eq. (4.24)]. One finds that the energy produced inside the cavity oscillating with (4.27) is very well fitted by a power law $\mathcal{E}(t) = 7.727 \times (\epsilon t)^2$. But this is exactly the behavior predicted by Eq. (4.24) for the detuned sinusoidal motion with $\delta n = 0.001$ (thus $\gamma = 1$). Why does the cosine motion with $\omega_{\rm cav} = 2\pi$ lead to the same behavior for the energy as the detuned sinusoidal motion? The reason is, that one has to formulate the resonance condition more precisely: An exact resonance occurs, if the external frequency $\omega_{\rm cav}$ is twice the eigenfrequency of a cavity mode defined with respect to the average position of the mirror, i.e. if

$$\omega_{\rm res} = 2\Omega_n^{<l>} \equiv \frac{2\,n\,\pi}{<l>}. \tag{4.28}$$

Here $< l >$ denotes the average position of the oscillating mirror. Whereas for the cavity motion (4.7) the average position of the moving mirror is identical to the initial size l_0, it is $< l >= l_0 + \epsilon$ in case of Eq. (4.27). Thus, Eq. (4.27) is not a resonant cavity motion for $\omega_{\rm cav} = 2\Omega_n^{\rm in}$, but a detuned one! The detuning parameter is $\Delta = 2\Omega_n^{\rm in} - \omega_{\rm res} = 2\Omega_n^{\rm in}(< l > - l_0)/< l >$. For $n = 1$ and $l_0 = 1$ this reduces to $\Delta = 2\pi \left(\frac{\epsilon}{1+\epsilon}\right) \simeq 2\pi\,\epsilon$, hence $\delta n = \epsilon = 0.001$ and thus $\gamma = 1$ [cf. Eq. (4.21)]. This explains why the energy inside the cavity is described by Eq. (4.24).
Consequently, by replacing the cavity frequency $\omega_{\rm cav} = 2\pi$ in (4.27) by $\omega_{\rm cav} = 2\,\pi/(1 + \epsilon)$, i.e. no detuning, the result for the cosine motion should coincide with the one for the sinusoidal motion, and be described by Eqs. (4.10) and (4.11). This is confirmed by the numerical simulations and demonstrated in Figs. 4.10 (a) and (b). With the "corrected frequency", the time evolution of the number of created particles is now qualitatively as well as quantitatively in very good agreement with the analytical predictions (4.10) and (4.11).

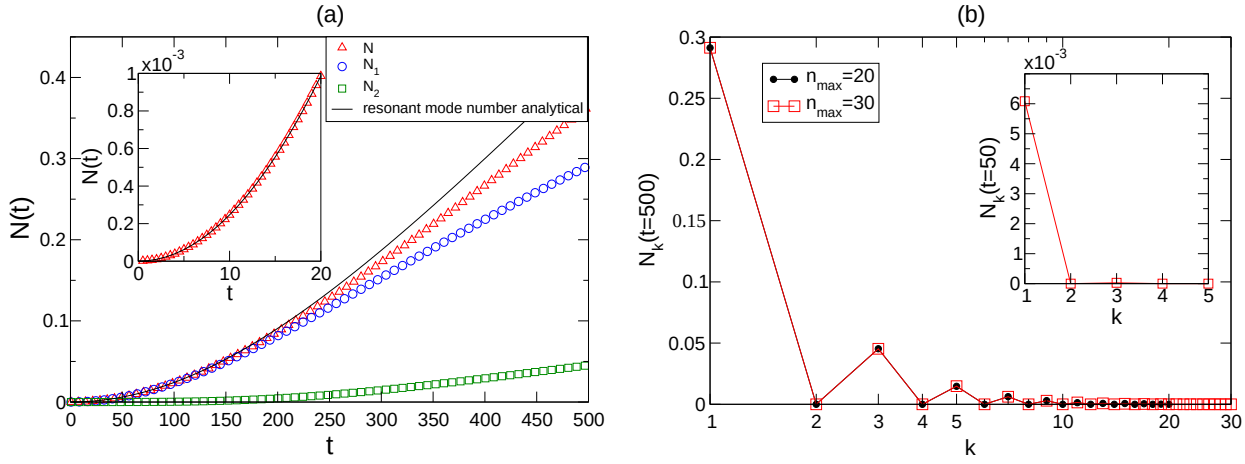

Figure 4.9: (a) Time evolution of the occupation number in a one-dimensional cavity oscillating with (4.27) and frequency $\omega_{\rm cav} = 2\pi$ ($l_0 = 1$) and amplitude $\epsilon = 0.001$. The solid line represents the analytical prediction (4.10) derived for the cavity motion (4.7). (b) Particle spectrum corresponding to (a).

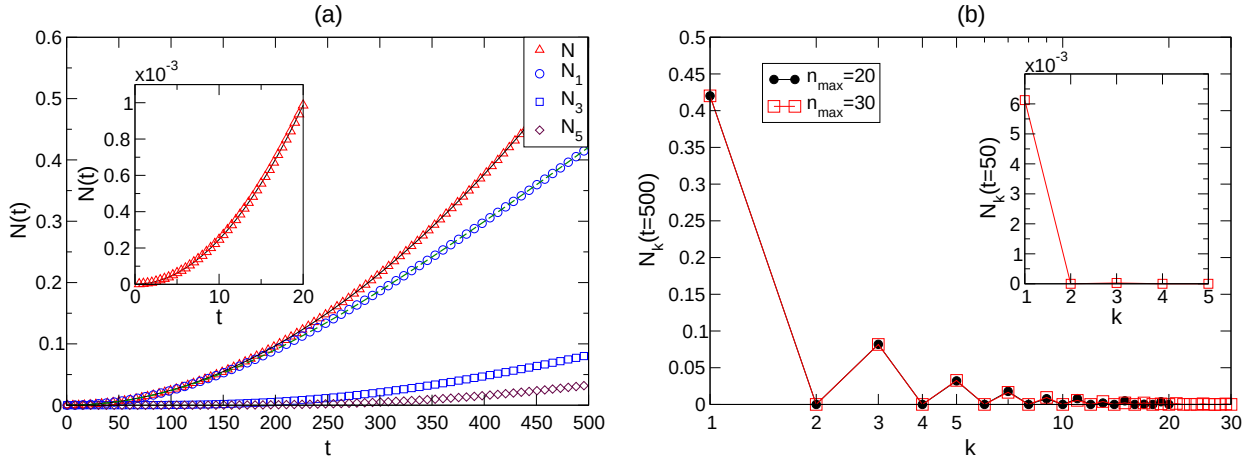

Figure 4.10: (a) Time evolution of the occupation number in a one-dimensional cavity oscillating with (4.27) and frequency $\omega_{\rm cav} = 2\pi/(1+\epsilon)$, i.e. the "true resonance" frequency. The solid and dotted lines represent Eqs. (4.10) and (4.11), respectively. (b) Particle spectrum corresponding to (a).

4.5 Discussion and final remarks

The main purpose of the work presented in this Chapter has been to test the very concept of investigating the dynamical Casimir effect fully numerically. Even though not very realistic, the model of a one-dimensional cavity represents a very good playground for testing the numerics, in particular the scenario of a vibrating cavity with its strong intermode coupling. Thereby, the results of the numerical simulations are entirely in perfect agreement with the variety of available analytical predictions. This may be regarded as not very exciting but, nevertheless, it leads to two conclusions. On the one hand it has demonstrated that the analytical results derived in the literature by means of approximations are indeed correct within their range of validity. On the other hand and not less important, it is a "proof of concept". One has a numerical formalism at hand, which allows to investigate particle production due to moving boundaries fully numerically which can be applied to scenarios where less is known analytically than in the simple model discussed here.

Chapter 5

Photon creation in a three-dimensional vibrating cavity

5.1 The electromagnetic field in a dynamical cavity

Let me begin by recalling that the free Maxwell equations describing the electromagnetic field in a region where there are no sources (charges and currents), are (see, e.g., [158])

$$\begin{aligned} \nabla \mathbf{E}(t,\mathbf{x}) &= 0\ ,\ \ \nabla \mathbf{B}(t,\mathbf{x}) = 0, & (5.1)\\ \nabla \wedge \mathbf{E}(t,\mathbf{x}) &= -\partial_t \mathbf{B}(t,\mathbf{x})\ ,\ \ \nabla \wedge \mathbf{B}(t,\mathbf{x}) = \partial_t \mathbf{E}(t,\mathbf{x})\ . & (5.2)\end{aligned}$$

Consider now a perfectly reflecting flat boundary (ideal mirror) with normal vector $\hat{\mathbf{x}}$ pointing into the x -direction. The ideality of the mirror requires that the electromagnetic field is subject to the boundary conditions (see, e.g.,[158])

$$\begin{aligned} \mathbf{E}_{\|}|_{\text{mirror}} = 0 \quad &\Leftrightarrow \quad \hat{\mathbf{x}} \wedge \mathbf{E}|_{\text{mirror}} = 0 & (5.3)\\ \mathbf{B}_{\perp}|_{\text{mirror}} = 0 \quad &\Leftrightarrow \quad \hat{\mathbf{x}} \cdot \mathbf{B}|_{\text{mirror}} = 0. & (5.4)\end{aligned}$$

Here $\|$ and $\perp$ denote the components of the field parallel and perpendicular to the mirror, respectively.

If the mirror is in motion, the boundary conditions (5.3,5.4) have to be imposed in the comoving Lorentz frame in which the mirror is instantaneously at rest [163]. I shall follow here the standard approach, where this problem is tackled by a decomposition of the fields into transverse-electric (TE) and transverse-magnetic (TM) modes [155, 156, 169, 42].
The decomposition reads

$$\begin{aligned} \mathbf{E}(t,\mathbf{x}) &= \mathbf{E}^{(\mathrm{TE})}(t,\mathbf{x}) + \mathbf{E}^{(\mathrm{TM})}(t,\mathbf{x}) & (5.5)\\ \mathbf{B}(t,\mathbf{x}) &= \mathbf{B}^{(\mathrm{TE})}(t,\mathbf{x}) + \mathbf{B}^{(\mathrm{TM})}(t,\mathbf{x}) & (5.6)\end{aligned}$$

with

$$\mathbf{E}^{(\mathrm{TE})}(t,\mathbf{x}) \cdot \hat{\mathbf{x}} = 0\ ,\ \ \mathbf{B}^{(\mathrm{TM})}(t,\mathbf{x}) \cdot \hat{\mathbf{x}} = 0. \tag{5.7}$$

The main step is to introduce two *different* vector potentials $\mathbf{A}^{(\mathrm{TE})}$ and $\mathbf{A}^{(\mathrm{TM})}$ for each polarization trough [155]

$$\begin{aligned} \mathbf{E}^{(\mathrm{TE})} &= -\partial_t \mathbf{A}^{(\mathrm{TE})}\ ,\ \ \mathbf{E}^{(\mathrm{TM})} = \nabla \wedge \mathbf{A}^{(\mathrm{TM})} & (5.8)\\ \mathbf{B}^{(\mathrm{TE})} &= \nabla \wedge \mathbf{A}^{(\mathrm{TE})}\ ,\ \ \mathbf{B}^{(\mathrm{TM})} = \partial_t \mathbf{A}^{(\mathrm{TM})}. & (5.9)\end{aligned}$$

This ansatz is suggested by the invariance of the free Maxwell equations under the duality transformation $\mathbf{E} \to \mathbf{B}$, $\mathbf{B} \to -\mathbf{E}$ [155]. With these definitions the decompositions (5.5) and (5.6) read

$$\begin{aligned} \mathbf{E}(t,\mathbf{x}) &= -\partial_t \mathbf{A}^{(\mathrm{TE})}(t,\mathbf{x}) + \nabla \wedge \mathbf{A}^{(\mathrm{TM})}(t,\mathbf{x}) & (5.10)\\ \mathbf{B}(t,\mathbf{x}) &= \nabla \wedge \mathbf{A}^{(\mathrm{TE})}(t,\mathbf{x}) + \partial_t \mathbf{A}^{(\mathrm{TM})}(t,\mathbf{x}). & (5.11)\end{aligned}$$

Both potentials are subject to the Coulomb gauge, i.e.

$$\nabla \cdot \mathbf{A}^{(\mathrm{TE/TM})} = 0 \tag{5.12}$$

and satisfy the wave equation

$$\Box_{(4)} \mathbf{A}^{(\mathrm{TE/TM})}(t, \mathbf{x}) = 0. \tag{5.13}$$

Recall that the corresponding scalar potentials are identically zero due to the absence of sources.
From the definition of the vector potentials (5.8) and (5.9) jointly with Eqs. (5.7) it follows the important result that

$$\mathbf{A}^{(\mathrm{TE})} \cdot \hat{\mathbf{x}} = 0 \quad \text{and} \quad \mathbf{A}^{(\mathrm{TM})} \cdot \hat{\mathbf{x}} = 0. \tag{5.14}$$

Ergo, the newly introduced vector potentials are both invariant under a boost in the x-direction.

Consider now the following situation. In the Laboratory frame Σ the position of the moving mirror is given by $x_{\mathrm{mirror}} = l(t)$. At a given time t_0 the mirror is located at $l(t_0)$. For times t sufficiently close to t_0, the position of the mirror is given by $x_{\mathrm{mirror}} = \dot{l}(t_0)(t - t_0) + l(t_0)$; it moves uniformly with velocity $v(t_0) = \dot{l}(t_0)$. The frame $\Sigma'(t_0)$ moving with this trajectory represents the instantaneously comoving frame at time t_0 [169]. Hence, the coordinates in both frames are related via the Lorentz transformation

$$x = \gamma\,(x' + vt') + l(t_0)\ , \quad t = \gamma\,(t' + vx') + t_0\ , \quad \mathbf{x}_{\|} = \mathbf{x}'_{\|} \tag{5.15}$$

with $\gamma = 1/\sqrt{1 - v^2}$.

In the instantaneous rest frame Σ' of the mirror the fields satisfy the boundary conditions (5.3,5.4), i.e.

$$\hat{\mathbf{x}} \wedge \mathbf{E}'(t' = 0, x' = 0, \mathbf{x}'_{\|}) = 0 \quad \text{and} \quad \hat{\mathbf{x}} \cdot \mathbf{B}'(t' = 0, x' = 0, \mathbf{x}'_{\|}) = 0. \tag{5.16}$$

From the decomposition of the fields in TE- and TM-components one finds the corresponding conditions for the vector potentials

$$\partial_{t'} \mathbf{A}^{(\mathrm{TE})\,\prime}(t' = 0, x' = 0, \mathbf{x}'_{\|}) = 0 \tag{5.17}$$

$$\partial_{x'} \mathbf{A}^{(\mathrm{TM})\,\prime}(t' = 0, x' = 0, \mathbf{x}'_{\|}) = 0. \tag{5.18}$$

Using that

$$\partial_{t'} = \gamma\,(v\partial_x + \partial_t) \quad \text{and} \quad \partial_{x'} = \gamma\,(\partial_x + v\partial_t)\ , \tag{5.19}$$

as well as that $\mathbf{A}^{(\mathrm{TE})}$ and $\mathbf{A}^{(\mathrm{TM})}$ are invariant under a boost in the x-direction one arrives at

$$\gamma(v\partial_x + \partial_t)\mathbf{A}^{(\mathrm{TE})}(t = t_0, x = l(t = t_0), \mathbf{x}_{\|}) = 0\ , \tag{5.20}$$

$$\gamma(\partial_x + v\partial_t)\mathbf{A}^{(\mathrm{TM})}(t = t_0, x = l(t = t_0), \mathbf{x}_{\|}) = 0. \tag{5.21}$$

For the TE-potential, $\gamma(v\partial_x + \partial_t)$ is just the total derivative d/dt. This implies that $\mathbf{A}^{(\mathrm{TE})}(t, x = l(t), \mathbf{x}_{\|})$ has to be constant since t_0 is arbitrary. One can set this constant to zero without loss of generality. Therefore, the boundary conditions for the vector potentials at the moving mirror are

$$\mathbf{A}^{(\mathrm{TE})}(t, x = l(t), \mathbf{x}_{\|}) = 0 \tag{5.22}$$

$$(\partial_x + v\partial_t)\mathbf{A}^{(\mathrm{TM})}(t, x = l(t), \mathbf{x}_{\|}) = 0. \tag{5.23}$$

The TE-mode vector potential obeys a Dirichlet boundary condition while the TM-mode vector potential is subject to a generalized Neumann boundary condition, i.e. a mixture of a Neumann boundary condition and a time-derivative, which I have already derived in Section 3.3.2 starting from the general variational principle [cf. Eq. (3.30)].

In the following I shall consider a rectangular cavity made of perfectly conducting walls (ideal mirrors) of dimensions $\{(0, l_x = l(t)), (0, l_y)(0, l_z)\}$, with the right wall following a prescribed trajectory $l(t)$ (cf. Fig. 5.1).

Using the just outlined considerations on the boundary conditions, it has been shown explicitely in [42] that the behavior of each component of the TE vector field inside an ideal cavity is related to that of a scalar

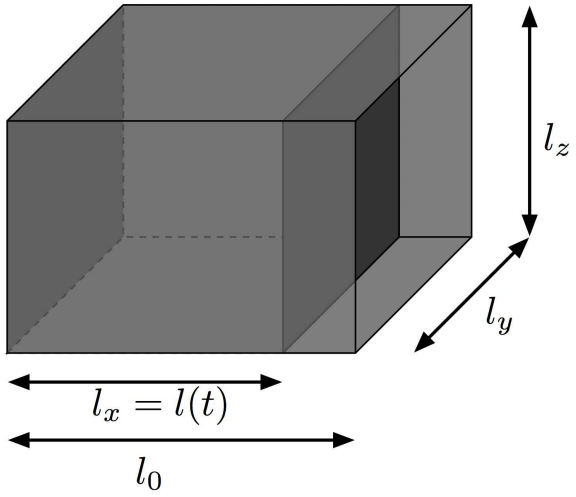

Figure 5.1: A three-dimensional cavity made of perfectly conducting walls. The right wall undergoes a prescribed trajectory $l(t)$.

field subject to Dirichlet boundary conditions at all cavity walls. Similarly, the dynamics of TM-modes can be mapped onto the problem of a scalar field subject to the generalized Neumann boundary conditions. Therefore, the dynamics of the electromagnetic field (and thus the problem of photon creation) inside a dynamical rectangular cavity can be split up into two separate boundary value problems for the two different polarizations

$$\Box_{(4)}\Phi(t,\mathbf{x}) = 0 \quad \text{with} \quad \begin{cases} \Phi|_{\text{all walls}} = 0 \quad \text{for TE} - \text{modes} \\ (v\partial_t + \partial_x)\Phi|_{x=l(t)} = \partial_x\Phi|_{\text{static walls}} = 0 \quad \text{for TM} - \text{modes} \end{cases} . \tag{5.24}$$

By this analogy, the number of created photons in TE- and TM - modes equals the number of created scalar particles subject to Dirichlet and (generalized) Neumann boundary conditions, respectively [42]. In the next section I shall discuss the TE-modes in detail.

5.2 Transverse electric modes

As I have just outlined, the study of photon production inside a rectangular ideal cavity is equivalent to the study of the production of scalar particles. For TE-modes, the problem is described by the wave equation

$$\Box_{(4)}\Phi(t,\mathbf{x}) = [\partial_t^2 - \triangle_{(3)}]\Phi(t,\mathbf{x}) = 0 \tag{5.25}$$

for a massless scalar field $\Phi(t,\mathbf{x})$ subject to Dirichlet boundary conditions at all walls of the cavity.
As in section 3.1, at any moment in time the field can be written as

$$\Phi(t,\mathbf{x}) = \sum_{\mathbf{n}} q_{\mathbf{n}}(t)\phi_{\mathbf{n}}(t,\mathbf{x}) \tag{5.26}$$

with canonical variables $q_{\mathbf{n}}(t)$ and functions

$$\phi_{\mathbf{n}}(t,\mathbf{x}) \quad = \quad \sqrt{\frac{2}{l(t)}}\sin\left[\frac{n_x\pi}{l(t)}x\right]\sqrt{\frac{2}{l_y}}\sin\left[\frac{n_y\pi}{l_y}y\right]\sqrt{\frac{2}{l_z}}\sin\left[\frac{n_z\pi}{l_z}z\right] \tag{5.27}$$

ensuring Dirichlet boundary conditions at all cavity walls [41]. The functions $\phi_{\mathbf{n}}(t,\mathbf{x})$ form an orthonormal and complete set of instantaneous eigenfunctions of the Laplacian $-\triangle_{(3)}$ with time-dependent eigenvalues

$$\Omega_{\mathbf{n}}(t) = \pi\sqrt{\left(\frac{n_x}{l(t)}\right)^2 + \left(\frac{n_y}{l_y}\right)^2 + \left(\frac{n_z}{l_z}\right)^2}. \tag{5.28}$$

Each field mode is labeled by three integers $n_x, n_y, n_z = 1, 2, ...$ for which I use the abbreviation $\mathbf{n} = (n_x, n_y, n_z)$. Inserting the expansion (5.26) into the field equation (5.25), multiplying it by $\phi_{\mathbf{m}}(t, x)$ and integrating over the spatial dimensions leads to the equation of motion for the canonical variables $q_{\mathbf{n}}(t)$

$$\ddot{q}_{\mathbf{n}}(t) + \Omega^2_{\mathbf{n}}(t) q_{\mathbf{n}}(t) + 2 \sum_{\mathbf{m}} M_{\mathbf{mn}}(t) \dot{q}_{\mathbf{m}}(t) + \sum_{\mathbf{m}} \left[\dot{M}_{\mathbf{mn}}(t) - N_{\mathbf{nm}}(t) \right] q_{\mathbf{m}}(t) = 0 \tag{5.29}$$

which is of the same form as for the one-dimensional case studied in section 3.1. The time-dependent coupling matrices $M_{\mathbf{nm}}(t)$ and $N_{\mathbf{nm}}(t)$ are given by [41]

$$\begin{aligned} M_{\mathbf{nm}} &= \int_0^{l(t)} dx \int_0^{l_y} dy \int_0^{l_z} dz \, \dot{\phi}_{\mathbf{n}}(t, \mathbf{x}) \phi_{\mathbf{m}}(t, \mathbf{x}) \\ &= \frac{\dot{l}(t)}{l(t)} \begin{cases} (-1)^{n_x + m_x} \dfrac{2 n_x m_x}{m_x^2 - n_x^2} \delta_{n_y m_y} \delta_{n_z m_z} & \text{if } n_x \neq m_x \\ 0 & \text{if } n_x = m_x \end{cases} \end{aligned}$$

and

$$N_{\mathbf{nm}} = \sum_{\mathbf{k}} M_{\mathbf{nk}} M_{\mathbf{mk}}. \tag{5.30}$$

Thus, $M_{\mathbf{nm}} = M_{n_x m_x} \delta_{n_y m_y} \delta_{n_z m_z}$ with $M_{n_x m_x}$ the coupling matrix (3.5) of the one-dimensional case. In Eq. (5.29), for a given mode (n_x, n_y, n_z), the coupling matrix (5.30) yields couplings of $q_{(n_x, n_y, n_z)}$ to $q_{(m_x, n_y, n_z)}$ and to $\dot{q}_{(m_x, n_y, n_z)}$ only, i.e. entirely summations over m_x appear. Modes of different quantum numbers with respect to the non-dynamical cavity dimensions are not coupled. The quantum numbers corresponding to the y- and z-directions enter the equations of motion only globally. This allows me to make the identifications

$$q_n(t) \equiv q_{(n_x, n_y, n_z)}(t) \;\text{ and }\; \Omega_n(t) \equiv \Omega_{(n_x, n_y, n_z)}(t) = \sqrt{\left[\frac{n\pi}{l(t)} \right]^2 + k_\parallel^2} \tag{5.31}$$

with $n \equiv n_x$ and the wave number

$$k_\parallel = \pi \sqrt{\left(\frac{n_y}{l_y} \right)^2 + \left(\frac{n_z}{l_z} \right)^2} \tag{5.32}$$

associated with the non-dynamical cavity dimensions. Because all summations over $\mathbf{m} = (m_x, m_y, m_z)$ involving the coupling matrix (5.30) reduce to summations over a single quantum number $m \equiv m_x$, Eq. (5.29) is equivalent to the differential equation describing a massive scalar field on a time-dependent interval $[0, l(t)]$ (one-dimensional cavity) when $k_\parallel$ is identified with the mass of the field

$$\mathfrak{m} = k_\parallel = \frac{M}{l_0}. \tag{5.33}$$

M is a dimensionless parameter which I shall use in the numerics and $l_0 = l(t_{\text{in}})$ is the initial position of the moving mirror.

The analogy between TE-mode photons and massless scalar particles in a three-dimensional cavity implies, that the number of produced TE-polarized photons equals the number of scalar particles of "mass" $k_\parallel$ created in a one-dimensional cavity $[0, l(t)]$. Production of TE-polarized photons in a three-dimensional dynamical cavity can therefore be studied numerically with the formalism introduced in Chapter 3.

5.3 Known analytical results

In what follows, I consider again the periodic trajectory

$$l(t) = l_0 \left[1 + \epsilon \sin(\omega_{\rm cav}\, t)\right] \ , \ \epsilon \ll 1. \tag{5.34}$$

Recall that two field modes l and k are coupled whenever one of the conditions given by Eq. (4.9) is satisfied. While for a massless field in a one-dimensional cavity mode coupling always occurs due to the equidistance of the frequency spectrum, only a few or even no modes may be coupled for TE-modes since the effective mass m (higher dimensionality of the problem) breaks the equidistance.
In a resonantly vibrating cavity $\omega_{\rm cav} = 2\Omega_n^{\rm in}$ with not one of these conditions fulfilled, the number of TE-mode photons created in the resonant mode n increases exponentially in time [41]

$$\mathcal{N}_n(t) = \sinh^2(n\,\gamma_n\,\epsilon\,t) \ \text{ with } \ \gamma_n = \frac{n}{2\,\Omega_n^{\rm in}} \left(\frac{\pi}{l_0}\right)^2 . \tag{5.35}$$

Here I have translated the results for three-dimensional cavities to the case of massive scalar particles according to Eq. (5.33).
By means of multiple scale analysis the authors of [41] also studied the resonance case $\omega_{\rm cav} = 2\Omega_n^{\rm in}$ with two coupled modes n and k satisfying

$$3\Omega_n^{\rm in} = \Omega_k^{\rm in}. \tag{5.36}$$

For the particular case $n = 1$ and $k = 5$ analytical expressions for the number of TE-mode photons are derived in [41]. Given a mode n, I can couple it to a particular mode k by tuning the mass M (or equivalently $k_\parallel$) such that the condition (5.36) is fulfilled. It is important to note, that coupling between modes does occur even if Eq. (4.9) is detuned, i.e. if Eq. (4.9) is satisfied by the frequencies $\Omega_k^{\rm in}$ and $\Omega_l^{\rm in}$ only approximately. The particular case of two modes n and k satisfying

$$(3+\kappa)\Omega_n^{\rm in} = \Omega_k^{\rm in} \tag{5.37}$$

without additional couplings to higher modes is studied in [62]. For sufficiently small κ (i.e., $\kappa < \epsilon$) the two modes n and k are still resonantly coupled and the number of particles produced in both modes increasing exponentially with time.

5.4 Numerical results for TE-modes

In the following I restrict myself to the discussion of the the main resonance case $\omega_{\rm cav} = 2\Omega_1^{\rm in}$. Higher resonances are briefly discussed in the corresponding publication mentioned in the introduction. In Fig. 5.2 the number of particles created in the resonant mode $n = 1$ is shown for masses $M = 0.2, 0.7, 2$ and 3.5 and compared to the analytical prediction Eq. (5.35) [1]. For $M = 0.7, 2$ and 3.5 the numerical results are well described by Eq. (5.35) which is valid provided that the resonant mode $n = 1$ is not coupled to other modes. But for the mass $M = 0.2$ the numerical result for $\mathcal{N}_1(t)$ disagrees with the analytical prediction (5.35). This shall now be discussed in detail.
Figure 5.2 (b) shows the corresponding particle spectra at time $t = 6700$. As one infers from these spectra, the mode which becomes excited most is indeed the resonant mode $n = 1$ for masses $M = 3.5, 2$ and 0.7. However, also higher modes become excited but the corresponding particle numbers are several orders of magnitude smaller than the number of particles created in the resonant mode. For $M = 0.7$, for example, the mode $k = 3$ is clearly excited. Figure 5.3 (a) shows the number of particles created in the modes $k = 1, 2$ and 3 for the mass parameter $M = 0.7$ in detail. The difference in the numerical values of $\mathcal{N}_1$ and $\mathcal{N}_3$ is so large that the contribution of $\mathcal{N}_3$ to the total particle number is negligible such that $\mathcal{N} \simeq \mathcal{N}_1$. From Fig. 5.3 (a) one could conclude that $\mathcal{N}_2$ behaves in the same way as $\mathcal{N}_3$ but shows superimposed oscillations. However, the high resolution figures provide a more detailed view on the time evolution of $\mathcal{N}_k(t)$ for modes $k = 2$ and 3. In the upper panel of Fig. 5.3 (a) the resolution in which the numerical results are shown is not sufficient in order to resolve the details which are visible in the lower panel plots of Fig. 5.3 (a). These high resolution pictures reveal that $\mathcal{N}_3$ increases exponentially in time with oscillations superimposed on an average particle number

[1] In this section I use the general notion "particles" for massive scalar particles, or equivalently, TE-mode photons. Furthermore, I call M the mass of the particle, having in mind that it corresponds to the wave number $k_\parallel$ for TE-mode photons.

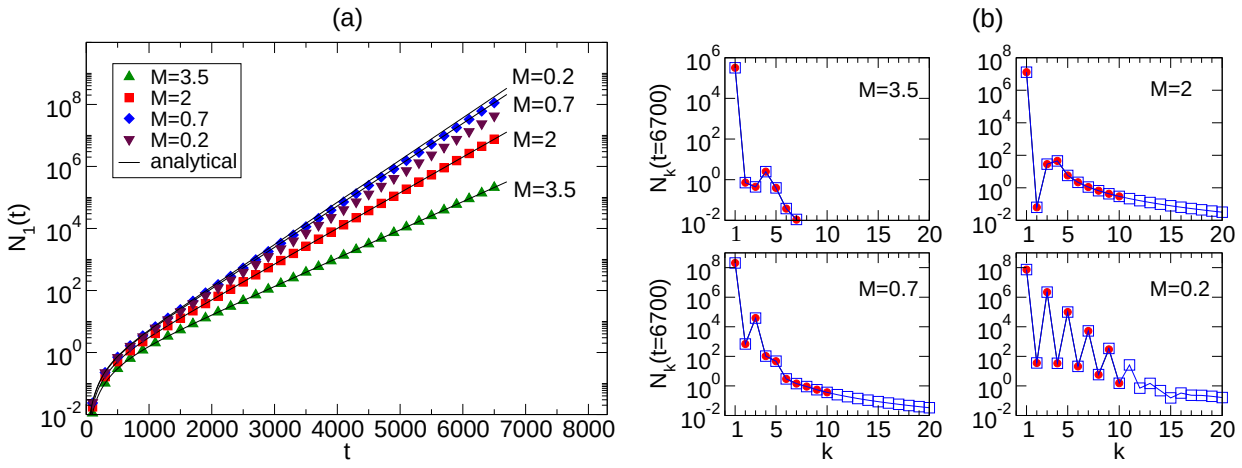

Figure 5.2: (a) Number of particles created in the resonance mode $n = 1$ for mass parameters $M = 0.2, 0.7, 2,$ and 3.5 in comparison with the analytical prediction (5.35). (b) Particle spectrum for different mass parameters $M = 3.5, 2, 0.7$ and $M = 0.2$ at time $t = 6700$ corresponding to (a). The spectra are shown for $n_{\max} = 10$ (dots) and $n_{\max} = 20$ (squares) to demonstrate numerical stability.

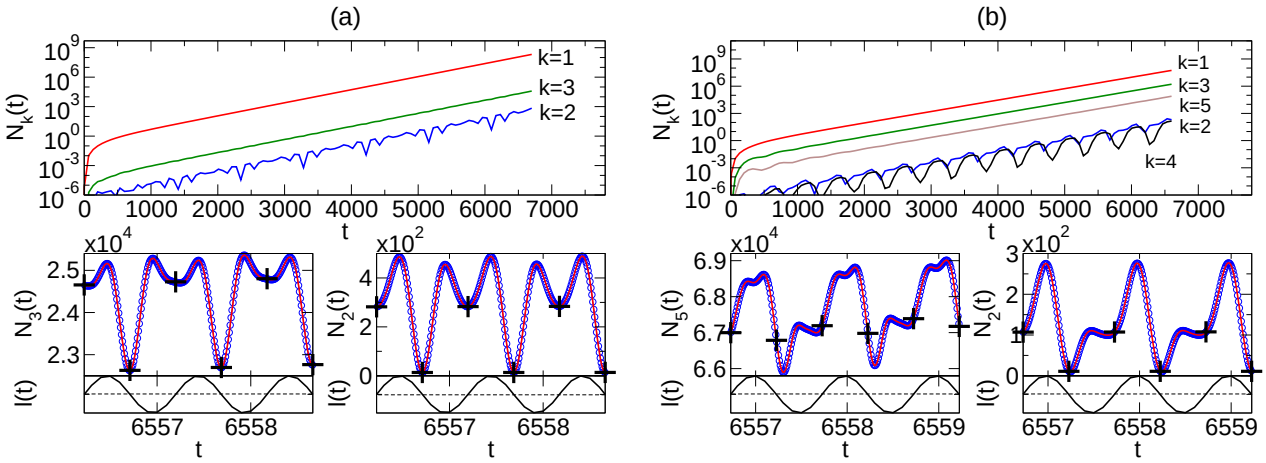

Figure 5.3: (a) Number of particles created in the modes $k = 1$, 2 and 3 for $M = 0.7$ and (b) number of particles created in the modes $k = 1, 2, 3, 4$ and 5 for $M = 0.2$, corresponding to the spectrum shown in Fig. 5.2 (b). The small plots are high resolution figures for the two time resolutions $\Delta t = 0.01$ (circles) and $\Delta t = 0.005$ (solid lines). The particle numbers calculated for times at which the mirror has returned to its initial position are accented by "+" and the background motion is shown for comparison as well.

whereas $\mathcal{N}_2$ itself oscillates strongly with an amplitude negligibly small compared to $\mathcal{N}_1$.
The small scale oscillations in the particle numbers are correlated with the periodic motion of the mirror which is depicted in the high resolution plots of Fig. 5.3 as well. One infers that the particle numbers show oscillations also when the expectation value (3.56) is calculated only for times at which the mirror has returned to its initial position l_0, i.e. if one uses Eq. (3.75). However, when calculating the particle number only after a full period of the mirror oscillations, no small scale oscillations in the particle numbers are left.

The observation that also higher modes become excited (even though they are very much suppressed) is explained by the fact, that two modes k and l are coupled even if Eq. (4.9) is not exactly satisfied by the two frequencies Ω_k^{in} and Ω_l^{in}. For $M = 0.7$ the equation $3\Omega_1^{\text{in}} = \Omega_k^{\text{in}}$ has no solution for integer k. Thus taking Eq. (4.9) as an exact equation only the resonant mode $n = 1$ should become excited and particle creation should take place in this mode exclusively. Inserting $M = 0.7$ one finds the solution $k \approx 3.07$ which is apparently

close enough to the integer value $k = 3$ to excite that mode.
For smaller values of M the solution of $3\Omega_1^{\text{in}} = \Omega_k^{\text{in}}$ approaches the value $k = 3$ and one has to expect that for sufficiently small values of M the mode coupling becomes again so strong that Eq. (5.35) does no longer describe the numerical results. This is the case for $M = 0.2$ yielding $k \approx 3.005$ for which a strong coupling between the modes $n = 1$ and $k = 3$ occurs. Furthermore, from Eq. (4.9) and the coupling of $n = 1$ to $k = 3$ follows $2\Omega_1^{\text{in}} + \Omega_3^{\text{in}} = \Omega_l^{\text{in}}$ which has $l \approx 5.004$ as solution, hence the mode $k = 3$ is coupled to the mode $l = 5$. In the same way the mode 5 is coupled to the mode 7. Thus interpreting Eq. (4.9) as $\omega_{\text{cav}} \simeq |\Omega_k^{\text{in}} \pm \Omega_l^{\text{in}}|$ explains the numerically computed particle spectrum for $M = 0.2$ [cf. Fig. 5.2 (b)] which shows similar features as the spectrum obtained for the massless case [cf. section 4.4.1].

One observes that for $M = 0.2$ also even modes become excited (like also for $M = 0.7$) which is not the case for $M = 0$, i.e. in the case of a one-dimensional cavity. These modes are dragged by the strongly excited modes (odd modes) and rapidly oscillate (like $\mathcal{N}_2$ for $M = 0.7$) with an amplitude several orders of magnitude smaller compared to $\mathcal{N}_1$, $\mathcal{N}_3$ and $\mathcal{N}_5$. In Fig. 5.3 (b) I show the number of particles created in the modes $k = 1$ to 5 for $M = 0.2$ to illustrate the just-stated. As for $M = 0.7$ the number of particles created in the odd modes increases exponentially showing oscillations superimposed on an average particle number, while the number of particles created in the even modes $k = 2$ and $k = 4$ consists mainly of oscillations with amplitudes much smaller compared to the number of particles created in the odd modes.

The fact that mode coupling occurs even if Eq. (4.9) is not satisfied exactly is well known. One can rewrite the expression $3\Omega_n^{\text{in}} \simeq \Omega_k^{\text{in}}$ to get $(3 + \kappa)\Omega_n^{\text{in}} = \Omega_k^{\text{in}}$ [Eq. (5.37)]. As mentioned at the end of the former section, for sufficiently small κ the modes n and k are still resonantly coupled, provided that no coupling to higher modes exists [62]. However, the case of two detuned coupled modes does not apply to the scenario discussed here. Decreasing the detuning, i.e. reducing the value of M, does not only strengthen the coupling between the modes $n = 1$ and $k = 3$ which would lead to an exponential growth of the particle number in both modes, but also enhances the coupling strength to higher modes $k = 5, 7, ...$ because the frequency spectrum becomes equidistant as $M \to 0$. The convergence of the numerical results towards the analytical expressions for the massless case is demonstrated below.

To study in more detail how the number of produced particles depends on the mass, I have performed numerical simulations for a wide range of values for M. The results are summarized in Fig. 5.4 in a "mass spectrum", where the number of particles created in the resonant mode $\mathcal{N}_1(t = 2000)$ is plotted as a function of M and compared to the analytical prediction Eq. (5.35). Particular values of M for which Eq. (4.9) gives integer solutions, i.e. exact (un-detuned) intermode coupling, are marked by arrows. Numerical results for these values are not included in the spectrum. Cases with exact coupling shall be discussed below.
The numerical values for $\mathcal{N}_1$ perfectly agree with the analytical prediction (5.35) for values of M larger than roughly $M \approx 0.6$. For masses smaller than this threshold value, the number of created particles is smaller compared to the analytical prediction. The mass spectrum has a maximum at $M \approx 0.4$, i.e. the production of particles in the resonant mode is most efficient for this particular mass. When $M < 0.4$ the number of created particles drops down and approaches the $M = 0$ result. The appearance of a maximum in the mass spectrum is clear from the above discussion. For the particular value $M = 0.4$ the equation $3\Omega_1^{\text{in}} = \Omega_k^{\text{in}}$ leads to a value $k = 3.02$ which is close enough to the integer solution $k = 3$ to couple this mode strongly to the resonant mode. On the other hand, the coupling to higher modes is still suppressed. Figure 5.5 (a) shows the particle spectrum obtained for $M = 0.4$ for different times, and in Fig. 5.5 (b) the time evolution of the number of particles created in the modes $k = 1, 2, 3$ and 4 is plotted. For the even modes $k = 2$ and 4 the same oscillating behavior is observed as for $M = 0.7$ and $M = 0.2$. But the coupling of the mode $k = 3$ to the mode $n = 1$ damps the evolution of the resonant mode.
For increasing masses larger than $M = 0.4$ the excitation of higher modes becomes more and more suppressed [cf Fig. 5.2 (a)]. Accordingly, the numerical results match the analytical expression (5.35) predicting that the number of created particles decreases with increasing mass. Decreasing the mass below $M = 0.4$ enhances the strength of the intermode coupling which results in a damping of the resonant mode $n = 1$. Consequently the number of particles produced in the resonant mode (and also the total particle number) is smaller than predicted analytically.

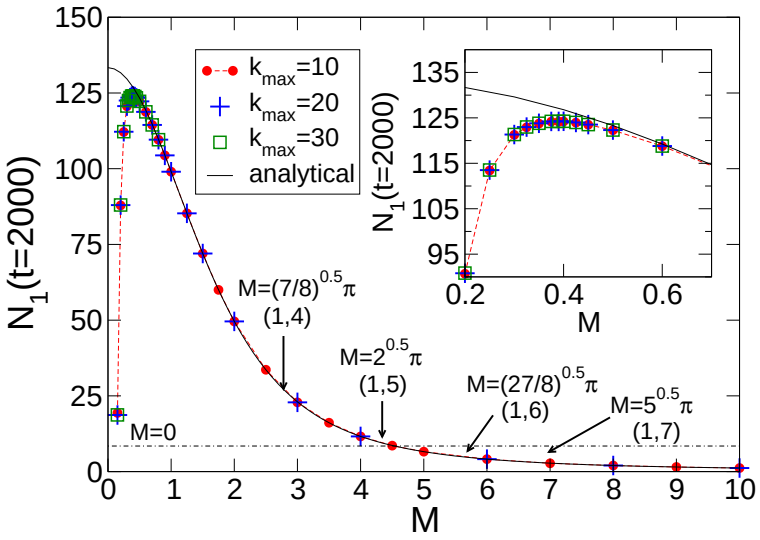

Figure 5.4: Number of particles created in the resonance mode $n = 1$ at time $t = 2000$ as a function of the mass parameter M. The solid line shows the analytical prediction Eq. (5.35). Arrows pointing towards particular values of M mark masses for which Eq. (5.35) is not valid because of exact intermode coupling. The coupled modes are given in brackets $[(1, k)]$. No numerical results are shown in the plot for these cases. Most of the numerical results are shown for different values of the cutoff $n_{\max}$ to underline stability.

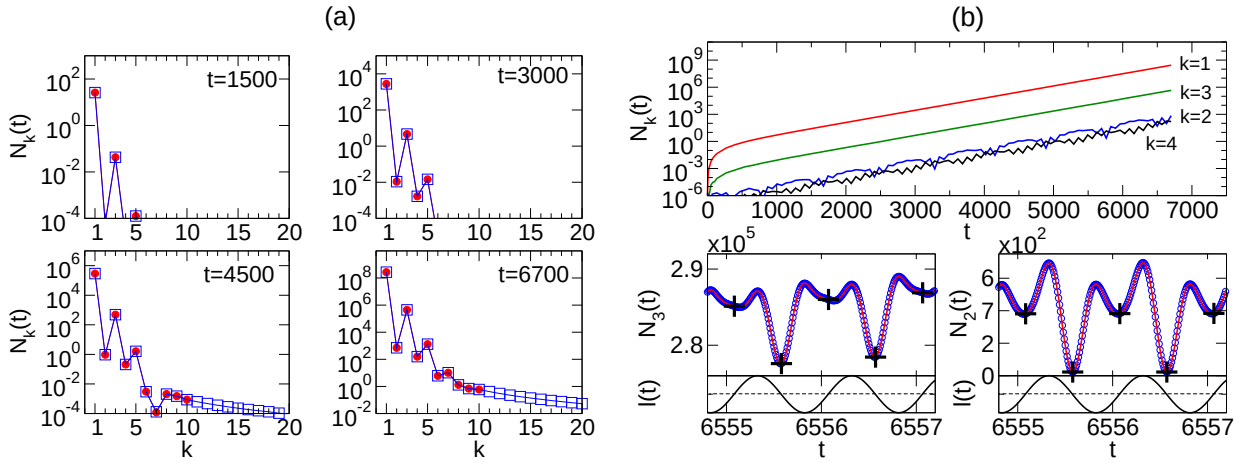

Figure 5.5: (a) Particle spectra for mass parameter $M = 0.4$ at times $t = 1500, 3000, 4500$ and 6700. Each spectrum is shown for values $n_{\max} = 10$ (dots) and $n_{\max} = 20$ (squares) to indicate numerical stability. (b) Upper panel: number of particles created in the modes $k = 1, 2, 3$ and 4 for the mass parameter $M = 0.4$ corresponding to the spectra shown in (a). Lower panels: $\mathcal{N}_3(t)$ and $\mathcal{N}_2(t)$ in each case for the two resolutions $\Delta t = 0.01$ (circles) and $\Delta t = 0.005$ (solid lines).

When studying the limit $M \to 0$, the numerical results should converge towards the well known results for the massless case studied in Section 4.4.1. This is demonstrated in Fig. 5.6 where the total particle number and the number of particles created in the resonant mode $n = 1$ are depicted for $M = 0.2, 0.15, 0.1$ and 0.05 up to $t = 500$ and compared with the analytical predictions for $M = 0$ [cf. Eqs. (4.10) and (4.11), Fig. 4.2 (c)]. While for $M = 0.2$ the total particle number $\mathcal{N}(t)$ is still mainly given by $\mathcal{N}_1(t)$, a divergency between $\mathcal{N}(t)$ and $\mathcal{N}_1(t)$ starts to become visible for $M = 0.15$, i.e. the influence of the intermode coupling gains importance. For $M = 0.1$ the numerical results are close to the analytical $M = 0$-results and are virtually identical with them for $M = 0.05$.

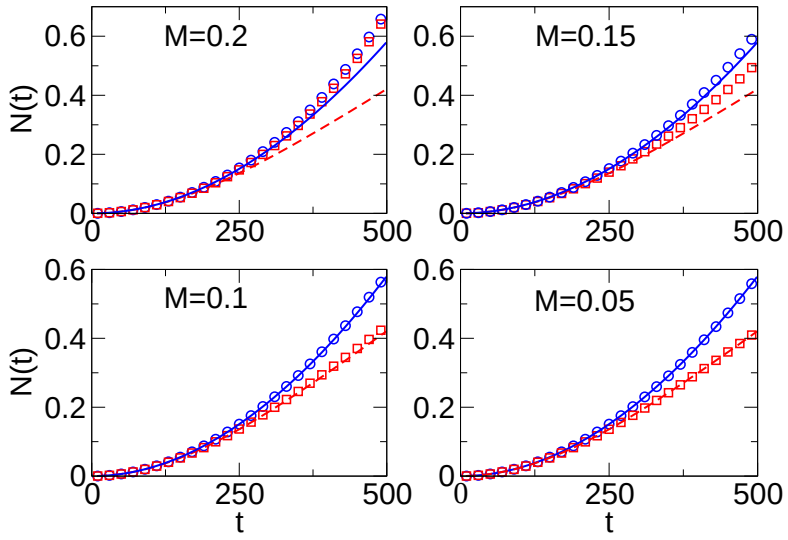

Figure 5.6: Total particle number $\mathcal{N}$ (circles) and number of particles created in the resonant mode $\mathcal{N}_1$ (squares) for mass parameters $M = 0.2, 0.15, 0.1$ and 0.05 together with the analytical predictions for the massless case Eq. (4.10) (dashed line) and Eq. (4.11) (solid line) to demonstrate the convergence of the solutions towards the $M = 0$ case. The cut-off parameter $n_{\max} = 30$ was used in the simulations.

I now turn to cases with exact coupling between two modes which takes place if Equation (4.9) has integer solutions. Exact coupling between two modes n and k occurs if Eq. (5.36) is satisfied. In [41] the authors derive analytical expressions (Eqs. (54) and (55) of [41]) for the case that the TE-mode $\Omega^{\rm in}_{(1,1,1)}$ (resonant mode) is coupled to the mode $\Omega^{\rm in}_{(5,1,1)}$, i.e. $3\Omega^{\rm in}_{(1,1,1)} = \Omega^{\rm in}_{(5,1,1)}$ is fulfilled. This particular case is equivalent to the coupling of the massive modes $n = 1$ and $k = 5$ if $M = \sqrt{2}\pi$ ($l_0 = 1$). Figure 5.7 (a) shows the particle spectrum at four different times. The cutoff parameter $n_{\max} = 20$ guarantees stability of the numerical results.

The numerical simulations confirm the prediction that virtually only the modes $n = 1$ and $k = 5$ become excited and particles are produced exclusively in the two coupled modes. Thereby the rate of particle creation is equal for the two modes. In Fig. 5.7 (b) I show the numerical results for $\mathcal{N}_1(t)$ and $\mathcal{N}_5(t)$ and compare them with the analytical expressions Eq. (54) and Eq. (55) of [41] derived via multiple scale analysis (MSA). Whereas the numerical results agree quite well with the analytical prediction of [41] for long times, one observes a discrepancy between the numerical results and the analytical predictions for "shorter times" up to $t \approx 3000$ ($\epsilon\pi\, t = 3\pi$). For long times, the analytical predictions nicely reproduce the large scale oscillations in the exponentially increasing particle numbers. But while the analytical expressions predict that for times $t < 500$ $\mathcal{N}_1$ and $\mathcal{N}_5$ increase with the same rate, I find from the numerical simulations that the production of particles in the mode $k = 5$ sets in after the production of particles in the $n = 1$-mode. Apart from the differences for short times the numerical results are well described by the analytical predictions of [41]. The discrepancy between the analytical predictions and the numerical results for short times is due to the fact that the multiple scale analysis in [41] only considers the resonant coupled modes, but for short enough times, all modes should be treated on an equal footing [49].
As a second example of exact coupling between two modes I show in Fig. 5.8 the numerical results obtained for $M = \sqrt{7/8}\pi$ for which the mode $n = 1$ is coupled to the mode $k = 4$.

Let me finally discuss another case with exact coupling of two modes which impressively demonstrates that strong coupling between modes k and l occurs even if Eq. (4.9) is satisfied only approximately. For $M = \sqrt{5}\pi$ equation (4.9) predicts that the mode $n = 1$ is exactly coupled to the mode $k = 7$. The equation $2\Omega^{\rm in}_1 = \Omega^{\rm in}_l - \Omega^{\rm in}_7$ is not satisfied by an integer l, but has the solution $l \approx 12.04$ which is close to the integer $l = 12$. Thus one expects a coupling of the mode $k = 7$ to the mode $l = 12$. In addition, one finds that the equation $2\Omega^{\rm in}_1 = \Omega^{\rm in}_m - \Omega^{\rm in}_{12}$ has solution $m \approx 16.96$, hence $l = 12$ is coupled to $m = 17$. In the same way the equation $2\Omega^{\rm in}_1 = \Omega^{\rm in}_j - \Omega^{\rm in}_{17}$ which is solved by $j \approx 21.93$ leads to a coupling between the modes $m = 17$ and $j = 22$. Hence, from the numerical simulations, one expects to find a particle spectrum which shows that particle creation takes place

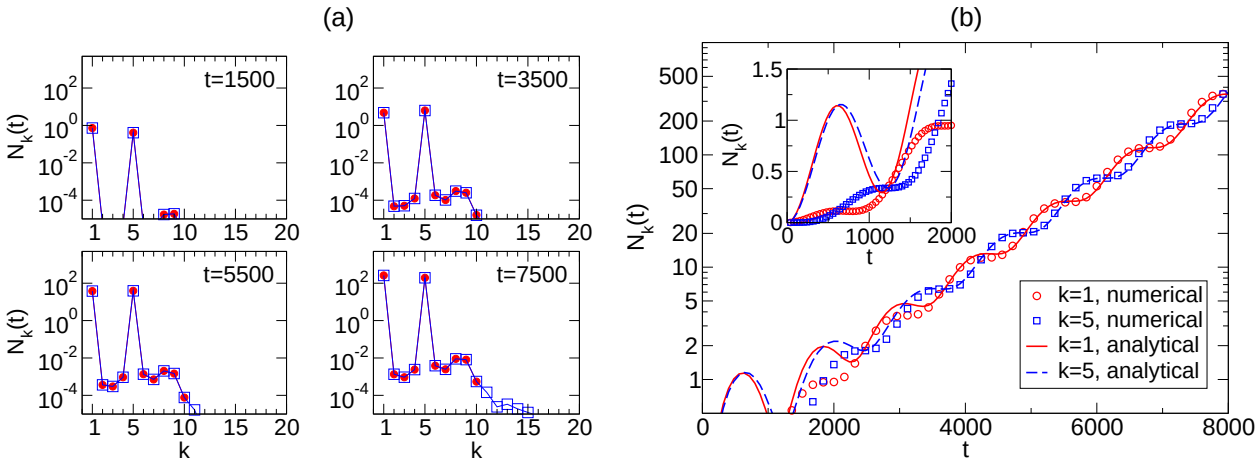

Figure 5.7: (a) Particle spectra for $\omega_{\rm cav} = 2\Omega_1^{\rm in}$ and mass parameter $M = \sqrt{2}\pi$ yielding exact coupling between the modes $n = 1$ and $k = 5$. Dots correspond to $n_{\rm max} = 10$ and squares to $n_{\rm max} = 20$. (b) Number of particles created in the modes $n = 1$ and $k = 5$ corresponding to the particle spectra depicted in (a). The numerical results are compared to the analytical predictions Eq. (54) [solid line] and Eq. (55) [dashed line] of [41]. The numerical results shown correspond to the cut-off parameter $n_{\rm max} = 20$.

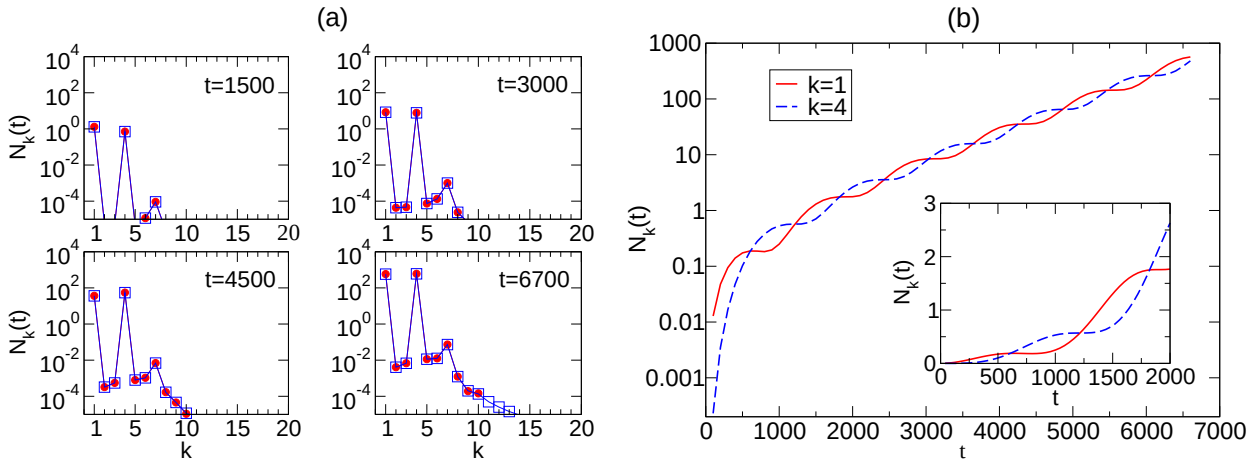

Figure 5.8: (a) Particle spectra for $\omega_{\rm cav} = 2\Omega_1^{\rm in}$ and mass parameter $M = \sqrt{7/8}\pi$ yielding exact coupling between the modes $n = 1$ and $k = 4$. Dots correspond to $n_{\rm max} = 10$ and squares to $n_{\rm max} = 20$. (b) Number of particles created in the modes $n = 1$ and $k = 4$ for $\omega_{\rm cav} = 2\Omega_1^{\rm in}$ and mass parameter $M = \sqrt{7/8}\pi$ corresponding to the particle spectra depicted in (a).

in the modes $k = 1, 7, 12, 17$ and 22. This is demonstrated in Fig. 5.9 (a) where the numerically evaluated particle spectrum is depicted for times $t = 500, 1000, 1500$ and 2000. The cutoff parameter $n_{\rm max} = 50$ ensures numerical stability in the integration range considered [2]. The corresponding number of created particles $\mathcal{N}_k(t)$ is shown in Fig. 5.9 (b) for the modes $k = 1, 7$ and 17.

Without having done a detailed analysis I find, as a reasonable approximation, that a mode l is (strongly) coupled to a given mode k whenever the ratio $|l - \tilde{l}|/l$ with $\tilde{l}$ denoting the solution of $2\Omega_n^{\rm in} = |\Omega_{\tilde{l}}^{\rm in} \pm \Omega_k^{\rm in}|$ is of the order of or smaller than 10^{-3}, i.e. of the order or smaller than ϵ used in the simulations.

[2] From Fig. 5.9 (a) one observes that also the mode $l = 27$ is weakly coupled. The equation $2\Omega_1^{\rm in} = \Omega_l^{\rm in} - \Omega_{22}^{\rm in}$ has the solution $l \approx 26.92$ which explains the excitation of the mode $l = 27$.

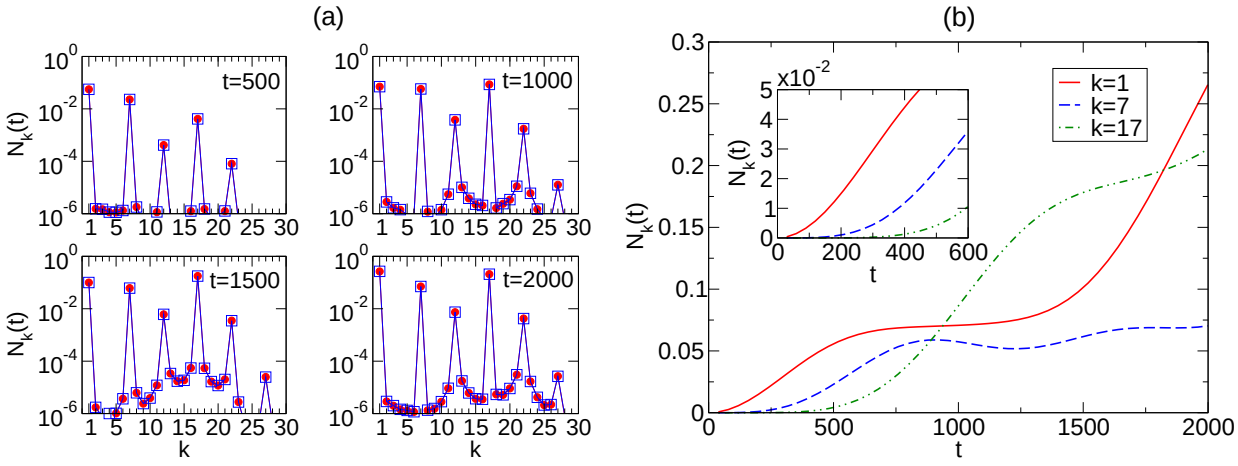

Figure 5.9: (a) Particle spectra for $\omega_{\rm cav} = 2\Omega_1^{\rm in}$ and mass parameter $M = \sqrt{5}\pi$. Dots correspond to $n_{\rm max} = 40$ and squares to $n_{\rm max} = 50$. (b) Number of particles created in the modes $n = 1$, $k = 7$ and $l = 17$ for $\omega_{\rm cav} = 2\Omega_1^{\rm in}$ and mass parameter $M = \sqrt{5}\pi$ corresponding to the particle spectra depicted in (a).

5.5 Discussion

The analogy between massive scalar particles and transverse electric photons in a three-dimensional rectangular cavity allows to interpret the presented numerical results in the following way: Consider a three-dimensional rectangular cavity with equally sized non-dynamical dimensions $l_y = l_z \equiv l_\parallel$. I parameterize the size of $l_\parallel$ in terms of the initial position l_0 of the dynamical cavity wall by introducing $\ell = l_\parallel/l_0$. If I restrict myself for simplicity to the case $n_y = n_z \equiv n_\parallel$, the dimensionless mass parameter M reads

$$M = l_0 k_\parallel = \sqrt{2}\left(\frac{n_\parallel \pi}{\ell}\right). \tag{5.38}$$

Therefore, for fixed $n_\parallel$, any value of M corresponds to a particular realization, i.e. size ℓ, of the non-dynamical cavity dimensions. Since I have shown that for a particular value M the production of massive scalar particles in the resonant mode is maximal, it is possible to maximize the production of TE-photons in a three-dimensional rectangular cavity by tuning the size ℓ of the non-dynamical cavity dimensions.

For instance, for $\omega_{\rm cav} = 2\Omega_1^{\rm in}$ the creation of massive scalar particles in the resonant mode $n = 1$ is most efficient for $M = 0.4$ (cf. Fig. 5.4). This corresponds to the three-dimensional case with $\omega_{\rm cav} = 2\Omega_{(1,1,1)}^{\rm in}$ and $\ell \approx 11$. Hence by designing the three-dimensional cavity such that $l_\parallel \approx 11\, l_0$ the production of TE-mode photons in the resonant mode $(1,1,1)$ can be maximized. In order to maximize the creation of TE-photons in the mode $(1,2,2)$ when $\omega_{\rm cav} = 2\Omega_{(1,2,2)}^{\rm in}$, the size $l_\parallel$ of the non-dynamical dimensions has to be doubled, i.e $l_\parallel \approx 22\, l_0$.
The strong coupling case $\omega_{\rm cav} = 2\Omega_1^{\rm in}$ with $M = 0.2$ where the analytical prediction (5.35) does not describe the numerical results due to enhanced intermode coupling [cf. Fig. 5.2] corresponds to the lowest TE-mode $(1,1,1)$ in a cavity of size $l_\parallel \approx 22\, l_0$.

Similarly one can arrange the size of the cavity such that particular modes are exactly coupled, i.e. Eq. (5.36) is satisfied. For instance, resonant coupling of the TE-modes $(1,1,1)$ and $(4,1,1)$ corresponds to $\omega_{\rm cav} = 2\Omega_1^{\rm in}$ with $M = \sqrt{7/8}\pi$ [cf Fig. 5.8] and is therefore realized in a cavity of size $l_\parallel \approx 1.5\, l_0$. Finally, choosing $l_\parallel \approx 0.63\, l_0$, i.e. $M = \sqrt{5}\pi$, couples the TE-modes $(1,1,1)$, $(7,1,1)$,$(12,1,1)$, $(17,1,1)$ and $(22,1,1)$ in the resonance case $\omega_{\rm cav} = 2\Omega_{(1,1,1)}^{\rm in}$ [cf Fig. 5.9].

In summary, the mass spectrum Fig. 5.4 can be interpreted in the following way if I set $n_\parallel = 1$ and $\omega_{\rm cav} = 2\Omega_{(1,1,1)}^{\rm in}$: For $l_\parallel = l_0$, i.e. cubic cavity, the modes $(1,1,1)$ and $(5,1,1)$ are resonantly coupled (see Fig. 5.7). Enlarging $l_\parallel$ with respect to l_0 increases the production of resonance mode photons $(1,1,1)$ until $l_\parallel \approx 1.5\, l_0$ ($M = \sqrt{7/8}\pi$) is approached where the modes $(1,1,1)$ and $(4,1,1)$ are exactly coupled, see Fig. 5.8. When increasing $l_\parallel$ further, photon creation in the TE-mode $(1,1,1)$ becomes more and more efficient and is

perfectly described by Eq. (5.35). Reaching $l_{\|} \approx 7.4\, l_0$ ($M \approx 0.6$, the threshold) the intermode coupling starts to become noticeable causing slight deviations of the numerical results from the analytical prediction. For $l_{\|} \approx 11\, l_0$ ($M \approx 0.4$), the production of TE-mode photons is most efficient. Thereby, the number of photons created in the mode $(1,1,1)$ is smaller than the analytical prediction Eq. (5.35) because of the coupling of the modes $(1,1,1)$ and $(3,1,1)$. When increasing $l_{\|}$ beyond $\approx 11\, l_0$, the strength of the intermode coupling is enhanced drastically, and consequently the number of produced TE-mode photons decreases rapidly. For $l_{\|} \approx 22\, l_0$, for instance, the mode $(1,1,1)$ is (strongly) coupled to the modes $(3,1,1)$ and $(5,1,1)$ [cf. Fig. 5.2(b)]. Reducing $l_{\|}$ with respect to l_0 (i.e. going to masses $M > \sqrt{2}\pi$) lowers the efficiency of photon creation in the resonant mode.

5.6 Outlook: TM-modes

The used formalism can, after some modifications resulting in a larger complexity of the numerics, also be employed to study the evolution of TM-modes. As the formalism depends inherently on the existence of a complete and orthonormal set of functions satisfying the BC's, the generalized Neumann BC $(\partial_x + v\partial_t)\Phi|_{l(t)} = 0$ cannot be treated directly using the (t,x)-coordinates. For a Neumann BC an orthonormal and complete set of functions is given by cosine functions, see footnote 3 in Section 3.4.3. In order to deal with the generalized Neumann BC, one can perform a particular coordinate transformation $(t,x) \to (\eta,\xi)$ involving the motion of the mirror itself. It is described in detail in [42]. The effect of this coordinate transformation is that, in the new coordinates, the mirror is still moving but the BC at the moving mirror becomes a usual Neumann BC $\partial_\xi \Phi|_{l(\eta)} = 0$. Then, a complete set of functions which can be used to expand the field are cosine functions $\phi_n(\eta,\xi) = \sqrt{2/l(\eta)}\cos(n\pi\,\xi/l(\eta))$. Being relatively complicated to deal with analytically without approximations, its numerical implementation is involved but straight forward. This is actually an ongoing project.

5.7 Observing quantum vacuum radiation

In contrast to its static counterpart, an experimental verification of the dynamical Casimir effect is still lacking. But before I briefly discuss experimental proposals, I should mention other phenomena and developments within the dynamical Casimir effect which are of importance in this context. So far, I have used the term "dynamical Casimir effect" for the production of photons by a moving mirror, for example in an empty cavity. A second possibility, and which goes under the same name, is the creation of photons from vacuum fluctuations in a cavity with space-time dependent dielectric properties [55, 141, 107, 191, 211]. For example, filling a whole cavity with a homogeneous medium described by a time-dependent permittivity $\epsilon(t)$ is analogous to introducing an effective cavity length $l_{\text{effective}}(t) = \sqrt{\epsilon(t)}l_0$ [211]. Worth mentioning are also studies of non-perfect boundary conditions [193, 194] and corrections due to finite temperature effects [176, 198, 106], two important and still not completely resolved (realistic BC's) problems which I do not consider in this thesis.

The main difficulty in designing an experiment aimed to verify the dynamical Casimir effect is that typical resonance frequencies of microwave cavities are of the order of gigahertz. From the experimental point of view, it is very difficult to construct a macroscopic mechanical device involving a wall oscillating at such a high frequency. However, progress is being made in this direction and a concrete experiment has been proposed [117, 118, 26].
A second proposal currently under debate which overcomes the mechanical problem is to mimic the mechanical motion of the mirror through a semiconducting layer whose reflectivity is driven by a laser at gigaherz frequencies [43, 22] (see also [5, 54, 196]).
Given the effort which is currently undertaken, it seems to be possible that the experimental verification of the phenomenon of quantum vacuum radiation will be accomplishable in the near future. One main result of this work, namely the finding that the rate of photon production can be maximized by tuning the size of the cavity, may be helpful for optimizing such an experiment.

Part II

Dynamical Casimir effect in braneworld cosmology

Chapter 6

The cosmological standard model

6.1 The observable Universe and the cosmological standard model

In this section I shall give a brief, by far not complete, description of the standard model of cosmology based on [151, 53, 129, 143].
The appropriate unit which is used by cosmologists to express distances in the Universe is *megaparsec*, abbreviated as Mpc. Thereby $1\,\mathrm{Mpc} = 3.26 \times 10^6$ light years which corresponds to $\simeq 3.1 \times 10^{22}\,\mathrm{m}$.
Galaxies, which may be regarded as the building blocks of the Universe, have a size of roughly 0.1 Mpc (large galaxies like our own). This includes a dark halo surrounding the galaxy which extends roughly 10 times as far and contains of order 10 times as much mass as the visible matter (stars, etc.) making up the galaxies. As the name suggests, the dark halo, made out of what is called dark matter (some, yet unknown, very weakly interacting form of matter), is not directly accessible through observations, but is needed to explain the rotation curves of the galaxies. The distance between the galaxies is roughly 1 Mpc with many of them existing in gravitationally bound clusters which contain several thousands of galaxies. Big clusters can reach a size of order 5 Mpc, so-called superclusters are even larger. Those are regions of space with a higher density than the average. On scales larger than 100 Mpc, however, the Universe, or more precisely the distribution of matter in it, appears to be very homogeneous.
On those scales where it is homogeneous, the Universe expands isotropically, i.e. the distance between any pair of galaxies is proportional to a universal *scale factor* a [cf. Eq. (6.2)] . That the Universe is expanding was discovered in 1929 by Hubble who found that galaxies move away from us (and from each other) with a speed $v = H\,d$ proportional to their distance d. The proportionality factor H is called *Hubble parameter*. Its value today is usually parameterized as

$$H_0 = 100\,h\,\frac{\mathrm{km}}{\mathrm{s}\cdot\mathrm{Mpc}} \tag{6.1}$$

with the numerical value $h \simeq 0.7$. Here and in the following I use the subscript "0" to denote the today's value of quantities.
The assumption of homogeneity and isotropy, i.e. the absence of a preferred place and a preferred direction, on large scales ($> 100\,\mathrm{Mpc}$) is the so-called *cosmological principle*. It implies that the spacetime geometry of the Universe is described by the *Friedmann-Lemaître-Robertson-Walker* -metric [cf. Eq. (6.2)]. Nowadays, the strongest evidence for the cosmological principle is the high level of isotropy of the Cosmic Microwave Background (CMB).
The CMB is a uniform background of photons with black body spectrum and a temperature of $\simeq 2.73\,\mathrm{K}$. It was discovered in 1965 by Penzias and Wilson and its precise measurements with missions like COBE (COsmic Background Explorer) and WMAP (Wilkinson Microwave Anisotropy Probe) have turned cosmology into a high precision science. The origin of the CMB radiation, first predicted by Gamov in 1948, lies in the very early Universe. It provides strong support for the picture of a hot and dense beginning of the Universe, the so-called *Hot Big Bang*. In such a dense initial phase until about 300,000 years after the Big Bang, the matter was fully ionized. Photons were tightly coupled to baryons and leptons through collision processes like Thomson scattering with cross section σ_T, leading to a black body spectral distribution of the photons. But as the Universe expands, the photon temperature decreases like $T \propto 1/a$. At a temperature of $\simeq 3000\,\mathrm{K}$, corresponding to an age of the Universe of $\simeq 300,000$ years, or equivalently energies $\simeq 0.25\,\mathrm{eV}$ much below the hydrogen ionization threshold (13.6 eV), the electrons combined with protons to form hydrogen atoms. The

result was a sudden decrease of the free electron density n_e and consequently the photon-electron interaction rate (Thomson scattering) $\Gamma \sim n_e \sigma_T$ became small compared to the expansion rate, $H \ll \Gamma$. After this *decoupling of matter and radiation*, the photons traveled freely through the Universe, maintaining the black body spectrum. Until today, their temperature has decreased down to 2.73 K due to expansion. Streaming nearly freely and undisturbed to us, the CMB radiation provides us with a snapshot of the Universe when it was only $\sim 300,000$ years old. Photons coming to us from different directions in the sky should have exactly the same temperature if the Universe was completely isotropic at the time of last scattering. Experiments have revealed that fluctuations ΔT in the CMB temperature exist, the so-called *CMB anisotropies*, which are of the order of $\Delta T/T \sim 10^{-5}$ (up to the dipole). This demonstrates that the Universe at last scattering was not perfectly but still very isotropic. The capability to explain the existence of the CMB radiation is a big success of the Hot Big Bang standard model.
Another important building block of the standard model is nucleosynthesis, i.e. the formation of nuclei from protons and neutrons, which took place at a temperature of $T \sim 1\,\mathrm{TeV}$ when the Universe was $\simeq 180$ seconds old. Based on the Hot Big Bang scenario, it succeeds to predict the measured abundances of light elements like hydrogen, helium, lithium and deuterium. Its predictions are very sensitive to the expansion rate H and thus to the total energy density [154, 23]. Therefore, the underlying particle theory, in particular what is called the effective number of species g_* at time of nucleosynthesis which is related to the energy density, is constraint. More importantly for this work, nucleosynthesis puts constraints on additional contributions to the total energy density (radiation), notably on the contribution of gravitational waves [154] (see Section 10.4.1).
As long as the Universe was younger than $t_{\mathrm{eq}} \simeq 3,000$ years, most of the the energy in the Universe was in the form of radiation. At time of "equality" t_{eq}, matter started to dominate over radiation and the Universe entered the matter era. Relatively recently, the Universe has become dominated by a yet unknown component called dark energy. Its density contributes to 70% to the total density and remains (relatively) constant with time, causing the Universe to accelerate. Structure formation leading to the large scale structure in the Universe set in when the Universe was $t \simeq 2 \times 10^8$ years old and has its origin in the small initial density perturbations which we observe as CMB anisotropies [172].

Despite its success in explaining the Hubble expansion of the Universe, the existence of the CMB radiation and the abundance of light elements via nucleosynthesis, the standard cosmological model had a number of shortcomings:

1. *Flatness problem*: Why is the Universe so close of being flat?
2. *Horizon problem*: Why do causally disconnected regions appear to be so similar?
3. *Origin of perturbations*: What mechanism did produce the small density perturbations we observe in the CMB and which are the seeds for structure formation?
4. *Monopole porblem*: Why do not we observe "dangerous relics" from early phase transitions like magnetic monopoles and other topological defects?

I shall abandon the idea to enter here into the details of all the problems since, as it is not directly related to the topic of this thesis, this would be too far-reaching. For a very pedagogical introduction see [144].
An idea which simultaneously solves all four cosmological puzzles is *inflation* [146, 88]. The basic idea of inflationary models is that, before the radiation era, the Universe underwent a period of superluminal expansion. One example is a so-called de Sitter phase, where the scale factor grows exponentially. Even an conclusive embedding of the paradigm of inflation into a more fundamental theory is still lacking, the agreement of its predictions with observations is very compelling.
In the remaining part of this Chapter I shall give a summary of basic equations governing the dynamics of an homogeneous and isotropic Universe and introduce gravitational waves.

6.2 Geometry of the Universe

Adopting the cosmological principle, the four-dimensional spacetime in the Universe is described by the Friedmann-Lemaître-Robertson-Walker (FLRW) metric [53, 206, 129]

$$ds^2 = g_{\mu\nu} dx^\mu dx^\nu = -d\tau^2 + a^2(\tau) dl^2 \quad \text{with} \quad dl^2 = \frac{dr^2}{1 - K\, r^2} + r^2 \left(d\theta^2 + \sin^2\theta d\varphi^2 \right) \tag{6.2}$$

where r, θ and φ are *comoving* polar coordinates and τ is the *proper* or *cosmological time* measured by a free-falling observer. The constant K determines the curvature of spacetime. It is positive for closed models, negative for open models and zero for a flat Universe. In the latter case, it is more convenient to replace the polar coordinates in (6.2) by euclidian coordinates, i.e. $dl^2 = \delta_{ij} dx^i dx^j$. The comoving coordinates remain fixed for any object which does not undergo any other motion except the expansion of the Universe itself. The expansion of the Universe is expressed in the *scale factor* $a(\tau)$.

The radial physical distance at proper time τ between us ($r = 0$) and an object at (fixed) comoving distance r is given by

$$r_{\text{phys}}(\tau) = a(\tau) \int_0^r \frac{dr'}{\sqrt{1 - Kr'^2}}. \tag{6.3}$$

In a flat Universe it is $r_{\text{phys}}(\tau) = a(\tau) r$, hence physical distances evolve with time due to cosmological expansion. If one assumes that there are no *peculiar velocities*, i.e. velocities with respect to the comoving coordinates, the velocity $v_{\text{phys}}(\tau)$ of an object at physical radial distance $r_{\text{phys}}(\tau)$ is

$$v_{\text{phys}}(\tau) = H(\tau) r_{\text{phys}}(\tau) \tag{6.4}$$

with the *Hubble parameter*

$$H(\tau) \equiv \frac{1}{a(\tau)} \frac{d\, a(\tau)}{d\tau}. \tag{6.5}$$

Equation (6.4) is the famous Hubble law stating that due to the expansion of the Universe all objects move away from each other. Thereby the escape velocities of, e.g. galaxies, are proportional to their distances. Another important quantity is the so-called *Hubble radius*

$$R_H = \frac{1}{H} \tag{6.6}$$

which roughly gives the distance light has been able to travel since the beginning of the Universe. Its todays value is $R_{H_0} \simeq 3000 h^{-1}\, Mpc$ [129] which is the radius of the observable Universe. Two times the Hubble radius $2R_H$ gives the *horizon size*. Regions in the Universe separated by a distance less than the horizon size are in causal contact.

It is sometimes convenient to work with *conformal time* η defined by

$$\eta = \int^\tau \frac{d\tau'}{a(\tau')} \tag{6.7}$$

in which the FRW-metric takes the form

$$ds^2 = a^2(\eta) \left[-d\eta^2 + dl^2 \right]. \tag{6.8}$$

The Hubble parameter $\mathcal{H}$ defined with respect to conformal time is related to H via

$$\mathcal{H} \equiv \frac{1}{a} \frac{d\, a}{d\eta} = H\, a. \tag{6.9}$$

6.3 Friedmann equations and cosmological solutions

The form of the FLRW-metric (6.2) is completely determined by the symmetry requirements of the cosmological principle. The only "unknown" is the scale factor a, or more precisely, its evolution in time, which is determined by the matter content of the Universe via the Einstein equations.

6.3.1 Einstein equations

In general relativity the dynamical variable is the metric $g_{\mu\nu}$ describing the gravitational field. The Einstein equations relate $g_{\mu\nu}$, i.e. the geometry of the spacetime, to the matter content in the Universe

$$G_{\mu\nu} + \Lambda_4 g_{\mu\nu} = \kappa_4 T_{\mu\nu}. \tag{6.10}$$

Λ_4 is a cosmological constant and κ_4 is the gravitational coupling constant. It is related to Newton's constant G_4 and the (four-dimensional) Planck mass $m_{\rm Pl}$ through

$$\kappa_4 = \frac{1}{M_4^2} = 8\pi G_4 = \frac{8\pi}{m_{\rm Pl}^2} \tag{6.11}$$

where $M_4 = m_{\rm Pl}/\sqrt{8\pi}$ is the *reduced Planck mass*.
The curvature is encoded in the Einstein tensor

$$G_{\mu\nu} = R_{\mu\nu} - \frac{1}{2} R\, g_{\mu\nu} \tag{6.12}$$

where $R_{\mu\nu}$ is the Ricci tensor and R the curvature scalar $R = R^\mu_\mu$. The Ricci tensor is defined as $R_{\mu\nu} = R^\gamma{}_{\mu\gamma\nu}$ where $R_{\gamma\delta\mu\nu}$ is the Riemann tensor

$$R^\mu_{\nu\lambda\rho} = \Gamma^\mu{}_{\nu\rho|\lambda} - \Gamma^\mu{}_{\nu\lambda|\rho} + \Gamma^\mu{}_{\sigma\lambda}\Gamma^\sigma{}_{\nu\rho} - \Gamma^\mu{}_{\sigma\rho}\Gamma^\sigma{}_{\nu\lambda} \tag{6.13}$$

with Christoffel symbols

$$\Gamma^\mu{}_{\lambda\rho} = \frac{1}{2} g^{\nu\sigma} \left(g_{\sigma\lambda|\rho} + g_{\sigma\rho|\lambda} - g_{\lambda\rho|\sigma} \right). \tag{6.14}$$

The matter content is described by the energy momentum tensor $T_{\mu\nu}$. Since the cosmological constant term has the form of vacuum energy it could be as well counted as part of the energy momentum tensor on the right hand side of the equation. The Einstein tensor satisfies the contracted Bianchi identities $G^{\mu\nu}{}_{||\nu} = 0$ in accordance with the local conservation law for the energy momentum tensor $T^{\mu\nu}{}_{||\nu} = 0$.

From the Lagrangian viewpoint, Einstein's equations in vacuum, i.e. $\Lambda_4 = 0$ and $T_{\mu\nu} = 0$, arise in a very natural way from variation of the *Einstein-Hilbert* action

$$\mathcal{S}_{\rm EH} = \frac{1}{2\kappa_4} \int \sqrt{-g}\, R\, d^4x \tag{6.15}$$

with respect to the metric $g_{\mu\nu}$ since [206, 217]

$$\frac{\delta\left(\sqrt{-g}\, R\right)}{\delta g^{\mu\nu}} = \sqrt{-g} \left(R_{\mu\nu} - \frac{1}{2} R\, g_{\mu\nu} \right) . \tag{6.16}$$

The full Einstein equations (6.10) follow accordingly from variation of the action

$$\mathcal{S} = \frac{1}{2\kappa_4} \int \sqrt{-g}\, \left(R - 2\Lambda_4 \right)\, d^4x + \mathcal{S}_{\rm matter} . \tag{6.17}$$

$\mathcal{S}_{\rm matter}$ is the action of the matter in the Universe whose variation with respect to the metric defines the energy momentum tensor [cf. Eq. (3.103)].

6.3.2 Friedmann equations

In order to solve Einsteins equation for the metric (6.2), i.e. to find the dynamics of the scale factor $a(\tau)$, one has to specify the energy momentum tensor. The most general form of $T_{\mu\nu}$ compatible with homogeneity and isotropy, i.e. compatible with the metric (6.2), is an energy momentum tensor which has the form of a *perfect fluid*

$$T_{\mu\nu} = \rho u_\mu u_\nu + P \left(g_{\mu\nu} + u_\mu u_\nu \right) \tag{6.18}$$

where u^μ is the four-velocity field of the fluid in the local rest frame $u^\mu = (1, \mathbf{0})$ [217, 206], i.e.

$$T^\mu_\nu = \mathrm{diag}\left(-\rho, P, P, P \right). \tag{6.19}$$

Here ρ is the energy density and P the pressure of the matter contained in the Universe. Both quantities can depend on time only.
Inserting the energy momentum tensor into the Einstein equations and evaluating the components of $G_{\mu\nu}$

for the metric (6.2) leads to the desired equations describing the evolution of the scale factor. From the 00-component one obtains the so-called *first Friedmann equation*

$$H^2 + \frac{K}{a^2} = \frac{\kappa_4}{3}\rho + \frac{\Lambda_4}{3} \tag{6.20}$$

with the Hubble parameter H defined in (6.5). It describes the expansion rate of the Universe depending on the energy content, the curvature and the cosmological constant. Combining the 11-component of the Einstein equations with the first Friedmann equation leads to the *second Friedmann equation*

$$\frac{1}{a}\frac{d^2\,a}{d\tau^2} = -\frac{\kappa_4}{6}\,(\rho + 3\,P) + \frac{\Lambda_4}{3}. \tag{6.21}$$

6.3.3 Continuity equation

As already noted in Section 3.6.3 on quantum field theory in a curved spacetime, the local conservation law $T^{\nu}_{\mu\,||\nu} = 0$ does in general (no Killing vectors) not lead to conserved quantities due to energy exchange with the gravitational field. However, when applied to the perfect fluid energy momentum tensor the $\nu = 0$ component yields the *continuity equation*

$$\frac{d\,\rho}{d\tau} = -3\,H\,(\rho + P)\ , \tag{6.22}$$

which describes (locally) the change of the energy density in a FLRW-Universe. The first term on the right hand side describes the dilution of energy due to the expansion of the Universe and the second term corresponds to the work done by pressure [143].
Note, that the two Friedmann equations (6.20), (6.21) and the continuity equation (6.22) are not all independent of each other, but only two of them. The continuity equation can be used, for example, to integrate the second Friedmann equation which leads to the first Friedmann equation.

6.3.4 Cosmological solutions

The energy density ρ and pressure P are often related via an equation of state

$$P = w\,\rho \tag{6.23}$$

where w is a constant. In this case, the continuity equation (6.22) can easily be integrated

$$\rho = \rho_0 a^{-3(1+w)}\ . \tag{6.24}$$

ρ_0 is an integration constant. Assuming that the Universe is flat, the first Friedmann equation can be solved with the aid of (6.24). Solutions corresponding to different kinds of matter are

- $w = 0$: non-relativistic matter (baryons)

$$\rho_{\rm m} \propto a^{-3}\ , \quad a \propto \tau^{2/3} \tag{6.25}$$

- $w = 1/3$: ultra-relativistic matter (radiation)

$$\rho_{\rm rad} \propto a^{-4}\ , \quad a \propto \tau^{1/2} \tag{6.26}$$

- $w = -1$: cosmological constant (vacuum energy)

$$\rho_{\Lambda_4} = \text{const.}\ , \quad a \propto e^{\tau}\ . \tag{6.27}$$

6.3.5 Critical density

The *critical density* $\rho_{\rm crit}$ is defined as the density which leads to a flat Universe with vanishing cosmological constant. Hence, from the first Friedmann equation

$$\rho_{\rm crit} = \frac{3\,H^2}{\kappa_4}. \tag{6.28}$$

With the parameterization (6.1) for the Hubble radius, the critical density today is $\rho_{\rm crit} = 1.88\, h^2\, 10^{-29}{\rm g/cm}^3$ [53]. With the aid of the critical density, the first Friedmann equation can be cast into a form which is useful for parameter estimations. One introduces the dimensionless density parameter Ω_i of some matter/energy component i as the ratio of the corresponding energy density ρ_i with respect to the critical density:

$$\Omega_i \equiv \frac{\rho_i}{\rho_{\rm crit}}. \tag{6.29}$$

The first Friedmann equation suggests to define an *effective curvature density* ρ_K

$$\rho_K = -\frac{3\,K^2}{\kappa_4\, a^2}\ . \tag{6.30}$$

Then, dividing by H^2, the first Friedmann equation is cast into the simple form

$$1 = \Omega_K + \Omega + \Omega_{\Lambda_4} \tag{6.31}$$

which relates all the matter components in a very instructive way. Here I do not have assigned any subscript to $\Omega = \rho/\rho_{\rm crit}$ since it is in general a composition of different components (radiation, baryons, etc).

6.4 Cosmological perturbations and gravitational waves

6.4.1 Cosmological perturbation theory

The smallness of the anisotropies in the CMB teach us that the early Universe can be described in a good first approximation by the FLRW-metric (6.2). Since at time of recombination the deviations from isotropy and homogeneity have been very small ($\sim 10^{-5}$) the deviations of the "real" early Universe from the FLRW-model can be studied perturbatively, i.e. by linearizing the equations around the FLRW-model. Cosmological perturbation theory is nowadays a very well developed tool and to give a broad introduction into this subject would be out of proportion for this thesis. I shall rather briefly outline the main ideas and then discuss only tensor perturbations (gravity waves) more detailed since their evolution in braneworld cosmology is the main subject of the following sections. References for cosmological perturbation theory are, for example, [207, 68, 165, 126, 12].
In the following I assume, as indicated by observations, that the Universe is flat, i.e. $K = 0$ in (6.2) such that $dl^2 = \delta_{ij} dx^i dx^j$. In addition I work in conformal time η instead of cosmic time τ. Consider now a perturbed metric

$$\tilde{g}_{\mu\nu} = g_{\mu\nu} + a^2\, \gamma_{\mu\nu} \tag{6.32}$$

where $g_{\mu\nu}(\eta) = a^2(\eta)\, \eta_{\mu\nu}$ is the flat FLRW-metric in conformal time. The perturbation $\gamma_{\mu\nu}$, assumed to be small, can be decomposed in components according to their transformation properties with respect to three-dimensional rotations. It contains scalar (spin-0), vector (spin-1) and tensor (spin-2) degrees of freedom. In linear perturbation theory, all those perturbations evolve independently of each other. This follows very generally from the so-called *decomposition theorem* (see, e.g.,[207, 53]). Consequently, the equations governing their dynamics are not coupled to each other which allows to treat them separately. There are, however, more degrees of freedom in the metric than physical modes; some are just gauge artifacts. Metric perturbations can thus be changed by gauge transformations, i.e. infinitesimal coordinate transformations. Only six physical degrees of freedom remain: two scalars, two vectors and two tensors, where tensor perturbations turn out to be gauge invariant. Scalar degrees of freedom correspond to the generalization of Newtonian gravity, vectors describe gravito-magnetism and tensors correspond to gravity waves [144]. Calculations can be performed by introducing gauge invariant quantities obeying gauge invariant equations of motion, like the so-called *Bardeen potentials* for the scalar degrees of freedom. Gauge invariant cosmological perturbation theory is nowadays not only very well developed, but also rather technical [68, 207]. Another way to proceed is to fix a gauge from the beginning and to use variables which are not gauge invariant. Their equations of motions have the correct number of independent solutions [144]. However, one has to be careful when extracting a physical meaning out of gauge dependent perturbations. Physical quantities, of course, are gauge invariant.
I shall now consider tensor perturbations in more detail.

6.4.2 Gravitational waves

Tensor perturbations of the metric are parameterized as [207, 53]

$$ds^2 = a^2(\eta)(\eta_{\mu\nu}dx^\mu dx^\nu + 2h_{\mu\nu}dx^\mu dx^\nu). \tag{6.33}$$

Here and in the following I restrict myself to a flat FLRW-spacetime and work in conformal time η. Tensor perturbations $h_{\mu\nu}(\eta, \mathbf{x})$ satisfy the *transverse traceless* (TT) gauge conditions

$$h_{00} = h_{0i} = h^i{}_i = h^j_{i\ |j} = 0, \tag{6.34}$$

and remain invariant under gauge transformations (see, e.g., [207]). The perturbed metric allowing for tensor perturbations can hence be written as

$$ds^2 = a^2(\eta)\left[-d\eta^2 + (\delta_{ij} + 2h_{ij})\, dx^i dx^j\right]. \tag{6.35}$$

Transversality and vanishing trace imply that tensor perturbations have two degrees of freedom, i.e. two polarization states $h_\times, h_+$. It is convenient to go into Fourier space. Introducing the unitary constant transverse-traceless polarization tensors $e^\bullet_{ij}(\mathbf{k})$ where $\bullet$ denotes the two polarizations, $h_{ij}(\eta, \mathbf{x})$ can be decomposed as

$$h_{ij}(\eta, \mathbf{x}) = \int \frac{d^3k}{(2\pi)^{3/2}} \sum_{\bullet=+,\times} e^{i\mathbf{k}\cdot\mathbf{x}} e^\bullet_{ij}(\mathbf{k}) h_\bullet(\eta, \mathbf{k})\ . \tag{6.36}$$

The polarization tensors satisfy (e.g.,[207])

$$e^\bullet_{ij} = e^\bullet_{ji}\ ,\ \ e^{\bullet\ i}_{\ i} = 0\ ,\ \ k^i e^\bullet_{ij}(\mathbf{k}) = 0\ ,\ \ e^\bullet_{ij}(-\mathbf{k}) = \left(e^\bullet_{ij}(\mathbf{k})\right)^*\ , \tag{6.37}$$

as well as

$$e^{\bullet\ j}_i(\mathbf{k}) \left[e^{i\ \bullet'}_j(\mathbf{k})\right]^* = \delta_{\bullet\bullet'}\ . \tag{6.38}$$

Note that the last relation implies

$$\sum_\bullet e^\bullet_{ij}(\mathbf{k}) \left(e^{\bullet\ ij}(\mathbf{k})\right)^* = 2\ . \tag{6.39}$$

Demanding that h_{ij} be real leads to

$$h^*_\bullet(\eta, \mathbf{k}) = h_\bullet(\eta, -\mathbf{k})\ . \tag{6.40}$$

If one fixes a coordinate system in which $\mathbf{k} = k\,\hat{z}$, i.e. the wave propagates into the z-direction, the perturbation has the form

$$h_{ij} = \begin{pmatrix} h_+ & h_\times & 0 \\ h_\times & -h_+ & 0 \\ 0 & 0 & 0 \end{pmatrix}. \tag{6.41}$$

From the linearly perturbed Einstein equations it follows that the tensor amplitudes $h_\bullet(\eta; k)$ satisfy a damped wave equation

$$\frac{\partial^2}{\partial\eta^2} h_\bullet(\eta, \mathbf{k}) + 2\mathcal{H}\frac{\partial}{\partial\eta} h_\bullet(\eta, \mathbf{k}) + k^2 h_\bullet(\eta, \mathbf{k}) = 0. \tag{6.42}$$

$\mathcal{H}$ is the Hubble parameter in conformal time [cf. Eq. (6.9)]. Furthermore it is assumed that the Universe is filled with a perfect fluid only, i.e. anisotropic stresses (perturbations of the energy momentum tensor) are absent. Equation (6.42) describes the propagation of tensor perturbations or gravity waves which are "propagating ripples in the spacetime curvature" on scales much smaller than the characteristic scales of the background, i.e. the Hubble radius in the cosmological context. Quantization of this equation leads to the definition of gravitons, i.e. massless spin-2 particles. This will be discussed below in more detail.
Deriving Equation (6.42) from the variation of the Einstein-Hilbert action (6.15) is tedious [207, 165]. The result is that the quadratic part of the Einstein-Hilbert action which corresponds to tensor perturbations reads [207]

$$\mathcal{S}^{(2)} = \frac{1}{2\kappa_4}\int d\eta \int d^3x a^2 \left[\left(\frac{\partial}{\partial\eta} h^i{}_k\right)\left(\frac{\partial}{\partial\eta} h^k{}_i\right) - h^i{}_{k|l} h^{k\ \ |l}_{\ i}\right]\ . \tag{6.43}$$

Here it is important to note that the indices are lowered and raised with respect to δ_{ij}. Inserting the expansion (6.36) and using the properties of the polarization tensors leads to

$$\mathcal{S}^{(2)} = \frac{1}{2\kappa_4}\int d\eta \int d^3k\, a^2 \sum_\bullet \left[\left|\frac{\partial}{\partial\eta} h_\bullet(\eta, \mathbf{k})\right|^2 - k^2 |h_\bullet(\eta, \mathbf{k})|^2\right]. \tag{6.44}$$

The Euler-Lagrange equations give now immediately (6.42).

6.5 Amplification of gravitational waves and inflation

As mentioned earlier, the shortcomings of the standard big bang scenario are solved by an early epoch of acceleration, called inflation. In Eq. (6.42) the dynamics of the scale factor enters into the friction term. It comes certainly not as a surprise that the problem of gravitational waves in a FLRW-Universe belongs to the class of scenarios discussed in the first part of the thesis; external field problems. Hence, depending on the background motion, amplification of gravitational waves may take place, in particular during inflation. Consequently, after quantization and provided that a meaningful vacuum and particle definition is possible, this corresponds to the creation of gravitons, i.e. massless spin-2 particles. This shall now be discussed.

6.5.1 Quantum generation of gravity waves

If one introduces a new variable

$$q_\bullet(\eta,\mathbf{k}) = \frac{1}{\sqrt{\kappa_4}} h_\bullet(\eta,\mathbf{k})\, a(\eta)\ , \tag{6.45}$$

Equation (6.42) takes the familiar form of an oscillator

$$\frac{\partial^2 q_\bullet(\eta,\mathbf{k})}{\partial\eta^2} + \Omega^2(\eta,k) q_\bullet(\eta,\mathbf{k}) = 0 \tag{6.46}$$

with background dependent *frequency* or *effective mass*

$$\Omega^2(\eta,k) = k^2 - \frac{\partial\mathcal{H}}{\partial\eta} - \mathcal{H}^2 = k^2 - \frac{1}{a}\frac{\partial^2 a}{\partial\eta^2}\ . \tag{6.47}$$

Note, that in a radiation dominated Universe $a \propto \eta$ and thus $\Omega^2(\eta,k) = k^2$. The solutions to (6.46) are then just plane waves. The factor $1/\sqrt{\kappa_4}$ in (6.45) has been introduced to make $q_\bullet(\eta,k)$ canonically normalized. Indeed, Eq. (6.46) can be derived from the Hamiltonian [144]

$$H = \sum_\bullet \frac{1}{2}\int d^3k \left[|p_\bullet(\eta,\mathbf{k})|^2 + k^2|q_\bullet(\eta,\mathbf{k})|^2 + 2\mathcal{H}p_\bullet(\eta,\mathbf{k})q_\bullet(\eta,\mathbf{k})\right] \tag{6.48}$$

with canonical momentum

$$p_\bullet(\eta,\mathbf{k}) = \frac{\partial}{\partial\eta} q_\bullet(\eta,-\mathbf{k}) - \mathcal{H} q_\bullet(\eta,-\mathbf{k})\ . \tag{6.49}$$

This canonical Hamiltonian follows directly from the action for $q_\bullet(\eta,\mathbf{k})$ which is obtained by inserting (6.45) into the action (6.44).
Formally one can now promote the canonical variable $q_\bullet(\eta,\mathbf{k})$ to an operator and expand it in annihilation and creation operators

$$\hat{q}_\bullet(\eta,\mathbf{k}) = v(\eta,k)\hat{a}_{\mathbf{k},\bullet} + v^*(\eta,k)\hat{a}^\dagger_{-\mathbf{k},\bullet}\ , \tag{6.50}$$

and demand the commutation relations

$$\left[\hat{a}_{\mathbf{k},\bullet}, \hat{a}^\dagger_{\mathbf{k}',\bullet'}\right] = \delta_{\bullet\bullet'}\delta^{(3)}(\mathbf{k}-\mathbf{k}')\ ,\ \ [\hat{a}_{\mathbf{k},\bullet}, \hat{a}_{\mathbf{k}',\bullet'}] = \left[\hat{a}^\dagger_{\mathbf{k},\bullet}, \hat{a}^\dagger_{\mathbf{k}',\bullet'}\right] = 0\ . \tag{6.51}$$

Then, the complex functions $v(\eta,\mathbf{k})$ are also solutions to (6.46). Of course, the vacuum state $|0\rangle$ onto which these operators act and their very meaning as particle operators has to be justified. In Chapter 3 this was done by demanding that the motion of the background ceases for some initial and final time such that the canonical Hamiltonian describing the quantized field becomes the usual collection of independent oscillators and corresponds to the energy of the field. Here in the cosmological context, and in particular in an inflationary scenario as I shall discuss below, a particle interpretation can be given for modes which are deep inside the horizon. Those modes with physical wavelength

$$\lambda_{\rm phys} \sim a/k \tag{6.52}$$

much smaller than the Hubble radius $1/H$ behave virtually as Minkowski modes. Since, in that limit, $k \gg aH = \mathcal{H}$, and thus the Hamiltonian (6.48) and the equation of motion (6.46) reduce to the standard oscillator types. Consequently,

$$v(\eta,k) = \frac{1}{\sqrt{2k}} e^{-ik\eta}\ ,\ \ k \gg aH \tag{6.53}$$

is a positive frequency solution which can be used to define an annihilation operator.

A background of gravitational waves generated during inflation, for example, could be observed due to its contribution to the anisotropies of the CMB or directly in future gravity wave experiments. Related to observations can be the power spectrum $\mathcal{P}_h(k)$ and the energy density ρ_h of the gravitational waves, which I shall now define.

6.5.2 Power spectrum

The power spectrum of gravitational waves is defined as (see, e.g., [207])

$$\frac{(2\pi)^3}{k^3}\mathcal{P}_h(k)\delta^{(3)}(\mathbf{k}-\mathbf{k}') = \sum_{\bullet}\langle 0|\hat{h}_\bullet(\eta,\mathbf{k})\hat{h}^\dagger_\bullet(\eta,\mathbf{k}')|0\rangle \tag{6.54}$$

with [cf. Eqs. (6.45), (6.50)]

$$\hat{h}_\bullet(\eta,\mathbf{k}) = \sqrt{\kappa_4}\,\frac{\hat{q}_\bullet(\eta,\mathbf{k})}{a}. \tag{6.55}$$

Note that different authors adopt different definitions for the power spectrum, in particular when the distribution of numerical factors like π is concerned. Using the commutation relations readily leads to

$$\mathcal{P}_h(k) = 2\,\frac{k^3}{(2\pi)^3}\frac{\kappa_4}{a^2}|v(\eta,k)|^2, \tag{6.56}$$

i.e., the power spectrum is completely determined by the solutions $v(\eta,k)$.

6.5.3 Energy density

In an averaged sense, it is also possible to associate an *effective* energy-momentum tensor with gravitational waves (see [207, 154] and in particular [159] for a careful discussion). The effective energy-momentum tensor is defined as (recall that the perturbed metric is $\eta_{\mu\nu}+2h_{\mu\nu}$)

$$T^{\rm GW}_{\mu\nu} = \frac{1}{\kappa_4}\left\langle h_{\rho\sigma||\mu}h^{\rho\sigma}{}_{||\nu}\right\rangle. \tag{6.57}$$

where "$||$" denotes the covariant derivative with respect to the unperturbed background metric, and the bracket stands for a four-dimensional average over regions of several wave lengths [207]. For the TT-gauge (6.34) the energy density ρ_h of gravitational radiation is then given by the 00-component of (6.57)

$$\rho_h = \frac{1}{\kappa_4}\left\langle(\partial_\tau h_{ij})(\partial_\tau h^{ij})\right\rangle = \frac{1}{\kappa_4\,a^2}\left\langle(\partial_\eta h_{ij})(\partial_\eta h^{ij})\right\rangle\ . \tag{6.58}$$

6.5.4 De-Sitter inflation

As an explicit example, let me finally discuss the generation of gravitational waves during inflation in the limit of an exact de Sitter stage. It is assumed that an inflationary phase takes place between two times τ_i and τ_f and the Universe enters a radiation dominated stage for times $\tau > \tau_f$. Exact de Sitter inflation is characterized by $a(\tau) = e^{H\tau}$ with $H = $ const and thus $\eta = -1/\mathcal{H}$ with $\eta \in (-\infty, 0)$. The differential equation for the functions $v(\eta,k)$ takes the form

$$\frac{\partial^2}{\partial\eta^2}v(\eta,k) + \left(k^2 - \frac{2}{\eta^2}\right)v(\eta,k) = 0\ . \tag{6.59}$$

The solution with the right asymptotics, i.e. which for $k \gg \mathcal{H}$ or equivalently $-k\eta \gg 1$ behaves as (6.53) is given by

$$v(\eta,k) = \frac{1}{\sqrt{2k}}\left(1 - \frac{i}{k\,\eta}\right)e^{-ik\eta}. \tag{6.60}$$

During de Sitter inflation, the Hubble radius $R_H = 1/H$ remains constant while the physical wavelength of the modes gets stretched $\lambda_{\rm phys} \sim e^{H\tau}/k$; they leave the horizon. Eventually, in a subsequent radiation and later matter dominated stage when the Hubble radius increases, they re-enter the horizon. Those perturbations

on super-Hubble scales, i.e. $k \ll aH$, are the ones which contribute to the CMB anisotropies. In the long wavelength limit $k \to 0$ the equation of motion for $v(\eta, k)$ reduces to

$$\frac{\partial^2}{\partial\eta^2} v(\eta, k) + \frac{1}{a}\frac{\partial^2 a}{\partial\eta^2} v(\eta, k) = 0 \ , \tag{6.61}$$

which has two solutions $v_1 \propto a$ and $v_2 \propto a \int d\eta/a^2$. Since the second one is a decaying solution it implies that $h_\bullet$ is approximately constant. Consequently, on super-Hubble scales the primordial spectrum of gravitational waves which enters observable quantities can be evaluated at the end of inflation. The corresponding large wavelength solution, i.e. $k \ll aH$ or $\eta k \to 0$, is

$$v(\eta, k) = \frac{iaH}{\sqrt{2k^3}} \ , \quad k \ll aH \ . \tag{6.62}$$

Inserting this expression into (6.56) leads to

$$\mathcal{P}_h(k) = \frac{\kappa_4 \, H^2}{(2\pi)^3} \ . \tag{6.63}$$

The power spectrum of gravitational waves generated during de Sitter inflation does not depend on the wave number k. Such a *scale invariant* spectrum is sometimes called *Harrison - Zel'dovich* spectrum.
Other inflationary models like power-law inflation where the Hubble parameter is not constant predict a nearly scale invariant spectrum of perturbations, not only for tensor but also for scalar perturbations. Thereby the scale invariance of the tensor spectrum is parameterized by the *spectral tilt* n_T, with $n_T = 0$ corresponding to scale invariance. The spectral tilt is given in terms of the so-called slow roll parameters. Those are linked to the features of the potential which the so-called *inflaton* field is rolling down when it drives the inflationary phase.
The approximate scale invariance of the power spectrum is a striking prediction of inflation and is nowadays confirmed by CMB observations with an impressive precision [144].

Chapter 7

Extra dimensions and braneworlds

In this section I shall give a brief introduction to extra dimensions and braneworld models. The presented material is partly based on the reviews [190, 136, 69, 173, 185].

7.1 Extra dimensions - An overview

The idea that our Universe has more than three spatial dimensions goes back to the 1920s. In an attempt to unify gravity and electromagnetism Theodor Kaluza [110] and Oscar Klein [119] discovered that the four-dimensional gravitational and electromagnetic fields can be understood as the components of the metric tensor in a theory with a compact fifth-dimension.
The quest for a theory unifying gravity and gauge interactions has led to theories and models that involve new extra spatial dimensions. Nowadays, the most successful candidate for such a unified theory is *String theory* [177, 178] whose fundamental constituents are no longer point particles, but one-dimensional objects called strings. Characterized by a *tension* (energy per unit length) their excitations give rise to states representing various massless and massive particles, including a massless spin-2 state, the graviton. Since superstring theory can be consistently formulated only in ten spacetime dimensions, extra dimensions are a natural ingredient for string theory.

If extra dimensions are compactified ("curled up") on, e.g., a torus of small radii with sizes of the order of the Planck length $L_p \sim 10^{-35}\,\mathrm{m}$, they would be completely hidden to experiments explaining why our world looks four dimensional. But if they were larger, what would be their influence in our four-dimensional world? One striking feature of models with extra dimensions is that a massless field defined in a theory involving compact extra dimensions would appear as an entire tower of massive fields when seen from four dimensions. Thereby the masses correspond to the (quantized) momenta of the field modes with respect to the extra dimensions and are thus inversely related to their size. Similarly, a higher dimensional massive field looks like a collection of massive fields, usually called the *Kaluza-Klein tower*, where the original mass is lifted by the (quantized) momenta with respect to the extra dimensions. Since this is true for any standard model field, compact extra dimensions imply the existence of identical copies of standard model particles but with different masses, notably a massive photon. From the fact that no such Kaluza-Klein particles have been seen in colliders so far leads to upper bounds on the size of the compact dimensions of the order of $\sim (200\mathrm{GeV})^{-1}$ or $\sim 10^{-18}$m. Explicit derivations are given in 7.2.
On the other hand, the presence of extra dimensions modifies Newton's law on small scales, i.e. on scales smaller or comparable to the size of the extra dimensions. If n is the number of extra dimensions, the gravitational force on small scales is $\propto 1/r^{2+n}$. The fact that Newton's law has been tested down to scales of ~ 0.1mm only leaves the possibility for large extra dimensions, provided that the Kaluza-Klein bound can be evaded. With such large extra dimensions it is possible to address the *hierarchy problem*, i.e. the vast unnatural discrepancy between the Planck scale $\sim 10^{19}$GeV and the electroweak scale $\sim 1\,\mathrm{TeV} = 10^3\,\mathrm{GeV}$ since the fundamental gravity scale departs from the Planck scale once extra dimensions are introduced. I shall discuss this more detailed in 7.3.

The Kaluza-Klein bound on the size of the extra dimension is evaded in the *braneworld scenario* where the standard model of particle physics is constrained to live on a hypersurface, a so-called *3-brane*. Extra dimen-

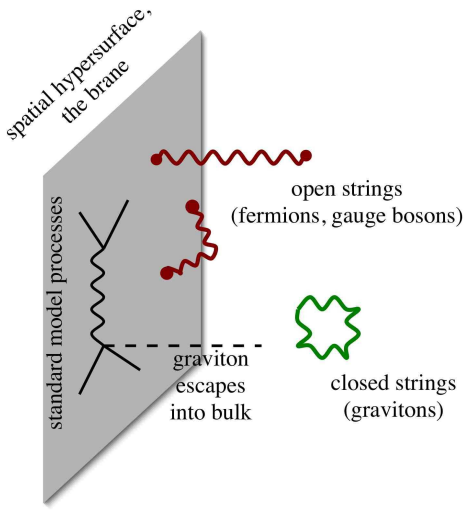

Figure 7.1: Pictorial presentation of the braneworld idea: a 3-brane in a higher-dimensional bulk. While standard model fields (open strings) are confined to the brane, gravitons (closed strings) propagate in the whole bulk.

sions can then be probed by gravity only. In 7.4 I briefly introduce the *ADD-brane model*. "ADD" stands for Arkani-Hamed, Dimopoulos and Dvali who introduced such a brane model in 1998 [6] in order to solve the hierarchy problem. Only one year later Randall and Sundrum presented there braneworld models, *RS-models I and II*. While in the ADD model the brane is considered as a hypersurface within a higher dimensional flat spacetime, the *bulk*, it is treated as physical self-gravitating object in the RS case. The bulk is five dimensional and has a negative cosmological constant $\Lambda_5 < 0$, implying that the fifth dimension is a slice of an Anti de-Sitter space. Such curved extra dimensions are usually referred to as *warped extra dimensions*. While in the RS I model [181] with two flat branes at the edges of the bulk, the warping leads to an interesting solution of the hierarchy problem, it localizes four-dimensional gravity on the brane in the RS II model [182] with one brane. Chapter 8 is devoted to the discussion of the RS scenario and its extension to braneworld cosmology.

The idea that the standard model is confined to a hypersurface is a picture that resembles *D-brane* constructions in string theory [179, 180, 8]. Thereby "D" stands for *Dirichlet*. Following Polchinski, "D-branes are extended objects, topological defects in a sense, defined by the property that strings can end on them". In String theory, standard model particles correspond to open strings and are naturally confined to a hypersurface since their endpoints are attached to the D-brane. Gravitons, on the other hand, correspond to closed strings and therefore propagate in the whole higher-dimensional space, cf. Figure 7.1. The braneworld setup consisting of hypersurfaces onto which standard model fields are confined does therefore naturally arise in String theory. For realizations within several string models see, e.g., [94, 95, 3, 201, 108].

Even though the braneworld picture has received a lot of attention since 1998/99 it is important to mention that similar ideas involving the localizing fermions on walls date back to the 1980's [189].

7.2 Kaluza-Klein modes

To demonstrate the appearance of Kaluza-Klein (KK) modes and their consequences in models with extra dimensions I shall consider a free non-interacting massive real scalar field $\Phi(x^\mu, y)$ in a five-dimensional Minkowski spacetime where the fifth dimension is compactified on a circle of radius R. The coordinates of the usual four-dimensional spacetime are denoted by x^μ and the extra dimension by y. Compactifying the fifth dimension on a circle means that the points y and $y + 2\pi R$ are identified. This implies the periodicity condition

$$\Phi(x^\mu, y) = \Phi(x^\mu, y + 2\pi R) \tag{7.1}$$

for the field Φ. The dynamics of the field is governed by the Klein-Gordon equation [1]

$$\left[\Box_{(5)} - \mathfrak{m}^2\right] \Phi(x^\mu, y) = 0 \tag{7.2}$$

with

$$\Box_{(5)} = \Box_{(4)} + \partial_y^2 = -\partial_t^2 + \triangle_3 + \partial_y^2. \tag{7.3}$$

Separability of the equation allows to expand a solution in eigenfunctions of ∂_y^2, i.e. a Fourier decomposition with respect to the extra dimension:

$$\Phi(x^\mu, y) = \sum_{n=0}^{\infty} \phi_n(x^\mu) e^{i\,n\,y/R}. \tag{7.4}$$

The spectrum of ∂_y^2 is discrete due to the periodicity condition (7.1) and takes the values $(n/R)^2$ for $n = 0, 1, 2, ...$, which is nothing else than the squared momentum associated with the fifth dimension. Consequently, every mode $\phi_n(x^\mu)$ satisfies the usual four-dimensional Klein-Gordon equation

$$\left[\Box_{(4)} - m_n^2\right] \phi_n(x^\mu) = 0 \tag{7.5}$$

with an "effective mass"

$$m_n = \sqrt{\mathfrak{m}^2 + \left(\frac{n}{R}\right)^2} \tag{7.6}$$

which depends on the size (compactification radius) of the extra dimension. This shows that a five-dimensional massive field is equivalent to a collection of (infinitely many) four-dimensional fields of masses m_n forming the KK tower. The lowest mode is the *zero mode* $n = 0$ which is constant throughout the extra dimension. Discussed here only for the simple case of a scalar field, the same is of course true for any standard model field. Hence a signature of an extra dimension would be the detection of such KK modes. For an observer in usual four-dimensional spacetime who does not know about the extra dimension, KK particles appear as copies of usual four-dimensional particles but with different masses. Therefore, KK particles related to such a compact extra dimension should be detectable in colliders if the energy scale reached in colliders exceeds the mass of the KK particles. That no KK particles have been seen so far gives us an upper bound on the size R of the compact extra dimension. Assuming that $1/R \gg \mathfrak{m}$, the mass of the first KK mode is $\sim 1/R$ such that an energy scale of $E \gtrsim 1/R$ is needed to excite that mode. Nowadays, the typical energy scale reached in colliders is $\sim 200\text{GeV}$, which translates into a limit for the maximal radius $R_{\max}$ of the compact extra dimension

$$R_{\max} \sim 10^{-18}\,\text{m} \tag{7.7}$$

(see, e.g.,[136]). At energy scales much lower than this threshold, physics is effectively four dimensional and one can integrate out the dependence on the extra dimension to obtain an effective low energy theory.

7.3 Gravity and extra dimensions

So far I have shown what the existence of extra dimensions implies for standard model fields: the existence of KK particles. Now I shall discuss how gravity, in particular Newton's law, is modified in the presence of extra dimensions. Thereby I consider a flat $D = d+1$ dimensional spacetime with $d = 3+n$ spatial dimensions where n denotes the number of extra dimensions. First I assume the extra dimensions to be non-compact to derive Newton's law generalized for higher dimensions. Then I shall discuss the case of compact extra dimensions, address the hierarchy problem and comment on experimental bounds. The material presented in this Section is partly based on [136, 69, 16] while the original argument goes back to Arkani-Hamed, Dimopoulos and Dvali [6].

7.3.1 Non-compact extra dimensions

Let $\mathbf{F}$ be the force exerted on a test mass m a distance r away from a point mass M generating the gravitational field $\mathbf{g} = \nabla_{(d)}\phi$. ϕ is the gravitational potential in the presence of d spatial dimensions. It is determined by the Poisson equation

$$\triangle_{(d)}\phi = \text{Area}(S_{(d-1)}) G_D\, \rho_M \tag{7.8}$$

[1] Note the different sign in front of the mass term with respect to the first part of the thesis since here in the second part I work with the metric signature $(-, +, ..., +)$ which is more common in cosmology.

where Area$(S_{(d-1)})$ is the area of the surface of the $d-1$ - dimensional sphere $S_{d-1} = \partial\mathcal{V}_d$ of radius r enclosing the d-dimensional volume $\mathcal{V}_d$ with the mass M in its center. With M being a point mass, the mass density is just $\rho_M = M\delta(r)$. G_D denotes Newton's constant in the D-dimensional spacetime.
The force exerted on the test mass m reads

$$\mathbf{F} = m\mathbf{g} \ . \tag{7.9}$$

Applying Gauss' law gives

$$\int_{\mathcal{V}_d} (\nabla_{(d)}\mathbf{F}) d\mathcal{V} = \int_{\partial\mathcal{V}_d} \mathbf{F} d\mathbf{S} \ , \tag{7.10}$$

where $d\mathcal{V}$ and $d\mathbf{S}$ denotes the volume element of $\mathcal{V}$ and surface element of $S_{(d-1)}$, respectively. Since the force is perpendicular onto every surface element $d\mathbf{S}$, the surface integral is simple to evaluate

$$\int_{\partial\mathcal{V}_d} \mathbf{F} d\mathbf{S} = F(r)\, r^{d-1}\, \text{Area}(S_{(d-1)}). \tag{7.11}$$

Equating the volume integral by using (7.8)

$$\int_{\mathcal{V}_d} (\nabla_{(d)}\mathbf{F}) d\mathcal{V} = m \int_{\mathcal{V}_d} (\nabla_{(d)}\mathbf{g}) d\mathcal{V} = m \int_{\mathcal{V}_d} (\triangle_{(d)}\phi) d\mathcal{V} = m\, \text{Area}(S_{(d-1)})\, G_D\, M \tag{7.12}$$

leads finally to Newton's law for $d = 3 + n$ spatial dimensions:

$$F(r) = G_D \frac{m\, M}{r^{2+n}} \ . \tag{7.13}$$

Due to the presence of the extra dimensions, i.e. the additional space, the field lines are diluted which is reflected by the additional factor $1/r^n$.

7.3.2 Compact extra dimensions

The above derivation of Newton's law (7.13) for a D-dimensional spacetime has been performed under the assumption that the extra dimensions are non-compact. In order to calculate the gravitational force in the presence of n compactified dimensions one uses an approach based on decompactification. One considers the infinite extension of extra dimensional space consisting of copies of the original compact spacetime leading to a lattice of masses. It is assumed that all compact dimensions have the same size R.
If $r \ll R$, the influence of all the copies of the mass M (mirror masses) is negligible and the force exerted on the test mass m is described by Eq. (7.13). For the opposite limit $r \gg R$, the lattice looks like a hypersurface (i.e. a line for $n = 1$) of mass density M/R^n and the test mass feels the copies. The force can be evaluated by forming a $n + 2$ - dimensional cylinder C of length L and radius r around the mass distribution. Applying Gauss' law to this configuration implies the usual Newton's law

$$F = \frac{\text{Area}(S_{(d-1)})}{4\pi\, R^n} G_D \frac{m\, M}{r^2} \ . \tag{7.14}$$

The force exerted on a mass m due to the gravitational field generated by the mass M behaves like $1/r^2$ even in the presence of compact dimensions of size R if $r \gg R$, i.e. gravity on large scales behaves four dimensional. However, comparing (7.14) with Newton's law in four dimensions gives an important relation between the four-dimensional Newton constant G_4 and the fundamental D-dimensional Newton constant G_D:

$$G_4 = \frac{\text{Area}(S_{(n+2)})}{4\pi\, R^n} G_D \ \text{ with } \ \text{Area}(S_{(n+2)}) = \frac{2\,\pi^{(n+3)/2}}{\Gamma((n+3)/2)} \tag{7.15}$$

where Γ denotes the Gamma function [1].
In summary, in the presence of compact extra dimensions, Newton's law is changed on small scales $r \ll R$ to $\propto 1/r^{n+2}$ while it remains unchanged on large scales $r \gg R$. Thereby the four-dimensional Newton constant G_4 is related to the fundamental D-dimensional one G_D by (7.15). Consequently, the existence of compactified extra dimensions is, in principle, observable in gravitational strength experiments using for example torsion pendulums. The smallest distances r probed in such experiments so far are $r \simeq$ several μm and no deviation from the $1/r^2$ behavior has been found (see 7.3.4). Gravity strength experiments lead thus to an upper bound on the size of extra dimensions of

$$R_{\max} \sim \text{several } \mu\text{m} \tag{7.16}$$

which is many orders of magnitude larger than the constraint (7.7) coming from the fact that no KK particles have been seen in colliders. Therefore, within a braneworld scenario where the standard model fields are confined to a brane and the KK constraint (7.7) does not apply, the extra dimensions can be rather large. This can be exploited to address the hierarchy problem.

7.3.3 The hierarchy problem

The reduced Planck mass M_4 appearing as the prefactor in the Einstein-Hilbert action of general relativity defines the energy scale of gravity. Its numerical value is

$$M_4 = \frac{1}{\sqrt{8\pi\, G_4}} = \frac{m_{\rm Pl}}{\sqrt{8\pi}} = 2.44 \times 10^{18}\text{GeV}. \tag{7.17}$$

In contrast, the electroweak scale $M_{\rm EW}$ – the energy scale of the standard model of particle physics – is $M_{\rm EW} \simeq 1\,\text{TeV} = 10^3\,\text{GeV}$, i.e. 10^{15} times smaller than M_4! To explain this vast difference in the scales poses the so-called *hierarchy problem*, which can be rephrased as: Why is gravity so much weaker than the other fundamental forces?
One attempt to address this rather unnatural huge separation of scales is to use the relation (7.15). If higher dimensions exist, the fundamental scale of gravity is given by G_D rather than G_4. Introducing the D-dimensional (fundamental) Planck mass M_D via

$$(D-2)\,\text{Area}(S_{(D-2)})G_D = M_D^{-(D-2)} \tag{7.18}$$

(recall that $D = 4+n$), which follows from dimensional arguments, the relation (7.15) can be cast into

$$M_4^2 \sim M_D^{(n+2)} R^n. \tag{7.19}$$

Thereby, R^n is (not counting factors of π) the volume of the internal space, i.e. the volume of the compact extra dimensions, which here are assumed to be of equal size. This allows to lower the fundamental gravity scale M_D by tuning the volume of the extra dimensions. Fixing M_D at the electroweak scale $M_D \sim M_{\rm EW}$, for example, leads to

$$R \sim 10^{30/n-19}\,\text{m}. \tag{7.20}$$

While the case $n = 1$ with $R \sim 10^{11}\,\text{m}$ is excluded since Newtonian gravitation would be modified on solar system scales, already the case $n = 2$ with $R \sim 1\,\text{mm}$ comes close to the small scales up to which gravity has been tested so far [cf. Eq. (7.16)]. Consequently, in a braneworld scenario, where the KK constraint (7.7) does not apply, the hierarchy problem can be solved by using "large" extra dimensions.

7.3.4 Gravity strength experiments

In the presence of extra dimensions, the deviation of Newton's law from the $1/r^2$ behavior should become visible when probing scales comparable to the size of the extra dimensions. However, because of the weakness of gravity compared to electromagnetic interactions, such experiments are very difficult to perform. Here I shall briefly comment on recent experimental results obtained by using torsion-balance experiments [98, 97, 111] of the Washington group (see also [96, 204, 38]).
Usually, the deviation from the Newtonian potential is parameterized by a Yukawa addition to the familiar $1/r$ potential

$$V(r) \propto \frac{1}{r}\left(1 + \alpha e^{-r/\lambda}\right) \tag{7.21}$$

where α is a dimensionless strength parameter and λ a length scale [74].
The experimental results are summarized in an $\alpha - \lambda$ - exclusion plot. Two such plots are depicted in Figure 7.2, corresponding to the results as of 1999 and 2007, demonstrating the progress which has been made in recent years. The shown plots have been compiled of many different experiments. I shall not comment on all features and information contained in the plots but rather refer the interested reader to the original papers [97, 111] where these pictures have been taken from.
Here I shall stress only two facts. First of all, note that in 1999 the Casimir force experiments of Lamoreaux [133, 134] which I have briefly described in 2.1 helped to constrain the allowed region in the $\alpha - \lambda$ - parameter

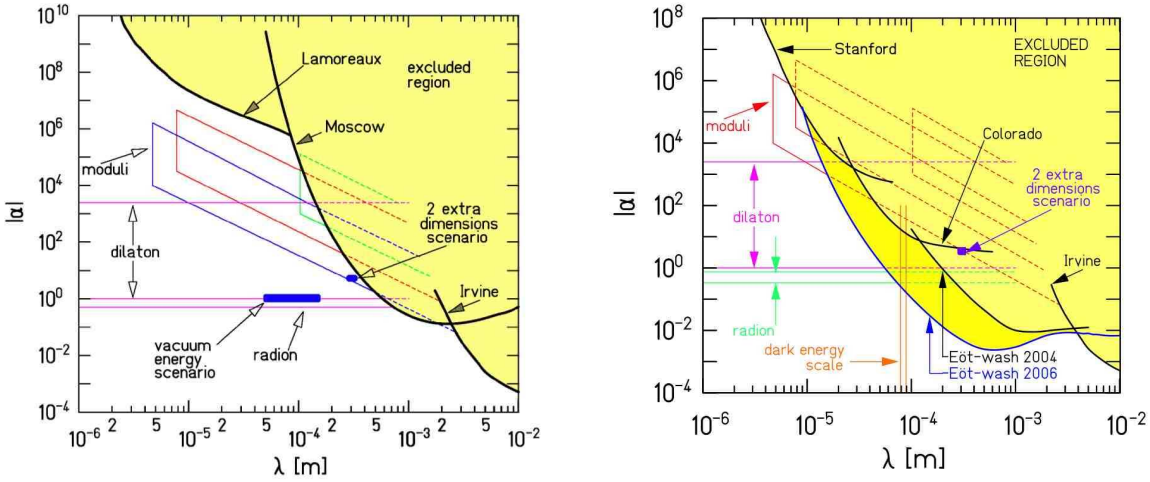

Figure 7.2: Constraints on Yukawa violations of the gravitational $1/r^2$ law as of 1999 (left panel) and 2007 (right panel). The shaded region is excluded at the 95% confidence level. Results compiled of different experiments are depicted. Pictures are taken from [97, 111].

space. Secondly, for the ADD models α is of order one and λ corresponds to the size of the extra dimensions [136]. At present, for $|\alpha| = 1$ the constraint on λ is [111].

$$\lambda \lesssim 56\,\mu\,\mathrm{m}\ . \tag{7.22}$$

7.4 ADD braneworlds

Let me now finally introduce the already mentioned ADD braneworld model more detailed. In 1998 Arkani-Hamed, Dimopoulos and Dvali [6] introduced the following model: As bulk spacetime they consider a *flat* spacetime of dimension $D = 3 + 1 + n$. Thereby n is again the number of "large" extra compact dimensions. The line element of the global spacetime reads

$$ds^2 = \eta_{AB} dx^A dx^B = \eta_{\mu\nu} dx^\mu dx^\nu + \delta_{ab} dy^a dy^b \tag{7.23}$$

where the x^A's are the coordinates of the bulk, the x^μ's of the usual four-dimensional Minkowski spacetime and the x^a's the coordinates of the extra dimensions, i.e. $x^A = (x^\mu, x^a)$. As before, $\eta_{\mu\nu}$ is the four-dimensional Minkowski metric and δ_{ab} the Kronecker-delta. It is assumed for simplicity that the compact dimensions are all of the same size, and one identifies $x^a = x^a + 2\pi R$.
So far, the setup is the same as in the original KK-picture, i.e. one has the possibility to "solve" the hierarchy problem through the relation (7.19) but on the other hand is subject to the constraint that no KK particles of standard model fields have been seen in colliders. To evade the constraint (7.7) on the size of the extra dimensions it is assumed that the standard model fields do not live in the whole bulk but are confined to a sub-space, a so-called *p-brane*. A p-brane is a spatial hypersurface of dimension p and thus sweeps out a $p+1$-dimensional spacetime. In the ADD model, the four-dimensional Universe we see is assumed to be such a world sheet defined by a 3-brane onto which the standard model is confined. As I have outlined in 7.1, such objects do naturally arise in String theory. Since standard model fields do not propagate into the extra dimensions, the KK constraint (7.7) does no loner apply and the extra dimensions can be probed by gravity only. Such a model has a very rich phenomenology for high-energy particle physics [82] as well as cosmology [7].

Chapter 8

The Randall-Sundrum models and brane cosmology

8.1 Warped geometry

The ADD setup discussed in 7.4 consists of a flat 3-brane in a higher dimensional bulk of flat geometry. But a brane itself is a physical object with an energy density $\mathcal{T}$, called *brane tension*. The brane itself produces a gravitational field. Taking the self-gravity of the brane into account and introducing a bulk cosmological constant Λ_5 which, as is shown below, is negative, leads to a bulk spacetime which is a portion of Anti-de Sitter (AdS). Many novel properties emerge within such a model. This braneworld scenario was first introduced by Randall and Sundrum in 1999 [181, 182].

I now derive the Randall-Sundrum setup in detail. Thereby I shall mainly follow [136, 190]. Consider a five-dimensional bulk with cosmological constant Λ_5 but otherwise empty and a 3-brane of tension $\mathcal{T}$. The brane is assumed to be Minkowskian, i.e. four-dimensional Poincaré invariance is imposed. One can now show [181, 136, 69, 190, 152] that the most general ansatz for the metric compatible with the symmetry requirements is given by

$$ds^2 = g_{AB}dx^A dx^B = a^2(z)\eta_{\mu\nu}dx^\mu dx^\nu + dz^2 \tag{8.1}$$

where $x^A = (x^\mu, z)$ with x^μ denoting the coordinates of the Minkowski slices and z the extra-dimension. The factor $a(z)$ is called the *warp factor* which is the new ingredient in this model with non-factorizable geometry. In order to determine the bulk geometry, i.e. in particular the warp factor $a(z)$, one has to solve the five-dimensional Einstein equations

$$G_{AB} + \Lambda_5 g_{AB} = \kappa_5 T_{AB} \tag{8.2}$$

where T_{AB} is the energy momentum tensor and κ_5 the five-dimensional gravitational coupling constant

$$\kappa_5 = 6\pi^2 G_5 = \frac{1}{M_5^3}\ . \tag{8.3}$$

M_5 and G_5 are the five-dimensional (fundamental) reduced Planck mass and Newton constant, respectively. Since I have assumed that the bulk is empty and I have already incorporated Λ_5 on the left hand side, T_{AB} contains just the brane tension $\mathcal{T}$. Putting the brane at $z = 0$, T_{AB} is of the form

$$T_{AB} = -\mathcal{T}\delta^\mu_A \delta^\nu_B \eta_{\mu\nu}\delta(z). \tag{8.4}$$

The self-gravitating brane acts as a delta function source for the gravitational field.
In the bulk where $G_{AB} + \Lambda_5 g_{AB} = 0$, Einstein's equation reduces to

$$\left(\frac{\partial_z a}{a}\right)^2 = -\frac{\Lambda_5}{6} \tag{8.5}$$

implying that (for a non-trivial solution) the five-dimensional cosmological constant has to be negative, $\Lambda_5 < 0$. Note, that if $\Lambda_5 = 0$, the ADD scenario is recovered. The warp factor can take two possible solutions:

$$a(z) = \begin{cases} e^{+z/L} \\ e^{-z/L} \end{cases} \tag{8.6}$$

where I have introduced the AdS curvature scale L defined by

$$\Lambda_5 = -\frac{6}{L^2}. \tag{8.7}$$

Einstein's equation contains a δ-function singularity at the position of the brane. This can be dealt with in the same way δ-function potentials are treated in quantum mechanics. The dynamical equation, the Schrödinger equation in QM and here Einstein's equation, is integrated over a small interval including the δ-function. Letting the interval shrink to zero, assuming that the field, the wave function in QM and here the metric field g_{AB}, is smooth at the position of the δ-function singularity leads to a jump in the first derivative of the field. The strength of this jump is related to the properties of the potential.
Using that

$$G_{\mu\nu} = 3\partial_z \left(a\partial_z a\right)\eta_{\mu\nu} \tag{8.8}$$

gives, with $\epsilon > 0$ and small,

$$\int_{-\epsilon}^{+\epsilon} dz \left[3\partial_z \left(a\partial_z a\right) + a^2\Lambda_5\right]\eta_{\mu\nu} = \kappa_5 \int_{-\epsilon}^{+\epsilon} dz T_{\mu\nu}\delta(z) = -\mathcal{T}\kappa_5\eta_{\mu\nu} \tag{8.9}$$

such that, since $a(z)$ is taken to be continuous at $z = 0$,

$$3a\partial_z a|_{-\epsilon}^{+\epsilon} = -\kappa_5\mathcal{T}. \tag{8.10}$$

In the limit $\epsilon \to 0$ and setting without loss of generality $a(0) = 1$ leads to a jump in the derivative of a which is related to the five-dimensional gravitational coupling and the brane tension. Finally, $\mathbb{Z}_2$-symmetry is imposed across the brane, i.e. the coordinates z and $-z$ are identified. This implies that $a(z)$ has to be even and $\partial_z a(z)$ odd. Consequently, the total jump in the first derivative of the warp factor at $z = 0$ is given by

$$\partial_z a(+\epsilon) = -\frac{\kappa_5\mathcal{T}}{6}. \tag{8.11}$$

This relation is called *junction condition* and I shall derive it below in a more general form.
The junction condition and the $\mathbb{Z}_2$-symmetry imply that, depending on whether the brane tension is positive or negative, one has two different solutions for the warp factor:

$$\text{positive tension brane } \mathcal{T} > 0: \quad a(z) = e^{-|z|/L} \text{ with } \frac{1}{L} = \frac{\kappa_5\,\mathcal{T}}{6} \tag{8.12}$$

$$\text{negative tension brane } \mathcal{T} < 0: \quad a(z) = e^{|z|/L} \text{ with } \frac{1}{L} = -\frac{\kappa_5\,\mathcal{T}}{6}\ . \tag{8.13}$$

The relation between the AdS curvature scale L and the brane tension just follows from the junction condition (8.11) and the particular solution. Combining these relations with (8.7) leads to the *Randall-Sundrum-fine tuning* condition

$$-\Lambda_5 = \frac{6}{L^2} = \frac{\kappa_5^2\mathcal{T}^2}{6}\ . \tag{8.14}$$

In summary, for a flat brane of positive tension the bulk geometry is

$$ds^2 = e^{-2|z|/L}\eta_{\mu\nu}dx^\mu dx^\nu + dz^2 \tag{8.15}$$

where the brane position is $z = 0$.

Later on I shall use *Poincaré coordinates* (x^μ, y) with

$$y = Le^{z/L} \tag{8.16}$$

which bring the metric into the conformally flat form

$$ds^2 = \left(\frac{L}{y}\right)^2 \left[\eta_{\mu\nu}dx^\mu dx^\nu + dy^2\right], \tag{8.17}$$

where now the brane position is $y = L$. Note that these coordinates do not cover the whole AdS spacetime but only a slice of it [136].

8.2 Randall-Sundrum models

8.2.1 Randall-Sundrum model I

The first model proposed by Randall and Sundrum (RS) [181] consists of a spacetime with a single $S^1/\mathbb{Z}_2$ orbifold extra dimension. Two flat 3-branes with opposite tensions reside at the orbifold fixed points. Within this construction involving two branes, Eq. (8.15) is still the bulk solution. In this particular case, one usually uses an angular coordinate ϕ with $z = r_c\phi$ where $-\pi \leq \phi \leq \pi$ and r_c is the radius of the compactified dimension. The metric reads

$$ds^2 = e^{-2r_c|\phi|/L}\eta_{\mu\nu}dx^\mu dx^\nu + r_c^2 d\phi^2 \ . \tag{8.18}$$

The two 3-branes are located at $\phi = 0$ (positive tension brane) and $\phi = \pi$ (negative tension brane) and the points $(x^\mu, -\phi)$ and (x^μ, ϕ) are identified. Since the spacetime in between the two branes is a slice of AdS_5, the RS I geometry can be interpreted as two portions of AdS_5 which are glued together at the two brane positions. Similar orbifold constructions arise within the context of M theory [94, 95, 221] and in [215] it is demonstrated how such a model may be obtained from String theory compactifications.
Standard model fields are confined on the negative tension brane called the *visible brane* which represents our Universe. The positive tension brane has fundamental scale M_5 and is called the *hidden brane*. An important consequence of the warp factor is that the four-dimensional Planck mass M_4 on the visible brane is related to the fundamental scale M_5 via

$$M_4^2 = M_5^3\, L\, \left[1 - e^{-2r_c\pi/L}\right] . \tag{8.19}$$

Since M_4 depends only weakly on r_c in the large r_c/L limit, M_4 is of the order of M_5. Furthermore, the exponential factor in the spacetime metric implies that any fundamental mass parameter m_0 of a field confined on the visible brane corresponds to a physical mass [181]

$$m = m_0 e^{-r_c\pi/L} \ . \tag{8.20}$$

Therefore, for $k/L \simeq 10$ the weak scale $\sim 1\,TeV$ is generated from a fundamental scale M_5 of the order of the Planck scale. Here I have followed the original Randall Sundrum paper [181] where the Planck scale is considered to be the fundamental scale. One could as well regard the TeV scale as the fundamental scale and the Planck scale as derived scale as I have done it in 7.3.3. Technically this can be established by a change of coordinates [181]. This mechanism does not require very larger hierarchies among the fundamental parameters and thus represents an appealing solution to the hierarchy problem. However, the radius r_c, i.e. the separation between the two branes, corresponds to a massless scalar field, the *radion*, which has to be stabilized in order to recover four-dimensional relativity at low energies [152, 136, 83, 209].

8.2.2 Randall-Sundrum model II

The RS II-model contains only one positive tension brane at position $y = L$ (or $z = 0$) representing our Universe. It may be thought of as arising from sending the negative tension brane in the RS I model off to infinity. From (8.19) it follows immediately that the energy scales are related via

$$M_5^3 = \frac{M_4^2}{L} \quad \text{or} \quad \kappa_5 = L\kappa_4 \ . \tag{8.21}$$

From now on I shall work exclusively in Poincaré coordinates (8.17). For the Poincaré metric, the full geometry of the spacetime is obtained by replacing the "left hand side", $0 < y < L$, of AdS by a second copy of the "right hand side". The superscripts "$_>$" and "$_<$" are used for the bulk sides with $y > y_b$ and $y < y_b$, respectively. In terms of the coordinate y, the value of y decreases continuously from ∞ to L and then jumps to $-L$ over the brane whereafter it continues to decrease. At the brane position, $y_b^> = L$, $y_b^< = -L$, the metric function $(L/y)^2$ has a kink. The advantage of the metric Eq. (8.15) is that the variable z does not jump.
Another way of seeing (8.21) is to consider the five-dimensional Einstein Hilbert action ($\mathfrak{R}$ is the Ricci scalar for the five-dimensional metric (8.17) with determinant g)

$$S = \frac{1}{2\,\kappa_5}\int dx^4 dy \sqrt{-g}\,\mathfrak{R} \ . \tag{8.22}$$

Integrating out the dependence on the extra dimension leads to the four-dimensional Einstein-Hilbert action if one identifies the pre-factor with the reduced Planck mass

$$M_4^2 = M_5^3 \int_{-\infty}^{+\infty} dy \left(\frac{L}{y}\right)^3 = 2\, M_5^3 \int_L^{+\infty} dy \left(\frac{L}{y}\right)^3 = M_5^3\, L\ . \tag{8.23}$$

Even the fifth-dimension is infinite, the integration remains finite due to the warp factor. Comparing this relation with (7.19) shows that it corresponds to the case of one compactified extra dimension of size L. For that reason, the mechanism of relating the energy scales via a warping of the extra dimension is called *effective compactification*.

Another important feature of the RS II model is that it localizes four-dimensional gravity on the brane. In order to discuss this, one has to study perturbations of the metric, in particular the tensor perturbation h_{ij} – the spin-2 graviton. Since it depends on the fifth dimension, it has a KK-decomposition in addition to a massless zero mode which corresponds to the standard four-dimensional graviton. I shall introduce perturbation theory and discuss the evolution equations in detail in 8.5 and Chapter 9. Here, I shall only address the standard four-dimensional graviton, and anticipate that its wave function (profile) $\Psi_0(y)$ with respect to the extra dimension is described by

$$-\partial_y^2 \Psi_0(y) + \frac{15}{4\,y^2}\Psi_0(y) = 0 \tag{8.24}$$

together with the boundary (junction) condition

$$\left(\partial_y + \frac{3}{2\,y}\right)\Psi_0|_{y=L} = 0. \tag{8.25}$$

These follow directly from the Eqs. (9.99) and (9.100) discussed in 9.5.4 which describe the evolution of tensor perturbations for the more general case of a moving brane by restriction to a fixed brane and an infinite bulk. The solution to (8.24) satisfying (8.25) which is normalizable, i.e. $2\int_L^\infty |\Psi_0|^2 = 1$, is readily found

$$\Psi_0(y) = \frac{L}{y^{3/2}}\ . \tag{8.26}$$

Its probability profile $\Psi_0^2(y)$ decreases rapidly for increasing values of y. This shows that the standard four-dimensional graviton is localized on the brane (at $y = L$).
Another way to see this localization qualitatively is to combine the wave equation (8.24) and the boundary condition (8.25) to a Schrödinger equation

$$-\partial_y^2 \Psi_0(y) + V(y)\Psi_0(y) = 0 \tag{8.27}$$

with volcano-type potential

$$V(y) = \frac{15}{4\,y^2} - \frac{3}{L}\,\delta(|y| - L)\ . \tag{8.28}$$

That Eq. (8.27) is indeed equivalent to the above boundary value problem is obvious. This is because Eq. (8.27) follows from the perturbed Einstein equation which contains a delta-function confining the energy momentum tensor (here only the brane tension) to the brane. Integrating it over a small interval across the brane and demanding continuity of Ψ_0 is what leads to the junction condition (8.25) [cf. Sections 8.1 and 8.5].
The vulcano-type potential peaks as $|y| \to L$ but has a negative singularity right at $|y| = L$, i.e. at the position of the brane. It is well known from quantum mechanics that such a delta-function potential supports a single normalizable bound state, whose wave function peaks at $y = L$ [182]. This state is the standard four-dimensional graviton (8.26). Its localization is the physical reason why gravity still behaves as four-dimensional on the brane [173].
For the massive KK gravitons which are traces of the five-dimensional nature of gravity, the potential (8.28) acts as a barrier. I shall discuss this in Section 9.5.4 in detail within the more general context of a moving brane.

For completeness, let me finally quote from [152] how the four-dimensional gravitational potential produced by a mass M, to which the KK-modes contribute, behaves within the RS II model. For small distances, $r \ll L$ one obtains

$$V(r) \approx \frac{G_4\, M\, L}{r^2} \tag{8.29}$$

which reflects the fact that the potential becomes truly five dimensional on small scales. On large scales $r \gg L$, it behaves as

$$V(r) \approx \frac{G_4 M}{r}\left(1+\frac{2L^2}{3r^2}\right), \tag{8.30}$$

i.e. it has a small correction at low energies from extra-dimensional effects. Table-top experiments of Newton's law require

$$L \lesssim 0.1\,\text{mm}. \tag{8.31}$$

8.3 Junction conditions

In this section I introduce the junction conditions in a more formal way. I shall not explicitely derive them in order to avoid the presentation of too many technical details which can be found in the literature.
Let me first introduce some important geometrical quantities. Consider a 3-brane in a five-dimensional bulk with metric g_{AB}. The worldsheet of the brane defines a four-dimensional spacetime, i.e. a submanifold of the bulk, which can be parameterized by coordinates ξ^λ. One can then define a brane embedding $x^A = X_b^A(\xi^\lambda)$ describing the brane position in the bulk. With the aid of this parameterization, it is now possible to define four vectors, forming a basis of vectors tangent to the brane $e_\mu = e_\mu^A \partial_A$ via

$$e_\mu^A = \frac{\partial X_b^A(\xi^\lambda)}{\partial \xi^\mu} \tag{8.32}$$

and the unit normal vector $n = n^A \partial_A$ to the brane through [1]

$$g_{AB} e_\mu^A n^B = 0 \;\text{ and }\; g_{AB} n^A n^B = 1. \tag{8.33}$$

The bulk metric induces a metric on the brane, the *first fundamental form* or *induced metric*. From the bulk perspective it is given by

$$q_{AB} = g_{AB} - n_A n_B, \tag{8.34}$$

which, after contraction with the tangent vectors, can be identified as the brane metric [136]

$$q_{\mu\nu} = q_{AB} e_\mu^A e_\nu^B = g_{AB} e_\mu^A e_\nu^B \ . \tag{8.35}$$

Consider now the RS II case with the metric (8.17) and a brane at $y = y_b = L$ (or equivalently $z = 0$ for the metric (8.15)) as described in 8.2.2. Denoting the energy momentum tensor on the brane by $S_{\mu\nu}$, the five-dimensional Einstein equation reads

$$G_{AB} + \Lambda_5 g_{AB} = \kappa_5 T_{AB} = \kappa_5 \delta_A^\mu \delta_B^\nu S_{\mu\nu} \delta(y - y_b) \tag{8.36}$$

where I have assumed that no matter is present in the bulk. The delta function enforces in the classical theory the string theory idea that Standard Model fields are confined to the brane. As already explained above, to avoid the delta function, one can integrate Eq. (8.36) along the extra dimensions from $y = y_b - \epsilon$ to $y = y_b + \epsilon$, and take the limit $\epsilon \to 0$. This leads to the so-called Israel-Darmois junction conditions [139, 200, 50, 102, 159] at the brane position. These read

$$[g_{\mu\nu}] \equiv g_{\mu\nu}^{>} - g_{\mu\nu}^{<} = 0 \ , \tag{8.37}$$

$$[K_{\mu\nu}] \equiv K_{\mu\nu}^{>} - K_{\mu\nu}^{<} = \kappa_5 \left(S_{\mu\nu} - \frac{1}{3} S q_{\mu\nu}\right) \equiv \kappa_5 \widehat{S}_{\mu\nu} \ , \tag{8.38}$$

where I have used the superscript notation ("$>$", "$<$") of 8.2.2. $S = S_\mu^\mu$ is the trace of the brane energy momentum tensor, $q_{\mu\nu}$ the induced metric (8.35) and $K_{\mu\nu}$ the *extrinsic curvature* or *second fundamental form* of the brane. It can be expressed purely in terms of the internal brane coordinates [52, 168, 69]

$$K_{\mu\nu} = -\frac{1}{2}\left[g_{AB}\left(e_\mu^A \partial_\nu n^B + e_\nu^A \partial_\mu n^B\right) + e_\mu^A e_\nu^B n^C \partial_C g_{AB}\right] \ . \tag{8.39}$$

[1] Note that here we have a timelike hypersurface with spacelike normals.

Equation (8.38) is usually referred to as the *second junction condition*. This important relation links the extrinsic curvature of the brane to the matter content on the brane. The first junction condition simply states that the induced metric, the first fundamental form, $q_{\mu\nu}$ [Eq. 8.35] be continuous across the brane. Note that the sign of the extrinsic curvature is not uniquely defined in the literature. Here I use the convention of [69] [2].

In the case of interest, the background spacetime consists of two copies of the part of AdS with $y \geqslant y_b = L$. The coordinate y jumps from $y = L$ to $y = -L$ across the brane. Due to $\mathbb{Z}_2$ - symmetry, i.e. the two sides of the brane are mirror images, the first junction condition is trivially fulfilled. In addition one has $K^{>}_{\mu\nu} = -K^{<}_{\mu\nu}$ so that the second junction condition reduces to

$$[K_{\mu\nu}] = 2K^{>}_{\mu\nu} = \kappa_5 \widehat{S}_{\mu\nu} \ . \tag{8.40}$$

Assuming a brane tension only, $S_{\mu\nu} = -\mathcal{T} q_{\mu\nu}$, and $y_b = L$ one finds

$$[K_{00}]\Big|_{y_b=L} = -\frac{2}{L} = -\frac{1}{3}\kappa_5 \mathcal{T} \text{ and } \ [K_{ii}]\Big|_{y_b=L} = \frac{2}{L} = \frac{1}{3}\kappa_5 \mathcal{T} \ , \tag{8.41}$$

leading to the Randall-Sundrum-fine tuning condition (8.14).

8.4 Brane cosmology

So far, I have considered a self-gravitating brane which is supposed to represent our Universe at a fixed position in the bulk. Now I shall assume that also matter in form of an energy momentum tensor of a perfect fluid exists on the brane. The AdS metric (8.17) is then still a solution to the five-dimensional Einstein equation. As a consequence of the matter on the brane, the brane position will be time-dependent; in other words, the brane is moving through the static AdS bulk [131, 101]. The induced metric on the brane is the FLRW-metric with the scale factor directly linked to the position of the brane in the bulk. In that way, the motion of the brane through AdS naturally mimics the expansion of the Universe. The dynamics of the scale factor is governed by the *modified Friedmann* equation for brane cosmology which follows from the second junction condition. That the brane is moving through the static AdS bulk is of course a coordinate-dependent picture. By using other coordinates (Gaussian normal coordinates) the brane position is fixed, but the bulk spacetime itself becomes time-dependent [3] [13, 166, 216, 14]. In the following I shall work with the picture of a brane moving through the static AdS bulk since, when studying five-dimensional tensor perturbations in this setup, the similarities to the dynamical Casimir effect discussed in the first part of the thesis become evident.

Let me begin by again writing down the AdS metric (8.17)

$$ds^2 = \frac{L^2}{y^2}\left[-dt^2 + \delta_{ij}dx^i dx^j + dy^2\right] . \tag{8.42}$$

The time coordinate t is conformal time of the AdS bulk. Denoting by η the conformal time of an observer on the brane, and the position of the brane in the bulk by y_b, the brane metric induced by the bulk metric (8.42) is

$$ds^2 = \frac{L^2}{y_b^2}\left[-\left(1 - \left(\frac{dy_b}{dt}\right)^2\right)dt^2 + \delta_{ij}dx^i dx^j\right] = a^2(\eta)\left[-d\eta^2 + \delta_{ij}dx^i dx^j\right] \ , \tag{8.43}$$

i.e. a flat FLRW-metric. The scale factor $a(\eta)$ is related to the position of the brane in the bulk $y_b(t)$ through

$$a(\eta) = \frac{L}{y_b(t)}. \tag{8.44}$$

The brane motion induces a γ-factor which relates the conformal time η on the brane to the conformal time t of the bulk:

$$d\eta = \sqrt{1 - \left(\frac{dy_b}{dt}\right)^2}\, dt \equiv \gamma^{-1} dt \ . \tag{8.45}$$

[2] The extrinsic curvature is in general defined as $K_{AB} = -q^C_A \, n_{B\,\|C}$, or in terms of the Lie-derivative $K_{AB} = -\frac{1}{2}\mathcal{L}_n q_{AB} = -\frac{1}{2}\left(n^C \, q_{AB\,\|C} + q_{CB}\, n^C_{\ \|A} + q_{AC}\, n^C_{\ \|B}\right)$, and describes the bending of the brane with respect to the bulk spacetime [136, 152, 69, 206].

[3] The explicit transformation between the two coordinate systems is given in [167].

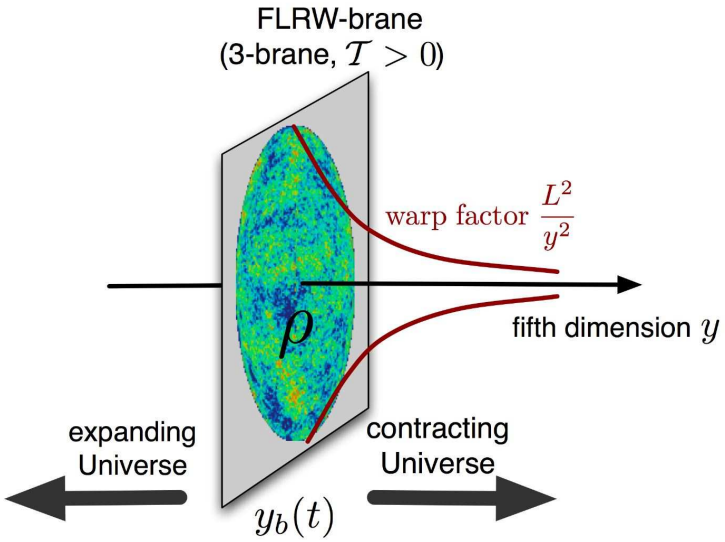

Figure 8.1: Pictorial presentation of a cosmological (FLRW-) brane, i.e. a brane with FLRW-metric (8.43), endowed with brane tension $\mathcal{T} > 0$ and energy density ρ of usual cosmological matter [cf. Eq. (6.19)] moving through five-dimensional AdS. For increasing values of $y_b(t)$ the Universe is contracting while it is expanding for decreasing values of $y_b(t)$ according to Eq. (8.44).

By means of the relation (8.44) any particular dynamics of the scale factor corresponds to a motion of the brane through AdS. When the brane is moving towards decreasing values of y the Universe is expanding while it is contracting for the opposite case (see Figure 8.1).
It is useful to introduce the velocity v of the brane via

$$v \equiv \frac{dy_b}{dt} = -LH\gamma^{-1} = -\frac{LH}{\sqrt{1+L^2H^2}} \tag{8.46}$$

such that

$$\gamma = \frac{1}{\sqrt{1-v^2}} = \sqrt{1+L^2H^2}. \tag{8.47}$$

H is the Hubble parameter (6.9)

$$H = (\partial_\eta a)/(a^2) = a^{-1}\mathcal{H} = -L^{-1}\gamma v. \tag{8.48}$$

Consider now an homogeneous and isotropic total energy momentum tensor on the brane

$$S^\mu_\nu = T^\mu_\nu - \mathcal{T}\delta^\mu_\nu. \tag{8.49}$$

Here $\mathcal{T}$ denotes again the brane tension and T^μ_ν is the energy momentum tensor of particles and fields confined on the brane, given by Eq. (6.19).
Evaluating the second junction condition gives

$$[K_{00}]\Big|_{y_b} = -2\frac{1+L^2H^2+L^2(\partial_\tau H)}{L\sqrt{1+L^2H^2}} = \kappa_5(\rho+P) - \frac{\kappa_5}{3}(\rho+\mathcal{T}) \,, \tag{8.50}$$

$$[K_{ij}]\Big|_{y_b} = 2a^2\frac{\sqrt{1+L^2H^2}}{L}\,\delta_{ij} = \frac{\kappa_5}{3}a^2(\rho+\mathcal{T})\,\delta_{ij} \,, \tag{8.51}$$

which leads to the two equations ($\partial_\eta = a\partial_\tau$)

$$\kappa_5(\rho+\mathcal{T}) = 6\frac{\sqrt{1+L^2H^2}}{L} \,, \tag{8.52}$$

$$\kappa_5(\rho + P) = -\frac{2L(\partial_\eta H)}{a\sqrt{1 + L^2H^2}} \ . \tag{8.53}$$

Taking the square of (8.52) yields

$$H^2 = \frac{\kappa_5^2}{18}\mathcal{T}\rho\left(1 + \frac{\rho}{2\mathcal{T}}\right) + \frac{\kappa_5^2\mathcal{T}^2}{36} - \frac{1}{L^2} \tag{8.54}$$

while combining (8.52) and (8.53) results in

$$(\partial_\eta\rho) = -3Ha(\rho + P) \ . \tag{8.55}$$

Equation (8.55) is the usual continuity equation of four-dimensional cosmology which holds since all the matter is confined on the brane and the bulk is empty [136, 152], and Eq. (8.54) is called the *modified Friedmann equation* for brane cosmology [131, 13]. Inspection of this equation reveals that one can define a four-dimensional cosmological constant $\Lambda_4 = \kappa_5^2\mathcal{T}^2/6 - 3/L^2$. However, imposing the RS fine tuning condition (8.14) yields $\Lambda_4 = 0$.

The new feature of the modified Friedmann equation is its dependence on the energy density. While for the ordinary four-dimensional Friedmann equation (6.20) $H^2 \propto \rho$, one has $H^2 \propto \rho^2$ in brane cosmology if $\rho \gg \mathcal{T}$. For usual matter with $\rho + P > 0$, ρ decreases during expansion and at sufficiently late time $\rho \ll \mathcal{T}$. Then one can neglect the ρ^2-term and the ordinary 4-dimensional Friedmann equation is recovered if one sets

$$\kappa_4 = \frac{1}{6}\kappa_5^2\mathcal{T}. \tag{8.56}$$

But, in addition [cf. Eq. (8.12)]

$$L = \frac{6}{\kappa_5\mathcal{T}} \quad \text{so that} \quad \kappa_4 = \frac{\kappa_5}{L} \ . \tag{8.57}$$

Note that, although for a de Sitter brane the density is simply constant, $\rho = -P = $ const. and there is no late time approximation, Eq. (8.53) implies that the Hubble rate remains constant and the usual exponential expansion is reproduced. Only the relation between the expansion rate H and the brane density ρ is modified.

Putting everything together, the modified Friedmann equation becomes

$$H^2 = \frac{\kappa_4\rho}{3}\left(1 + \frac{\rho}{2\mathcal{T}}\right). \tag{8.58}$$

Note that for a non-flat brane ($K \neq 0$), the $\frac{K}{a^2}$-term would appear in (8.58) as in (6.20). While the dynamics of the Universe in brane cosmology remains unchanged at late times when $\rho \ll \mathcal{T}$, it is modified in the early Universe due to $H^2 \propto \rho^2$, i.e. in the high-energy regime. Cosmological observations impose a lower limit on the brane tension $\mathcal{T}$. Significant deviations from usual general relativity must take place before nucleosynthesis which is very sensitive to the expansion rate , thus

$$\mathcal{T} > (1\,\mathrm{MeV})^4 \ , \tag{8.59}$$

implying for the five-dimensional Planck mass [69, 152]

$$M_5 > 10^4\mathrm{GeV} \ . \tag{8.60}$$

Hence, if the brane tension is for example given by the electroweak scale $\mathcal{T} \geq (1\,\mathrm{TeV})^4$, the observed low energy cosmology is not affected.

If the matter on the brane has an equation of state $P = w\rho$ with $w = $ const., Eq. (8.58) can be integrated [69, 152]. Using *cosmological time* τ on the brane, i.e. $H = (\partial_\tau a)/a$, and (6.24) leads to

$$a(\tau) = a_0\left[\tau\left(\tau + \tau_{\mathcal{T}}\right)\right]^{1/[3(1+w)]} \tag{8.61}$$

with ($w > -1$)

$$\tau_{\mathcal{T}} = \frac{m_{\mathrm{Pl}}}{\sqrt{3\pi\mathcal{T}}(1+w)} < (1+w)^{-1} \times 10^{-9}\ \mathrm{seconds} \ , \tag{8.62}$$

where for the inequality the bound (8.59) has been used. In the limit $\mathcal{T} \to \infty$, i.e. $\tau_{\mathcal{T}} \to 0$, the usual four-dimensional behavior from general relativity is recovered. For times $\tau \ll \tau_{\mathcal{T}}$ the evolution differs from standard cosmology while for "late times" $\tau \gg \tau_{\mathcal{T}}$ it is the usual one. During a radiation dominated stage with $w = 1/3$, for example, one finds $a \propto \tau^{1/4}$ for high energies (early times), instead of the usual (low energy) $a \propto \tau^{1/2}$ behavior.

A qualitative analysis of the Friedmann equations in braneworld cosmology is given in [29, 30]. For a discussion of inflation in the braneworld scenario see the review [152] and the references therein.

8.5 Tensor perturbations in a RS braneworld

Perturbation theory in braneworld cosmology has been extensively studied and developed. To give a detailed introduction into this subject would exceed the frame of this thesis (and the knowledge of its author). A comprehensive list of references can be found in, e.g., Chapter 6 of [152]. Here, I shall concentrate only on tensor perturbations, in particular on the degree of freedom of the five-dimensional graviton which appears as four-dimensional graviton in our Universe. The presentation is partly based on [152, 136, 52, 67].
The spin-2 graviton in five dimensions is represented by a transverse traceless metric perturbation h_{AB} and has five spin sates. In our Universe, i.e. projected onto the brane, four of those five degrees of freedom (polarizations) of the five-dimensional graviton field are felt as the four-dimensional spin-2 graviton h_{ij} and a vector perturbation Σ_i which is the spin-1 *gravi-vector*. Both have two polarizations. The fifth degree of freedom felt on the brane is a scalar perturbation which is called *gravi-scalar*. All three different types of perturbations evolve independently from each other, depend on the extra dimension and satisfy the same wave equation. Therefore, having the KK-decomposition in mind, each of these perturbations appears as a tower of KK modes on the brane. In the following I restrict myself to the investigation of the modes h_{ij}, i.e. to the four-dimensional spin-2 gravitons on the brane, which I shall just call tensor perturbations. The massless zero mode of h_{ij}, mass in the sense of the KK-decomposition, corresponds to the standard four-dimensional graviton.
The bulk metric allowing for tensor perturbations of the spatial three-dimensional geometry at fixed y reads (compare with Section 6.4.2) [136, 52]

$$ds^2 = \frac{L^2}{y^2}\left[-dt^2 + (\delta_{ij} + 2h_{ij})dx^i dx^j + dy^2\right] \ , \tag{8.63}$$

where the perturbation now depends on the extra dimension $h_{ij} = h_{ij}(t, \mathbf{x}, y)$ and satisfies

$$h^i_i = \partial_i h^i_j = 0 \ . \tag{8.64}$$

From the perturbed five-dimensional Einstein equation

$$\delta G_{AB} = -\Lambda_5 \delta g_{AB} = \frac{6}{L^2}\delta g_{AB} \ , \tag{8.65}$$

where I have used the RS fine tuning (8.14), it follows that the tensor modes satisfy the wave equation for minimally coupled massless scalar fields in AdS_5 [89, 90, 138]

$$\left[\partial_t^2 - \triangle_{(3)} - \partial_y^2 + \frac{3}{y}\partial_y\right] h_{ij}(t, \mathbf{x}, y) = 0 \ , \tag{8.66}$$

where $\triangle_{(3)}$ is the Laplacian of three-dimensional flat space. Transversality and vanishing trace implies that h_{ij} has only two independent degrees of freedom, the two polarizations $\bullet = \times$ and $\bullet = +$, such that h_{ij} can be decomposed into spatial Fourier modes like in Eq. (6.36)

$$h_{ij}(t, \mathbf{x}, y) = \int \frac{d^3k}{(2\pi)^{3/2}} \sum_{\bullet=+,\times} e^{i\mathbf{k}\cdot\mathbf{x}} e^{\bullet}_{ij}(\mathbf{k}) h_\bullet(t, y, \mathbf{k}) \ , \tag{8.67}$$

where $e^{\bullet}_{ij}(\mathbf{k})$ are the unitary constant transverse-traceless polarization tensors (6.37,6.38) which form a basis of the two polarization states. For h_{ij} to be real one has to require

$$h^*_\bullet(t, y, \mathbf{k}) = h_\bullet(t, y, -\mathbf{k}). \tag{8.68}$$

Inserting the expansion (8.67) into (8.66) leads to the two-dimensional wave equation for the tensor amplitudes $h_\bullet(t, y, \mathbf{k})$

$$\left[\partial_t^2 + k^2 - \partial_y^2 + \frac{3}{y}\partial_y\right] h_\bullet(t, y, \mathbf{k}) = 0 \ . \tag{8.69}$$

This equation describes the perturbations in the entire bulk but it does not involve any time-dependence. As I shall show now, the time-dependence enters through a boundary condition for the perturbation at the moving brane as a consequence of the second junction condition.
The perturbed second junction condition at the brane reads

$$[\delta K_{\mu\nu}]\Big|_{y_b} = \kappa_5 \delta \widehat{S}_{\mu\nu} \ , \tag{8.70}$$

leading to

$$\begin{aligned}[\delta K_{\mu\nu}]\Big|_{y_b} &= 2\frac{\sqrt{1+L^2H^2}}{L}\left[2h_{ij} - y_b\partial_y h_{ij} + y_b\frac{LH}{\sqrt{1+L^2H^2}}\partial_t h_{ij}\right]\Big|_{y_b} \\ &= \frac{\kappa_5}{3}\left[2(\rho+\mathcal{T})h_{ij} + 3P\Pi_{ij}^{(T)}\right]\Big|_{y_b} . \end{aligned} \tag{8.71}$$

Here $\Pi_{ij}^{(T)}$ denotes possible anisotropic stress perturbations in the brane energy-momentum tensor [69]. From now on I shall neglect the anisotropic stress perturbations for simplicity, $\Pi_{ij}^{(T)} \equiv 0$, since I am interested in the quantum production of free gravitons, not in the coupling of gravitational waves to matter. That is, I make the assumption that the Universe is filled with a perfect fluid. Some of the difficulties which appear when $\Pi_{ij}^{(T)} \neq 0$ are discussed in [31].
Using the background equations and the expansion of the tensor perturbation in Fourier modes (8.67), Eq. (8.71) can be cast into the form

$$\left[LH\partial_t h_\bullet(t,y,\mathbf{k}) - \sqrt{1+L^2H^2}\partial_y h_\bullet(t,y,\mathbf{k})\right]\Big|_{y_b(t)} = 0 . \tag{8.72}$$

Finally, with the definition of the brane velocity (8.46), it can be written as

$$\left(v\partial_t + \partial_y\right) h_\bullet(t,y,\mathbf{k})\big|_{y_b(t)} = 0 . \tag{8.73}$$

It is the time-dependence of the boundary condition caused by the moving brane which leads to a non-trivial time evolution for the tensor modes. The problem is now completely equivalent to the dynamical Casimir effect discussed for the scalar and electromagnetic fields in the first part of this thesis.
Two facts are worth stressing. First, the boundary problem for tensor perturbations is the same as for transverse-magnetic polarized modes of the electromagnetic field [cf. Section 5.1]. In this context, the boundary condition (8.73) has been called *generalized Neumann boundary condition* [cf. Eq. (5.24)]. Secondly, the boundary condition (8.73), here derived via the second junction condition (8.70), is also the only possible boundary condition which is compatible with the variational principle starting from an action for $h_\bullet(t,y,\mathbf{k})$, except under the (unphysical) assumption that $h_\bullet(t,y,\mathbf{k})$ is constant on the brane (e.g., Dirichlet boundary condition). The wave equation (8.69) and the boundary condition (8.73) follow directly form the variation of the action

$$\mathcal{S}^{(2)} = 2\,\frac{L^3}{2\kappa_5}\sum_\bullet \int dt \int d^3k \int_{y_b(t)}^{y_s}\frac{dy}{y^3}\left[|\partial_t h_\bullet(t,y,\mathbf{k})|^2 - |\partial_y h_\bullet(t,y,\mathbf{k})|^2 - k^2\,|h_\bullet(t,y,\mathbf{k}|^2\right] \tag{8.74}$$

by means of a similar calculation as the one shown in more detail for the model of a massive scalar field in a two-dimensional spacetime with moving boundaries in Section 3.3. The above action can be obtained from the second-order perturbation of the gravitational Lagrangian which is quite involved (see also Section 6.4.2). Notice the additional factor 2, which is due to $\mathbb{Z}_2$-symmetry.

After quantizing the tensor perturbations, the brane moving through the AdS bulk leads to the creation of gravitons from vacuum fluctuations in the same way the moving mirror leads to photon production in dynamical cavities as discussed in part one of the thesis. I shall therefore refer to this phenomenon as *dynamical Casimir effect for gravitons* which is the subject of the next Chapter and was the second main research topic of my thesis.

Chapter 9

Dynamical Casimir effect approach to graviton production by a moving brane

9.1 The problem and motivations

As I have shown in the preceding Chapter, at low energies the observed cosmological evolution is not affected within the braneworld scenario. However, perturbations on the brane, i.e in our Universe, carry five-dimensional effects like massive four-dimensional gravitons as discussed in Section 8.5. Described by the wave equation (8.69) and the time-dependent boundary condition (8.73) caused by the motion of the brane through the AdS bulk, the evolution of perturbations is highly non trivial. Depending on the particular brane trajectory, their amplitude may be significantly amplified leading to observable consequences, for example a stochastic gravitational wave background. (For a review of stochastic gravitational waves see [154].) This amplification mechanism is identical to the dynamical Casimir effect in dynamical cavities as discussed in the first part of the thesis. In the quantum field theoretical language, such an amplification corresponds to the creation of particles, here gravitons, out of vacuum fluctuations. Hence, in the same way the moving mirror in a dynamical cavity leads to the production of photons, the brane moving through the bulk causes the creation of gravitons. Thereby, not only the usual massless graviton might be produced, but also gravitons of the KK-tower can be excited. Those massive gravitons are of particular interest, since their energy density could eventually dominate the energy density of the Universe and spoil the phenomenology if their production is sufficiently copious.

The evolution of cosmological perturbations under the influence of moving brane has been the subject of many studies during recent years. Since one has to deal with a complicated partial differential equation and time-dependent boundary conditions the investigation of the evolution of perturbations in the background of a moving brane is quite complicated. Analytical progress has been made based on approximations like the "near brane limit" and a slowly moving brane [10, 11, 70, 125].
The case of de Sitter or quasi-de Sitter inflation on the brane has been investigated analytically in [85, 124, 153, 138]. In [138] it is demonstrated that during slow-roll inflation (modeled as a period of quasi-de Sitter expansion) the standard four-dimensional result for the amplitude of perturbations is recovered at low energies while it is enhanced at high energies.
However, most of the effort has gone into numerical simulations [91, 92, 93, 130, 99, 100, 121, 122, 123, 199], in particular in order to investigate the high energy regime. Thereby different coordinate systems have been used for which the brane is at rest, and different numerical evolution schemes have been employed in order to solve the partial differential equation. Recall that in coordinates in which the brane is not moving, the boundary condition simplifies significantly but the bulk metric becomes time dependent (see e.g.,[130]) what leads a priori not to a simpler problem. The above mentioned simulations are based on the classical evolution of the perturbations (most of them) but also on their quantum mechanical treatment, in particular [121, 122].

For this thesis I have chosen a different way of looking at the problem. In contrast to the above cited studies, I shall apply the dynamical Casimir effect formalism outlined in Chapter 3 to study the amplification of tensor perturbation, i.e. the production of gravitons, in braneworld cosmology. This approach and its numerical implementation, which has been employed to braneworld cosmology here for the first time, offers many advantages and differs from the cited numerical evolution schemes in different respects. The most important advantage

is the fact that this approach deals directly with the mode couplings described by the coupling matrices [1]. Hence, the complicated interaction between the four-dimensional graviton and the KK modes is not hidden within a numerical simulation, but can directly be investigated. Since the coupling matrices enter the system of differential equations describing the evolution of the Bogoliubov coefficients "analytically", different couplings between modes can be switched on and off artificially. This makes it possible to select the most relevant couplings and reveals the underlying physical effects in a very transparent way. As I shall show below, under certain circumstances it is then possible to find analytical solutions. Another advantage concerns the accuracy of the numerical simulations. Since the boundary motion is encoded in the coupling matrices the numerical problem is reduced to solving a system of coupled linear first-order ordinary differential equations which can be done with very high accuracy.

In the following I consider the setup of a flat FLRW-brane of positive tension representing our Universe which moves through the AdS_5 bulk with a time-dependent position $y_b(t)$. Additionally, a second brane is introduced at a fixed position $y_s > y_b(t)$. The fixed brane serves as a regulator brane for the numerics in RS II-type models [182] and as a "real" brane in the spirit of ekpyrotic models about which I shall say more in Chapter 10. For reasons discussed below in detail, I shall assume that the velocity of the brane is small, but the brane trajectory otherwise not restricted. This setup is generic enough to study many interesting effects and is depicted in Fig. 9.1 for better illustration.

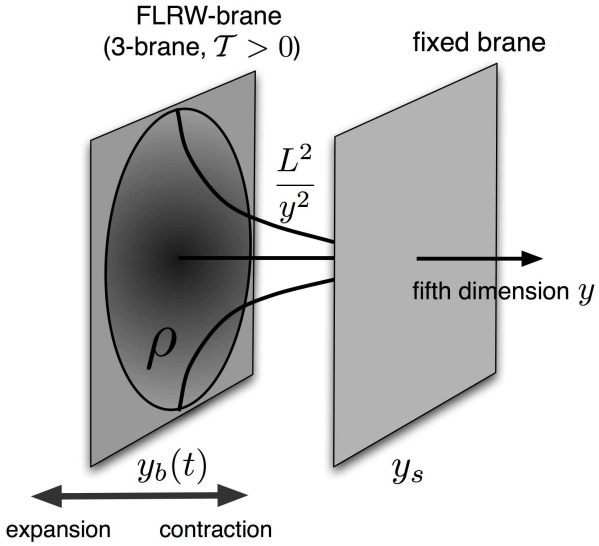

Figure 9.1: Two branes in an AdS_5 spacetime. The physical brane is to the left. While it is approaching the fixed brane its scale factor is decreasing, and when it moves away from the fixed brane the physical brane is expanding. The value of the warp factor as function of the extra dimension y is also indicated.

9.2 Canonical formulation in the low energy limit

9.2.1 Introductionary remarks

The treatment of the dynamical Casimir effect expounded in Chapter 3 relies on the existence of eigenfunctions of the spatial part of the wave equation which obey the time-dependent boundary condition. As already mentioned there, this is not practicable for the junction condition (8.73) involving a time derivative ∂_t. One possibility is to use a different coordinate system in which the boundary conditions at both branes are of Neumann type. Such a coordinate transformation has been proposed in [42] for the treatment of the transverse-magnetic modes in a dynamical cavity (cf. Section 5.6). In this work I shall proceed otherwise. I use an approximation for the junction condition at low energies, supposing a small brane velocity. As I shall

[1] Note that in [11] a similar approach involving coupling matrices has been used. However, perturbatively only, and not in the complexity presented in this Chapter.

demonstrate, if this approximation is done consistently, the equations following from the full five-dimensional theory reproduce exactly the behavior of the four-dimensional graviton. Hence, at low energies, the evolution of the usual four-dimensional graviton is not modified by effects related to the fifth dimension; its equation of motion is reproduced automatically. This is certainly not a proof of the goodness of the approximation but provides me with confidence that this treatment of five-dimensional perturbations should be valid at low energies where four-dimensional physics is in perfect agreement with observations. Eventually, of course, this has to be confirmed by implementing the full junction condition for which this work and the used numerics provides a very reliable starting point.

9.2.2 Mode expansion

The restriction to late times and low energies is characterized by [cf. Eqs. (8.58)]

$$\rho\mathcal{T} \gg \rho^2 \ , \ \ |LH| \ll 1 \ \text{ and therefore } \ |v| \ll 1. \tag{9.1}$$

One particular example which I shall consider below is a radiation dominated dynamics of the brane. Since in this limit $\gamma \simeq 1$ (cf. Eq. (8.45)), the conformal time on the brane η agrees roughly with the five-dimensional conformal time coordinate t. Thus I set $t = \eta$, and I do not distinguish between these times in the following. Because of $|v| \ll 1$, I now assume that in the low energy limit the junction condition (8.73) at the position of the moving brane can be replaced by a Neumann boundary condition. The graviton amplitude is then subject to the boundary conditions

$$\partial_y h_\bullet|_{y_b} = \partial_y h_\bullet|_{y_s} = 0 \ . \tag{9.2}$$

This is the basic approximation (assumption) which most of the remaining material is based on.
Given the boundary conditions (9.2), a canonical formulation, i.e. a description of the graviton field and its dynamics in terms of field modes in the spirit of the dynamical Casimir effect can now be achieved. I introduce instantaneous real eigenfunctions $\phi_\alpha(t, y)$ of the spatial part of the differential operator (8.69)

$$\left[-\partial_y^2 + \frac{3}{y}\partial_y\right]\phi_\alpha(t,y) = -y^3\partial_y\left[y^{-3}\partial_y\phi_\alpha(t,y)\right] = m_\alpha^2(t)\phi_\alpha(t,y) \tag{9.3}$$

and impose the boundary conditions (9.2) for these eigenfunctions. This forms a Sturm-Liouville problem at any given time t. Consequently, the set of eigenfunctions $\{\phi_\alpha(t,y)\}_{\alpha=0}^{\infty}$ is complete and orthonormal with respect to the inner-product

$$(\phi_\alpha, \phi_\beta) = 2\int_{y_b}^{y_s}\frac{dy}{y^3}\phi_\alpha(t,y)\phi_\beta(t,y) = \delta_{\alpha\beta}. \tag{9.4}$$

The completeness relation of the eigenfunctions ϕ_α reads

$$2\sum_\alpha \phi_\alpha(t,y)\phi_\alpha(t,\tilde{y}) = \delta(y-\tilde{y})y^3 \ . \tag{9.5}$$

Note the factor 2 in front of both expressions which takes into account the $\mathbb{Z}_2$-symmetry.
The case $\alpha = 0$ with $m_0 = 0$ is the zero-mode, i.e. the massless four-dimensional graviton. Its general solution in accordance with the boundary conditions is just a constant with respect to the extra dimension, $\phi_0(t,y) = \phi_0(t)$, and is fully determined by the normalization condition $(\phi_0, \phi_0) = 1$:

$$\phi_0(t) = \frac{y_s y_b(t)}{\sqrt{y_s^2 - y_b^2(t)}}. \tag{9.6}$$

For $\alpha = n \in \{1, 2, 3, \cdots, \}$ with eigenvalues $m_n > 0$ the general solution of (9.3) is a combination of the Bessel functions $J_2\left(m_n(t)\, y\right)$ and $Y_2\left(m_n(t)\, y\right)$. The particular combination is determined by the boundary condition at the moving brane. The remaining boundary condition at the fixed brane selects the possible values for the eigenvalues $m_n(t)$, the KK masses. Explicitly, the solutions $\phi_n(t,y)$ corresponding to the KK modes are given by

$$\phi_n(t,y) = N_n(t) y^2 \mathcal{C}_2\left(m_n(t)\, y\right) \tag{9.7}$$

where I have defined

$$\mathcal{C}_\nu(m_n y) = Y_1(m_n y_b)J_\nu(m_n y) - J_1(m_n y_b)Y_\nu(m_n y). \tag{9.8}$$

The normalization reads

$$N_n(t, y_b, y_s) = \left[\frac{1}{y_s^2 \mathcal{C}_2^2(m_n\, y_s) - \left(2/(m_n \pi)\right)^2} \right]^{\frac{1}{2}} \tag{9.9}$$

where I have used that (see [1] Eq. (9.1.16))

$$\mathcal{C}_2(m_n\, y_b) = \frac{2}{\pi\, m_n\, y_b}\ . \tag{9.10}$$

N_i can be simplified further by using

$$\mathcal{C}_2(m_n\, y_s) = \frac{Y_1(m_n\, y_b)}{Y_1(m_n\, y_s)} \frac{2}{\pi\, m_n\, y_s} \tag{9.11}$$

leading to

$$N_n = \frac{m_n \pi}{2} \left[\frac{Y_1^2(m_n y_s)}{Y_1^2(m_n y_b) - Y_1^2(m_n y_s)} \right]^{\frac{1}{2}}. \tag{9.12}$$

Note that it is possible to have $Y_1^2(m_n\, y_s) - Y_1^2(m_n\, y_b) = 0$. But then $Y_1^2(m_n y_s) = Y_1^2(m_n y_b) = 0$ and Eq. (9.12) has to be understood as a limit. For that reason, the expression (9.9) for the normalization is used in the numerical simulations. Its denominator remains always finite.
The spectrum of time-dependent KK masses $\{m_n(t)\}_{i=1}^{\infty}$ is determined by the condition

$$\mathcal{C}_1\left(m_n(t) y_s\right) = 0. \tag{9.13}$$

This condition poses the first difficulty which requires numerical work: Because the zeros of the cross product of the Bessel functions J_1 and Y_1 are not known analytically in closed form, the KK-spectrum has to be determined by solving Eq. (9.13) numerically [2].
An important quantity which I need below is the rate of change $\dot{m}_n/m_n$ of a KK-mass given by

$$\hat{m}_n \equiv \frac{\dot{m}_n}{m_n} = \hat{y}_b\, \frac{4}{m_n^2\, \pi^2}\, N_n^2 \tag{9.14}$$

where the rate of change of the brane motion

$$\hat{y}_b(t) \equiv \frac{\dot{y}_b}{y_b} \simeq -Ha = -\frac{\dot{a}}{a} = -\mathcal{H} \tag{9.15}$$

is just the Hubble parameter on the brane. From now on, an over-dot always denotes the derivative with respect to t.

9.2.3 Equations of motion

On account of the completeness of the eigenfunctions $\phi_\alpha(t, y)$ the gravitational wave amplitude $h_\bullet(t, y, \mathbf{k})$ can now be expanded in these eigenfunctions

$$h_\bullet(t, y, \mathbf{k}) = \sqrt{\frac{\kappa_5}{L^3}} \sum_{\alpha=0}^{\infty} q_{\alpha,\mathbf{k},\bullet}(t) \phi_\alpha(t, y). \tag{9.16}$$

The coefficients $q_{\alpha,\mathbf{k},\bullet}(t)$ are canonical variables describing the time-evolution of the five-dimensional perturbations and the factor $\sqrt{\kappa_5/L^3}$ has been introduced in order to render the $q_{\alpha,\mathbf{k},\bullet}$'s canonically normalized. The first term in the expansion $\alpha = 0$ corresponds to the usual four-dimensional graviton, and the succesive terms $\alpha \geq 1$ to the tower of KK gravitons. In order to satisfy (8.68) ensuring that the perturbation is real, one has to impose the same condition for the canonical variables:

$$q^*_{\alpha,\mathbf{k},\bullet}(t) = q_{\alpha,-\mathbf{k},\bullet}(t). \tag{9.17}$$

As discussed in Section 3.3.2, imposing a Neumann boundary condition at a moving boundary does not lead to a free wave equation by means of variation of the action (8.74). Consequently, if one would insert the expansion

[2] Approximate expressions for the zeros can be found in [1].

(9.16) into the wave equation (8.69), one is led to an equation of motion for the variables $q_{\alpha,\mathbf{k},\bullet}(t)$ of the form (3.31). This equation cannot be derived by means of Hamiltonian equations of motion (3.27,3.28) since no associated Lagrangian and hence Hamiltonian exists while the boundary is in motion. The only consistent way to implement the boundary condition (9.2) is therefore to consider the action (8.74) as the starting point. Inserting the expansion (9.16) into the action (8.74) leads to the canonical action

$$\mathcal{S}^{(2)} = \frac{1}{2}\sum_{\bullet}\int dt \int d^3k \Big\{ \sum_{\alpha} \left[|\dot{q}_{\alpha,\mathbf{k},\bullet}|^2 - \Omega_{\alpha,k}^2 |q_{\alpha,\mathbf{k},\bullet}|^2 \right] + \sum_{\alpha\beta} \left[M_{\alpha\beta} \left(q_{\alpha,\mathbf{k},\bullet}\dot{q}_{\beta,-\mathbf{k},\bullet} + q_{\alpha,-\mathbf{k},\bullet}\dot{q}_{\beta,\mathbf{k},\bullet} \right) + N_{\alpha\beta} q_{\alpha,\mathbf{k},\bullet} q_{\beta,-\mathbf{k},\bullet} \right] \Big\}. \tag{9.18}$$

I have introduced the time-dependent frequency of a graviton mode

$$\Omega_{\alpha,k} = \sqrt{k^2 + m_\alpha^2} \ , \quad k = |\mathbf{k}| \ , \tag{9.19}$$

and the familiar coupling matrices

$$M_{\alpha\beta}(t) \equiv (\partial_t \phi_\alpha, \phi_\beta) \ , \quad N_{\alpha\beta}(t) \equiv (\partial_t \phi_\alpha, \partial_t \phi_\beta) \ , \tag{9.20}$$

which are given explicitely in 9.2.4. Introducing the canonically conjugate momentum

$$p_{\alpha,\mathbf{k},\bullet} = \frac{\partial L}{\partial \dot{q}_{\alpha,\mathbf{k},\bullet}} = \dot{q}_{\alpha,-\mathbf{k},\bullet} + \sum_{\beta} M_{\beta\alpha} q_{\beta,-\mathbf{k},\bullet} \tag{9.21}$$

leads, after Legendre transformation, to the Hamiltonian describing the evolution of the perturbations

$$H = \sum_{\bullet}\int d^3k \left\{ \frac{1}{2}\sum_{\alpha} \left[|p_{\alpha,\mathbf{k},\bullet}|^2 + \Omega_{\alpha,k}^2 |q_{\alpha,\mathbf{k},\bullet}|^2 \right] - \frac{1}{2}\sum_{\alpha\beta} M_{\beta\alpha} \left[q_{\beta,\mathbf{k},\bullet} p_{\alpha,\mathbf{k},\bullet} + p_{\alpha,\mathbf{k},\bullet} q_{\beta,\mathbf{k},\bullet} \right] \right\} \ , \tag{9.22}$$

where I have symmetrized the interaction term.
Consequently, the equations of motion for the canonical variables $q_{\alpha,\mathbf{k},\bullet}$ are

$$\ddot{q}_{\alpha,\mathbf{k},\bullet} + \Omega_{\alpha,k}^2 q_{\alpha,\mathbf{k},\bullet} + \sum_{\beta} \left[M_{\beta\alpha} - M_{\alpha\beta} \right] \dot{q}_{\beta,\mathbf{k},\bullet} + \sum_{\beta} \left[\dot{M}_{\alpha\beta} - N_{\alpha\beta} \right] q_{\beta,\mathbf{k},\bullet} = 0 \ . \tag{9.23}$$

The dynamical equations describing the evolution of tensor perturbations are identical to the ones describing the dynamics of a scalar field on a time-dependent interval (3.21). Here, the only difference is the appearance of the three-momentum $\mathbf{k}$. As in the case of the electromagnetic field discussed in Chapter 5, modes with different $\mathbf{k}$ do not couple due to translation invariance with respect to the directions parallel to the brane. The three-momentum enters the equations only via the frequency $\Omega_{\alpha,k}$, i.e. as a global quantity similar to the mass of the scalar field of Chapter 3. The motion of the brane through the bulk, i.e. the expansion of the Universe, is encoded in the time-dependent coupling matrices $M_{\alpha\beta}, N_{\alpha\beta}$. These mode couplings are caused by the time-dependent boundary condition $\partial_y h_\bullet(t,y,k)|_{y_b(t)} = 0$ which forces the eigenfunctions $\phi_\alpha(t,y)$ to be explicitly time dependent. In addition, the frequency of a KK mode is also time dependent since the distance between the two branes changes when the brane is in motion. Both time-dependencies can lead to the amplification of perturbations, i.e. graviton production. For the bouncing model which I shall discuss in the next Chapter, it turns out that the inter-mode coupling is the most important source for the production of KK gravitons.

9.2.4 Coupling matrices

The use of several identities of Bessel functions leads to the coupling matrices

$$M_{00} = \hat{y}_b \frac{y_s^2}{y_s^2 - y_b^2} \ , \tag{9.24}$$

$$M_{0m} = 0 \ , \tag{9.25}$$

$$M_{n0} = \frac{4N_n}{\pi m_n}\frac{\hat{y}_b}{y_b}\phi_0 = \hat{y}_b \, \frac{4}{\pi m_n} \, N_n \, \frac{y_s}{\sqrt{y_s^2 - y_b^2}} \ , \tag{9.26}$$

$$M_{nn} = \hat{m}_n \ , \tag{9.27}$$

$$M_{nm} = M_{nm}^{\mathrm{A}} + M_{nm}^{\mathrm{N}} \tag{9.28}$$

with

$$M^{\rm A}_{nm} = (\hat{y}_b + \hat{m}_n) y_b \frac{2\, m_n^2 N_n N_m}{m_m^2 - m_n^2} \times \\ \times \left[y_s\, \mathcal{C}_2(m_m y_s)\, \mathcal{J}_1(m_n y_s) - y_b\, \mathcal{C}_2(m_m y_b)\, \mathcal{J}_1(m_n y_b) \right] \tag{9.29}$$

where

$$\mathcal{J}_1(m_n\, y) = [J_2(m_n y_b) Y_1(m_n y) - Y_2(m_n y_b) J_1(m_n y)] \tag{9.30}$$

and

$$M^{\rm N}_{nm} = 2\, N_n N_m m_n \hat{m}_n \int_{y_b}^{y_s} dy y^2 \mathcal{C}_1(m_n y) \mathcal{C}_2(m_m y). \tag{9.31}$$

Eventually, this integral has to be solved numerically. Note that, because of the boundary conditions, one has the identity

$$\int_{y_b}^{y_s} dy y^2 \mathcal{C}_1(m_n y) \mathcal{C}_2(m_m y) = -\int_{y_b}^{y_s} dy y^2 \mathcal{C}_1(m_n y) \mathcal{C}_0(m_m y). \tag{9.32}$$

Furthermore, one can simplify

$$\mathcal{J}_1(m_n\, y_b) = \frac{2}{\pi m_n y_b}\ , \quad \mathcal{J}_1(m_n\, y_s) = \frac{2}{\pi m_n y_b} \frac{Y_1(m_n y_s)}{Y_1(m_n y_b)} \tag{9.33}$$

where the limiting value has to be taken for the last term whenever $Y_1(m_n y_b) = Y_1(m_n y_s) = 0$.

9.3 Recovering four-dimensional gravity

Before discussing the quantization of the perturbations, it is already possible to derive an important result from the equations of motion for $q_{\alpha,\mathbf{k},\bullet}$. Numerics indicate that the term M^N_{nm} appearing in M_{nm} has a similar amplitude like M^A_{nm}, thus M^A_{nm} can give us an order of magnitude estimate of M_{nm}. Here I'm mainly interested in the limit that the fixed brane goes to infinity, $y_s \to \infty$. Setting $\epsilon = y_b/y_s$ one finds $\hat{m}_n \propto y_b \epsilon^2$ for $\epsilon \to 0$. To lowest order in ϵ the elements of the coupling matrix reduce to

$$\begin{aligned} M_{00} &= -\mathcal{H}[1 + \mathcal{O}(\epsilon)]\ , \\ M_{0m} &= 0\ , \\ M_{n0} &= \mathcal{H}\mathcal{O}(\epsilon)\ , \\ M_{nn} &= \mathcal{H}\mathcal{O}(\epsilon^2)\ , \\ M_{nm} &= \mathcal{H}\mathcal{O}(\epsilon^2)\ . \end{aligned} \tag{9.34}$$

Hence, only the M_{00} matrix element survives the limit $\epsilon \to 0$. Recall that M_{00} expresses the coupling of the zero mode to the moving boundary. Since all other couplings disappear for $\epsilon \to 0$ all modes decouple from each other and, in addition, the canonical variables for the KK modes decouple from the brane motion itself. This leads to the following interesting result. At late times and in the limit $y_s \gg y_b$, the KK modes with non-vanishing mass evolve trivially and only the massless zero mode is coupled to the brane motion [3]. Explicitely, the equation of motion for the zero mode $\alpha = 0$ is

$$\ddot{q}_{0,\mathbf{k},\bullet} + \left[k^2 - \dot{\mathcal{H}} - \mathcal{H}^2 \right] q_{0,\mathbf{k},\bullet} = 0\ , \tag{9.35}$$

while for the KK modes $\alpha = n \neq 0$

$$\ddot{q}_{n,\mathbf{k},\bullet} + \left[k^2 + m_n^2 \right] q_{n,\mathbf{k},\bullet} = 0\ . \tag{9.36}$$

Equation (9.35) is identical to Eq. (6.46) describing the evolution of the canonical variable for the usual four-dimensional tensor perturbation. Consequently, the expressions for the canonical momentum (9.21) and the Hamiltonian (9.22) consistently reduce to the expressions (6.49) and (6.48) for the four-dimensional tensor

[3] It is easy to see that $\epsilon^{-1} \sum_\alpha M_{\alpha m}$ is bounded for all values of ϵ and therefore we do not have to fear that the infinite sum might contribute in the limit $\epsilon \to 0$.

perturbation. Since $\phi_0 \propto 1/a$ [cf. Eqs. (9.75,9.77) of Section 9.5.1], and the zero mode is not coupled to the KK modes, I find that the gravitational zero-mode on the brane

$$h_{0,\bullet}(t,\mathbf{k}) \equiv \sqrt{\frac{\kappa_5}{L^3}} q_{0,\mathbf{k},\bullet}\phi_0(t,y_b) \tag{9.37}$$

evolves according to

$$\ddot{h}_{0,\bullet}(t,\mathbf{k}) + 2\mathcal{H}\dot{h}_{0,\bullet}(t,\mathbf{k}) + k^2 h_{0,\bullet}(t,\mathbf{k}) = 0 \ , \tag{9.38}$$

This equation is valid everywhere in the bulk, and in particular on the physical brane where it reproduces exactly the equation for a four-dimensional gravity wave in a FLRW-Universe (6.42). This explicitly demonstrates that at low energies (late times) the homogeneous tensor perturbation equation in brane cosmology reduces to the four-dimensional tensor perturbation equation. Massive KK modes decouple completely from the massless mode in the one brane limit and their canonical variables evolve trivially [cf. Eq. (9.36)]. The dynamical Casimir effect approach also allows the following interesting association. The friction term $\propto \mathcal{H}$ in (9.38) can be related to time-dependent boundary condition since $M_{00} \simeq -\mathcal{H}$. It is a consequence of the motion of the brane through the AdS bulk (expansion of the Universe) and not due to the excitation of massive modes damping the evolution of the zero mode as claimed in [130].

An important comment is in order here concerning the Randall-Sundrum II model. In the limit $y_s \to \infty$ the fixed brane is sent off to infinity and one ends up with a single positive tension brane in AdS, i.e. the RS II model. Even though I have just shown that all couplings except M_{00} vanish in this limit, that does not imply that this is necessarily the case for the RS II setup. Strictly speaking, the above considerations are only valid in a two brane model with $y_s \gg 1$. Starting with the RS II model from the beginning, the coupling matrices do in general not vanish when calculated with the corresponding eigenfunctions which can be found in, e.g., [85].
These eigenfunctions are similar to (9.7) but with $m_n \to m$ continuous, and a different normalization $N(m)$. The M_{m0} coupling (m continuous), for instance, is given by $(4N(m)/(\pi m))(\hat{y}_b/y_b)\phi_0$, i.e. as in (9.26), but the normalization is different and non-vanishing. Hence, in general, M_{m0} does not vanish. The reason is, that when taking the limit $y_s \to \infty$, the discrete normalization N_n (Kronecker-δ_{nm} orthonormality) does not converge into the continuum normalization $N(m)$ ($\delta(n-m)$-function orthonormality). But what the above consideration demonstrates is that, if the couplings of the zero-mode to the KK-modes vanish, like in the $y_s \gg 1$ limit or in the low energy RS II model as observed in numerical simulations (see below), the standard evolution equation for the zero-mode emerges automatically from five-dimensional perturbation theory.

In summary, starting from five-dimensional perturbation theory, the above formalism does imply the usual evolution equation for the four-dimensional graviton in a FLRW-Universe in the limit of vanishing couplings. This serves as a very strong indication (but certainly not proof!) for the fact that the approach based on the approximation (9.2) and the expansion of the action in canonical variables rather than the wave equation is consistent and leads to results which should reflect the physics at low energies. A few more comments are in order to support this statement. First of all, if one would expand the wave equation in the set of functions ϕ_α introduced above, the equation of motion for the corresponding canonical variables would be of the form (3.31). While for (9.23) the term $\propto \dot{q}_{0,\mathbf{k},\bullet}$ vanishes in the limits discussed in this section, it does not for (3.31). This equation, which cannot be derived from a Hamiltonian, does not reproduce the usual evolution equation for massless gravitons in a FLRW-Universe. Moreover, in [130] the low energy RS II scenario has been studied numerically including the full junction condition (8.73) without approximations. Those numerical results show that the evolution of tensor perturbations on the brane is four dimensional, i.e. described by Eq. (6.42) derived here analytically. Combining these observations gives me confidence that the used approach based on the Neumann boundary condition approximation and the action as starting point for the canonical formulation is adequate for the study of tensor perturbations in the low energy limit. The many benefits this approach offers will become visible in the following.

9.4 Quantum generation of tensor perturbations

9.4.1 Preliminary remarks

In this section I present the treatment of quantum generation of tensor perturbations, based on the formulation of the dynamical Casimir effect introduced in the first part of the thesis. Even though the formulation is basically the same as for the scalar field, I shall repeat the important steps for tensor perturbations again for the sake of clarity and completeness.
I assume that asymptotically, i.e. for $t \to \pm\infty$ the physical brane approaches the Cauchy horizon, $y_b \to 0$, moving very slowly. Then, asymptotically, the coupling matrices vanish and the Kaluza-Klein masses are constant

$$\lim_{t\to\pm\infty} M_{\alpha\beta}(t) = 0 \ , \quad \lim_{t\to\pm\infty} m_\alpha(t) = \text{const.} \ . \tag{9.39}$$

In this limit, the system (9.23) of differential equations reduces to an infinite set of uncoupled harmonic oscillators and the Hamiltonian (9.22) can be diagonalized. This allows to introduce an unambiguous and meaningful particle concept, i.e. notion of gravitons (cf. Section 3.4).
As a matter of fact, in the numerical simulations, the brane motion has to be switched on and off at finite times. These times are denoted by $t_{\rm in}$ and $t_{\rm out}$, respectively. I shall introduce the vacuum states with respect to times $t < t_{\rm in} < 0$ and $t > t_{\rm out} > 0$ in the same way as I have done it in 3.4. In order to avoid spurious effects influencing the particle creation, one has to chose $t_{\rm in}$ small, respectively $t_{\rm out}$ large enough such that the couplings are effectively zero at those times. Checking the independence of the numerical results on the choice of $t_{\rm in}$ and $t_{\rm out}$ guarantees that these times correspond effectively to asymptotic states of the brane configuration.

9.4.2 Quantization, initial and final state

Canonical quantization of the gravity wave amplitude is performed by replacing the canonical variables $q_{\alpha,\mathbf{k},\bullet}$ by the corresponding operators $\hat{q}_{\alpha,\mathbf{k},\bullet}$

$$\hat{h}_\bullet(t,y,\mathbf{k}) = \sqrt{\frac{\kappa_5}{L^3}} \sum_\alpha \hat{q}_{\alpha,\mathbf{k},\bullet}(t)\phi_\alpha(t,y) \ , \tag{9.40}$$

where $\hat{q}_{\alpha,\mathbf{k},\bullet}$ satisfies equation (9.23).
Under the assumptions outlined above, the operator $\hat{q}_{\alpha,\mathbf{k},\bullet}$ can be written for times $t < t_{\rm in}$ as

$$\hat{q}_{\alpha,\mathbf{k},\bullet}(t < t_{\rm in}) = \frac{1}{\sqrt{2\Omega^{\rm in}_{\alpha,k}}} \left[\hat{a}^{\rm in}_{\alpha,\mathbf{k},\bullet} e^{-i\,\Omega^{\rm in}_{\alpha,k}\,t} + \hat{a}^{\rm in\dagger}_{\alpha,-\mathbf{k},\bullet} e^{i\,\Omega^{\rm in}_{\alpha,k}\,t}\right] \tag{9.41}$$

where I have introduced the initial-state frequency

$$\Omega^{\rm in}_{\alpha,k} \equiv \Omega_{\alpha,k}(t < t_{\rm in}). \tag{9.42}$$

This expansion ensures that (9.17) is satisfied. The set of annihilation and creation operators $\{\hat{a}^{\rm in}_{\alpha,\mathbf{k},\bullet},\ \hat{a}^{\rm in\dagger}_{\alpha,\mathbf{k},\bullet}\}$ corresponding to the notion of gravitons for $t < t_{\rm in}$ is subject to the usual commutation relations

$$\left[\hat{a}^{\rm in}_{\alpha,\mathbf{k},\bullet}, \hat{a}^{\rm in\dagger}_{\alpha',\mathbf{k}',\bullet'}\right] = \delta_{\alpha\alpha'}\delta_{\bullet\bullet'}\delta^{(3)}(\mathbf{k}-\mathbf{k}') \ , \tag{9.43}$$

$$\left[\hat{a}^{\rm in}_{\alpha,\mathbf{k},\bullet}, \hat{a}^{\rm in}_{\alpha',\mathbf{k}',\bullet'}\right] = \left[\hat{a}^{\rm in\dagger}_{\alpha,\mathbf{k},\bullet}, \hat{a}^{\rm in\dagger}_{\alpha',\mathbf{k}',\bullet'}\right] = 0. \tag{9.44}$$

For times $t > t_{\rm out}$, the operator $\hat{q}_{\alpha,\mathbf{k},\bullet}$ can be expanded in a similar manner,

$$\hat{q}_{\alpha,\mathbf{k},\bullet}(t > t_{\rm out}) = \frac{1}{\sqrt{2\Omega^{\rm out}_{\alpha,k}}} \left[\hat{a}^{\rm out}_{\alpha,\mathbf{k},\bullet} e^{-i\,\Omega^{\rm out}_{\alpha,k}\,t} + \hat{a}^{\rm out\,\dagger}_{\alpha,-\mathbf{k},\bullet} e^{i\,\Omega^{\rm out}_{\alpha,k}\,t}\right] \tag{9.45}$$

with final-state frequency

$$\Omega^{\rm out}_{\alpha,k} \equiv \Omega_{\alpha,k}(t > t_{\rm out}). \tag{9.46}$$

The annihilation and creation operators $\{\hat{a}^{\rm out}_{\alpha,\mathbf{k},\bullet}, \hat{a}^{\rm out\,\dagger}_{\alpha,\mathbf{k},\bullet}\}$ correspond to a meaningful definition of final state gravitons (they are associated with positive and negative frequency solutions for $t > t_{\rm out}$) and satisfy the same

commutation relations as the initial state operators.
Initial $|0,\mathrm{in}\rangle \equiv |0, t < t_{\rm in}\rangle$ and final $|0,\mathrm{out}\rangle \equiv |0, t > t_{\rm out}\rangle$ vacuum state are uniquely defined via

$$\hat{a}^{\rm in}_{\alpha,\mathbf{k},\bullet}|0,\mathrm{in}\rangle = 0\ ,\ \hat{a}^{\rm out}_{\alpha,\mathbf{k},\bullet}|0,\mathrm{out}\rangle = 0\ ,\ \ \forall\,\alpha,\ \mathbf{k},\ \bullet\ . \tag{9.47}$$

Recall that the notations $|0, t < t_{\rm in}\rangle$ and $|0, t > t_{\rm out}\rangle$ do not mean that the states are time dependent; states do not evolve in the Heisenberg picture. The operators counting the number of gravitons defined with respect to the initial and final vacuum state, respectively, are

$$\hat{N}^{\rm in}_{\alpha,\mathbf{k},\bullet} = \hat{a}^{\rm in\,\dagger}_{\alpha,\mathbf{k},\bullet}\hat{a}^{\rm in}_{\alpha,\mathbf{k},\bullet}\ ,\ \ \hat{N}^{\rm out}_{\alpha,\mathbf{k},\bullet} = \hat{a}^{\rm out\,\dagger}_{\alpha,\mathbf{k},\bullet}\hat{a}^{\rm out}_{\alpha,\mathbf{k},\bullet}\ . \tag{9.48}$$

The number of gravitons created during the motion of the brane for each momentum $\mathbf{k}$, quantum number α and polarization state $\bullet$ is given by the expectation value of the number operator $\hat{N}^{\rm out}_{\alpha,\mathbf{k},\bullet}$ of final-state gravitons with respect to the initial vacuum state $|0,\mathrm{in}\rangle$:

$$\mathcal{N}^{\rm out}_{\alpha,\mathbf{k},\bullet} = \langle 0,\mathrm{in}|\hat{N}^{\rm out}_{\alpha,\mathbf{k},\bullet}|0,\mathrm{in}\rangle. \tag{9.49}$$

If the brane undergoes a non-trivial dynamics between $t_{\rm in} < t < t_{\rm out}$, $\hat{a}^{\rm out}_{\alpha,\mathbf{k},\bullet}|0,\mathrm{in}\rangle \neq 0$ in general, i.e. graviton production takes place.
From (8.67), the expansion (9.40) and Eqs.(9.41), (9.45) it follows that the quantized tensor perturbation with respect to the initial and final vacuum state can be written as

$$\hat{h}_{ij}(t < t_{\rm in}, \mathbf{x}, y) = \sqrt{\frac{\kappa_5}{L^3}}\sum_{\bullet,\alpha}\int \frac{d^3k}{(2\pi)^{3/2}}\frac{\hat{a}^{\rm in}_{\alpha,\mathbf{k},\bullet}\,e^{-i\,\Omega^{\rm in}_{\alpha,k}\,t}}{\sqrt{2\Omega^{\rm in}_{\alpha,k}}}\,u^{\bullet}_{ij,\alpha}(t_{\rm in},\mathbf{x},y,\mathbf{k}) + \mathrm{h.c.} \tag{9.50}$$

and

$$\hat{h}_{ij}(t > t_{\rm out}, \mathbf{x}, y) = \sqrt{\frac{\kappa_5}{L^3}}\sum_{\bullet\alpha}\int \frac{d^3k}{(2\pi)^{3/2}}\frac{\hat{a}^{\rm out}_{\alpha,\mathbf{k},\bullet}\,e^{-i\,\Omega^{\rm out}_{\alpha,k}\,t}}{\sqrt{2\Omega^{\rm out}_{\alpha,k}}}\,u^{\bullet}_{ij,\alpha}(t_{\rm out},\mathbf{x},y,\mathbf{k}) + \mathrm{h.c.}\ , \tag{9.51}$$

respectively. I have introduced the basis functions

$$u^{\bullet}_{ij,\alpha}(t,\mathbf{x},y,\mathbf{k}) = e^{i\mathbf{k}\cdot\mathbf{x}}\,e^{\bullet}_{ij}(\mathbf{k})\,\phi_\alpha(t,y) \tag{9.52}$$

which, on account of $(e^{\bullet}_{ij}(\mathbf{k}))^* = e^{\bullet}_{ij}(-\mathbf{k})$, satisfy $(u^{\bullet}_{ij,\alpha}(t,\mathbf{x},y,\mathbf{k}))^* = u^{\bullet}_{ij,\alpha}(t,\mathbf{x},y,-\mathbf{k})$.

9.4.3 Time evolution

During the motion of the brane the time evolution of the tensor modes is described by the system of coupled differential equations (9.23). To account for the inter-mode couplings mediated by the coupling matrix $M_{\alpha\beta}$ the operator $\hat{q}_{\alpha,\mathbf{k},\bullet}$ is decomposed as

$$\hat{q}_{\alpha,\mathbf{k},\bullet}(t) = \sum_\beta \frac{1}{\sqrt{2\Omega^{\rm in}_{\beta,k}}}\left[\hat{a}^{\rm in}_{\beta,\mathbf{k},\bullet}\epsilon^{(\beta)}_{\alpha,k}(t) + \hat{a}^{\rm in\dagger}_{\beta,-\mathbf{k},\bullet}\epsilon^{(\beta)^*}_{\alpha,k}(t)\right]. \tag{9.53}$$

The complex functions $\epsilon^{(\beta)}_{\alpha,k}(t)$ also satisfy the system of coupled differential equations (9.23). With the ansatz (9.53) the quantized tensor perturbation at any time during the brane motion reads

$$\hat{h}_{ij}(t,\mathbf{x},y) = \sqrt{\frac{\kappa_5}{L^3}}\sum_{\bullet\alpha\beta}\int \frac{d^3k}{(2\pi)^{\frac{3}{2}}}\frac{\hat{a}^{\rm in}_{\beta,\mathbf{k},\bullet}}{\sqrt{2\Omega^{\rm in}_{\beta,k}}}\epsilon^{(\beta)}_{\alpha,k}(t)u^{\bullet}_{ij,\alpha}(t,\mathbf{x},y,\mathbf{k}) + \mathrm{h.c.}\ . \tag{9.54}$$

Due to the time dependence of the eigenfunctions ϕ_α, the time derivative of the tensor perturbation contains mode-coupling contributions. Using the orthnormality (9.4) and completeness (9.5) of the ϕ_α's it is readily shown that

$$\dot{\hat{h}}_\bullet(t,y,\mathbf{k}) = \sqrt{\frac{\kappa_5}{L^3}}\sum_\alpha \hat{p}_{\alpha,-\mathbf{k},\bullet}(t)\phi_\alpha(t,y) \tag{9.55}$$

where [cf. Eq. (9.21)]

$$\hat{p}_{\alpha,-\mathbf{k},\bullet}(t) = \dot{\hat{q}}_{\alpha,\mathbf{k},\bullet}(t) + \sum_\beta M_{\beta\alpha}\hat{q}_{\beta,\mathbf{k},\bullet}(t). \tag{9.56}$$

The coupling term $\propto M_{\beta\alpha}$ arises from the time dependence of the mode functions ϕ_α. Accordingly, the time derivative $\dot{\hat{h}}_{ij}$ reads

$$\dot{\hat{h}}_{ij}(t,\mathbf{x},y) = \sqrt{\frac{\kappa_5}{L^3}} \sum_{\bullet\alpha\beta} \int \frac{d^3k}{(2\pi)^{\frac{3}{2}}} \frac{\hat{a}^{\rm in}_{\beta,\mathbf{k},\bullet}}{\sqrt{2\Omega^{\rm in}_{\beta,k}}} f^{(\beta)}_{\alpha,k}(t) u^{\bullet}_{ij,\alpha}(t,\mathbf{x},y,\mathbf{k}) + \text{h.c.} \tag{9.57}$$

with [cf. Eq. (3.62)]

$$f^{(\beta)}_{\alpha,k}(t) = \dot{\epsilon}^{(\beta)}_{\alpha,k}(t) + \sum_\gamma M_{\gamma\alpha}(t)\epsilon^{(\beta)}_{\gamma,k}(t). \tag{9.58}$$

By comparing Eq. (9.50) and its time-derivative with Eqs. (9.54) and (9.57) at $t = t_{\rm in}$ one can read off the initial conditions for the functions $\epsilon^{(\beta)}_{\alpha,k}$ [cf. Eq. (3.66)]

$$\epsilon^{(\beta)}_{\alpha,k}(t_{\rm in}) = \delta_{\alpha\beta}\, \Theta^{\rm in}_{\alpha,k}\ , \quad \dot{\epsilon}^{(\beta)}_{\alpha,k}(t_{\rm in}) = \left[-i\Omega^{\rm in}_{\alpha,k}\delta_{\alpha\beta} - M_{\beta\alpha}(t_{\rm in})\right]\ \Theta^{\rm in}_{\beta,k} \tag{9.59}$$

with phase

$$\Theta^{\rm in}_{\alpha,k} = e^{-i\Omega^{\rm in}_{\alpha,k}\, t_{\rm in}}. \tag{9.60}$$

The choice of this phase for the initial condition is in principle arbitrary, I could as well set $\Theta^{\rm in}_{\alpha,k} = 1$. But with this choice, $\epsilon^{(\beta)}_{\alpha,k}(t)$ is independent of $t_{\rm in}$ for $t < t_{\rm in}$ and therefore it is also at later times independent of $t_{\rm in}$ if only I choose $t_{\rm in}$ sufficiently early. This is especially useful for the numerical work.

9.4.4 Bogoliubov transformations and first order system

The two sets of annihilation and creation operators $\{\hat{a}^{\rm in}_{\alpha,\mathbf{k},\bullet},\ \hat{a}^{\rm in\,\dagger}_{\alpha,\mathbf{k},\bullet}\}$ and $\{\hat{a}^{\rm out}_{\alpha,\mathbf{k},\bullet},\ \hat{a}^{\rm out\,\dagger}_{\alpha,\mathbf{k},\bullet}\}$ corresponding to the notion of initial-state and final-state gravitons are related via a Bogoliubov transformation. Matching the expression for the tensor perturbation Eq. (9.54) and its time derivative Eq. (9.57) with the final-state expression Eq. (9.51) and its corresponding time derivative one finds

$$\hat{a}^{\rm out}_{\beta,\mathbf{k},\bullet} = \sum_\alpha \left[\mathcal{A}_{\alpha\beta,k}(t_{\rm out})\hat{a}^{\rm in}_{\alpha,\mathbf{k},\bullet} + \mathcal{B}^*_{\alpha\beta,k}(t_{\rm out})\hat{a}^{\rm in\,\dagger}_{\alpha,-\mathbf{k},\bullet}\right] \tag{9.61}$$

with

$$\mathcal{A}_{\beta\alpha,k}(t_{\rm out}) = \frac{\Theta^{\rm out^*}_{\alpha,k}}{2}\sqrt{\frac{\Omega^{\rm out}_{\alpha,\rm k}}{\Omega^{\rm in}_{\beta,\rm k}}}\left[\epsilon^{(\beta)}_{\alpha,k}(t_{\rm out}) + \frac{i}{\Omega^{\rm out}_{\alpha,k}} f^{(\beta)}_{\alpha,k}(t_{\rm out})\right] \tag{9.62}$$

and

$$\mathcal{B}_{\beta\alpha,k}(t_{\rm out}) = \frac{\Theta^{\rm out}_{\alpha,k}}{2}\sqrt{\frac{\Omega^{\rm out}_{\alpha,\rm k}}{\Omega^{\rm in}_{\beta,\rm k}}}\left[\epsilon^{(\beta)}_{\alpha,k}(t_{\rm out}) - \frac{i}{\Omega^{\rm out}_{\alpha,k}} f^{(\beta)}_{\alpha,k}(t_{\rm out})\right] \tag{9.63}$$

where I shall stick to the phase $\Theta^{\rm out}_{\alpha,k}$ defined like $\Theta^{\rm in}_{\alpha,k}$ in (9.60) for completeness. Performing the matching for $t_{\rm out} = t_{\rm in}$ the Bogoliubov transformation has to be trivial, i.e. the Bogoliubov coefficients are subject to vacuum initial conditions

$$\mathcal{A}_{\alpha\beta,k}(t_{\rm in}) = \delta_{\alpha\beta}\ \ , \ \ \mathcal{B}_{\alpha\beta,k}(t_{\rm in}) = 0. \tag{9.64}$$

By means of Eq. (9.61) the number of generated final state gravitons (9.49), which is the same in every polarization state, is given by

$$\mathcal{N}^{\rm out}_{\alpha,k}(t \geq t_{\rm out}) = \sum_{\bullet=+,\times} \langle 0,{\rm in}|\hat{N}^{\rm out}_{\alpha,\mathbf{k},\bullet}|0,{\rm in}\rangle = 2\sum_\beta |\mathcal{B}_{\beta\alpha,k}(t_{\rm out})|^2. \tag{9.65}$$

As in section 3.5.2, I introduce auxiliary functions $\xi^{(\beta)}_{\alpha,k}(t), \eta^{(\beta)}_{\alpha,k}(t)$ via

$$\xi^{(\beta)}_{\alpha,k}(t) = \epsilon^{(\beta)}_{\alpha,k}(t) + \frac{i}{\Omega^{\rm in}_{\alpha,k}} f^{(\beta)}_{\alpha,k}(t)\ , \quad \eta^{(\beta)}_{\alpha,k}(t) = \epsilon^{(\beta)}_{\alpha,k}(t) - \frac{i}{\Omega^{\rm in}_{\alpha,k}} f^{(\beta)}_{\alpha,k}(t) \tag{9.66}$$

which are related to the Bogoliubov coefficients through

$$\mathcal{A}_{\beta\alpha,k}(t_{\rm out}) = \frac{\Theta^{\rm out^*}_{\alpha,k}}{2}\sqrt{\frac{\Omega^{\rm out}_{\alpha,k}}{\Omega^{\rm in}_{\beta,k}}}\left[\Delta^{+}_{\alpha,k}(t_{\rm out})\xi^{(\beta)}_{\alpha,k}(t_{\rm out}) + \Delta^{-}_{\alpha,k}(t_{\rm out})\eta^{(\beta)}_{\alpha,k}(t_{\rm out})\right] \tag{9.67}$$

$$\mathcal{B}_{\beta\alpha,k}(t_{\rm out}) = \frac{\Theta^{\rm out}_{\alpha,k}}{2}\sqrt{\frac{\Omega^{\rm out}_{\alpha,k}}{\Omega^{\rm in}_{\beta,k}}}\left[\Delta^{-}_{\alpha,k}(t_{\rm out})\xi^{(\beta)}_{\alpha,k}(t_{\rm out}) + \Delta^{+}_{\alpha,k}(t_{\rm out})\eta^{(\beta)}_{\alpha,k}(t_{\rm out})\right] \tag{9.68}$$

with

$$\Delta^{\pm}_{\alpha,k}(t) = \frac{1}{2}\left[1 \pm \frac{\Omega^{\rm in}_{\alpha,k}}{\Omega_{\alpha,k}(t)}\right]. \tag{9.69}$$

$\xi^{(\beta)}_{\alpha,k}(t)$ and $\eta^{(\beta)}_{\alpha,k}(t)$ satisfy the following system of first order differential equations:

$$\dot{\xi}^{(\beta)}_{\alpha,k}(t) = -i\left[a^{+}_{\alpha\alpha,k}(t)\xi^{(\beta)}_{\alpha,k}(t) - a^{-}_{\alpha\alpha,k}(t)\eta^{(\beta)}_{\alpha,k}(t)\right] - \sum_{\gamma}\left[c^{-}_{\alpha\gamma,k}(t)\xi^{(\beta)}_{\gamma,k}(t) + c^{+}_{\alpha\gamma,k}(t)\eta^{(\beta)}_{\gamma,k}(t)\right] \tag{9.70}$$

$$\dot{\eta}^{(\beta)}_{\alpha,k}(t) = -i\left[a^{-}_{\alpha\alpha,k}(t)\xi^{(\beta)}_{\alpha,k}(t) - a^{+}_{\alpha\alpha,k}(t)\eta^{(\beta)}_{\alpha,k}(t)\right] - \sum_{\gamma}\left[c^{+}_{\alpha\gamma,k}(t)\xi^{(\beta)}_{\gamma,k}(t) + c^{-}_{\alpha\gamma,k}(t)\eta^{(\beta)}_{\gamma,k}(t)\right] \tag{9.71}$$

with

$$a^{\pm}_{\alpha\alpha,k}(t) = \frac{\Omega^{\rm in}_{\alpha,k}}{2}\left\{1 \pm \left[\frac{\Omega_{\alpha,k}(t)}{\Omega^{\rm in}_{\alpha,k}}\right]^2\right\}\ ,\ \ c^{\pm}_{\gamma\alpha,k}(t) = \frac{1}{2}\left[M_{\alpha\gamma}(t) \pm \frac{\Omega^{\rm in}_{\alpha,k}}{\Omega^{\rm in}_{\gamma,k}}M_{\gamma\alpha}(t)\right]. \tag{9.72}$$

The vacuum initial conditions (9.64) entail the initial conditions

$$\xi^{(\beta)}_{\alpha,k}(t_{\rm in}) = 2\,\delta_{\alpha\beta}\,\Theta^{\rm in}_{\alpha,k}\ ,\ \ \eta^{(\beta)}_{\alpha,k}(t_{\rm in}) = 0. \tag{9.73}$$

The coefficients $\mathcal{B}_{\alpha\beta,k}(t_{\rm out})$ and therefore the number of produced gravitons can be directly deduced from the solutions to this system of coupled first order differential equations. In the next section I show how interesting observable quantities like the power spectrum and the energy density of gravitational waves can be expressed in terms of the number of created gravitons.

9.5 Power spectrum and energy density

9.5.1 Perturbations on the brane

By solving the system of coupled differential equations formed by Eqs. (9.70) and (9.71) the time evolution of the quantized tensor perturbation $\hat{h}_{ij}(t,\mathbf{x},y)$ can be completely reconstructed at any position y in the bulk. Accessible to observations is the imprint which the perturbations leave on the brane, i.e. in our Universe. Of particular interest is therefore the part of the tensor perturbation which resides on the brane. It is given by evaluating Eq. (8.67) at the brane position $y = y_b$ (see also [199])

$$\hat{h}_{ij}(t,\mathbf{x},y_b) = \int \frac{d^3k}{(2\pi)^{3/2}}\sum_{\bullet=+,\times} e^{i\mathbf{k}\cdot\mathbf{x}}e^{\bullet}_{ij}(\mathbf{k})\hat{h}_{\bullet}(t,y_b,\mathbf{k})\ . \tag{9.74}$$

The motion of the brane (expansion of the Universe) enters this expression via the eigenfunctions $\phi_\alpha[t,y_b(t)]$. I shall take (9.74) as the starting point to define observables on the brane.
The zero mode function $\phi_0(t)$, given in Eq. (9.6), does not depend on the extra dimension y. Noting that $\mathcal{C}_2(m_n y_b)$ is a Wronskian [cf. Eq. (9.10)], one reads off from Eq. (9.7) that the eigenfunctions on the brane $\phi_\alpha(t,y_b)$ are

$$\phi_\alpha(t,y_b) = y_b\,\mathcal{Y}_\alpha(y_b) = \frac{L}{a}\,\mathcal{Y}_\alpha(a) \tag{9.75}$$

where I have defined

$$\mathcal{Y}_0(a) = \sqrt{\frac{y_s^2}{y_s^2 - y_b^2}}\ \text{ and }\ \mathcal{Y}_n(a) = \sqrt{\frac{Y_1^2(m_n y_s)}{Y_1^2(m_n y_b) - Y_1^2(m_n y_s)}}, \tag{9.76}$$

for the zero and KK modes, respectively. One immediately is confronted with an interesting observation: the function $\mathcal{Y}_\alpha(a)$ behaves differently with the expansion of the Universe for the zero-mode $\alpha = 0$ and the KK-modes $\alpha = n$. This is evident in particular in the asymptotic regime $y_s \gg y_b$, i.e. $y_b \to 0$ ($|t|, a \to \infty$) where, exploiting the asymptotics of Y_1 (see [1]), one finds

$$\mathcal{Y}_0(a) \simeq 1\ , \quad \mathcal{Y}_n(a) \simeq \frac{L}{a}\frac{\pi m_n}{2}|Y_1(m_n y_s)| \simeq \frac{L}{a}\sqrt{\frac{m_n\,\pi}{2\,y_s}}\ . \tag{9.77}$$

Ergo, $\mathcal{Y}_0$ is constant while $\mathcal{Y}_n$ decays with the expansion of the Universe as $1/a$. For large n one can approximate $m_n \simeq n\pi/y_s$ and $Y_1(m_n y_s) \simeq Y_1(n\pi) \simeq (1/\pi)\sqrt{2/n}$ [1], so that

$$\mathcal{Y}_n(a) \simeq \frac{L m_n}{\sqrt{2\,n a}}, \quad \mathcal{Y}_n^2(a) \simeq \frac{\pi L^2 m_n}{2\,y_s a^2}\ . \tag{9.78}$$

In summary, the amplitude of the KK modes on the brane decreases faster with the expansion of the Universe than the amplitude of the zero mode. This leads to interesting consequences for the observable power spectrum and energy density and has a clear physical interpretation: It manifest the localization of usual gravity on the brane. As I shall show below, KK-gravitons which are traces of the five-dimensional nature of gravity escape rapidly from the brane.

9.5.2 Power spectrum

I define the power spectrum $\mathcal{P}(k)$ of gravitational waves on the brane as in four-dimensional cosmology [cf. Eq. (6.54)] by using the restriction of the tensor amplitude to the brane position (9.74):

$$\frac{(2\pi)^3}{k^3}\mathcal{P}(k)\delta^{(3)}(\mathbf{k}-\mathbf{k}') = \sum_{\bullet=\times,+}\left\langle 0,\mathrm{in}\middle|\hat{h}_\bullet(t,y_b,\mathbf{k})\hat{h}_\bullet^\dagger(t,y_b,\mathbf{k}')\middle|0,\mathrm{in}\right\rangle, \tag{9.79}$$

i.e. I consider the expectation value of the field operator $\hat{h}_\bullet$ with respect to the initial vacuum state at the position of the brane $y = y_b(t)$. In order to get a physically meaningful power spectrum, averaging over several oscillations of the gravitational wave amplitude has to be performed. Equation (9.79) describes the observable power spectrum imprinted in our Universe by the four-dimensional spin-2 graviton component of the five-dimensional tensor perturbation.
The explicit calculation of the expectation value is carried out in detail in Appendix A.1. The final result reads

$$\mathcal{P}(k) = \frac{1}{a^2}\frac{k^3}{(2\pi)^3}\frac{\kappa_5}{L}\sum_\alpha \mathcal{R}_{\alpha,k}(t)\,\mathcal{Y}_\alpha^2(a). \tag{9.80}$$

The function $\mathcal{R}_{\alpha,k}(t)$ can be expressed in terms of the Bogoliubov coefficients (9.62) and (9.63) if one considers t_{out} as a continuous variable t:

$$\mathcal{R}_{\alpha,k}(t) = \frac{\mathcal{N}_{\alpha,k}(t) + \mathcal{O}^{\mathcal{N}}_{\alpha,k}(t)}{\Omega_{\alpha,k}(t)}. \tag{9.81}$$

$\mathcal{N}_{\alpha,k}(t)$ is the instantaneous particle number [cf. Section 3.5.3] and the function $\mathcal{O}^{\mathcal{N}}_{\alpha,k}(t)$ is defined in Eq. (A.6), Appendix A.1. It is important to recall that $\mathcal{N}_{\alpha,k}(t)$ can in general not be interpreted as a physical particle number. For example zero modes with wave numbers such that $kt < 1$ cannot be considered as particles. They have not performed several oscillations and their energy density cannot be defined in a meaningful way. Equivalently, expressed in terms of the complex functions $\epsilon^{(\beta)}_{\alpha,k}$, one finds

$$\mathcal{R}_{\alpha,k}(t) = \sum_\beta \frac{|\epsilon^{(\beta)}_{\alpha,k}(t)|^2}{\Omega^{\mathrm{in}}_{\beta,k}} - \frac{1}{\Omega_{\alpha,k}(t)} + \mathcal{O}^{\epsilon}_{\alpha,k}(t), \tag{9.82}$$

with $\mathcal{O}^{\epsilon}_{\alpha,k}$ given in Eq. (A.7). Equation (9.80) together with (9.81) or (9.82) holds at all times.
If one is interested in the power spectrum at early times $kt \ll 1$, it is not sufficient to take only the instantaneous particle number $\mathcal{N}_{\alpha,k}(t)$ in Eq. (9.81) into account. This is due to the fact that even if the mode functions $\epsilon^{(\beta)}_{\alpha,k}$ are already oscillating, the coupling matrix entering the Bogoliubov coefficients might still have a non-trivial time dependence [cf. Eq. (10.25)]. In the next chapter I shall show explicitly, that in a radiation dominated

bounce particle creation, especially of the zero-mode, only stops on sub-Hubble times, $kt > 1$, even if the mode functions are plane waves right after the bounce [cf, e.g., Figs. 10.1, 10.2, 10.4] Therefore, in order to determine the perturbation spectrum of the zero mode, one has to make use of the full expression expression (9.82) and may not use (9.83), given below.
At late times, $kt \gg 1$ ($t > t_{\rm out}$) when the brane moves slowly, the couplings $M_{\alpha\beta}$ go to zero and particle creation has come to an end, both functions $\mathcal{O}^{\mathcal{N}}_{\alpha,k}$ and $\mathcal{O}^{\epsilon}_{\alpha,k}$ do not contribute to the observable power spectrum after averaging over several oscillations. Furthermore, the instantaneous particle number then equals the (physically meaningful) number of created final state gravitons $\mathcal{N}^{\rm out}_{\alpha,k}$ and the KK masses are constant. Consequently, the observable power spectrum at late times takes the form

$$\mathcal{P}(k, t > t_{\rm out}) = \frac{\kappa_4}{a^2}\frac{k^3}{(2\pi)^3}\sum_{\alpha}\frac{\mathcal{N}^{\rm out}_{\alpha,k}}{\Omega^{\rm out}_{\alpha,{\rm k}}}\mathcal{Y}^2_{\alpha}(a)\ , \tag{9.83}$$

where I have used that $\kappa_5/L = \kappa_4$ [cf. Eq. (8.57)]. Its dependence on the wave number k is completely determined by the spectral behavior of the number of created gravitons $\mathcal{N}^{\rm out}_{\alpha,k}$.
It is useful to decompose the power spectrum in its zero-mode and KK-contributions:

$$\mathcal{P} = \mathcal{P}_0 + \mathcal{P}_{KK}. \tag{9.84}$$

In the late time regime, using Eqs. (9.83) and (9.77), the zero-mode power spectrum reads

$$\mathcal{P}_0(k, t > t_{\rm out}) = \frac{\kappa_4}{a^2}\frac{k^2}{(2\pi)^3}\mathcal{N}^{\rm out}_{0,k}. \tag{9.85}$$

As expected for a usual four-dimensional tensor perturbation (massless graviton), on sub-Hubble scales the power spectrum decreases with the expansion of the Universe as $1/a^2$ [cf. Eq. (6.56)].
In contrast, the KK-mode power spectrum for late times, given by

$$\mathcal{P}_{\rm KK}(k, t > t_{\rm out}) = \frac{k^3}{a^4}\frac{\kappa_4 L^2}{32\pi}\sum_{n}\mathcal{N}^{\rm out}_{n,k}\frac{m_n^2}{\Omega^{\rm out}_{\rm n,k}}Y_1^2(m_n y_s), \tag{9.86}$$

decreases as $1/a^4$, i.e. with a factor $1/a^2$ faster than $\mathcal{P}_0$. The gravity wave power spectrum at late times is therefore dominated by the zero-mode power spectrum and looks four dimensional. Contributions to it arising from five-dimensional effects are scaled away rapidly as the Universe expands due to the $1/a^4$ behavior of $\mathcal{P}_{\rm KK}$.
In the limit of large masses $m_n y_s \gg 1$, $n \gg 1$ and for wave lengths $k \ll m_n$ such that $\Omega_{n,k} \simeq m_n$, the late-time KK-mode power spectrum can be approximated by

$$\mathcal{P}_{\rm KK}(k, t > t_{\rm out}) = \frac{k^3}{a^4}\frac{\kappa_4 L^2}{16\pi^2 y_s}\sum_{n}\mathcal{N}^{\rm out}_{n,k}\ , \tag{9.87}$$

where I have inserted Eq. (9.78) for $\mathcal{Y}^2_n(a)$. Note that, as discussed at the end of Section 3.4.3, the formal summation over the particle number might be ill defined if the brane trajectory contains unphysical features like discontinuities in the velocity. An appropriate regularization is then necessary, for example, by introducing (a physically motivated) cutoff.

9.5.3 Energy density

For a usual four-dimensional tensor perturbation $h_{\mu\nu}$ on a background metric $g_{\mu\nu}$ an associated effective energy momentum tensor can be defined unambiguously by (cf. Section 6.5.3, [207])

$$T_{\mu\nu} = \frac{1}{\kappa_4}\langle h_{\alpha\beta\|\mu}h^{\alpha\beta}{}_{\|\nu}\rangle\ , \tag{9.88}$$

where the bracket stands for averaging over several periods of the wave. The energy density of gravity waves is the 00-component of the effective energy momentum tensor. Here I shall use the same effective energy momentum tensor to calculate the energy density corresponding to the four-dimensional spin-2 graviton component of the five-dimensional tensor perturbation on the brane, i.e. for the perturbation $h_{ij}(t, \mathbf{x}, y_b)$ given by Eq. (9.74). It is important to remember here that in my low energy approach, and hence in particular at late times for which I want to calculate the energy density, the conformal time η on the brane is identical to the conformal

bulk time t. The energy density of four-dimensional spin-2 gravitons on the brane produced during the brane motion is then given by (see also [199])

$$\rho = \frac{1}{\kappa_4\, a^2} \left\langle \left\langle 0, \mathrm{in}|\dot{\hat{h}}_{ij}(t,\mathbf{x},y_b)\dot{\hat{h}}^{ij}(t,\mathbf{x},y_b)|0,\mathrm{in}\right\rangle \right\rangle . \tag{9.89}$$

Here the outer bracket denotes averaging over several oscillations, which (in contrast to the power spectrum) I embrace from the very beginning. The factor $1/a^2$ comes from the fact that an over-dot indicates the derivative with respect t. A detailed calculation is carried out in Appendix A.2 leading to the result

$$\rho = \frac{1}{a^4}\sum_\alpha \int \frac{d^3k}{(2\pi)^3}\Omega_{\alpha,k}\mathcal{N}_{\alpha,k}(t)\mathcal{Y}^2_\alpha(a) \tag{9.90}$$

where again $\mathcal{N}_{\alpha,k}(t)$ is the instantaneous particle number. At late times $t > t_{\rm out}$ after particle creation has ceased, the energy density is therefore given by

$$\rho = \frac{1}{a^4}\sum_\alpha \int \frac{d^3k}{(2\pi)^3}\Omega^{\rm out}_{\alpha,\rm k}\,\mathcal{N}^{\rm out}_{\alpha,k}\,\mathcal{Y}^2_\alpha(a). \tag{9.91}$$

This expression looks at first sight very similar to a "naive" definition of energy density as integration over momentum space and summation over all quantum numbers α of the energy $\Omega^{\rm out}_{\alpha,\rm k}\,\mathcal{N}^{\rm out}_{\alpha,k}$ of created gravitons. (Note that the graviton number $\mathcal{N}^{\rm out}_{\alpha,k}$ already contains the contributions of both polarizations [see Eq. (9.65)].) However, the important difference is the appearance of the function $\mathcal{Y}^2_\alpha(a)$ which exhibits a different dependence on the scale factor for the zero mode compared to the KK modes.
Let me decompose the energy density into zero mode and KK contributions

$$\rho = \rho_0 + \rho_{KK}. \tag{9.92}$$

For the energy density of the massless zero mode one then obtains

$$\rho_0 = \frac{1}{a^4}\int \frac{d^3k}{(2\pi)^3}\, k\,\mathcal{N}^{\rm out}_{0,k}\ . \tag{9.93}$$

This is the expected behavior; the energy density of standard four-dimensional gravitons scales like radiation. In contrast, the energy density of the KK modes at late times is found to be

$$\rho_{\rm KK} = \frac{L^2}{a^6}\frac{\pi^2}{4}\sum_n \int \frac{d^3k}{(2\pi)^3}\Omega^{\rm out}_{n,k}\,\mathcal{N}^{\rm out}_{n,k}\,m_n^2 Y_1^2(m_n y_s), \tag{9.94}$$

i.e. it decays like $1/a^6$. As the Universe expands, the energy density of massive gravitons on the brane is therefore rapidly diluted. The total energy density of gravitational waves in the Universe at late times is dominated by the standard four-dimensional graviton (massless zero-mode). In the large mass limit $m_n y_s \gg 1$,$n \gg 1$ the KK-energy density can be approximated by

$$\rho_{\rm KK} \simeq \frac{\pi L^2}{2a^6 y_s}\sum_n \int \frac{d^3k}{(2\pi)^3}\,\mathcal{N}^{\rm out}_{n,k}\,\Omega^{\rm out}_{n,k} m_n\ . \tag{9.95}$$

Due to the factor m_n coming from the function $\mathcal{Y}^2_n$, for the summation over the KK-tower to converge, the number of produced gravitons $\mathcal{N}^{\rm out}_{n,k}$ has to decrease faster than $1/m_n^3$ for large masses and not just faster than $1/m_n^2$ as one might naively expect.

9.5.4 Escaping of massive gravitons and localization of gravity

As I have shown above, power spectrum and energy density of the KK modes scale with the expansion of the Universe at late times, when particle production has ceased, as

$$\mathcal{P}_{\rm KK} \propto 1/a^4\ ,\ \ \rho_{\rm KK} \propto 1/a^6. \tag{9.96}$$

Both quantities decay by a factor $1/a^2$ faster than the corresponding expressions for the zero mode graviton. In particular the energy density of the KK particles on the brane behaves effectively like stiff matter [$w = 1$ in

Eq. (6.24)]. Mathematically, this difference arises from the distinct behavior of the functions $\mathcal{Y}_0(a)$ and $\mathcal{Y}_n(a)$ [cf. Eq. (9.77)] and is a direct consequence of the warping of the fifth dimension. But what is the underlying physics? As I shall discuss now, this scaling behavior for the KK particles has indeed a very appealing physical interpretation which is in the spirit of the Randall-Sundrum model.
First, the mass m_n is a comoving mass. The (instantaneous) 'comoving' frequency or energy of a KK-graviton is $\Omega_{n,k} = \sqrt{k^2 + m_n^2}$, with comoving wave number k. The physical mass of a KK mode measured by an observer on the brane with cosmic time $d\tau = adt$ is therefore m_n/a, i.e. the KK masses are redshifted with the expansion of the Universe. This comes from the fact that m_n is the wave number corresponding to the y-direction with respect to the bulk time t which corresponds to *conformal time* η on the brane and not to physical time. It implies that the energy of KK particles on a moving AdS brane is redshifted like that of massless particles. From this alone one would expect that the energy density of KK modes on the brane decays like $1/a^4$ (see also Appendix D of [85]).

Now, let me define the "wave function" for a graviton

$$\Psi_\alpha(t, y) = \frac{\phi_\alpha(t, y)}{y^{3/2}} \tag{9.97}$$

which, by virtue of $(\phi_\alpha, \phi_\alpha) = 1$, satisfies

$$2 \int_{y_b}^{y_s} dy \Psi_\alpha^2(t, y) = 1 \ . \tag{9.98}$$

From the expansion of the gravity wave amplitude Eq. (9.16) and the normalization condition it is clear that $\Psi_\alpha^2(t, y)$ gives the probability to find a KK graviton of mass m_α for a given (fixed) time t at position y in the $\mathbb{Z}_2$-symmetric AdS-bulk. Since ϕ_α satisfies Equation (9.3), the wave function Ψ_α satisfies the Schrödinger like equation

$$-\partial_y^2 \Psi_\alpha + \frac{15}{4\, y^2} \Psi_\alpha = m_\alpha^2 \Psi_\alpha \tag{9.99}$$

and the junction conditions (9.2) translate into

$$\left(\partial_y + \frac{3}{2\, y} \right) \Psi_\alpha|_{y=\{y_b, y_s\}} = 0. \tag{9.100}$$

In Fig. 9.2 I plot the evolution of $\Psi_1^2(t, y)$ under the influence of the brane motion Eq. (10.3) with $v_b = 0.1$ which I shall study in the next chapter, as an example. For this motion, the physical brane starting at $y_b \to 0$ for $t \to -\infty$ moves towards the static brane, corresponding to a contracting Universe. After a bounce, it moves back to the Cauchy horizon, i.e. the Universe expands. The second brane is placed at $y_s = 10L$ and y ranges from $y_b(t)$ to y_s. I set $\Psi_1^2 \equiv 0$ for $y < y_b(t)$, and the time-dependent KK mass m_1 is determined numerically from Eq. (9.13). As it is evident from this figure, Ψ_1^2 is effectively localized close to the static brane, i.e. the weight of the KK-mode wave function lies in the region of less warping, far from the physical brane. Thus the probability to find a KK mode is larger in the region with less warping. Since the effect of the brane motion on Ψ_1^2 is hardly visible in Fig. 9.2, I also show the behavior of Ψ_1^2 close to the physical brane in Fig. 9.3. This shows that Ψ_1^2 peaks also at the physical brane but with an amplitude roughly ten times smaller than the amplitude at the static brane. While the brane, coming from $t \to -\infty$, approaches the point of closest encounter Ψ_1^2 slightly increases and peaks at the bounce $t = 0$ where, as I shall show in the next Chapter, the production of KK particles takes place. Afterwards, for $t \to \infty$, when the brane is moving back towards the Cauchy horizon, the amplitude Ψ_1^2 decreases again and so does the probability to find a KK particle at the position of the physical brane, i.e. in our Universe. The parameter settings used in Figures 9.2 and 9.3 are typical parameters which I use in the numerical simulations described later on. However, the effect is illustrated even better if the second brane is closer to the moving brane. In Figure 9.4 I show Ψ_1^2 for the same parameters as in Figures 9.2 and 9.3 but now with $y_s = L$. In this case, the probability to find a KK particle on the physical brane is of the same order as in the region close to the second brane during times close to the bounce. However, as the Universe expands, Ψ_1^2 rapidly decreases at the position of the physical brane.

From Eqs. (9.75) and (9.77) it follows that $\Psi_n^2(t, y_b) \propto 1/a$. The behavior of the KK-mode wave function suggests the following interpretation: If KK gravitons are created on the brane, or equivalently in our Universe, they escape from the brane into the bulk as the brane moves back to the Cauchy horizon, i.e. when the

Universe undergoes expansion. This is the reason why the power spectrum and the energy density imprinted by the KK modes on the brane decrease faster with the expansion of the Universe than for the massless zero mode.
The zero mode, on the other hand, is localized at the position of the moving brane. The profile of ϕ_0 does not depend on the extra dimension, but the zero-mode wave function Ψ_0 does. Its square is

$$\Psi_0^2(t,y) = \frac{y_s^2 y_b^2}{y_s^2 - y_b^2}\frac{1}{y^3} \to \frac{y_b^2}{y^3} = \left(\frac{L}{a}\right)^2 \frac{1}{y^3} \quad \text{if} \quad y_s \gg y_b \ , \tag{9.101}$$

such that on the brane ($y = y_b$) it behaves as

$$\Psi_0^2(t,y_b) \simeq \frac{a}{L}. \tag{9.102}$$

Equation (9.101) shows that, at any time, the zero mode is localized at the position of the moving brane. In addition, Eq. (9.102) reveals that the "localization of the zero mode on the brane becomes stronger" as the Universe expands. For a better illustration I show Eq. (9.101) in Fig. 9.5 for the same parameters as in Fig. 9.4. This is the "dynamical analog" of the localization mechanism discussed in Section 8.2.2, and (9.101) corresponds to the generalization of (8.26) to the case of a moving brane.
As I have done it in Section 8.2.2 to obtain a intuitive physical description, I again rewrite the boundary value problem (9.99), (9.100) as

$$-\partial_y^2 \Psi_\alpha(t,y) + V(y,t)\Psi_\alpha(y,t) = m_\alpha(t)\Psi_\alpha(y,t) \tag{9.103}$$

with

$$V(y,t) = \frac{15}{4\,y^2} - \frac{3}{y_b(t)}\,\delta(|y| - y_b(t)) = \frac{15}{4\,y^2} - 3\frac{a(t)}{L}\,\delta(|y| - y_b(t)) \ , \tag{9.104}$$

where I have absorbed the boundary condition at the moving brane into the (instantaneous) volcano potential $V(y,t)$ and made use of $\mathbb{Z}_2$ symmetry. At any time, the potential (9.104) supports a single bound state, the four-dimensional graviton (9.101), and acts as a barrier for the massive KK modes. The potential, ensuring localization of four-dimensional gravity on the brane and the repulsion of KK modes, moves together with the brane through the fifth dimension. Note that with the expansion of the Universe, the "depth of the delta-function" becomes larger, expressing the fact that the localization of four-dimensional gravity becomes stronger at late times [cf. Eq. (9.102), Fig. 9.5].

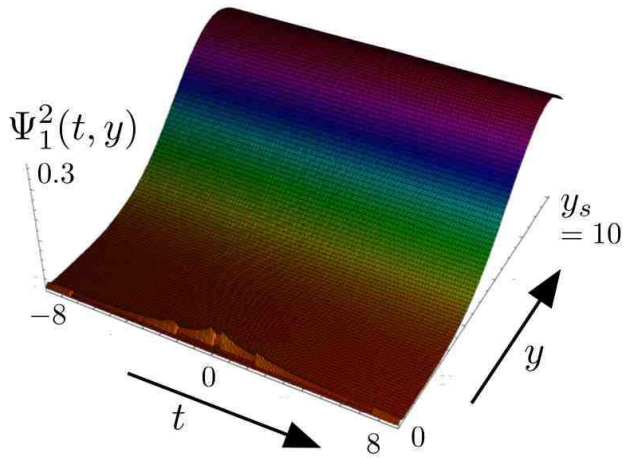

Figure 9.2: The evolution of $\Psi_1^2(t,y)$ which corresponds to the probability to find the lightest KK-graviton at time t at the position y in the AdS-bulk. The static brane is at $y_s = 10L$ and the maximal brane velocity is given by $v_b = 0.1$.

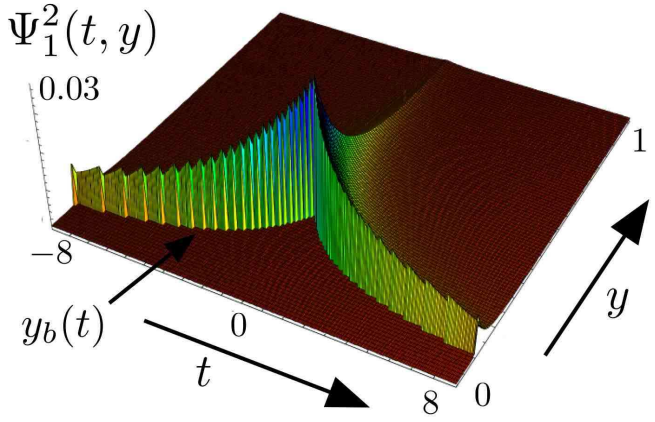

Figure 9.3: Evolution of $\Psi_1^2(t,y)$ as in Fig. 9.2 but zoomed into the bulk-region close to the moving brane.

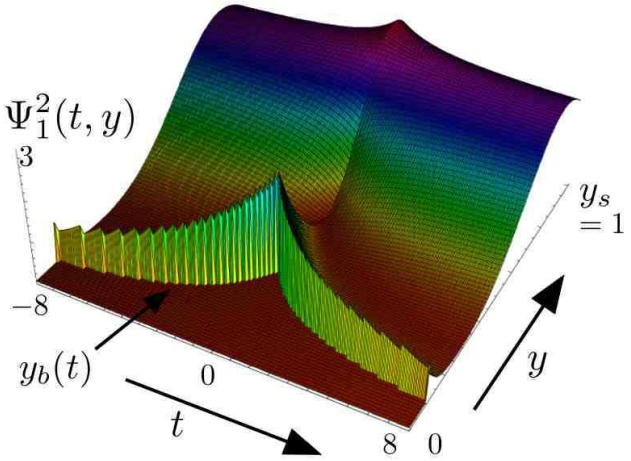

Figure 9.4: Evolution of $\Psi_1^2(t,y)$ for $y_s = L$ and $v_b = 0.1$.

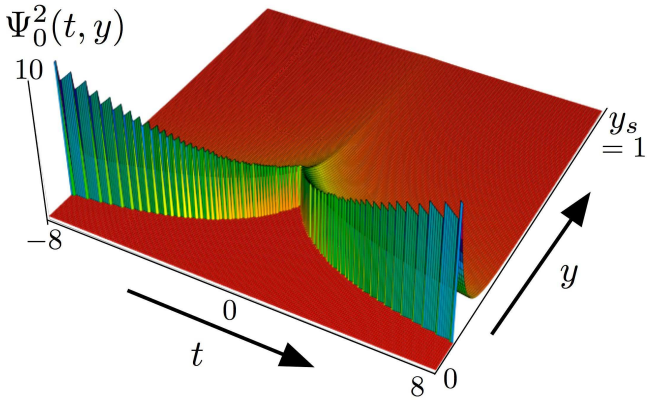

Figure 9.5: Localization of four-dimensional gravity on a moving brane: Evolution of $\Psi_0^2(t,y)$ for $y_s = L = 1$ and $v_b = 0.1$.

In summary, the different scaling behavior for the zero and KK modes on the brane is entirely a consequence of the geometry of the bulk spacetime, i.e. of the warping L^2/y^2 of the metric (8.42) [4]. It is simply a manifestation of the localization of gravity on the brane: as time evolves, the KK gravitons, which are traces of the five-dimensional nature of gravity, escape into the bulk and only the zero mode which corresponds to the usual four-dimensional graviton remains on the brane.

This, and in particular the scaling behavior (9.96), remains also true if the second brane is removed, i.e. in the limit $y_s \to \infty$, leading to the original Randall-Sundrum II model. By looking at (9.87) and (9.95) one could at first think that then the KK-power spectrum and energy density vanish and no traces of the KK gravitons could be observed on the brane since both expressions behave as $1/y_s$. But this is not the case since the spectrum of KK masses becomes continuous. In the continuum limit $y_s \to \infty$ the summation over the discrete spectrum m_n has to be replaced by an integration over continuous masses m in the following way:

$$\frac{1}{y_s}\sum_n f(m_n) \longrightarrow \frac{1}{\pi}\int dm\, f(m)\ . \tag{9.105}$$

f is some function depending on the spectrum, for example $f(m_n) = \mathcal{N}^{\rm out}_{n,k}$. The pre-factor $1/y_s$ in (9.87) and (9.95) therefore ensures the existence of the proper continuum limit of both expressions.
Another way of seeing this is to repeat the same calculations but using the eigenfunctions for the case with only one brane from the beginning. Those are δ-function normalized and can be found in, e.g., [85]. They are basically the same as (9.7) except that the normalization is different since it depends on whether the fifth dimension is compact or not. In particular, on the brane, they have the same scale factor dependence as (9.75).

At the end, the behavior found for the KK modes should not come as a surprise, since the RS II model has attracted lots of attention because of exactly this; it localizes usual four-dimensional gravity on the brane (cf. section 8.2.2, [182, 136, 190]). As I have shown here, localization of standard four-dimensional gravity on a moving brane via a warped geometry automatically ensures that the KK modes escape into the bulk as the Universe expands because their wave function has its weight in the region of less warping, resulting in an KK-mode energy density on the brane which scales like stiff matter.

An immediate consequence of this particular scaling behavior is that KK gravitons in an AdS braneworld cannot play the role of dark matter. Their energy density in our Universe decays much faster with the expansion than that of ordinary matter which is restricted to reside on the brane.

[4] Note that it does not depend on a particular type of brane motion and it should also be true in the high energy case which I do not consider here.

Chapter 10

Graviton production in a bouncing braneworld

10.1 The model

The model which I shall consider in the following is strongly motivated by the *ekpyrotic* or *cyclic Universe* and similar ideas [112, 109, 171, 205, 137, 113, 114, 115, 116, 210]. The scenario of the ekpyrotic Universe goes back to Khoury, Ovrut, Steinhardt and Turok [112] who suggested a three-brane cosmological model based on the Hořava-Witten [94, 95] and heteroic M-theory [148, 149, 150]. In this model, roughly speaking, the Hot Big Bang corresponds to the collision of two branes; a moving bulk brane which hits "our" brane, i.e. the observable Universe. Thereby, our brane is one of two bounding branes spanning an intervening bulk volume (the fifth dimension). While our brane, called the *visible brane* is of negative tension, the second boundary brane is of positive tension and called the *hidden brane*. Both branes are Minkowskian but the bulk is warped along the fifth dimension. In addition there is a bulk brane which is free to move and its collision with our brane defines the creation of the Hot Big Bang Universe. Within such a model, it seems to be possible to address all major cosmological problems (homogeneity, origin of density perturbations, monopole problem) without invoking the paradigm of inflation. For more details see [112] but also [109] for critical comments.
One important difference between the ekpyrotic model and standard inflation is that in the latter one density as well as tensor perturbations have a nearly scale invariant spectrum [cf. Section 6.5.4]. The ekpyrotic model, on the other hand, predicts a strongly blue gravitational wave spectrum with spectral tilt $n_T \simeq 2$ [112]. This blue spectrum is a key test for the ekpyrotic scenario since inflation always predicts a slightly red spectrum for gravitational waves. One method to detect a background of primordial gravitational waves of wavelengths comparable to the Hubble horizon today is the polarization of the cosmic microwave background. Since a strongly blue spectrum of gravitational waves is unobservably small for large length scales, the detection of gravitational waves in the cosmic microwave background polarization would falsify the ekpyrotic model [112].
It is important to mention that a blue spectrum of gravitational waves also appears in the *Pre-Big-Bang* models introduced by Veneziano and Gasparini [214, 81, 28, 27] (see also [66, 32]).

Here I shall consider a simple specific model which should be generic enough to cover important main features of the generation and evolution of gravitational waves in the background of a moving brane whose trajectory involves a bounce.
The setup is the scenario depicted in Fig. 9.1. Our Universe is represented by the positive tension FLRW-brane in the five-dimensional AdS bulk. (In that respect this model is more similar to the *pyrotechnic Universe* of Kallosh, Kofman and Linde [109] where the observable Universe is also represented by a positive tension brane rather than to the ekpyrotic model where our brane has negative tension.) First, the physical brane moves towards the static brane, initially the motion is very slow. During this phase the Universe is contracting, i.e. the scale factor on the brane decreases, the energy density on the brane increases and the motion becomes faster. I suppose that, at some more or less close encounter of the two branes which I call the bounce, some high energy mechanism which I do not want to specify in any detail, turns around the motion of the brane leading to an expanding Universe. Modeling the transition from contraction to subsequent expansion in any detail would require assumptions about unknown physics. I shall therefore ignore results which depend on the details of the transition. Finally the physical brane moves away from the static brane back towards the horizon

$y = 0$ with expansion first fast and then becoming slower as the energy density drops.

In particular I assume that the dynamics of the brane is driven by a radiation component on the brane in the low energy limit

$$P = \frac{1}{3}\rho \quad \text{and} \quad v \ll 1 \quad \text{so that} \quad \gamma \simeq 1 \, , d\eta \simeq dt \, . \tag{10.1}$$

In such a period, the dynamics of the scale factor on the brane is described by the usual Friedmann equation (6.20) with solution

$$a(t) = \frac{|t| + t_b}{L} \, , \quad t_b = \text{const.} > 0. \tag{10.2}$$

Recall that the conformal time on the brane η corresponds to the bulk time t in the low energy limit. The motion of the brane through the AdS bulk which mimics the above evolution of the scale factor on the brane is [cf. Eq. (8.44)]

$$y_b(t) = \frac{L^2}{|t| + t_b} \tag{10.3}$$

with velocity

$$v(t) = -\frac{\text{sign}(t) L^2}{(|t| + t_b)^2} = -HL \, . \tag{10.4}$$

Negative times describe a contracting phase, while positive times describe radiation dominated expansion. At $t = 0$, the scale factor exhibits a kink and the evolution equations are singular. The (free) parameter t_b determines the value of the scale factor a_b as well as the velocity of the brane v_b at the bounce

$$a_b = a(0) = \frac{t_b}{L} = \frac{1}{\sqrt{v_b}} \, , \quad v_b = |\dot{y}_b(0)| = \frac{L^2}{t_b^2}. \tag{10.5}$$

Apparently one has to demand $t_b > L$. Inspection of Equation (10.4) shows that the time-derivative of the Hubble parameter diverges at $t = 0$; it contains a δ-function [cf. Section 10.3.1]. This is the bounce which I shall not model in detail. I will have to introduce a cutoff in order to avoid ultraviolet divergencies in the total particle number and energy density which are due to this unphysical kink expressing my ignorance related to the physics driving the bounce. But I shall show that when the kink is smoothed out at some scale, the production of KK modes with masses larger than this scale is exponentially suppressed, and the divergency disappears.
One advantage of considering this particular brane motion is, that the two brane system has well defined asymptotic configurations such that the conditions (9.39) are naturally satisfied.

10.2 Numerical simulations

10.2.1 Preliminary remarks

In the numerical simulations I set $L = 1$, i.e. all dimensionful quantities are measured in units of the AdS_5 curvature scale. Starting at initial time $t_{\text{in}} \ll 0$ where the initial vacuum state $|0, \text{in}\rangle$ is defined the system (3.76,3.77) is evolved numerically up to final time t_{out}. Thereby I set $t_{\text{in}} = -2\pi N_{\text{in}}/k$ with $1 \leq N_{\text{in}} \in \mathbb{N}$, such that $\Theta^{\text{in}}_{0,k} = 1$ [cf. Eq. (9.60)]. This implies $\xi^{(0)}_0(t_{\text{in}}) = 2$, i.e. independent of the three-dimensional momentum k a (plane wave) zero-mode solution always performs a fixed number of oscillations between t_{in} and the bounce at $t = 0$ [cf. Eq. (9.73)]. The final particle spectrum at $\mathcal{N}^{\text{out}}_{\alpha,k,\bullet}$ is calculated at late times $t_{\text{out}} \gg 1$ when the brane approaches the Cauchy horizon and particle creation has ceased. This quantity is physically well defined and leads to the late-time power spectrum (9.83) and energy density (9.91) on the brane. For illustrative purposes, I also plot the instantaneous particle number $\mathcal{N}_{\alpha,k,\bullet}(t)$ which also determines the power spectrum at all times [cf Eq.(9.81)]. In this section I shall use the term *particle number* for both, the instantaneous particle number $\mathcal{N}_{\alpha,k,\bullet}(t)$ as well as the final state graviton number $\mathcal{N}^{\text{out}}_{\alpha,k,\bullet}$, keeping in mind that only the latter one is physically meaningful.

There are two physical input parameters for the numerical simulation; the maximal brane velocity v_b (i.e. t_b) and the position of the fixed brane y_s. The latter determines the number of KK modes which fall within a particular mass range. On the numerical side one has to specify N_{in} and t_{out}, as well as the maximum number

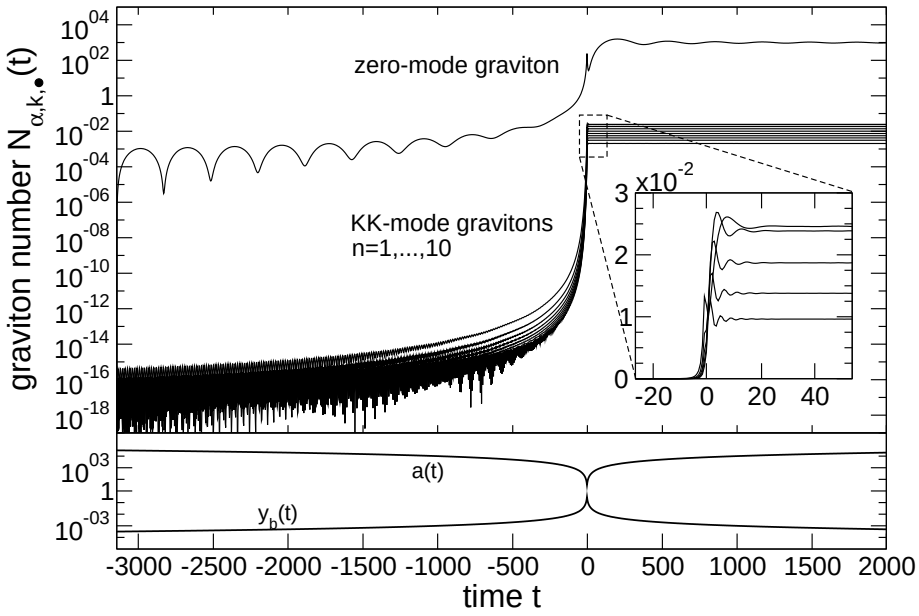

Figure 10.1: Evolution of the graviton number $\mathcal{N}_{\alpha,k,\bullet}(t)$ for the zero mode and the first ten KK modes for three-momentum $k = 0.01$ and $v_b = 0.1$, $y_s = 10$.

of KK modes $n_{\max}$ which one takes into account, i.e. after which KK mode the system of differential equations is truncated. The independence of the numerical results on the choice of the time parameters is checked and the convergence of the particle spectrum with increasing $n_{\max}$ is investigated. More detailed information on numerical issues including accuracy considerations are collected in Appendix B.1.
One strong feature of the brane motion (10.3) is its kink at the bounce $t = 0$. In order to study how particle production depends on the kink, I shall compare the motion (10.3) with the following motion which has a smooth transition from contraction to expansion ($L = 1$):

$$y_b(t) = \begin{cases} (|t| + t_b - t_s)^{-1} & \text{if } |t| > t_s \\ a + (b/2)t^2 + (c/4)t^4 & \text{if } |t| \leq t_s \end{cases} \tag{10.6}$$

with the new parameter t_s in the range $0 < t_s < t_b$. This motion is constructed such that its velocity at $|t| = t_s$ is the same as the velocity of the kink motion at the bounce. This will be the important quantity determining the number of produced gravitons. For $t_s \to 0$ the motion with smooth transition approaches (10.3). The parameters a, b and c are obtained by matching the motions and the first and second derivatives. Matching also the second derivative guarantees that possible spurious effects contributing to particle production are avoided. The parameter t_s has to be chosen small enough, $t_s \ll 1$, such that the maximal velocity of the smooth motion is not much larger than v_b in order to have comparable situations.
For reasons which will become obvious in the next two sections I shall discuss the cases of long $k \ll 1$ and short wavelengths $k \gg 1$, separately.

10.2.2 Generic results and observations for long wavelengths $k \ll 1$

Figure 10.1 displays the results of a numerical simulation for three-momentum $k = 0.01$, static brane position $y_s = 10$ and maximal brane velocity $v_b = 0.1$. Depicted is the graviton number for one polarization $\mathcal{N}_{\alpha,k,\bullet}(t)$ for the zero mode and the first ten KK modes as well as the evolution of the scale factor $a(t)$ and the position of the physical brane $y_b(t)$. Initial and final times are $N_{\text{in}} = 5$ and $t_{\text{out}} = 2000$, respectively. The KK-particle spectrum will be discussed in detail below. One observes that the zero mode particle number increases slightly with the expansion of the Universe towards the bounce at $t = 0$. Close to the bounce $\mathcal{N}_{0,k,\bullet}(t)$ increases drastically, shows a local peak at the bounce and, after a short decrease, grows again until the mode is sub-horizon ($kt \gg 1$). Inside the horizon $\mathcal{N}_{0,k,\bullet}(t)$ is oscillating around a mean value with diminishing amplitude. This mean value which is reached asymptotically for $t \to \infty$ corresponds to the number of generated final state zero mode gravitons $\mathcal{N}^{\text{out}}_{0,k,\bullet}$. Production of KK mode gravitons takes effectively place only at the bounce in a

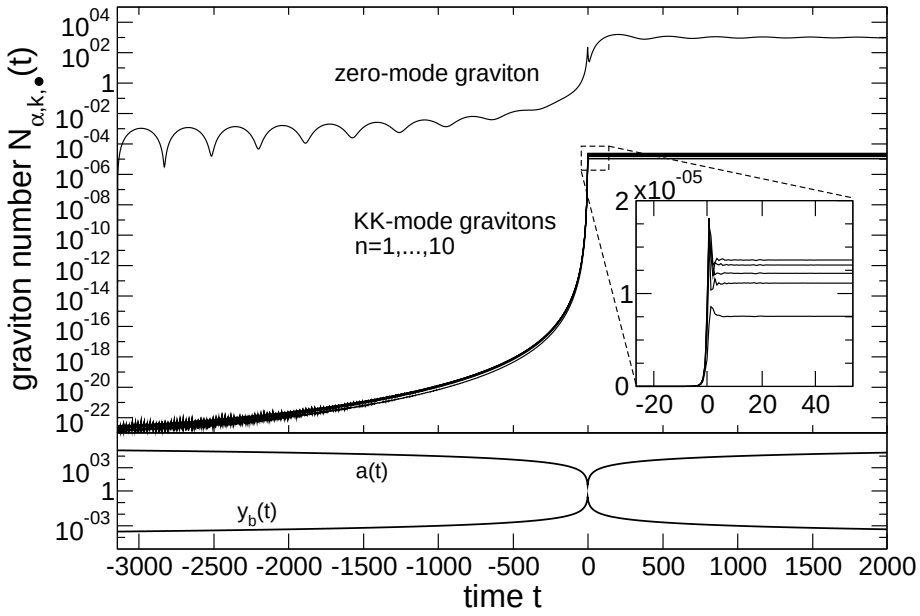

Figure 10.2: $\mathcal{N}_{n,k,\bullet}(t)$ for the zero mode and the first ten KK modes for the parameters of Fig. 10.1, but without coupling of the zero mode to the KK modes, i.e. $M_{i0} \equiv 0$.

step-like manner and the graviton number remains constant right after the bounce.
In Fig. 10.2 I show the numerical results obtained for the same parameters as in Fig. 10.1 but without coupling of the zero mode to the KK modes, i.e. $M_{n0} = 0$ (and thus also $N_{n0} = N_{0n} = 0$). One observes that the production of zero mode gravitons is virtually not affected by the artificial decoupling [1]. Note that even if $M_{0m} \equiv 0$ (see Eqs. 9.25), which is in general true for Neumann boundary conditions, the zero mode $q_{0,\mathbf{k},\bullet}$ couples in Eq. (9.23) to the KK modes via $N_{0m} = M_{00}M_{m0}$ and through the anti-symmetric combination $M_{\alpha\beta} - M_{\beta\alpha}$.
In contrast, the production of the first ten KK modes is heavily suppressed if $M_{n0} = 0$. The corresponding final-state graviton numbers $\mathcal{N}^{\rm out}_{n,k,\bullet}$ are reduced by four orders of magnitude. This shows that the coupling to the zero mode is essential for the production of massive gravitons. Later we will see that this is true for light KK gravitons only. If the KK masses exceed $m_n \sim 1$, they evolve independently of the four-dimensional graviton and their evolution is entirely driven by the intermode couplings M_{nm}. It will also turn out that the time-dependence of the KK mass m_n plays only an inferior role for the generation of massive KK modes. On the other hand, the effective decoupling of the evolution of the zero mode from the KK modes occurs in general as long as $k \ll 1$ is satisfied, i.e. for long-wavelengths. We will see that it is no longer true for short wavelengths $k \gg 1$.
The effective decoupling of the zero mode evolution from the KK modes makes it possible to derive analytical expressions for the number of zero mode gravitons, their power spectrum and energy density. The calculations are carried out in section 10.3.1.
In summary I would like to emphasize the important observation that for long wavelengths the amplification of the four dimensional gravity wave amplitude during the bounce is not affected by the evolution of the KK gravitons. One can therefore study the zero mode separately from the KK modes in this case.

10.2.3 Zero mode: long wavelengths $k \ll 1$

In Figure 10.3 I show the numerical results for the number of generated zero mode gravitons $\mathcal{N}_{0,k,\bullet}(t)$ and the evolution of the corresponding power spectrum $\mathcal{P}_0(k)$ on the brane for momentum $k = 0.01$, position of the static brane $y_s = 10$ and maximal brane velocity $v_b = 0.1$. The results have been obtained by solving the equations for the zero mode alone, i.e. without the couplings to the KK modes, since, as I have just shown, the evolution of the four-dimensional graviton for long wavelengths is not influenced by the KK modes. Thereby

[1] Quantitatively it is $\mathcal{N}_{0,k,\bullet}(t = 2000) = 965.01$ with and $\mathcal{N}_{0,k,\bullet}(t = 2000) = 965.06$ without M_{i0}. Note that this difference lies indeed within the accuracy of our numerical simulations (see Appendix B.3.)

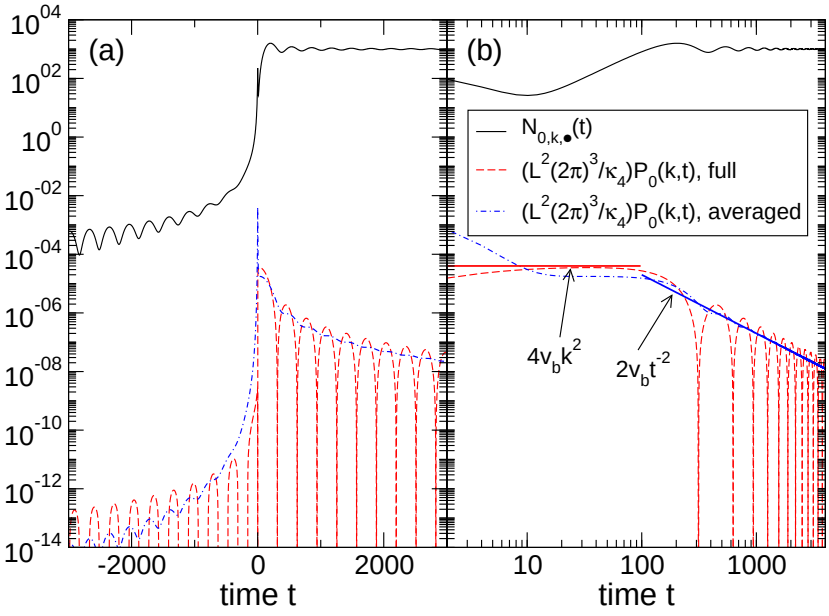

Figure 10.3: Time evolution of the number of created zero mode gravitons $\mathcal{N}_{0,k,\bullet}(t)$ and of the zero-mode power spectrum (9.80): (a) for the entire integration time; (b) for $t > 0$ only. Parameters are $k = 0.01$, $y_s = 10$ and $v_b = 0.1$. Initial and final time of integration are given by $N_{\rm in} = 10$ and $t_{\rm out} = 4000$, respectively. The power spectrum is shown with and without the term $\mathcal{O}^{\mathcal{N}}_{0,k,\bullet}$, i.e. before and after averaging, respectively, and compared with the analytical results.

the power spectrum is shown before and after averaging over several oscillations, i.e. employing Eq. (9.81) with and without the term $\mathcal{O}^{\mathcal{N}}_{0,k}$, respectively. Right after the bounce where the generation of gravitons is initiated and which is responsible for the peak in $\mathcal{N}_{0,k,\bullet}$ at $t = 0$, the number of gravitons first decreases again. Afterwards $\mathcal{N}_{0,k,\bullet}$ grows further until the mode enters the horizon at $kt = 1$. Once on sub-horizon scales $kt \gg 1$, the number of produced gravitons oscillates with a diminishing amplitude and asymptotically approaches the final state graviton number $\mathcal{N}^{\rm out}_{0,k,\bullet}$. During the growth of $\mathcal{N}_{0,k,\bullet}$ after the bounce, the power spectrum remains practically constant. Within the range of validity it is in good agreement with the analytical prediction (10.32) yielding $(L^2(2\pi)^3/\kappa_4)\mathcal{P}_0(k,t) = 4v_b(kL)^2$. When particle creation has ceased, the full power spectrum Eq.(9.80) starts to oscillate with an decreasing amplitude. The time-averaged power spectrum obtained by using Eq. (9.81) without the $\mathcal{O}^{\mathcal{N}}_{0,k}$-term is perfectly in agreement with the analytical expression Eq. (10.30) which gives $(L^2(2\pi)^3/\kappa_4)\mathcal{P}_0(k,t) = 2v_b(L/t)^2$. Note that at early times, the time-averaged power spectrum behaves not in the same way as the full one, demonstrating the importance of the term $\mathcal{O}^{\mathcal{N}}_{0,k}$.
Figure 10.4 shows a summary of numerical results for the number of created zero mode gravitons $\mathcal{N}_{0,k,\bullet}(t)$ for different values of the three-momentum k. The maximum velocity at the bounce is $v_b = 0.1$ and the second brane is at $y_s = 10$. These values are representative. Other values in accordance with the considered low-energy regime do not lead to a qualitatively different behavior. Note that the evolution of the zero mode does virtually not depend on the value of y_s as long as $y_s \gg y_b(0)$ (see below). Initial and final integration times are given by $N_{\rm in} = 5$ and $t_{\rm out} = 20000$, respectively.
For sub-horizon modes I compare the final graviton spectra with the analytical prediction (10.26). Both are in perfect agreement. On super-horizon scales where particle creation has not ceased yet $\mathcal{N}_{0,k,\bullet}$ is independent of k. The corresponding time-evolution of the power spectra $\mathcal{P}_0(k,t)$ is depicted in Fig. 10.5. For the sake of clarity, only the results for $t > 0$, i.e. after the bounce, are shown in both figures.

The numerical simulations and the calculations of section 10.3.1 reveal that the power spectrum for the four-dimensional graviton for long wavelengths is blue on super-horizon scales, as expected for an ekpyrotic scenario. The analytical calculations performed in section 10.3.1 rely on the assumption that $y_b \ll y_s$ and $t_{\rm in} \to -\infty$. Figure 10.6 shows the behavior of the number of generated zero mode gravitons of momentum $k = 0.01$ in dependence on the inter-brane distance and the initial integration time. The brane velocity at the bounce is $v_b = 0.1$ which implies that at the bounce the moving brane is at $y_b(0) = \sqrt{v_b} \simeq 0.316$ ($L = 1$). In case of a

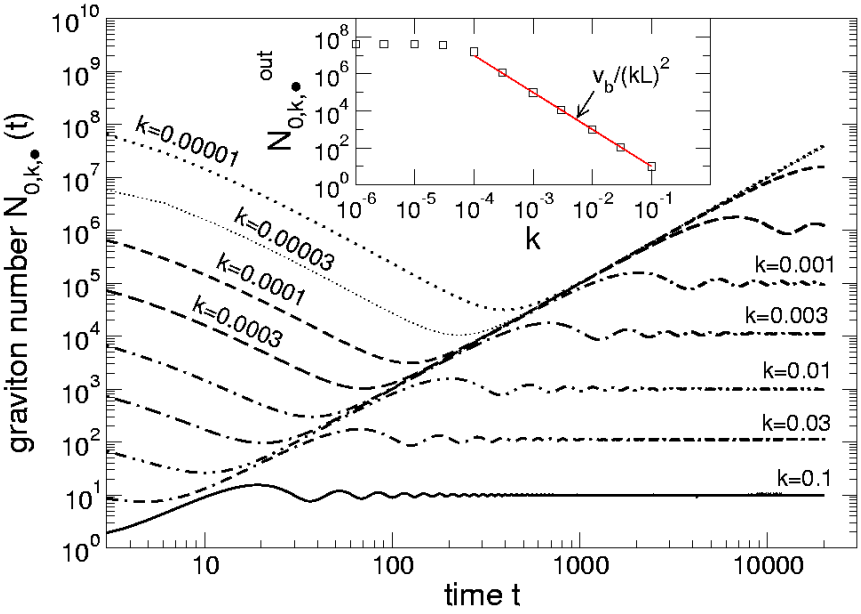

Figure 10.4: Numerical results for the time evolution of the number of created zero mode gravitons $\mathcal{N}_{0,k,\bullet}(t)$ after the bounce $t > 0$ for different three-momenta k. The maximal brane velocity at the bounce is $v_b = 0.1$ and the second brane is positioned at $y_s = 10$. In the final particle spectrum the numerical values are compared with the analytical prediction Eq. (10.26). Initial and final time of integration are given by $N_{\rm in} = 5$ and $t_{\rm out} = 20000$, respectively.

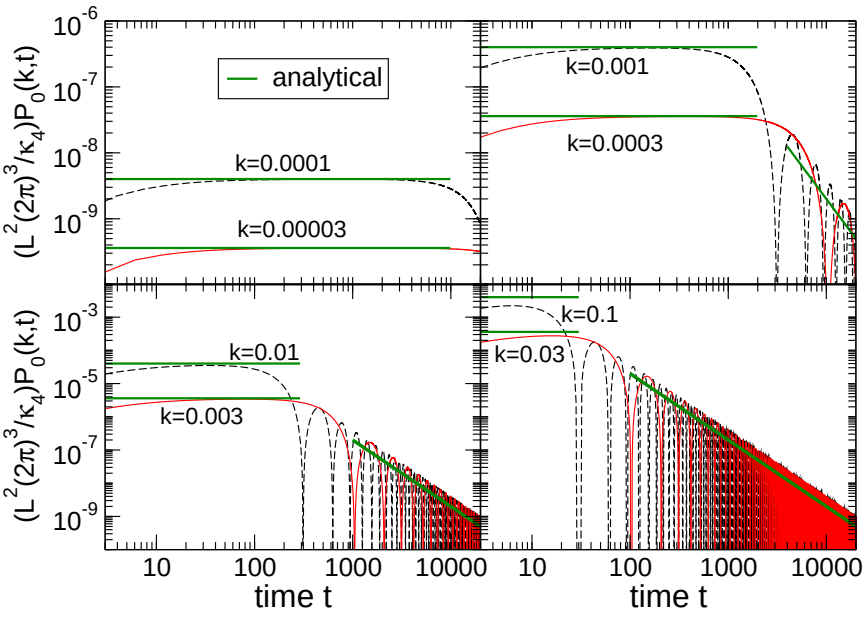

Figure 10.5: Evolution of the zero mode power spectrum after the bounce $t > 0$ corresponding to the values and parameters of Fig. 10.4. The numerical results are compared to the analytical predictions Eqs. (10.30) and (10.32).

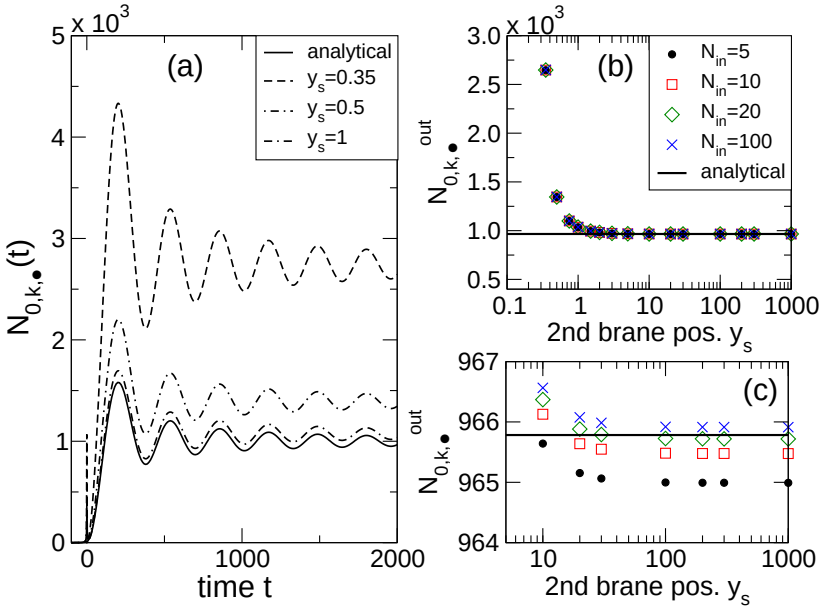

Figure 10.6: Dependence of the zero mode particle number on inter-brane distance and initial integration time for momentum $k = 0.01$, maximal brane velocity $v_b = 0.1$ in comparison with the analytical expression Eq. (10.25). (a) Evolution of the instantaneous particle number $\mathcal{N}_{0,k,\bullet}(t)$ with initial integration time given by $N_{\rm in} = 5$ for $y_s = 0.35, 0.5$ and 1. (b) Final zero mode graviton spectrum $\mathcal{N}_{0,k,\bullet}(t_{\rm out} = 2000)$ for various values of y_s and $N_{\rm in}$. (c) Close-up view of (b) for large y_s.

close encounter of the two branes as for $y_s = 0.35$, the production of massless gravitons is strongly enhanced compared to the analytical result. But as soon as $y_s \gtrsim 1$, (i.e. $y_s \gtrsim L$) the numerical result is very well described by the analytical expression Eq. (10.25) derived under the assumption $y_s \gg y_b$. For $y_s \gtrsim 10$ the agreement between both is very good. From panels (b) and (c) one infers that the numerical result becomes indeed independent of the initial integration time when increasing $N_{\rm in}$. Note that in the limit $N_{\rm in} \gg 1$ the numerical result is slightly larger than the analytical prediction but the difference between both is negligibly small. This confirms the correctness and accuracy of the analytical expressions derived in Section 10.3.1 for the evolution of the zero mode graviton.

10.2.4 Kaluza-Klein-modes: long wavelengths $k \ll 1$

Because the creation of KK gravitons ceases right after the bounce [cf Fig. 10.1] one can stop the numerical simulation and read out the number of produced KK gravitons $\mathcal{N}^{\rm out}_{n,k,\bullet}$ at times for which the zero mode is still super-horizon.

Even though Eq. (9.13) cannot be solved analytically, the KK masses can be approximated by $m_n \simeq n\pi/y_s$. This expression is the better the larger the mass. Consequently, for the massive modes the position of the second brane y_s determines how many KK modes belong to a particular mass range Δm.

In Figure 10.7 I show the KK graviton spectra $\mathcal{N}^{\rm out}_{n,k,\bullet}$ for three-momentum $k = 0.001$ and second brane position $y_s = 100$ for maximal brane velocities $v_b = 0.1, 0.3$ and 0.5. For any velocity v_b two spectra obtained with $n_{\rm max} = 60$ and 80 KK modes taken into account in the simulation are compared to each other. This reveals that the numerical results are stable up to a KK mass $m_n \simeq 1$. One infers that first, $\mathcal{N}^{\rm out}_{n,k,\bullet}$ grows with increasing mass until a maximum is reached. The position of the maximum shifts slightly towards larger masses with increasing brane velocity v_b. Afterwards, $\mathcal{N}^{\rm out}_{n,k,\bullet}$ declines with growing mass. Until the maximum is reached, the numerical results for the KK-particle spectrum are very stable. This already indicates that the KK-intermode couplings mediated by M_{nm} are not very strong in this mass range. In Figure 10.8 I show the final KK particle spectrum for the same parameters as in Fig. 10.7 but for three-momentum $k = 0.01$ and

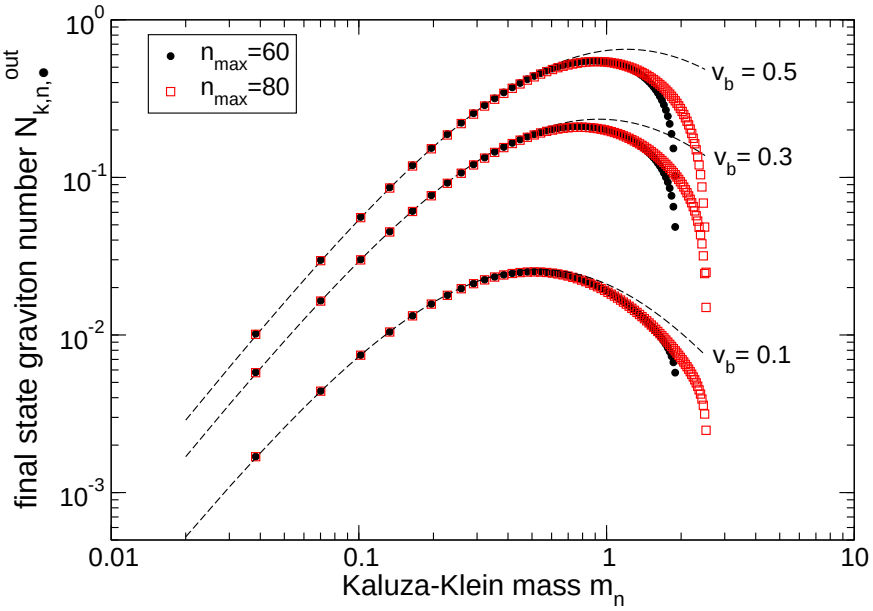

Figure 10.7: Final state KK graviton spectra for $k = 0.001$, $y_s = 100$, different maximal brane velocities v_b and $N_{\rm in} = 1$, $t_{\rm out} = 400$. The numerical results are compared with the analytical prediction Eq. (10.44) (dashed line).

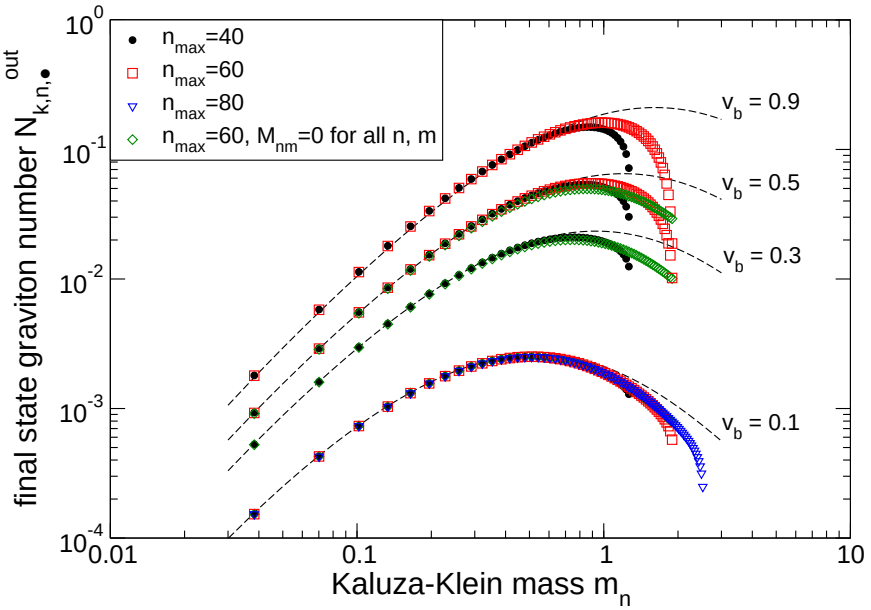

Figure 10.8: Final state KK graviton spectra for $k = 0.01$, $y_s = 100$, different v_b and $N_{\rm in} = 1$, $t_{\rm out} = 400$. The numerical results are compared with the analytical prediction Eq. (10.44) (dashed line). For $v_b = 0.3, 0.5$ the spectra obtained without KK-intermode and self-couplings ($M_{nm} \equiv 0 \,\forall\, n, m$) are shown as well.

the additional velocity $v_b = 0.9$ [2]. One observes the same qualitative behavior as in Fig. 10.7. In addition I show numerical results obtained for $v_b = 0.3$ and 0.5 without the KK-intermode and self couplings, i.e. I have set $M_{nm} \equiv 0 \; \forall \, n, m$ by hand. One infers that for KK masses, depending slightly on the velocity v_b but at least up to $m_n \simeq 1$, the numerical results for the spectra do not change when the KK-intermode coupling is switched off. Consequently, the evolution of *light*, i.e. $m_n \lesssim 1$, KK gravitons is virtually not affected by the KK-intermode coupling.
In addition I find that also the time-dependence of the KK masses is not important for the production of light KK gravitons which is explicitly demonstrated below. Thus, production of light KK gravitons is driven by the zero mode evolution only. This allows me to find an analytical expression, Eq. (10.44), for the number of produced light KK gravitons in terms of exponential integrals. The calculations which are based on several approximations are performed in Section 10.3.3.
In Figs. 10.7 and 10.8 the analytical prediction (10.44) for the spectrum of final state gravitons has already been included (dashed lines). Within its range of validity it is in excellent agreement with the numerical results obtained by including the full KK-intermode coupling. It perfectly describes the dependence of $\mathcal{N}^{\rm out}_{n,k,\bullet}$ on the three-momentum k and the maximal velocity v_b. For small velocities $v_b \lesssim 0.1$ it is also able to reproduce the position of the maximum. This reveals that the KK-intermode coupling is negligible for light KK gravitons and that their production is entirely driven by their coupling to the four-dimensional graviton.
The analytical prediction is very precious for testing the goodness of the parameters used in the simulations, in particular the initial time $t_{\rm in}$ (respectively $N_{\rm in}$). Since it has been derived for real asymptotic initial conditions, $t_{\rm in} \to -\infty$, its perfect agreement with the numerical results demonstrates that the values for $N_{\rm in}$ used in the numerical simulations are large enough. No spurious initial effects contaminate the numerical results.
Note, that the numerical values for $\mathcal{N}^{\rm out}_{n,k,\bullet}$ in the examples shown are all smaller than one. However, for smaller values of k than the ones which we consider here for purely numerical reasons, the number of generated KK-mode particles is enhanced since $\mathcal{N}^{\rm out}_{n,k,\bullet} \propto 1/k$ as can be inferred from Eq. (10.44) in the limit $k \ll m_n$.

If one goes to smaller values of y_s, fewer KK modes belong to a particular mass range. Hence, with the same or similar number of KK modes as taken into account in the simulations so far, I can study the behavior of the final particle spectrum for larger masses. These simulations shall reveal the asymptotical behavior of $\mathcal{N}^{\rm out}_{n,k,\bullet}$ for $m_n \to \infty$ and therefore the behavior of the total graviton number and energy density. Due to the kink in the brane motion one cannot expect that the energy density of produced KK-mode gravitons is finite when summing over arbitrarily high frequency modes. Eventually, I will have to introduce a cutoff setting the scale at which the kink-approximation [cf. Eqs. (10.2) - (10.4)] is no longer valid. This is the scale where the effects of the underlying unspecified high-energy physics which drive the transition from contraction to expansion become important. The dependence of the final particle spectrum on the kink will be studied later on in this section in detail.

In Figures 10.9 and 10.10 I show KK graviton spectra for $y_s = 10$ and three-momentum $k = 0.01$ and $k = 0.1$. The analytical expression Eq. (10.44) is depicted as well and the spectra are always shown for at least two values of $n_{\rm max}$ to indicate up to which KK mass stability of the the numerical results is guaranteed. Now, only two KK modes are lighter than $m = 1$. For these modes the analytical expression Eq. (10.44) is valid and in excellent agreement with the numerical results, in particular for small brane velocities $v_b \sim 0.1$. As before, the larger the velocity v_b the more visible is the effect of the truncation of the system of differential equations at $n_{\rm max}$.
For $k = 0.01$ the spectrum seems to follow a power law decrease right after the maximum in the spectra. In case of $v_b = 0.1$ the spectrum is numerically stable up to masses $m_n \simeq 20$. In the region $5 \lesssim m_n \lesssim 20$ the spectrum is very well fitted by a power law $\mathcal{N}^{\rm out}_{n,k,\bullet} \propto m_n^{-2.7}$. Also for larger velocities the decline of the spectrum is given by the same power within the mass ranges where the spectrum is numerically stable. For $k = 0.1$, however, the decreasing spectrum bends over at a mass around $m_n \simeq 10$ towards a less steep decline. This is in particular visible in the two cases with $v_b = 0.1$ and 0.3 where the first 100 KK modes have been taken into account in the simulation. The behavior of the KK mode particle spectrum can therefore not be described by a single power law decline for masses $m_n > 1$. It shows more complicated features instead, which depend on the parameters. I shall demonstrate that this bending over of the decline is related to the coupling properties of the KK modes and to the kink in the brane motion. But before I come to a detailed discussion of these issues, let me briefly confront numerical results of different y_s to demonstrate a scaling behavior.

[2] Such a high brane velocity is of course not consistent with a Neumann boundary condition Eq. (9.2) at the position of the moving brane.

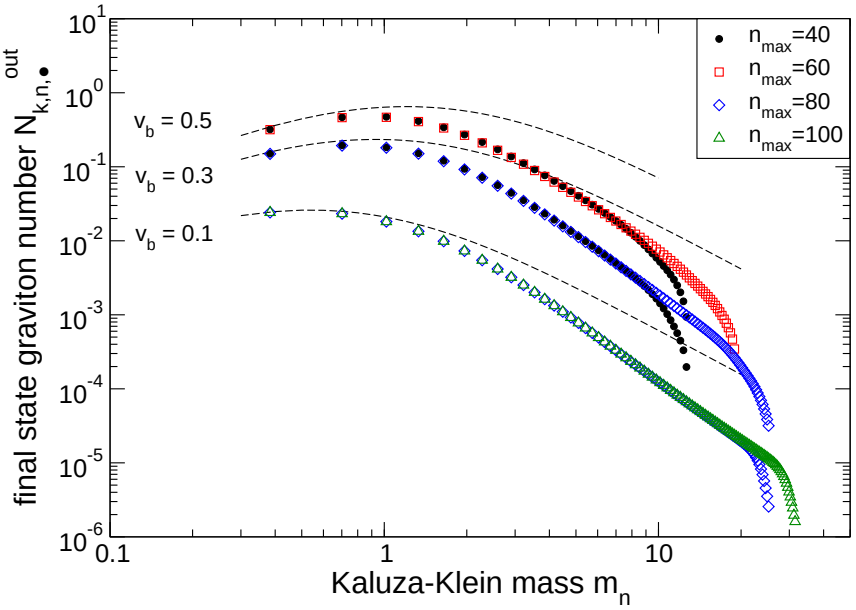

Figure 10.9: Final state KK graviton spectra for $k = 0.01$, $y_s = 10$, different maximal brane velocities v_b and $N_{\rm in} = 2$, $t_{\rm out} = 400$. The numerical results are compared with the analytical prediction Eq. (10.44) (dashed line).

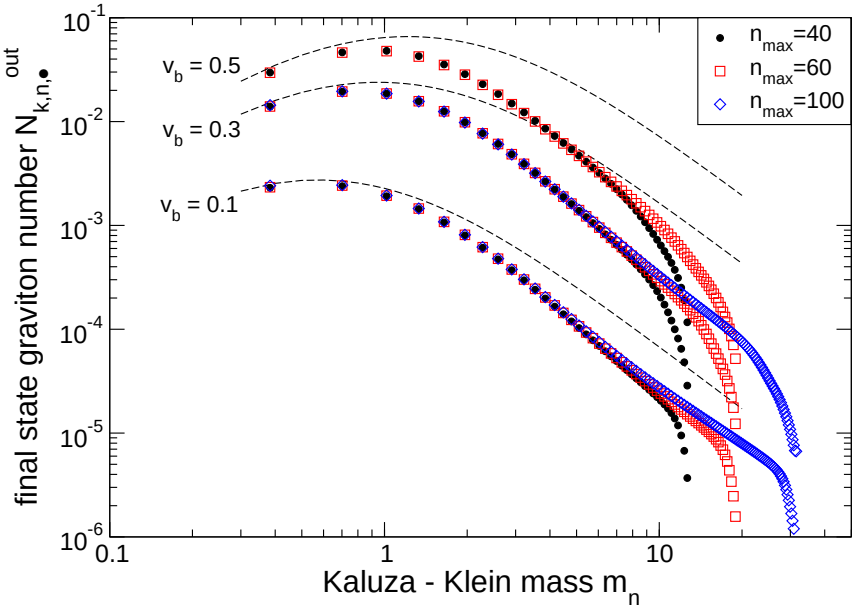

Figure 10.10: Final state KK graviton spectra for $k = 0.1$, $y_s = 10$, different maximal brane velocities v_b and $N_{\rm in} = 2$, $t_{\rm out} = 400$. The numerical results are compared with the analytical prediction Eq. (10.44) (dashed line).

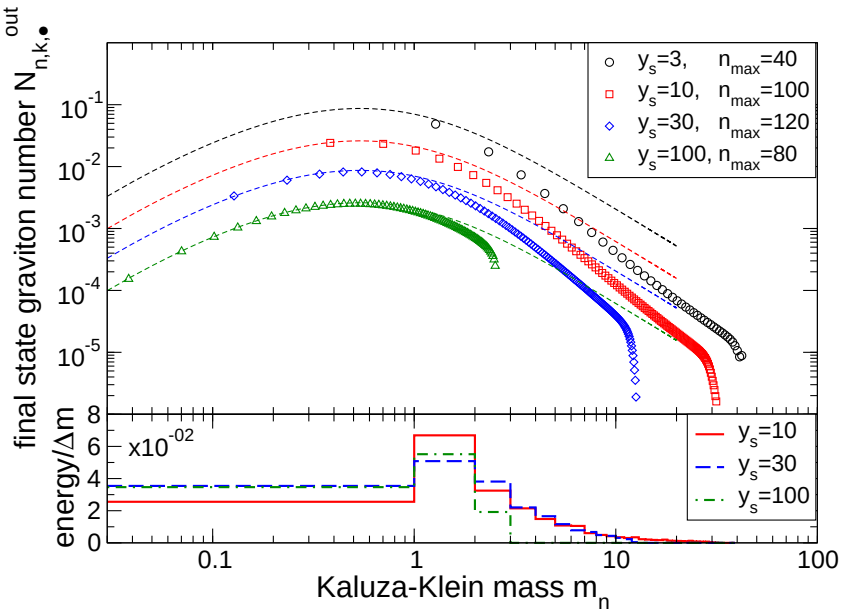

Figure 10.11: Upper panel: Final state KK particle spectra for $k = 0.01$, $v_b = 0.1$ and different $y_s = 3, 10, 30$ and 100. The analytical prediction Eq. (10.44) is shown as well (dashed line). Lower panel: Energy $\Omega^{out}_{n,k}\mathcal{N}^{out}_{n,k,\bullet}$ of the produced final state gravitons binned in mass intervals $\Delta m = 1$ for $y_s = 10, 30, 100$.

In the upper panel of Figures 10.11 and 10.12 I compare the final KK-spectra for several positions of the second brane $y_s = 3, 10, 30$ and 100 obtained for a maximal brane velocity $v_b = 0.1$ for $k = 0.01$ and 0.1, respectively. One observes that the shapes of the spectra are identical. The bending over in the decline of the spectrum at masses $m_n \sim 1$ is very well visible for $k = 0.1$ and $y_s = 3, 10$. For a given KK mode n the number of particles produced in this mode is the larger the smaller y_s. But the smaller y_s, the less KK modes belong to a given mass interval Δm. The energy transferred into the system by the moving brane, which is determined by the maximum brane velocity v_b, is the same in all cases. Therefore, the total energy of the produced final state KK gravitons of a given mass interval Δm should also be the same, independent of how many KK modes are contributing to it. This is demonstrated in the lower panels of Figs. 10.11 and 10.12 where the energy $\Omega^{out}_{n,k}\mathcal{N}^{out}_{n,k,\bullet}$(in units of L) of the generated KK gravitons binned in mass intervals $\Delta m = 1$ is shown [3]. One observes that, as expected, the energy transferred into the production of KK gravitons of a particular mass range is the same (within the region where the numerical results are stable), independent of the number of KK modes lying in the interval. This is in particular evident for $y_s = 30, 100$. The discrepancy for $y_s = 10$ is due to the binning. As I shall discuss below in detail, the particle spectrum can be split into two different parts. The first part is dominated by the coupling of the zero mode to the KK modes (as shown above), whereas the second part is dominated by the KK-intermode couplings and is virtually independent of the wave number k. As long as the coupling of the zero mode to the KK modes is the dominant contribution to KK particle production it is $\mathcal{N}^{out}_{n,k,\bullet} \propto 1/k$ [cf. Eq. (10.44)]. Hence, $\mathcal{E}^{out}_{n,k,\bullet} = \Omega^{out}_{n,k}\mathcal{N}^{out}_{n,k,\bullet} \propto 1/k$ if $m_n \gg k$. This explains why the energy per mass interval Δm is one order larger for $k = 0.01$ (cf Fig. 10.11) than for $k = 0.1$ (cf Fig. 10.12) .

Let me now discuss the KK-spectrum for large masses. The qualitative behavior of the spectrum $\mathcal{N}^{out}_{n,k,\bullet}$ and the mass at which the decline of the spectrum changes are independent of y_s. This is demonstrated in Figure 10.13 where KK-spectra for $v_b = 0.1$, $k = 0.1$, $y_s = 10$ [cf Fig. 10.10] and $y_s = 3$ [cf Fig. 10.12] are shown. The results obtained by taking the full intermode-coupling into account are compared to results of simulations where I have switched off the coupling of the KK modes to each other as well as their self-coupling ($M_{nm} \equiv 0 \; \forall \, n, m$). Furthermore I display the results for the KK-spectrum obtained by taking only the KK-intermode couplings into account, i.e. $M_{n0} = M_{nn} = 0 \; \forall \, n$. One infers that for the lowest masses the spectra obtained with all couplings are identical to the ones obtained without the KK-intermode ($M_{nm} = 0, n \neq m$)

[3] The energy for the case $y_s = 3$ is not shown because no KK mode belongs to the first mass interval.

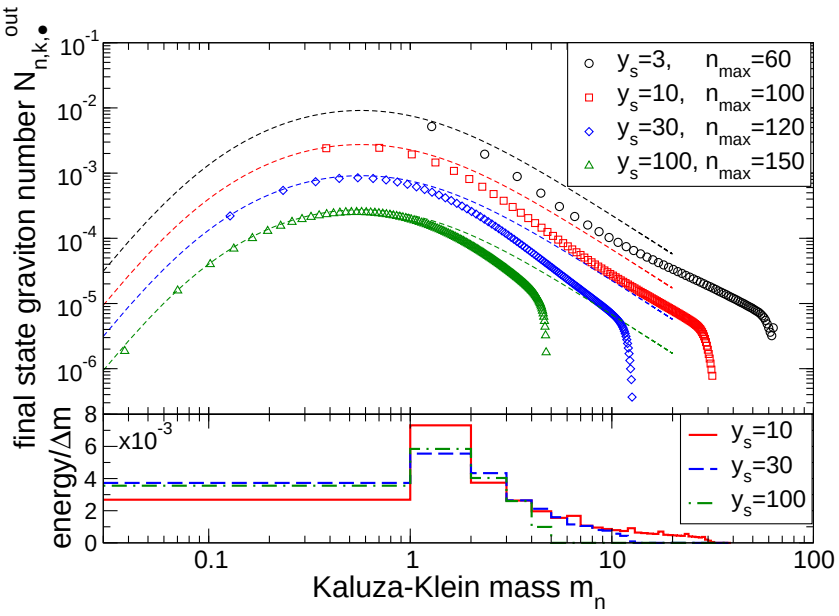

Figure 10.12: Upper panel: Final state KK particle spectra for $k = 0.1$, $v_b = 0.1$ and different $y_s = 3, 10, 30$ and 100. The analytical prediction Eq. (10.44) is shown as well (dashed line). Lower panel: Energy $\Omega^{out}_{n,k}\mathcal{N}^{out}_{n,k,\bullet}$ of the produced final state gravitons binned in mass intervals $\Delta m = 1$ for $y_s = 10, 30, 100$.

and self-couplings ($M_{nn} = 0$). Hence, as already seen before, the primary source for the production of light KK gravitons is their coupling to the evolution of the four-dimensional graviton. In this mass range, the contribution to the particle creation coming from the KK-intermode couplings is very much suppressed and negligibly small.

For masses $m_n \simeq 4$ a change in the decline of the spectrum sets in and the spectrum obtained without the coupling of the KK modes to the zero mode starts to diverge from the spectrum computed by taking all the couplings into account. While the spectrum without the KK-intermode couplings decreases roughly like a power law $\mathcal{N}^{out}_{n,k,\bullet} \propto m_n^{-3}$ the spectrum corresponding to the full coupling case changes its slope towards a power law decline with less power. At this point the KK-intermode couplings gain importance and the coupling of the KK modes to the zero mode looses influence. For a particular mass $m_c \simeq 9$ the spectrum obtained including the KK-intermode couplings only, crosses the spectrum calculated by taking into account exclusively the coupling of the KK modes to the zero mode. After the crossing, the spectrum obtained by using only the KK-intermode couplings approaches the spectrum of the full coupling case. Both agree for large masses. Thus for large masses $m_n > m_c$ the production of KK gravitons is dominated by the couplings of the KK modes to each other and is not influenced anymore by the evolution of the four-dimensional graviton. This crossing defines the transition between the two regimes mentioned before: for masses $m_n < m_c$ the production of KK gravitons takes place due to their coupling to the zero mode M_{n0}, while it is entirely caused by the intermode couplings M_{nm} for masses $m_n > m_c$.

Decoupling of the evolution of the KK modes from the dynamics of the four-dimensional graviton for large masses implies that KK-spectra obtained for the same maximal velocity are independent of the three-momentum k. This is demonstrated in Fig. 10.14 where I compare spectra obtained for $v_b = 0.1$ and $y_s = 3$ but different k. As expected, all spectra converge towards the same behavior for masses $m_n > m_c$.

Figure 10.15 shows KK particle spectra for $k = 0.1$,$v_b = 0.1$ and $y_s = 3$ obtained for different couplings. This plot visualizes how each particular coupling combination contributes to the production of KK gravitons. It shows, as already mentioned before but not shown explicitly, that the M_{nn} coupling which is the rate of change of the corresponding KK mass [cf. Eqs. (9.14),(9.27)] is not important for the production of KK gravitons. Switching it off does not affect the final graviton spectrum. I also show the result obtained with all couplings but with $\alpha^+_{nn}(t) = \Omega^{in}_{n,k}$ and $\alpha^-_{nn}(t) = 0$, i.e. the time-dependence of the frequency has been neglected [cf. Eq. (9.72)]. One observes that in this case the spectrum for larger masses is quantitatively slightly different but has a identical qualitative behavior. If, on the other hand, all the couplings are switched

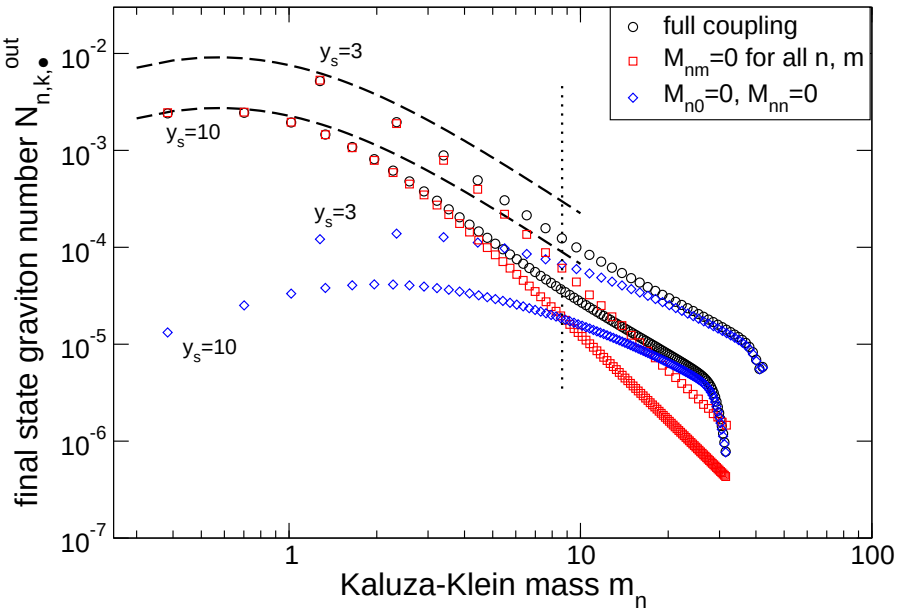

Figure 10.13: KK particle spectra for three-momentum $k = 0.1$, maximum brane velocity $v_b = 0.1$ and $y_s = 3$ and 10 with different couplings taken into account. The dashed lines indicates again the analytical expression Eq. (10.44).

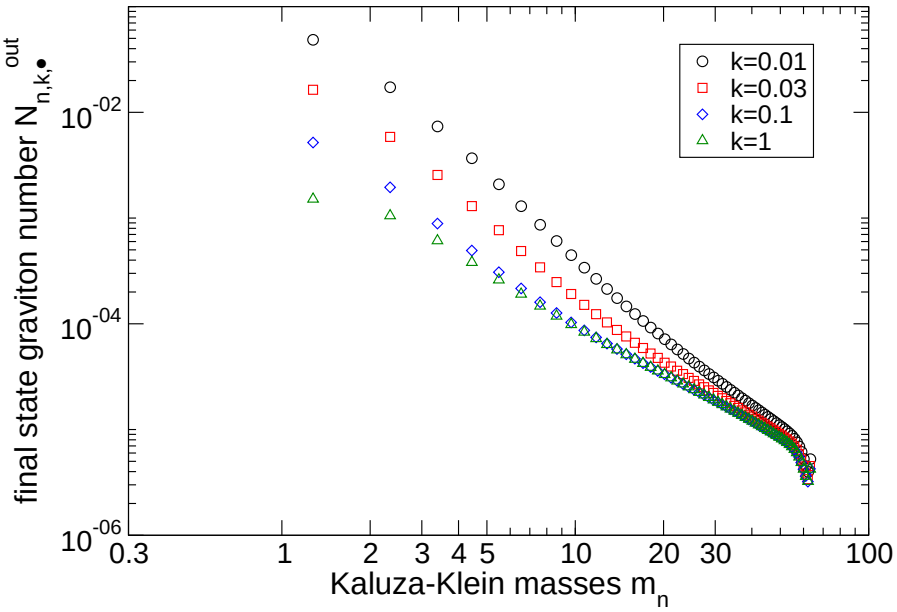

Figure 10.14: Comparison of KK particle spectra for $y_s = 3$, $v_b = 0.1$ and three-momentum $k = 0.01$, 0.03, 0.1 and 1 demonstrating the independence of the spectrum on k for large masses. $n_{\max} = 60$ KK modes have been taken into account in the simulations.

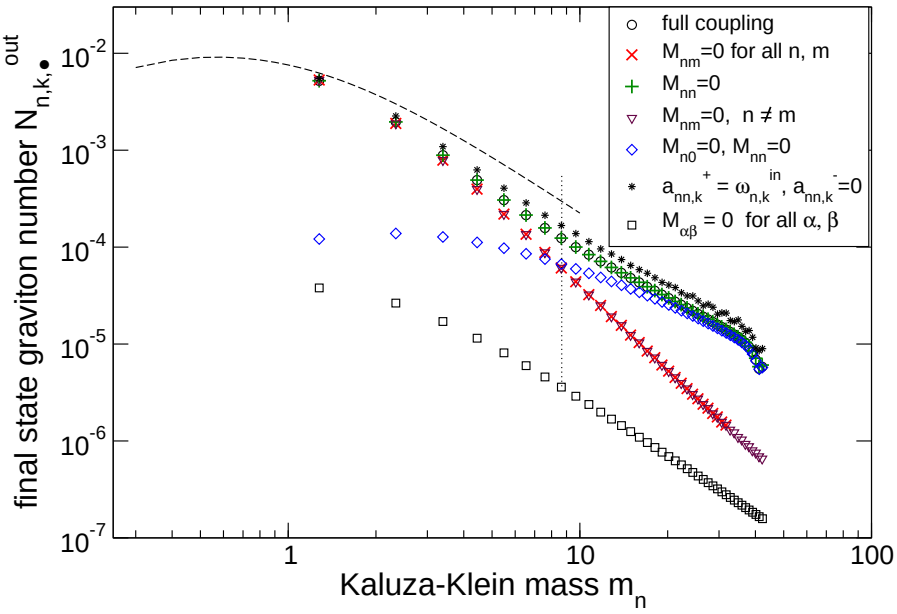

Figure 10.15: KK particle spectra for three-momentum $k = 0.1$, maximum brane velocities $v_b = 0.1$ and $y_s = 3$ for $n_{\max} = 40$ obtained for different coupling combinations.

off $M_{\alpha\beta} \equiv 0 \; \forall \, \alpha, \beta$ and only the time-dependence of the frequency $\Omega_{n,k}$ is taken into account, the spectrum changes drastically. Not only the number of produced gravitons is now orders of magnitude smaller but also the spectral tilt changes. For large masses it behaves as $\mathcal{N}_{n,k,\bullet} \propto m_n^{-2}$. Consequently, the time-dependence of the graviton frequency itself plays only an inferior role for production of KK gravitons.
The bottom line is that the main sources of the production of KK gravitons is their coupling to the evolution of the four-dimensional graviton (M_{n0}) and their couplings to each other (M_{nm}, $n \neq m$) for small and large masses, respectively. Both are caused by the time-dependent boundary condition. The time-dependence of the oscillator frequency $\Omega_{n,k} = \sqrt{m_n^2(t) + k^2}$ is virtually irrelevant. Note that this situation is very different from ordinary inflation where there are no boundaries and particle production is due entirely to the time dependence of the frequency [4].

The behavior of the KK-spectrum, in particular the mass m_c at which the KK-intermode couplings start to dominate over the coupling of the KK modes to the zero mode depends only on the three-momentum $k = |\mathbf{k}|$ and the maximal brane velocity v_b. This is now discussed. In Figure 10.16 I show KK particle spectra for $y_s = 10$, $v_b = 0.1$, $n_{\max} = 100$ and three-momenta $k = 0.01$ and 0.1. Again, the spectra obtained by taking all the couplings into account are compared to the case where only the coupling to the zero mode is switched on. One observes that for $k = 0.01$ the spectrum is dominated by the coupling of the KK modes to the zero mode up to larger masses than it is the case for $k = 0.1$. For $k = 0.01$ the spectrum obtained taking into account M_{i0} only is identical to the spectrum obtained with the full coupling up to $m_n \simeq 10$. In case of $k = 0.1$ instead, the spectrum is purely zero mode dominated only up to $m_n \simeq 5$. Hence, the smaller the three-momentum k the larger is the mass range for which the KK-intermode coupling is suppressed, and the coupling of the zero mode to the KK modes is the dominant source for the production of KK gravitons. As long as the coupling to the zero mode is the primary source of particle production, the spectrum declines with a power law $\propto m_n^{-3}$. Therefore, in the limiting case $k \to 0$ when the coupling of the zero mode to the KK modes dominates particle production also for very large masses it is $\mathcal{N}^{\rm out}_{n \gg 1, k \to 0, \bullet} \propto 1/m_n^3$.

Figure 10.17 shows KK graviton spectra obtained for the same parameters as in Fig. 10.16 but for fixed $k = 0.1$ and different maximal brane velocities v_b. Again, the spectra obtained by taking all the couplings into account are compared with the spectra to which only the coupling of the KK modes to the zero mode contributes. The mass up to which the spectra obtained with different couplings are identical changes only

[4] Note, however, that the time-dependent KK mass $m_j(t)$ enters the intermode-couplings.

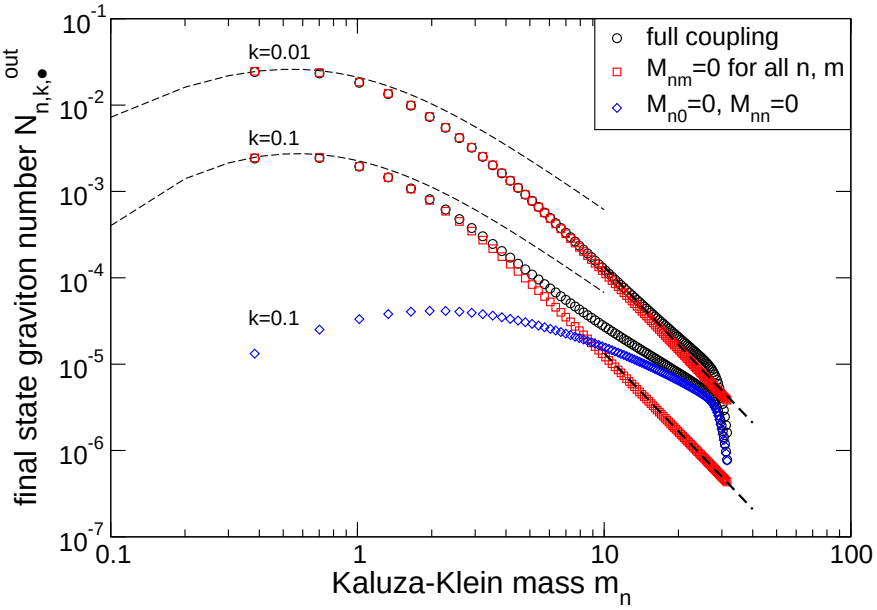

Figure 10.16: KK particle spectra for $y_s = 10$, $v_b = 0.1$, $n_{\max} = 100$ and three-momentum $k = 0.01$ and 0.1 with different couplings taken into account. The thin dashed lines indicates Eq. (10.44) and the thick dashed line Eq. (10.9).

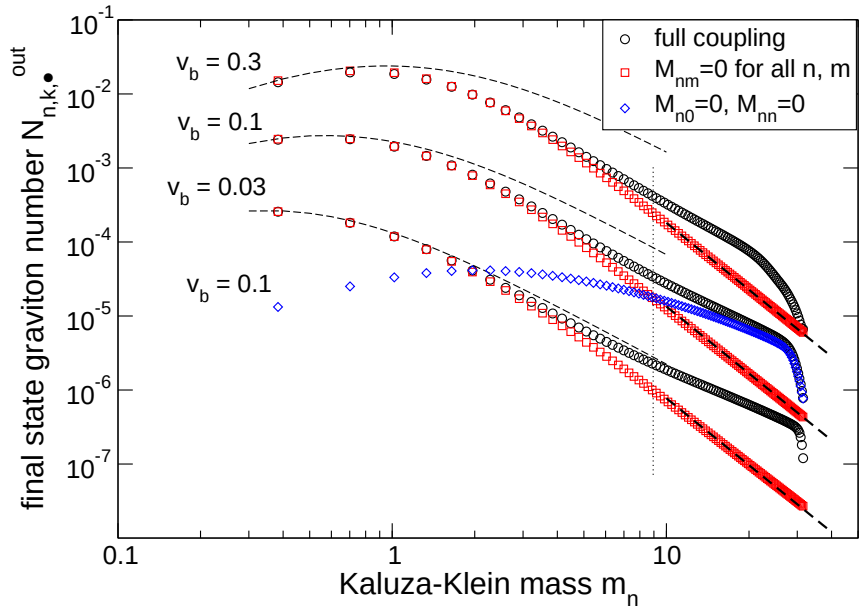

Figure 10.17: KK particle spectra for three-momentum $k = 0.1$,$y_s = 10$ and maximum brane velocities $v_b = 0.03, 0.1$ and 0.3 with $n_{\max} = 100$. As in Fig. 10.16 different couplings have been taken into account and thin dashed lines indicates Eq. (10.44) and the thick dashed line Eq. (10.9).

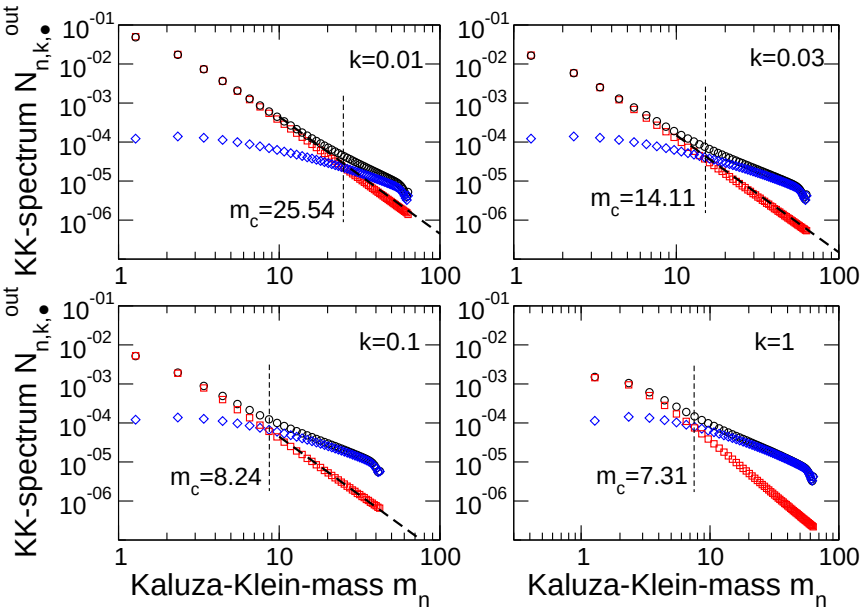

Figure 10.18: KK particle spectra for three-momentum $k = 0.01$, 0.03, 0.1 and 1 for $y_s = 3$ and maximum brane velocity $v_b = 0.1$ with different couplings taken into account where the notation is like in Fig. 10.17. From the crossing of the $M_{nn} = M_{nm} = 0$ – and $M_{nn} = M_{n0} = 0$ – results we determine the k-dependence of $m_c(k, v_b)$. The thick dashed line indicates Eq. (10.9).

slightly with the maximal brane velocity v_b. Therefore, the dependence of m_c on the velocity is rather weak even if v_b is changed by an order of magnitude, but nevertheless evident.
This behavior of the spectrum can indeed be understood qualitatively. In Section 10.3.3 I demonstrate that the coupling strength of the KK modes to the zero mode at the bounce $t = 0$, where production of KK gravitons takes place, is proportional to

$$\frac{\sqrt{v_b}}{k}. \tag{10.7}$$

The larger this term the stronger is the coupling of the KK modes to the zero mode, and thus the larger is the mass up to which this coupling dominates over the KK-intermode couplings. Consequently, the mass at which the tilt of the KK particle spectrum changes depends strongly on the three-momentum k but only weakly on the maximal brane velocity due to the square root behavior of the coupling strength. This explains qualitatively the behavior obtained from the numerical simulations.

An approximate expression for $m_c(k, v_b)$ can be obtained from the numerical simulations. In Figure 10.18 I depict the KK particle spectra for three-momentum $k = 0.01$, 0.03, 0.1 and 1 for $y_s = 3$ and maximum brane velocity $v_b = 0.1$ with different couplings taken into account. The legend is as in Fig. 10.17. From the crossings of the $M_{nm} = 0$, $n \neq m$ and $M_{nn} = M_{n0} = 0$ results one can determine the k-dependence of m_c. Note that the spectra are not numerically stable for large masses, but they are stable in the range where m_c lies [cf., e.g., Fig. 10.20, for $k = 0.1$]. Using the data for $k = 0.01, 0.03$ and 0.1 one finds $m_c(k, v_b) \propto 1/\sqrt{k}$.
In Fig. 10.19 KK graviton spectra are displayed for $k = 0.1$, $y_s = 3$ and maximal brane velocities $v_b = 0.3, 0.2, 0.1, 0.08, 0.05$ and 0.03 with different couplings taken into account. It is in principle possible to determine the v_b-dependence of m_c from the crossings of the $M_{ij} = 0$, $i \neq j$- and $M_{ii} = M_{i0} = 0$ results as done for the k-dependence. However, the values for m_c displayed in the Figures indicate that the dependence of m_c on v_b is very weak. From the given data it is not possible to obtain a good fitting formula (as a simple power law) for the v_b-dependence of m_c. (In the range $0.1 \leq v_b \leq 0.3$ a very good fit is $m_c = 1.12\pi v_b^{0.13}/\sqrt{k}$.) The reason is twofold. First of all, given the complicated coupling structure, it is *a priori* not clear that a simple power law dependence exists. Recall that also the analytical expression for the particle number Eq. (10.44) has not a simple power law velocity dependence. Moreover, for the number of modes taken into account ($n_{\max} = 40$) the numerical results are not stable enough to resolve the weak dependence of m_c on v_b with a high enough accuracy. (But it is good enough to perfectly resolve the k-dependence.) The reason for the slow convergence

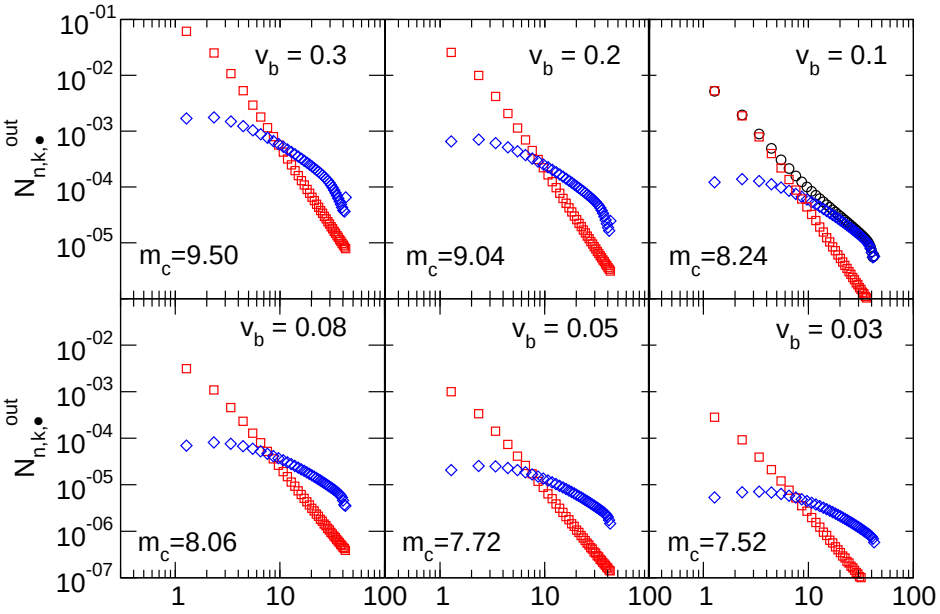

Figure 10.19: KK graviton spectra for three-momentum $k = 0.1$, $y_s = 3$ and maximal brane velocities $v_b = 0.3, 0.2, 0.1, 0.08, 0.05$ and 0.03 with different couplings taken into account where the notation is like in Fig. 10.17. From the crossing of the $M_{nn} = M_{nm} = 0$ – and $M_{nn} = M_{n0} = 0$ – results we determine the v_b-dependence of m_c.

of the numerics will become clear below. As we shall see, the corresponding energy density is dominated by masses much larger than m_c. Consequently the weak dependence of m_c on v_b is not very important in that respect and therefore does not need to be determined more precisely. However, combining all the data I can give as a fair approximation

$$m_c(k, v_b) \simeq \frac{\pi\, v_b^\alpha}{L\sqrt{k\,L}}, \quad \text{with} \quad \alpha \simeq 0.1. \tag{10.8}$$

Taking $\alpha = 0.13$ for $0.1 \leq v_b \leq 0.3$ and $\alpha = 0.08$ for $0.03 \leq v_b \leq 0.1$ fits the given data reasonably well.

As we have seen, as long as the zero mode is the dominant source of KK particle production, the final KK graviton spectrum can be approximated by a power law decrease m_n^{-3}. I can combine the presented numerical results to obtain a fitting formula valid in this regime:

$$\mathcal{N}^{\rm out}_{n\gg 1, k\ll 1, \bullet} = \frac{\pi}{k\, y_s}\frac{(v_b)^{2.37}}{(L\, m_n)^3}, \quad \text{for} \quad \frac{1}{L} < m_n < m_c. \tag{10.9}$$

This fitting formula is shown in Figs. 10.16 10.17 and 10.18 and is in reasonable good agreement with the numerical results. Since Eq. (10.9) together with (10.8) is an important result, I have reintroduced dimensions, i.e. the AdS scale L which is set to one in the simulations, in both expressions.

Let me now discuss the slope of the KK graviton spectrum for masses $m_n \to \infty$ since it determines the contribution of the heavy KK modes to the energy density. In Figure 10.20 I show KK graviton spectra obtained for three-momentum $k = 0.1$, second brane position $y_s = 3$ and maximal brane velocities $v_b = 0.01, 0.03$ and 0.1. Up to $n_{\rm max} = 100$ KK modes have been taken into account in the simulations. One immediately is confronted with the observation that the convergence of the KK graviton spectra for large m_n is very slow. This is since those modes, which are decoupled from the evolution of the four-dimensional graviton, are strongly affected by the kink in the brane motion. Recall that the production of light KK gravitons with masses $m_n \ll m_c$ is virtually driven entirely by the evolution of the massless mode. Those light modes are not so sensitive to the discontinuity in the velocity of the brane motion. To be more precise, their primary source of excitation is the evolution of the four-dimensional graviton but not the kink which, as I shall discuss now, is responsible for the production of heavy KK gravitons $m_n \gg m_c$.

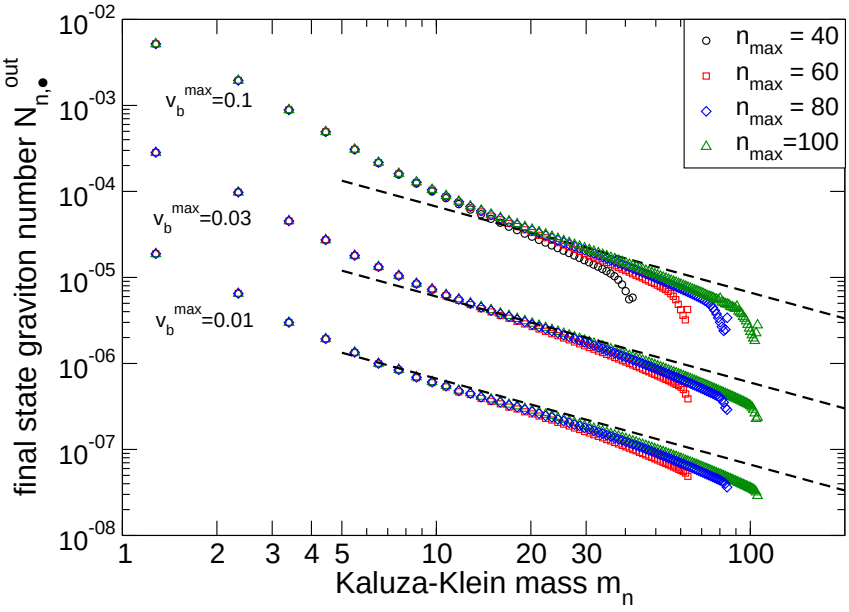

Figure 10.20: KK particle spectra for $k = 0.1$, $y_s = 3$ and maximal brane velocities $v_b = 0.01, 0.03, 0.1$ up to KK masses $m_n \simeq 100$ compared with an $1/m_n$ decline. The dashed lines indicate the approximate expression (10.11) which describes the asymptotic behavior of the final KK particle spectra reasonably well, in particular for $v_b < 0.1$.

As discussed in section 3.5.2 and demonstrated in section 4.2, a discontinuity in the velocity will always lead to a divergent total particle number. Arbitrary high frequency modes are excited by the kink since the acceleration diverges there. Due to the excitation of KK gravitons of arbitrarily high masses one cannot expect that the numerical simulations show a satisfactory convergence behavior which allows to determine the slope by fitting the data. However, it is nevertheless possible to give a quantitative expression for the behavior of the KK graviton spectrum for large masses. The studies of the usual dynamical Casimir effect on a time-dependent interval are very useful for this purpose.

In section 4.2 I have discussed particle production on a time-dependent interval $[0, l(t)]$ for the boundary motion $l(t) = l_0 + v\,t$ with $v =$ const. in detail. I have demonstrated that the particle spectrum behaves as $\propto v^2/\Omega_n$ where $\Omega_n = n\pi/l_0$ is the frequency of a massless scalar particle. This divergent behavior and the resulting slow convergence of the numerical results shown in Fig. 4.1 is caused by the discontinuities in the velocity appearing when the motion is switched on and off.
At the kink in the brane-motion the total change of the velocity is $2v_b$, similar to the case for the linear motion where the discontinuous change of the velocity is $2v$. Consequently one may conclude that for large KK masses $m_n \gg m_c$ for which the evolution of the KK modes is no longer affected by their coupling to the four-dimensional graviton the KK graviton spectrum behaves as [5]

$$\mathcal{N}^{\rm out}_{n,k,\bullet} \propto \frac{(v_b)^2}{m_n} \quad \text{for} \quad m_n \gg m_c \; . \tag{10.10}$$

If I assume that the spectrum declines like $1/m_n$ and use that the numerical results for masses $m_n \simeq 20$ are virtually stable one finds $\mathcal{N}^{\rm out}_{n,k,\bullet} \propto v_b^{2.08}/m_n$ which describes the asymptotics of the numerical results well.
As for the uniform motion [cf. Fig. 4.1], the slow convergence of the numerical results towards the $1/m_n$ behavior is well visible for large masses $m_n \gg m_c$ which do no longer couple to the four-dimensional graviton. This is a strong indication for the statement that the final graviton spectrum for large masses behaves indeed like (10.10). It is therefore possible to give a single simple expression for the final KK particle spectrum for

[5] Note that the discussion in section 4.2 refers to Dirichlet boundary conditions. For Neumann boundary conditions considered here, the zero mode and its asymmetric coupling play certainly a particular role. However, as we have shown, for large masses only the KK-intermode couplings are important. Consequently, there is no reason to expect that the qualitative behavior of the spectrum for large masses depends on the particular kind of boundary condition.

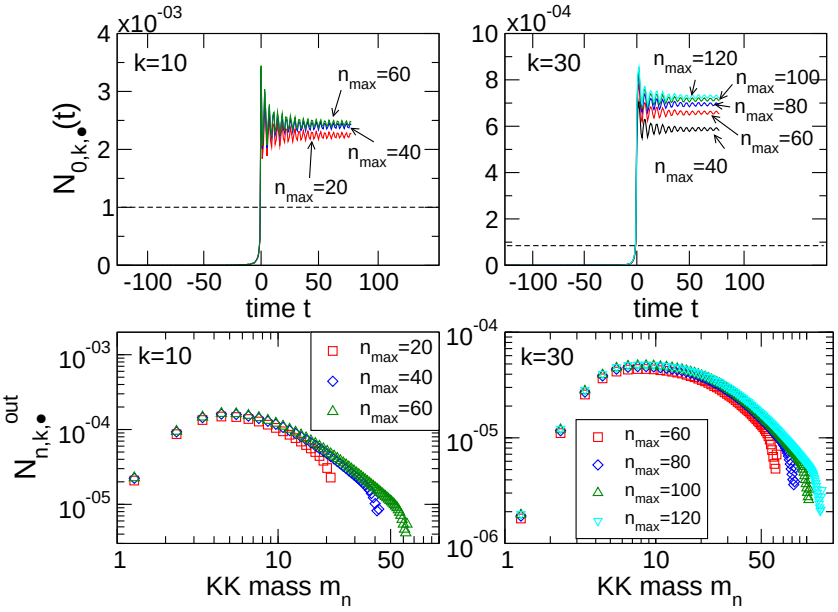

Figure 10.21: Evolution of the zero mode particle number $\mathcal{N}_{0,k,\bullet}(t)$ and final KK graviton spectra $\mathcal{N}^{\rm out}_{n,k,\bullet}$ for $y_s = 3$, maximal brane velocity $v_b = 0.1$ and three-momenta $k = 10$ and 30. The dashed line in the upper plots indicate Eq. (10.26) (divided by two) demonstrating the value of the number of produced zero mode gravitons without coupling to the KK modes.

large masses which comprises all the features of the spectrum even quantitatively reasonably well [cf. dashed lines in Fig. 10.20]

$$\mathcal{N}^{\rm out}_{n,k,\bullet} \simeq 0.2 \frac{v_b^2}{\Omega^{\rm out}_{n,k}\, y_s} \quad \text{for} \quad m_n \gg m_c \ . \tag{10.11}$$

The $1/y_s$-dependence is compelling. It follows immediately from the considerations on the energy and the scaling behavior discussed above [cf. Figs. 10.11 and 10.12]. For completeness we now write $1/\Omega^{\rm out}_{n,k}$ instead of the KK mass m_n only, since what matters is the total energy of a mode. Throughout this section this has not been important since I considered only $k \ll 1$ such that $\Omega^{\rm out}_{n,k}$ becomes independent of k for large masses $m_n \gg k$ [cf. Fig. 10.14].

10.2.5 Short wavelengths $k \gg 1$

For short wave lengths $k \gg 1$ (short compared to the AdS-curvature scale L set to one in the simulations) a completely new and very interesting effect appears. The behavior of the four-dimensional graviton mode changes drastically. I find that the zero mode now couples to the KK gravitons and no longer evolves virtually independently of the KK modes, in contrast to the behavior for long wavelengths.
In Fig. 10.21 I show the evolution of the zero mode graviton number $\mathcal{N}_{0,k,\bullet}(t)$ and final KK graviton spectra $\mathcal{N}^{\rm out}_{n,k,\bullet}$ for $y_s = 3$, maximal brane velocity $v_b = 0.1$ and three-momenta $k = 10$ and 30. One observes that the evolution of the four-dimensional graviton depends on the number of KK modes $n_{\rm max}$ taken into account, i.e. the zero mode couples to the KK gravitons. For $k = 10$ the first 60 KK modes have to be included in the simulation in order to obtain a numerically stable result for the zero mode. In the case of $k = 30$ one already needs $n_{\rm max} \simeq 100$ in order to achieve numerical stability for the zero mode.
Figure 10.22 displays the time-evolution of the number of produced zero mode gravitons $\mathcal{N}_{0,k,\bullet}(t)$ for $y_s = 3$ and $v_b = 0.1$. For large k the production of massless gravitons takes place only at the bounce since these short wavelength modes are sub-horizon right after the bounce. Corresponding KK particle spectra for $k = 10, 30$ are depicted in Figs. 10.21 and 10.23. The inset in Fig. 10.22 shows the resulting final four-dimensional graviton spectrum $\mathcal{N}^{\rm out}_{0,k,\bullet}$, which is very well fitted by an inverse power law $\mathcal{N}^{\rm out}_{0,k,\bullet} = 0.02/(k - 1.8)$ [6]. Consequently, for

[6] The momenta $k = 5, 10, 20, 30$ and 40 have been used to obtain the fit. Fitting the spectrum for $k = 20, 30$ and 40 to a power law gives $\mathcal{N}^{\rm out}_{0,k,\bullet} \propto k^{-1.1}$.

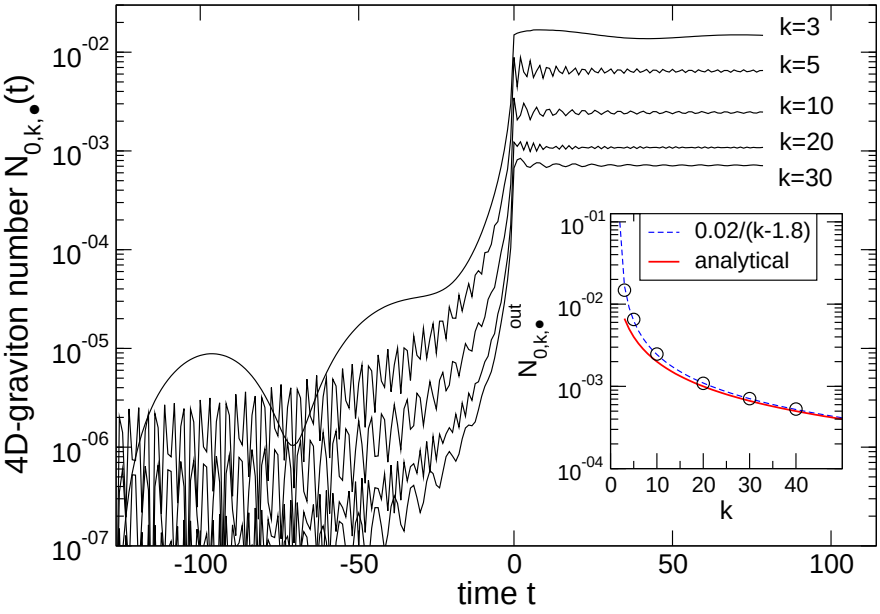

Figure 10.22: 4D-graviton number $\mathcal{N}_{0,k,\bullet}(t)$ for $k = 3, 5, 10, 20$ and 30 with $y_s = 3$ and maximal brane velocity $v_b = 0.1$. The small plot shows the final graviton spectrum $\mathcal{N}^{\rm out}_{0,k,\bullet}$ together with a fit to the inverse law $a/(k+b)$ [dashed line] and the analytical fitting formula Eq. (10.33) [solid line]. For $k = 10$ and 30 the corresponding KK graviton spectra are shown in Fig. 10.21.

$k \gg 1$ the zero mode particle number $\mathcal{N}^{\rm out}_{0,k,\bullet}$ declines like $1/k$ only, in contrast to the $1/k^2$ behavior found for $k \ll 1$.

The dependence of $\mathcal{N}^{\rm out}_{0,k,\bullet}$ on the maximal brane velocity v_b also changes. In Fig. 10.23 I show $\mathcal{N}_{0,k,\bullet}(t)$ together with the corresponding KK graviton spectra for $y_s = 3$, $k = 5$ and 10 in each case for different v_b. Using $n_{\rm max} = 60$ KK modes in the simulations guarantees numerical stability for the zero mode. The velocity dependence of $\mathcal{N}^{\rm out}_{0,k,\bullet}$ is not given by a simple power law as it is the case for $k \ll 1$. This is not very surprising since now the zero mode couples strongly to the KK modes [cf. Fig. 10.21]. For $k = 10$, for example, one finds $\mathcal{N}^{\rm out}_{0,k,\bullet} \propto v_b^{1.4}$ if $v_b \lesssim 0.1$.

As in the long wavelengths case, the zero mode particle number does not depend on the position of the static brane y_s even though the zero mode now couples to the KK modes. This is demonstrated in Fig. 10.24 where the evolution of the zero mode particle number $\mathcal{N}_{0,k,\bullet}(t)$ and the corresponding KK graviton spectra with $k = 10$, $v_b = 0.1$ for the two values $y_s = 3$ and 10 are shown. One needs $n_{\rm max} = 60$ for $y_s = 30$ in order to obtain a stable result for the zero mode which is not sufficient in the case $y_s = 10$. Only for $n_{\rm max} \simeq 120$ the zero mode solution approaches the stable result which is identical to the result obtained for $y_s = 3$.
What is important is not the number of the KK modes the four-dimensional graviton couples to, but rather a particular mass $m_{\rm zm} \simeq k$. The zero mode couples to all KK modes of masses below $m_{\rm zm}$ no matter how many KK modes are lighter. Recall that the value of y_s just determines how many KK modes belong to a given mass interval Δm since, roughly, $m_n \simeq n\pi/y_s$. The KK-spectra for $k \geq 1$ show the same scaling behavior as demonstrated for long wavelengths in Figs. 10.11 and 10.12.

The production of four-dimensional gravitons of short wavelengths takes place on the expense of the KK modes. In Fig. 10.25 I show the numerical results for the final KK particle spectra with $v_b = 0.1$, $y_s = 3$ and $k = 3, 5, 10$ and 30 obtained for different coupling combinations. These spectra should be compared with those shown in Fig. 10.18 for the long wavelengths case. For $k \gtrsim 10$ the number of the produced lightest KK gravitons is smaller in the full coupling case compared to the situation where only the KK-intermode coupling is taken into account. In case $k = 30$, for instance, the numbers of produced gravitons for the first four KK modes are smaller for the full coupling case. This indicates that the lightest KK modes couple strongly to the zero mode. Their evolution is damped and graviton production in those modes is suppressed. The production

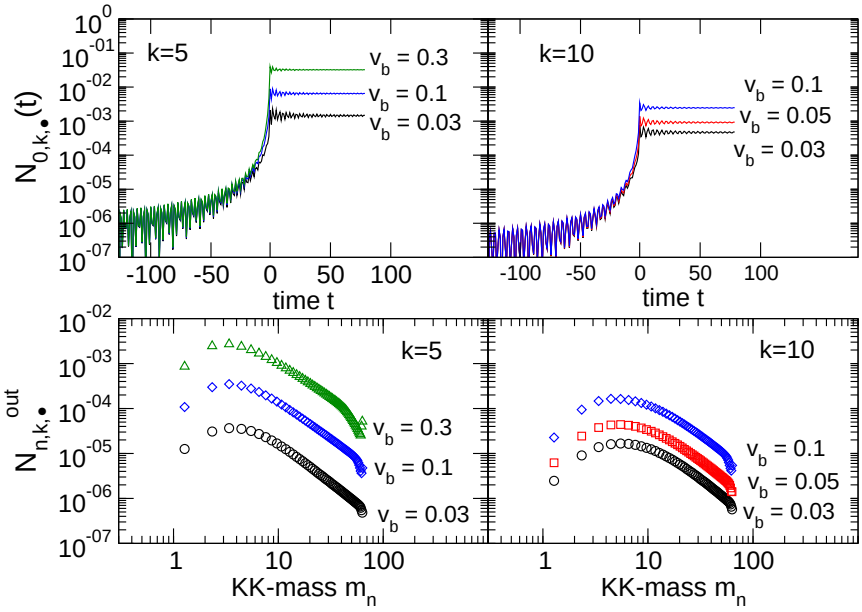

Figure 10.23: Zero mode particle number $\mathcal{N}_{0,k,\bullet}(t)$ and corresponding final KK particle spectra $\mathcal{N}^{\rm out}_{n,k,\bullet}$ for $y_s = 3$, $k = 5, 10$ and different maximal brane velocities v_b. $n_{\rm max} = 60$ guarantees numerically stable solutions for the zero mode.

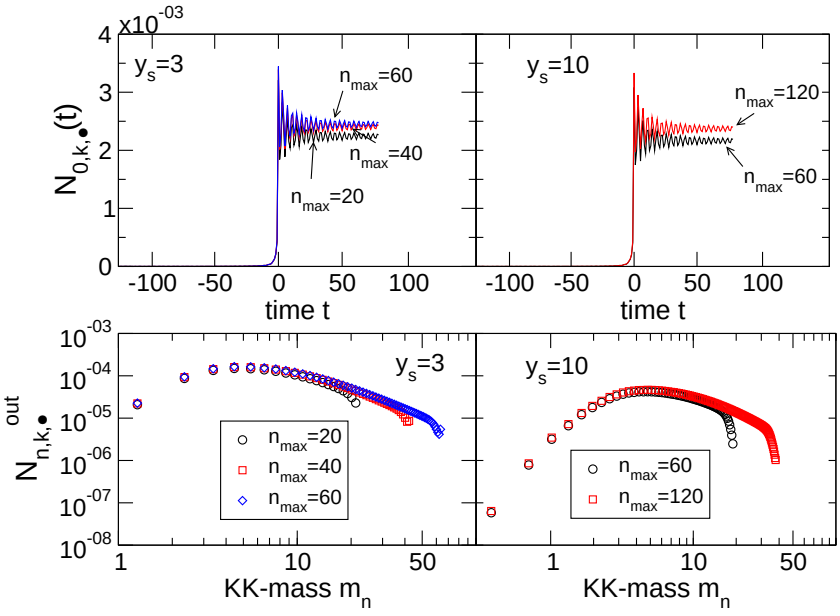

Figure 10.24: Zero mode particle number $\mathcal{N}_{0,k\bullet}(t)$ and corresponding KK graviton spectra for $k = 10$, $v_b = 0.1$ and 2nd brane positions $y_s = 3$ and 10.

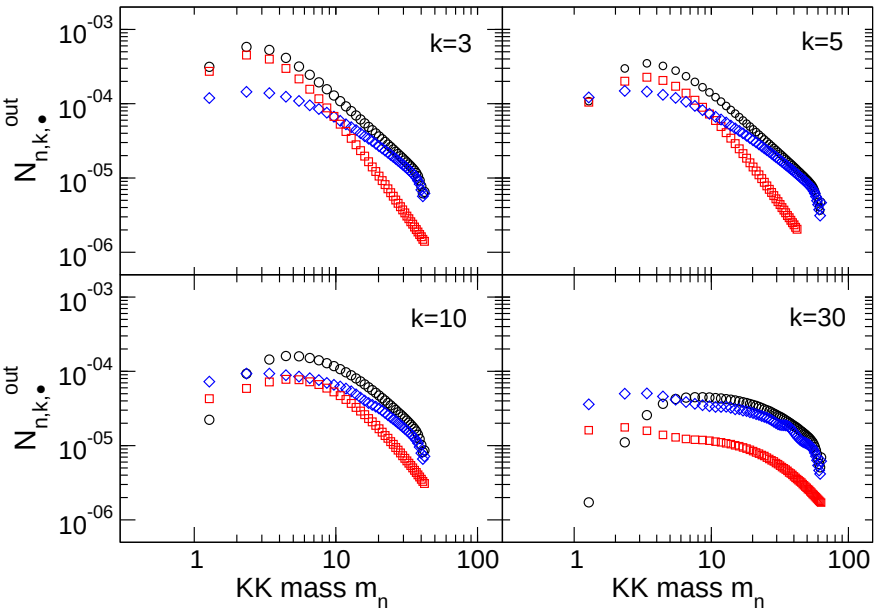

Figure 10.25: Final KK particle spectra $\mathcal{N}^{\rm out}_{n,k,\bullet}$ for $v_b = 0.1$, $y_s = 3$ and $k = 3, 5, 10$ and 30 and different couplings. Circles correspond to the full coupling case, squares indicate the results if $M_{nm} = M_{nn} = 0$, i.e. no KK-intermode couplings and diamonds correspond to $M_{n0} = 0$, i.e. no coupling of KK modes to the zero mode.

of zero mode gravitons on the other hand is enhanced compared to the long wavelengths case. For short wavelengths, the evolution of the KK modes therefore contributes to the production of zero mode gravitons. This may be interpreted as creation of zero mode gravitons out of KK-mode vacuum fluctuations.
As in the long wavelengths case, the KK particle spectrum becomes independent of k if $m_n \gg k$ and the evolution of the KK modes is dominated by the KK-intermode coupling. This is visible in Fig. 10.25 for $k = 3$ and 5. Also the bend in the spectrum when the KK-intermode coupling starts to dominate is observable. For $k = 10$ and 30 this regime with $m_n \gg k$ is not reached.

As I have shown before, in the regime $m_n \gg k$ the KK particle spectrum behaves as $1/\Omega^{\rm out}_{n,k}$ which will dominate the energy density of produced KK gravitons.
If $1 \ll m_n \lesssim k$, however, the zero mode couples to the KK modes and the KK graviton spectrum does not decay like $1/\Omega^{\rm out}_{n,k}$. This is demonstrated in Fig. 10.26 where the number of produced final state gravitons $\mathcal{N}^{\rm out}_{n,k,\bullet}$ is plotted as function of their frequency $\Omega^{\rm out}_{n,k}$ for parameters $v_b = 0.1$, $y_s = 3$ and $k = 5, 10, 20, 30$ and 40.
While for $k = 5$ the KK-intermode coupling dominates for large masses [cf. Fig. 10.25] leading to a bending over in the spectrum and eventually to an $1/\Omega^{\rm out}_{n,k}$-decay, the spectra for $k = 20, 30$ and 40 show a different behavior. All the modes are still coupled to the zero mode leading to a power-law decrease $\propto 1/(\Omega^{\rm out}_{n,k})^{\alpha}$ with $\alpha \simeq 2$. The case $k = 10$ corresponds to an intermediate regime. Also shown is the simple analytical expression given in Eq. (10.45) which describes the spectra reasonably well for large k (dashed line).
The KK particle spectra in the region $1 \ll m_n \lesssim k$ will also contribute to energy density since the cutoff scale is the same for the integration over k and the summation over the KK-tower (see Section 10.3.4 below).

10.2.6 A smooth transition

Let me finally investigate how the KK-graviton spectrum changes when the kink-motion (10.3) is replaced by the smooth motion (10.6). In Fig. 10.27 I show the numerical results for the final KK-graviton spectrum for $y_s = 3$, $v_b = 0.1$ and $k = 0.1$ for the smooth motion (10.6) with $t_s = 0.05, 0.015$ and 0.005. $n_{\rm max} = 60$ modes have been taken into account in the simulation and the results are compared to the spectrum obtained with the kink-motion (10.3). The parameter t_s defines the scale $L_s \simeq 2t_s$ at which the kink is smoothed, i.e. L_s corresponds to the width of the transition from contraction to expansion. From the numerical results one observes that KK modes of masses smaller than $m_s \simeq 1/L_s$ are not affected, but the production of KK-particles

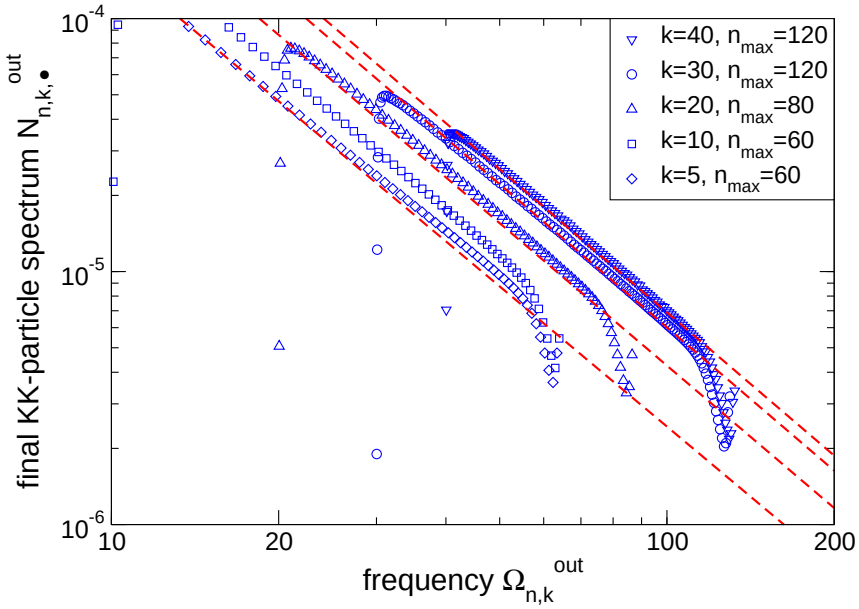

Figure 10.26: Final KK particle spectra $\mathcal{N}^{\rm out}_{n,k,\bullet}$ for $v_b = 0.1$, $y_s = 3$ and $k = 5, 10, 20, 30$ and 40. The dashed lines indicate Eq. (10.45) for $k = 10, 20, 30$ and 40. For $k \geq 20$, the simple analytical expression (10.45) agrees quite well with the numerical results.

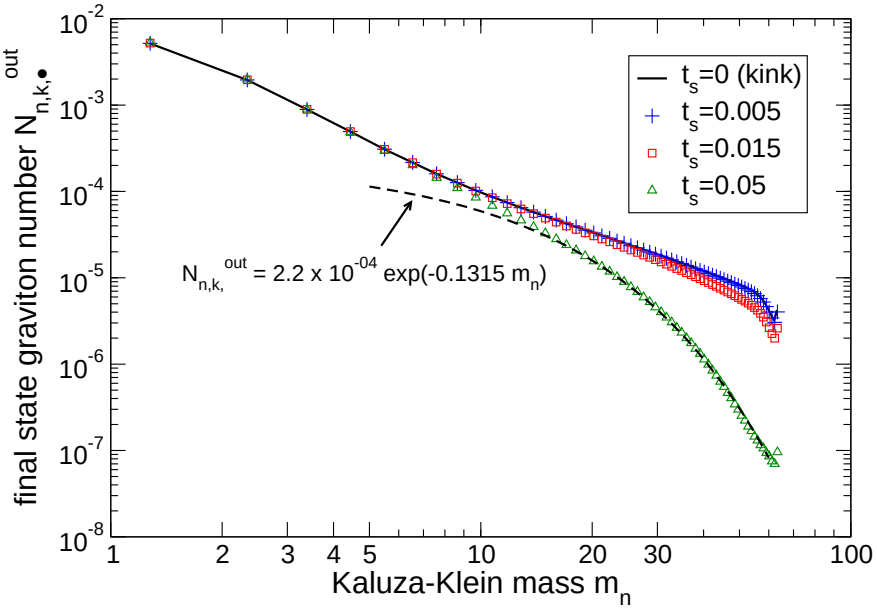

Figure 10.27: KK-particle spectrum for $y_s = 3$, $v_b = 0.1$ and $k = 0.1$ for the bouncing as well as smooth motions with $t_s = 0.005, 0.015$, and 0.05 to demonstrate the influence of the bounce. $n_{\rm max} = 60$ KK modes have been taken into account in the simulations and the result for the kink motion is shown as well.

of masses larger than m_s is exponentially suppressed. This is in particular evident for $t_s = 0.05$ where the particle spectrum for masses $m_n > 10$ has been fitted to a exponential decrease. Going to smaller values of t_s, the suppression of KK-mode production sets in for larger masses. For the example with $t_s = 0.005$, the KK-particle spectrum is identical to the one obtained with the kink-motion within the depicted mass range. In this case the exponential suppression of particle production sets in only for masses $m_n > 100$. Note that the exponential decay of the spectrum for the smooth transition from contraction to expansions also shows that no additional spurious effects due to the discontinuities in the velocity when switching the brane dynamics on and off occur. Consequently, $t_{\rm in}$ and $t_{\rm out}$ are appropriately chosen.

10.3 Analytical calculations and estimates

10.3.1 Zero mode: long wavelengths $k \ll 1/L$

The numerical simulations show that the evolution of the zero mode at large wavelengths is not affected by the KK modes. To find an analytical approximation to the numerical result for the zero mode, I neglect all the couplings of the KK modes to the zero mode by setting $M_{nm} = 0 \; \forall \; n, m$ and keeping M_{00} only. Then only the evolution equation for $\epsilon_0^{(\alpha)} \equiv \delta_0^\alpha \epsilon$ is important; it decouples and reduces to

$$\ddot{\epsilon} + [k^2 + \mathcal{V}(t)]\epsilon = 0 \; , \tag{10.12}$$

with "potential"

$$\mathcal{V} \;\; = \;\; \dot{M}_{00} - M_{00}^2 \; . \tag{10.13}$$

The corresponding vacuum initial conditions are [cf. Eq. (9.59); here I do not consider the unimportant phase]

$$\lim_{t\to-\infty} \epsilon \;\; = \;\; 1 \; , \quad \lim_{t\to-\infty} \dot{\epsilon} = -ik. \tag{10.14}$$

A brief calculation using the expression for M_{00} leads to

$$\mathcal{V} = \frac{y_s^2}{y_s^2 - y_b^2}\left[\frac{\ddot{y}_b}{y_b} + \frac{\dot{y}_b^2}{y_b^2}\frac{3y_b^2 - 2y_s^2}{y_s^2 - y_b^2}\right] = -\frac{y_s^2}{y_s^2 - y_b^2}\left[\mathcal{H}^2\left(1 - \frac{y_b^2}{y_s^2 - y_b^2}\right) + \dot{\mathcal{H}}\right] . \tag{10.15}$$

If one assumes that the static brane is much further away from the Cauchy horizon than the physical brane, $y_s \gg y_b$, it is simply

$$\mathcal{V} = -\mathcal{H}^2 - \dot{\mathcal{H}} \; , \tag{10.16}$$

and one recovers Eq. (9.35).
For the particular scale factor (10.2) one obtains

$$\mathcal{H} \;\; = \;\; \frac{\dot{a}}{a} = \frac{\mathrm{sign}(t)}{|t| + t_b} \qquad \text{and} \tag{10.17}$$

$$\dot{\mathcal{H}} \;\; = \;\; \frac{2\delta(t)}{t_b} - \frac{1}{(|t| + t_b)^2} \tag{10.18}$$

such that

$$\dot{\mathcal{H}} + \mathcal{H}^2 = \frac{2\delta(t)}{t_b} \; . \tag{10.19}$$

The δ-function in the last equation models the bounce. Without the bounce, i.e. for an eternally radiation dominated dynamics, one has $\mathcal{V} = 0$ and the evolution equation for ϵ would be trivial. With the bounce, the potential is just a δ-function potential with "height" proportional to $-2\sqrt{v_b}/L$

$$\mathcal{V} = -\frac{2\sqrt{v_b}}{L}\delta(t) \; , \tag{10.20}$$

where v_b is given in Eq (10.5). Equation (10.12) with potential (10.20) can be considered as a Schrödinger equation with δ-function potential. Its solution is a classical textbook problem. Since the approximated potential $\mathcal{V}$ vanishes for all $t < 0$ one has, with the initial condition (10.14),

$$\epsilon(t) = e^{-ikt} \; , \quad t < 0 \; . \tag{10.21}$$

Assuming continuity of ϵ through $t = 0$ and integrating the differential equation over a small interval $[0^-, 0^+]$ around $t = 0$ gives

$$0 = \int_{0_-}^{0_+} \left[\ddot{\epsilon} + \left(k^2 - \frac{2\sqrt{v_b}}{L}\delta(t)\right)\epsilon\right] = \dot{\epsilon}(0_+) - \dot{\epsilon}(0_-) - \frac{2\sqrt{v_b}}{L}\epsilon(0) \ . \tag{10.22}$$

Consequently, similar to the derivation of the junction condition in Chapter 8, the derivative $\dot{\epsilon}$ has a jump. This jump leads to particle creation. Using $\epsilon(0_+) = \epsilon(0) = \epsilon(0_-)$ and $\dot{\epsilon}(0_+) = \dot{\epsilon}(0_-) + \frac{2\sqrt{v_b}}{L}\epsilon(0)$ as initial conditions for the solution for $t > 0$, one obtains

$$\epsilon(t) = Ae^{-ikt} + Be^{ikt} \ , \quad t > 0 \tag{10.23}$$

with

$$A = 1 + i\frac{\sqrt{v_b}}{kL} \ , \quad B = -i\frac{\sqrt{v_b}}{kL} \ . \tag{10.24}$$

The Bogoliubov coefficient $\mathcal{B}_{00}$ after the bounce is then given by

$$\mathcal{B}_{00}(t \geq 0) = \frac{e^{-ikt}}{2}\left[\left(1 + i\frac{\mathcal{H}}{k}\right)\epsilon(t) - \frac{i}{k}\dot{\epsilon}(t)\right] \ , \tag{10.25}$$

where I have used that $M_{00} = -\mathcal{H}$ if $y_s \gg y_b$ [cf. Eq. (9.34)]. At this point the importance of the coupling matrix M_{00} becomes obvious. Even though the solution ϵ to the differential equation (10.12) is a plane wave right after the bounce, $|\mathcal{B}_{00}(t)|^2$ is not a constant due to the motion of the brane itself. Only once the mode is inside the horizon, i.e. $\mathcal{H}/k \ll 1$, $|\mathcal{B}_{00}(t)|^2$ is constant and the number of generated final state gravitons (for both polarizations) is given by

$$\mathcal{N}_{0,k}^{\text{out}} = 2|\mathcal{B}_{00}(kt \gg 1)|^2 = 2\left(\frac{1}{4}\left[|\epsilon|^2 + \frac{|\dot{\epsilon}|^2}{k^2}\right] - \frac{1}{2}\right) = \frac{2v_b}{(kL)^2} \tag{10.26}$$

where I have used that the Wronskian of ϵ, ϵ^* is $2ik$. As illustrated in Fig. 10.4 the expression (10.26) is indeed in excellent agreement with the (full) numerical results, not only in its k-dependence but also the amplitude agrees without any fudge factor. The evolution of the four-dimensional graviton mode and the associated generation of massless gravitons with momentum $k < 1/L$ can therefore be understood analytically.

In order to calculate the energy density, I have to take into account that the approximation of an exactly radiation dominated Universe with an instant transition breaks down on small scales. I assume this break down to occur at a lengths scale L_s, much smaller than L. In particular I shall take this scale to be the string scale, thus

$$L_s^3 = \kappa_5 \ , \tag{10.27}$$

which, by virtue of (8.57), implies that

$$\frac{L}{L_s} = \left(\frac{L_s}{L_{\text{Pl}}}\right)^2 \ . \tag{10.28}$$

L_s is the true width of the transition from collapse to expansion which is set to zero in the treatment. Modes with mode numbers $k \gg (2\pi)/L_s$ will not 'feel' the potential and are not generated. I therefore choose $k_{\max} = (2\pi)/L_s$ as the cutoff scale. Then, with Eq (9.93), one obtains for the energy density

$$\rho_0 = \frac{1}{2\,\pi^2 a^4}\int_0^{2\pi/L_s} dk k^3 \mathcal{N}_{0,k} \ . \tag{10.29}$$

For small wave numbers, $k < 1/L$, I can use the above analytical result for the zero mode particle number. However, as the numerical simulations have revealed, as soon as $k \geq 1/L$, the coupling of the four-dimensional graviton to the KK modes becomes important and for large wave numbers $\mathcal{N}_{0,k}^{\text{out}}$ decays only like $1/k$. Hence the integral (10.29) is entirely dominated by the upper cutoff. The contribution from long wavelengths to the energy density are negligible.

For the power spectrum, on the other hand, I am interested in cosmologically large scales, $1/k \simeq$ several Mpc or more, but not in short wavelengths $kL > 1$ dominating the energy density. Inserting the expression

for the number of produced long wavelength gravitons (10.26) into (9.83), the gravity wave power spectrum at late times becomes

$$\mathcal{P}_0(k) = \frac{2\,v_b}{(2\pi)^3}\frac{\kappa_4}{(aL)^2} \quad \text{for} \quad kt \gg 1. \tag{10.30}$$

This is the *asymptotic* power spectrum, when ϵ starts oscillating, hence inside the Hubble horizon, $kt \gg 1$. On super Hubble scales, $kt \ll 1$ when the asymptotic out-state of the zero mode is not yet reached, one may use Eq. (9.82) with

$$\mathcal{R}_{0,k}(t) = \frac{|\epsilon(t)|^2 - 1}{k} \simeq \frac{4v_b a^2}{k}\ . \tag{10.31}$$

For the $\simeq$ sign I assume $t \gg L$ and $t \gg t_b$ so that one may neglect terms of order t/L in comparison to $\sqrt{v_b}(t/L)^2$. I have also approximated $a = (t+t_b)/L \simeq t/L$. Inserting this in Eq. (9.80) yields

$$\mathcal{P}_0(k) = \frac{\kappa_4}{2\,\pi^3} v_b\, k^2\ , \qquad kt \ll 1\ . \tag{10.32}$$

Both expressions (10.30) and (10.32) are in good agreement with the corresponding numerical results, see Figs. 10.4,10.5 and 10.6.

10.3.2 Zero mode: short wavelengths $k \gg 1/L$

As I have demonstrated with the numerical analysis, as soon as $k \geq 1/L$, the coupling of the zero mode to the KK modes becomes important and for large wave numbers $\mathcal{N}^{\rm out}_{0,k,\bullet} \propto 1/k$. I obtain a good asymptotic behavior if I set

$$\mathcal{N}^{\rm out}_{0,k,\bullet} \simeq \frac{v_b}{5(kL)}. \tag{10.33}$$

This function and Eq. (10.26) (divided by two for one polarization) meet at $kL = 5$. Even though the approximation is not good in the intermediate regime it is very reasonable for large k [cf. Fig. 10.22]. Inserting this approximation into Eq (10.29) for the energy density, one finds that the integral is dominated entirely by the upper cutoff, i.e. by the blue, high energy modes:

$$\rho_0 \simeq \frac{16}{30}\frac{\pi}{a^4}\frac{v_b}{LL_s^3} \simeq \frac{1}{2}\frac{\pi}{a^4}\frac{v_b}{LL_s^3}. \tag{10.34}$$

The power spectrum associated with the short wavelengths $k > 1/L$ is not of interest since the gravity wave spectrum is measured on cosmologically large scales only, $k \ll 1/L$.

10.3.3 Light Kaluza-Klein modes and long wavelengths $k \ll 1/L$

The numerics indicates that light ($m_n < 1$) long wavelength Kaluza-Klein modes become excited mainly due to their coupling to the zero mode. Let me take only this coupling into account and neglect also the time-dependence of the frequency, setting $\Omega_{n,k}(t) \equiv \Omega^{\rm out}_{n,k} = \Omega^{\rm in}_{n,k}$. The Bogoliubov coefficients are then determined by the equations

$$\dot{\xi}_{n,k} + i\Omega^{\rm out}_{n,k}\xi_{n,k} = \frac{k}{2\Omega^{\rm out}_{n,k}} S_n(t;k) \tag{10.35}$$

$$\dot{\eta}_{n,k} - i\Omega^{\rm out}_{n,k}\eta_{n,k} = -\frac{k}{2\Omega^{\rm out}_{n,k}} S_n(t;k) \tag{10.36}$$

with the "source"

$$S_n(t;k) = (\xi_{0,k} - \eta_{0,k})\, M_{n0}\ . \tag{10.37}$$

I have defined $\xi_{\alpha,k} \equiv \xi^{(0)}_{\alpha,k}$ and $\eta_{\alpha,k} \equiv \eta^{(0)}_{\alpha,k}$. The source is known, since the evolution of the four-dimensional graviton is know. From the result for ϵ above and the definition of $\xi_{0,k}$ and $\eta_{0,k}$ in terms of ϵ and $\dot{\epsilon}$ one obtains

$$\xi_{0,k} - \eta_{0,k} = \frac{2i}{k}\left[-ik + \frac{1}{|t| + t_b}\right] e^{-itk}\ , \quad t < 0 \tag{10.38}$$

$$\xi_{0,k} - \eta_{0,k} = 2\left[1 + \frac{i}{kt_b} + \frac{1 - ikt_b}{k^2 t_b(t+t_b)}\right] e^{-itk} + 2\left[\frac{i}{kt_b} - \frac{1}{k^2 t_b(t+t_b)}\right] e^{itk}\ , \quad t > 0\ . \tag{10.39}$$

Furthermore, if $y_s \gg y_b$, one has [cf. Eq. (9.26)]

$$M_{n0} = 2\frac{\dot{y}_b}{y_b}\sqrt{\frac{Y_1(m_n y_s)^2}{Y_1(m_n y_b)^2 - Y_1(m_n y_s)^2}} \ . \tag{10.40}$$

Assuming $y_s m_n \gg 1$ and $y_b m_n \ll 1$ one can expand the Bessel functions and arrives at

$$M_{n0} \simeq \sqrt{\pi}\sqrt{\frac{m_n}{y_s}}\dot{y}_b = -\sqrt{\frac{\pi m_n L^2}{y_s}}\frac{L\,\mathrm{sign(t)}}{(|t|+t_b)^2} \ .$$

To determine the number of created final state gravitons, I only need to calculate $\eta_{n,k}$ [cf. Eq. (9.68)],

$$\mathcal{N}^{\rm out}_{n,k,\bullet} = |\mathcal{B}_{0n,k}(t_{\rm out})|^2 = \frac{1}{4}\frac{\Omega^{\rm out}_{n,k}}{k}|\eta_{n,k}(t_{\rm out})|^2 \ . \tag{10.41}$$

The vacuum initial conditions require $\lim_{t\to-\infty}\eta_{n,k} = 0$ so that $\eta_{n,k}$ is given by the particular solution

$$\eta_{n,k}(t) = \frac{k}{\Omega^{\rm out}_{n,k}}\int_{-\infty}^{t} S_j(t';k)e^{-it'\Omega^{\rm out}_{n,k}}dt' \ , \tag{10.42}$$

and therefore

$$\mathcal{N}^{\rm out}_{n,k,\bullet} = \frac{k}{4\Omega^{\rm out}_{n,k}}\left|\int_{-\infty}^{\infty} S_n(t;k)e^{-it\Omega^{\rm out}_{n,k}}dt\right|^2 \ , \tag{10.43}$$

where the integration range has been extended from $-\infty$ to $+\infty$ since the source is very localized around the bounce. This integral can be solved exactly. A somewhat lengthy but straight forward calculation gives

$$\begin{aligned}\mathcal{N}^{\rm out}_{n,k,\bullet} &= \frac{\pi m_n^5 L^4}{2\Omega^{\rm out}_{n,k}k y_s}\Big|2i\mathrm{Re}\left(e^{i(\Omega^{\rm out}_{n,k}+k)t_b}E_1(i(\Omega^{\rm out}_{n,k}+k)t_b)\right)\\ &+ (kt_b)^{-1}e^{i(\Omega^{\rm out}_{n,k}-k)t_b}E_1(i(\Omega^{\rm out}_{n,k}-k)t_b) - e^{i(\Omega^{\rm out}_{n,k}+k)t_b}E_1(i(\Omega^{\rm out}_{n,k}+k)t_b)\Big|^2 \ .\end{aligned} \tag{10.44}$$

Here E_1 is the exponential integral, $E_1(z) \equiv \int_z^\infty t^{-1}e^{-t}dt$. This function is holomorphic in the complex plane with a cut along the negative real axis, and the above expression is therefore well defined. Note that this expression does not give rise to a simple dependence of $\mathcal{N}^{\rm out}_{n,k,\bullet}$ on the velocity $v_b = (L/t_b)^2$. In the preceding Section we have seen that, within its range of validity, Eq. (10.44) is in excellent agreement with the numerical results (cf., for instance, Figs. 10.7 and 10.8).
As already mentioned before, this excellent agreement between the numerics and the analytical approximation demonstrates that the numerical results are not contaminated by any spurious effects.

10.3.4 Kaluza-Klein modes: asymptotic behavior and energy density

The numerical simulations show that the asymptotic KK-graviton spectra (i.e. for masses $m_n \gg 1$) decay like $1/\Omega^{\rm out}_{n,k}$ if $m_n \gg k$ and like $\left(1/\Omega^{\rm out}_{n,k}\right)^\alpha$ with $\alpha \simeq 2$ if $m_n \lesssim k$. The corresponding energy density on the brane is given by the summation of Eq. (9.95) over all KK modes up to the cutoff. Since the mass m_n is simply the momentum into the extra dimension, it is plausible to choose the same cutoff scale for both, the k-integral and the summation over the KK modes, namely $2\pi/L_s$. The main contribution to the four-dimensional particle density and energy density comes from $m_n \sim 2\pi/L_s$ and $k \sim 2\pi/L_s$, i.e. the blue end of the spectrum.
The large-frequency behavior of the final KK-spectrum can be approximated by

$$\mathcal{N}^{\rm out}_{n,k,\bullet} \simeq \frac{0.2v_b^2}{y_s}\begin{cases}\dfrac{1}{\Omega^{\rm out}_{n,k}} & \text{if } \ 1/L \lesssim k \lesssim m_n \\ 2^{(\alpha-1)/2}\dfrac{k^{\alpha-1}}{(\Omega^{\rm out}_{n,k})^\alpha} & \text{if } \ m_n \lesssim k \lesssim 2\pi/L_s\end{cases} \tag{10.45}$$

with $\alpha \simeq 2$ which is particularly good for large k. Both expression match at $m_n = k$ and are indicated in Figs. 10.20 and 10.26 as dashed lines. Given the complicated coupling structure of the problem and the

multitude of features visible in the particle spectra these compact expressions describe the numerical results reasonable well for all parameters. The deviation from the numerical results is at most a factor of two. This accuracy is sufficient in order to obtain a useful expression for the energy density from which bounds on the involved energy scales can be derived.
The energy density on the brane associated with the KK gravitons is given by [cf. Eq. (9.95)]

$$\rho_{\rm KK} \simeq \frac{L^2}{4\pi a^6 y_s} \sum_n \int dk k^2 \, \mathcal{N}^{\rm out}_{n,k,\bullet} \, \Omega^{\rm out}_{n,k} \, m_n \ . \tag{10.46}$$

Splitting the momentum integration into two integrations from 0 to m_n and m_n to the cutoff $2\pi/L_s$, and replacing the sum over the KK masses by an integral one obtains

$$\rho_{KK} \simeq C(\alpha) \frac{\pi^5 v_b^2}{a^6 y_s} \frac{L^2}{L_s^5} \ . \tag{10.47}$$

The power α in Eq. (10.45) enters the final result for the energy density only through the pre-factor $C(\alpha)$ which is of order unity.

10.4 Discussion

The numerical simulations have revealed many interesting effects related to the interplay between the evolution of the four-dimensional graviton and the KK modes. All features observed in the numerical results have been interpreted entirely on physical grounds and many of them are supported by analytical calculations and arguments. Having summarized the results for the power spectrum and energy densities in the preceding section, I'm now in the position to discuss the significance of these findings for brane cosmology.

10.4.1 Zero mode

For the zero-mode power spectrum I have found that

$$\mathcal{P}_0(k) = \frac{\kappa_4}{2\,\pi^3} v_b \begin{cases} k^2 & \text{if } \ kt \ll 1 \\ \frac{1}{2}(La)^{-2} & \text{if } \ kt \gg 1 \end{cases} \ . \tag{10.48}$$

Therefore, the gravity wave spectrum on large, super Hubble scales is blue with spectral tilt

$$n_T = 2 \ . \tag{10.49}$$

As I have explained in Section 10.1, this is a common feature of ekpyrotic and pre-Big Bang models. The amplitude of perturbations on CMB scales is of the order of $(H_0/m_{Pl})^2$, i.e. very suppressed on scales relevant for the anisotropies of the CMB. The fluctuations induced by these Casimir gravitons are much too small to leave any observable imprint on the CMB.

For the zero-mode energy density at late times, $kt \gg 1$, I have obtained [cf Eq. (10.34)]

$$\rho_{h0} \simeq \frac{1}{2} \frac{\pi}{a^4} \frac{v_b}{L L_s^3} \ . \tag{10.50}$$

In this section I denote the energy density of the zero mode by ρ_{h0} in order not to confuse it with the present density of the Universe. Recall that L_s is the scale at which my kinky approximation (10.2) of the scale factor breaks down, i.e. the width of the bounce. If this width is taken to zero, the energy density of gravitons is very blue and diverges. This is not so surprising, since the kink in $a(t)$ allows one to generate gravitons of arbitrary high energies. However, as the numerical simulations have shown, when I smooth the kink at some scale L_s, the production of modes with energies larger than $\simeq 1/L_s$ is exponentially suppressed [cf. Fig. 10.27]. This justifies the introduction of L_s as a cutoff scale.

In the following I shall determine the density parameter of the generated gravitons today and compare it to the nucleosynthesis bound. For this I need the minimal scale factor a_b [cf. Eq. (10.5)] and

$$H_b = \left| \frac{\dot{a}}{a^2} \right|_{t=0} \simeq \frac{v_b}{L} \ , \tag{10.51}$$

the maximal Hubble parameter, i.e. the Hubble parameter right after the bounce. (Recall that in the low energy approximation $t = \eta$.) Since at low energies the modified Friedmann equation (8.58) reduces to the standard one (6.20) (neglecting curvature and/or a cosmological constant), during the radiation era the radiation density is

$$\rho_{\rm rad} = \frac{3}{\kappa_4} H^2 = \frac{3}{\kappa_4 L^2} a^{-4} = \frac{3}{\kappa_4} H_b^2 \left(\frac{a_b}{a}\right)^4 . \tag{10.52}$$

In order to determine the density parameter of the generated gravitons today, i.e., at $t = t_0$, I use [cf. Section 6.3.5]

$$\Omega_{h0} = \frac{\rho_{h0}(t_0)}{\rho_{\rm crit}(t_0)} = \frac{\rho_{h0}(t_0)}{\rho_{\rm rad}(t_0)} \frac{\rho_{\rm rad}(t_0)}{\rho_{\rm crit}(t_0)} = \frac{\rho_{h0}(t_0)}{\rho_{\rm rad}(t_0)} \Omega_{\rm rad}. \tag{10.53}$$

The second factor $\Omega_{\rm rad}$ is the present radiation density parameter. For the factor $\rho_{h0}/\rho_{\rm rad}$, which is time independent since both ρ_{h0} and $\rho_{\rm rad}$ scale like $1/a^4$, I insert the above results and obtain, using $\kappa_4 = L_{\rm Pl}^2$,

$$\Omega_{h0} = \frac{\rho_{h0}}{\rho_{\rm rad}} \Omega_{\rm rad} = \frac{1}{2}\frac{\pi}{3} v_b \left(\frac{L_{Pl}}{L_s}\right)^2 \frac{L}{L_s} \Omega_{\rm rad} \simeq \frac{v_b}{2} \left(\frac{L_{Pl}}{L_s}\right)^2 \frac{L}{L_s} \Omega_{\rm rad} . \tag{10.54}$$

The nucleosynthesis bound [154] requests that

$$\Omega_{h0} \lesssim 0.1\, \Omega_{\rm rad} , \tag{10.55}$$

which translates into the relation

$$\frac{v_b}{2} \left(L_{Pl}/L_s\right)^2 \left(L/L_s\right) \lesssim 0.1 \tag{10.56}$$

which, at first sight, relates the different scales involved. But since I have chosen the cutoff scale L_s to be the higher-dimensional fundamental scale (string scale), Equation (10.56) reduces to

$$v_b \lesssim 0.2 \tag{10.57}$$

by virtue of Equation (10.28). All one has to require to be consistent with the nucleosynthesis bound is a small brane velocity which justifies the low energy approach. In all, I conclude that the model is not severely constrained by the zero mode. This result itself is remarkable. If there would be no coupling of the zero mode to the KK modes for small wavelengths the number of produced high energy zero-mode gravitons would behave as $\propto k^{-2}$ as it is the case for long wavelengths. The production of high energy zero-mode gravitons from KK gravitons enhances the total energy density by a factor of about L/L_s. Without this enhancement, the nucleosynthesis bound would not lead to any meaningful constraint and would not require $v_b < 1$.

10.4.2 KK modes

As derived above, the energy density of KK gravitons on the brane is dominated by the high energy gravitons and can be approximated by Eq. (10.47)

$$\rho_{KK} \simeq \frac{\pi^5 v_b^2}{a^6 y_s} \frac{L^2}{L_s^5} . \tag{10.58}$$

Let me evaluate the constraint induced from the requirement that the KK-energy density on the brane be smaller than the radiation density $\rho_{\rm KK}(t) < \rho_{\rm rad}(t)$ at all times. If this is not satisfied, back-reaction cannot be neglected and the results are no longer valid. Clearly, at early times this condition is more stringent than at late times since $\rho_{\rm KK}$ decays faster than $\rho_{\rm rad}$. Inserting the value of the scale factor directly after the bounce where the production of KK gravitons takes place, $a_b^{-2} = v_b$, one finds, using again the RS-fine tuning condition (10.28),

$$\left(\frac{\rho_{\rm KK}}{\rho_{\rm rad}}\right)_{\rm max} \simeq 100\, v_b^3 \left(\frac{L}{y_s}\right) \left(\frac{L}{L_s}\right)^2 . \tag{10.59}$$

If I use the largest value for the brane velocity v_b admitted by the nucleosynthesis bound $v_b \simeq 0.2$ and require that $\rho_{\rm KK}/\rho_{\rm rad}$ be (much) smaller than one for back-reaction effects to be negligible, I obtain the very stringent condition

$$\frac{L}{y_s} \ll \left(\frac{L_s}{L}\right)^2 . \tag{10.60}$$

Let me first discuss the largest allowed value for $L \simeq 0.1$mm. The RS-fine tuning condition then determines (10.28)

$$L_s = (LL_{Pl}^2)^{1/3} \simeq 10^{-22}\ \text{mm} \simeq 1/(10^6\ \text{TeV}). \tag{10.61}$$

In this case the brane tension is

$$\mathcal{T} = 6\kappa_4/\kappa_5^2 = 6L_{Pl}^2/L_s^6 = 6/(LL_s^3) \sim (10\,\text{TeV})^4. \tag{10.62}$$

Furthermore, one has

$$(L/L_s)^2 \simeq 10^{42} \text{ so that } y_s > L(L/L_s)^2 \simeq 10^{41}\,\text{mm} \simeq 3 \times 10^{15}\,\text{Mpc}, \tag{10.63}$$

which is about 12 orders of magnitude larger than the present Hubble scale! Also, since $y_b(t) \ll L$ in the low energy regime, and $y_s \gg L$ according to the inequality (10.60), the physical brane and the static brane are very far apart at all times. Note that the distance between the physical and the static brane is

$$d = \int_{y_b}^{y_s} \frac{L}{y} dy = L \log(y_s/y_b) \gtrsim L \gg L_s\ .$$

This situation is probably not very realistic. Some high energy, stringy effects are needed to provoke the bounce and one expects these to be relevant only when the branes are sufficiently close, i.e. at a distance of order L_s. But in this case the constraint (10.60) will be violated which implies that back-reaction will be relevant.
On the other hand, if one wants that $y_s \simeq L$ and back-reaction to be unimportant, then Eq. (10.59) implies that the bounce velocity has to be exceedingly small,

$$y_s \simeq L \quad \Rightarrow \quad v_b \lesssim 10^{-15}. \tag{10.64}$$

One might hope to find a way out of these conclusions by allowing the bounce to happen in the high energy regime. But then $v_b \simeq 1$ and the nucleosynthesis bound is violated since too many zero-mode gravitons are produced. Even if one disregards this limit for a moment, saying that the calculation presented here only applies in the low energy regime, $v_b \ll 1$, the modification coming from the high energy regime are not expected to alleviate the bounds. In the high energy regime one may of course have $y_b(t) \gg L$ and therefore the physical brane can approach the static brane arbitrarily closely without the latter having to violate (10.60). These results suggest that even in the scenario of a bounce at low energies, the back reaction from KK gravitons has to be taken into account. But this does not need to exclude the model.

Chapter 11

Conclusions

In this thesis, I have studied particle creation from vacuum fluctuations by moving boundaries - the dynamical Casimir effect - for two rather distinct scenarios: The production of photons in dynamical cavities and the generation of gravitons in braneworld cosmology.

The first part of the thesis was devoted to a comprehensive presentation of the dynamical Casimir effect within the framework of canonical quantization. Besides the detailed treatment of compatible boundary conditions which, at least to my knowledge, has been outlined for the dynamical Casimir effect in this form for the first time, I have tried to highlight the differences between the dynamical Casimir effect and other quantum vacuum radiation effects like particle creation in an expanding Universe and the Unruh effect.
By introducing a particular parameterization for the time-evolution of the field modes inside the dynamical cavity, I have derived a system of coupled first-order linear differential equations determining the evolution of the Bogoliubov coefficients. Physical quantities like the number of particles created during the dynamics of the mirror and the associated energy of the generated radiation are determined by the solutions to this system which can be found by applying standard numerics. This formalism allows for efficient numerical investigation of the dynamical Casimir effect for a variety of possible interesting scenarios where less or even nothing is known analytically.
As a first example, and as a testing ground for the numerics, I studied the creation of massless scalar particles in a one-dimensional cavity. After the historic example of a uniform motion, which I have used to demonstrate the role of discontinuities in the velocity of the mirror motion, I have employed the numerical formalism to trembling cavities, the most studied model of the dynamical Casimir effect. Thereby, the numerical results are entirely in agreement with analytical predictions derived by many authors for resonant as well as off-resonant mirror vibrations. This has demonstrated that the numerical simulations are a reliable tool and that the developed method is appropriate to study the dynamical Casimir effect fully numerically. Potential problems inherent in the method, in particular the matching problem due to discontinuities in the velocity of the boundary motion leading to spurious contributions to the total particle number, have been discussed. It has been shown that this effect is negligibly small for cavity vibrations with a sufficiently small amplitude.

As the main application of the formalism, the production of TE-mode photons in a three-dimensional rectangular vibrating cavity has been studied numerically for resonant wall oscillations. This is of great importance regarding current proposals for experiments aiming to verify the dynamical Casimir effect in the laboratory. I have found perfect agreement between numerical results and analytical predictions in the case that no modes are (strongly) coupled. When two field modes of frequency $\Omega_{\mathbf{l}}^{\text{in}}$ and $\Omega_{\mathbf{k}}^{\text{in}}$ are exactly coupled, i.e. $\omega_{\text{cav}} = |\Omega_{\mathbf{l}}^{\text{in}} \pm \Omega_{\mathbf{k}}^{\text{in}}|$ where ω_{cav} is the (resonant) cavity frequency, the numerical results agree with analytical predictions of [41] for sufficiently long times but disagree for short times. The discrepancy for short times is ascribed to properties of the multiple scale analysis used in [41].
The effects of the intermode coupling has been studied in detail which is only possible by means of numerical simulations. The numerical simulations have revealed that the efficiency of photon production in a resonantly vibrating rectangular cavity can be controlled and in particular maximized by tuning the cavity size. This important and indeed new result might be very useful for the optimization of planned dynamical Casimir experiments. The main resonance case $\omega_{\text{cav}} = 2\Omega_{(1,1,1)}^{\text{in}}$ has been discussed for a cavity with equally sized non-dynamical dimensions $l_{\parallel} = l_y = l_z$ in detail. I have shown that photon creation in the resonant mode $(1,1,1)$

is most efficient if the size $l_\parallel$ of the non-dynamical cavity dimensions is ≈ 11 times larger than the dynamical cavity dimension. The existence of a certain cavity size which maximizes photon creation is among other things explained by the fact, that intermode coupling takes place even if the coupling condition $\omega_{\rm cav} = |\Omega^{\rm in}_{\mathbf{l}} \pm \Omega^{\rm in}_{\mathbf{k}}|$ is satisfied only approximately. If $l_\parallel$ is larger than ≈ 11, the intermode coupling is so strong that higher frequency modes like $(3,1,1)$ and $(5,1,1)$ couple to the resonant mode $(1,1,1)$ and strongly damp its evolution. Furthermore the coupling of particular field modes by tuning the size of the cavity has been studied. The effects provoked by the intermode coupling can be studied in full detail only by means of numerical methods. The findings demonstrate that the intermode coupling in dynamical cavities plays an important role. Even if analytical results are known, numerical simulations are a very useful and indeed necessary tool because only they can completely account for the intermode coupling.

In the second part of the thesis, I have studied the evolution of tensor perturbations in braneworld cosmology by using the techniques developed for the standard dynamical Casimir effect. A model consisting of a moving and a fixed 3-brane embedded in a five-dimensional static AdS bulk has been considered. Regarding particle creation from vacuum, such a two-brane setup is analogous to the dynamical cavity considered in the first part. Applying the dynamical Casimir effect formulation to the study of tensor perturbations in braneworld cosmology represents an interesting alternative to other approaches existing in the literature so far and provides a new perspective on the problem.
First of all, the explicit use of coupling matrices allows to obtain detailed information about the effects of the intermode couplings generated by the time-dependent boundary conditions, i.e. the brane motion. This has enabled me to shown analytically that, at low energies (late time cosmology), all couplings except the zero-mode self coupling vanish if the fixed brane is far away from the physical brane. As a consequence, in this limit or in any other case where the zero mode decouples from the KK modes, the homogeneous tensor perturbation equation in brane cosmology automatically leads to the standard four-dimensional tensor perturbation equation. As I have argued in section 9.3, this result supports the assumption that the low energy physics is reasonably well described even if one replaces the full junction condition at the moving brane by a Neumann boundary condition.
Based on the expansion of the tensor perturbations in instantaneous eigenfunctions, I have introduced a consistent quantum mechanical formulation of graviton production by a moving brane. Observable quantities like the power spectrum and energy density can be directly deduced from quantum mechanical expectation values, in particular the number of gravitons created from vacuum fluctuations. The most surprising and at the same time most interesting fact which this approach has revealed is that the energy density of the massive gravitons decays like $1/a^6$ with the expansion of the Universe. At first this seems very disturbing. How can it be that massive modes on the brane scale like stiff matter rather than like ordinary massive particles, $\propto 1/a^3$? As I have explained in detail in Section 9.5.4, the reason for this is twofold. First, the mass of the modes, m_n is a 'comoving' mass and hence the dispersion relation of the particles is $\Omega^2_{n,k} = k^2 + m_n^2$, where k and $\Omega_{n,k}$ are comoving momentum and frequency as also pointed out in [85]. Alone, this would imply a $1/a^4$ behavior of the energy density, as for the massless mode. But there is an additional factor $1/a^2$ coming from the value of the mode function ϕ_n on the brane. This function is normalized in the bulk, but its value on the brane decreases. Physically this means, as time evolves, the probability that a KK graviton is concentrated close to the brane becomes smaller and smaller, i.e. the KK gravitons escape into the bulk. While the wave function of massive gravitons is repulsed away from the brane, the zero-mode wave function stays localized at the brane position with the localization becoming even stronger as the Universe expands. This is the localization of gravity: the five-dimensional aspects of it, like the KK gravitons, become less and less 'visible' on the brane with the expansion of the Universe. The $1/a^6$-scaling behavior remains valid also when the fixed brane is sent off to infinity and one ends up with a single braneworld in AdS, like in the original Randall-Sundrum II scenario. Consequently, Kaluza-Klein gravitons on a brane moving through an AdS bulk cannot play the role of dark matter.

As an explicit example, I have studied graviton production in a generic, ekpyrotic-inspired model of two branes bouncing at low energies, assuming that the energy density on the moving brane is dominated by a radiation component. The numerical results have revealed a multitude of interesting effects.
For long wavelengths $kL \ll 1$ (k being the co-moving momentum and L the curvature radius of AdS) the zero mode evolves virtually independently from the KK modes. Zero mode gravitons are generated by the self coupling of the zero mode to the moving brane. For the number of produced massless gravitons I have found the simple analytical expression $2v_b/(kL)$ with v_b being the bounce velocity of the brane. These long wave-

length modes are the once which are of interest for the zero-mode power spectrum which could also be derived analytically. As one expects for an ekpyrotic scenario, the zero-mode power spectrum is blue on super-horizon scales with spectral tilt $n_T = 2$. Hence, the spectrum of these Casimir gravitons has much too little power on large scales to affect the fluctuations of the cosmic microwave background.
The situation changes completely for short wavelengths $kL \gg 1$. In this wavelength range, the evolution of the zero mode couples strongly to the KK modes, and production of zero-mode gravitons takes place on the expense of KK-graviton production. The numerical simulation revealed that the number of produced short-wavelength massless gravitons is given by $2v_b/(5kL)$. It decays only like $1/k$ instead of the $1/k^2$-behavior found for long wavelengths. These short wavelength gravitons dominate the energy density. Comparing the energy density with the nucleosynthesis bound and taking the cutoff scale to be the string scale L_s, I have found that the model is not constrained by the zero mode. As long as $v_b \lesssim 0.2$, i.e. a low energy bounce as I have assumed from the very beginning, the nucleosynthesis bound is not violated.
More stringent bounds on the model come from the KK modes. Their energy density is dominated by the high energy modes which are produced due to the kink which models the transition from contraction to expansion. Imposing the reasonable requirement that the energy density of the KK modes on the brane be (much) smaller than the radiation density at all times in order for back-reaction effects to be negligible, has led to two cases. On the one hand, allowing the largest values for the AdS curvature scale $L \simeq 0.1$mm and the bounce velocity $v_b \simeq 0.2$, back-reaction can only be neglected if the fixed brane is very far away from the physical brane $y_s \sim 10^{41}$mm. As I have argued, this is not very realistic since some high energy, stringy effects provoking the bounce are expected to be relevant only when the branes are sufficiently close, i.e. $y_s \sim L_s$. On the other hand, by only requiring that $y_s \simeq L \gg L_s$, the bounce velocity has already to be exceedingly small, $v_b \lesssim 10^{-15}$, for back-reaction to be unimportant. Therefore, one of the main conclusions to take away from this final part of the thesis is that back reaction of massive gravitons has to be taken into account for a realistic bounce.

Many of the results presented here are based on numerical calculations. However, since the used approach provides the possibility to artificially switch on and off the mode couplings, I was able identify the primary sources driving the time evolution of the perturbations in different wavelength and KK-mass ranges. This has allowed me to understand many of the features observed in the numerical results on analytical grounds.
On the other hand, it is fair to say that most of the presented results rely on the low energy approach, i.e. on the approximation of the junction condition (generalized Neumann boundary condition) by a Neumann boundary condition. Even though I have given arguments for the goodness of this approximation, it has eventually to be confirmed by calculations which take the exact boundary condition into account. Therefore, the next step is to extend the formalism to generalized Neumann boundary conditions along the lines which I have briefly outlined in this thesis. The present formalism and in particular the available code represents an ideal starting point for this promising task. This will not only allow to study graviton production in the high energy regime of braneworld models, but also the investigation of TM-modes in dynamical cavities. Let me finally mention that the present model of two bouncing branes seems to be adequate to address the back reaction issue since the creation of Kaluza-Klein gravitons happens exclusively at the bounce.

Appendix A

On power spectrum and energy density calculation

A.1 Power spectrum

In order to calculate the power spectrum Eq. (9.79) I need to evaluate the expectation value

$$\langle \hat{h}_\bullet(t,y_b,\mathbf{k})\hat{h}^\dagger_\bullet(t,y_b,\mathbf{k}')\rangle_{\rm in} = \frac{\kappa_5}{L^3}\sum_{\alpha\alpha'}\phi_\alpha(t,y_b)\phi_{\alpha'}(t,y_b)\langle \hat{q}_{\alpha,\mathbf{k},\bullet}(t)\hat{q}^\dagger_{\alpha',\mathbf{k}',\bullet}(t)\rangle_{\rm in} \tag{A.1}$$

where I have used (9.40) and introduced the shortcut $\langle ...\rangle_{\rm in} = \langle 0,{\rm in}|...|0,{\rm in}\rangle$. Using the expansion (9.53) of $\hat{q}_{\alpha,\mathbf{k}\bullet}(t)$ in initial state operators and complex functions $\epsilon^{(\gamma)}_{\alpha,k}(t)$ one finds

$$\langle \hat{q}_{\alpha,\mathbf{k},\bullet}(t)\hat{q}^\dagger_{\alpha',\mathbf{k}',\bullet}(t)\rangle_{\rm in} = \sum_\beta \frac{\epsilon^{(\beta)}_{\alpha,k}(t)\,\epsilon^{(\beta)*}_{\alpha',k}(t)}{2\Omega^{\rm in}_{\beta,k}}\,\delta^{(3)}(\mathbf{k}-\mathbf{k}'). \tag{A.2}$$

From the initial conditions (9.59) it follows that the sum in (A.1) diverges at $t = t_{\rm in}$. This divergence is related to the usual normal ordering problem and can be removed by a subtraction scheme. However, in order to obtain a well defined power spectrum at all times, it is not sufficient just to subtract the term $(1/2)(\delta_{\alpha\alpha'}/\Omega^{\rm in}_{\alpha,k})\delta^{(3)}(\mathbf{k}-\mathbf{k}')$ which corresponds to $\langle \hat{q}_{\alpha,\mathbf{k},\bullet}(t_{\rm in})\hat{q}^\dagger_{\alpha',\mathbf{k}',\bullet}(t_{\rm in})\rangle_{\rm in}$ in the above expression. In order to identify all terms contained in the power spectrum one can use the instantaneous particle concept which allows to treat the Bogoliubov coefficients (9.62) and (9.63) as continuous functions of time [cf. section 3.5.3]. First I express the complex functions $\epsilon^{(\beta)}_{\alpha,k}$ in (A.2) in terms of $\mathcal{A}_{\gamma\alpha,k}(t)$ and $\mathcal{B}_{\gamma\alpha,k}(t)$. This is of course equivalent to calculating the expectation value using

$$\hat{q}_{\alpha,k\bullet}(t) = \frac{1}{\sqrt{2\Omega_{\alpha,k}(t)}}\left[\hat{a}_{\alpha,\mathbf{k},\bullet}(t)\Theta_{\alpha,k}(t) + \hat{a}^\dagger_{\alpha,-\mathbf{k},\bullet}(t)\Theta^*_{\alpha,k}(t)\right] \tag{A.3}$$

and the Bogoliubov transformation of the from (3.81). The result consists of terms involving the Bogoliubov coefficients and the factor $(1/2)(\delta_{\alpha\alpha'}/\Omega_{\alpha,k}(t))\delta^{(3)}(\mathbf{k}-\mathbf{k}')$, leading potentially to a divergence at all times. This term corresponds to $\langle 0,t|\hat{q}_{\alpha,\mathbf{k},\bullet}(t)\hat{q}^\dagger_{\alpha',\mathbf{k}',\bullet}(t)|0,t\rangle$, i.e. it is related to the normal ordering problem (zero-point energy) with respect to the instantaneous vacuum state $|0,t\rangle$. It can be removed by the subtraction scheme

$$\langle \hat{q}_{\alpha,\mathbf{k},\bullet}(t)\hat{q}^\dagger_{\alpha',\mathbf{k}',\bullet}(t)\rangle_{\rm in,phys} = \langle \hat{q}_{\alpha,\mathbf{k},\bullet}(t)\hat{q}^\dagger_{\alpha',\mathbf{k}',\bullet}(t)\rangle_{\rm in} - \langle 0,t|\hat{q}_{\alpha,\mathbf{k},\bullet}(t)\hat{q}^\dagger_{\alpha',\mathbf{k}',\bullet}(t)|0,t\rangle \tag{A.4}$$

where I use the subscript "phys" to denote the physically meaningful expectation value. Inserting this expectation value into (A.1), and using Eq. (9.75) I find

$$\langle \hat{h}_\bullet(t,y_b,\mathbf{k})\hat{h}_\bullet(t,y_b,\mathbf{k}')\rangle_{\rm in} = \frac{1}{a^2}\frac{\kappa_5}{L}\sum_\alpha \mathcal{R}_{\alpha,k}(t)\mathcal{Y}^2_\alpha(a)\delta^{(3)}(\mathbf{k}-\mathbf{k}') \tag{A.5}$$

with $\mathcal{R}_{\alpha,k}(t)$ defined in Eq. (9.81). The function $\mathcal{O}^{\mathcal{N}}_{\alpha,k}$ appearing in Eq. (9.81) is explicitely given by

$$\mathcal{O}^{\mathcal{N}}_{\alpha,k} = 2\,\Re\,\sum_\beta\left\{\Theta^2_{\alpha,k}\mathcal{A}_{\beta\alpha,k}\mathcal{B}^*_{\beta\alpha,k} + \Theta_{\alpha,k}\sum_{\alpha'\neq\alpha}\sqrt{\frac{\Omega_{\alpha,k}}{\Omega_{\alpha',k}}}\frac{\mathcal{Y}_{\alpha'}(a)}{\mathcal{Y}_\alpha(a)}\left[\Theta^*_{\alpha',k}\mathcal{B}^*_{\beta\alpha}\mathcal{B}_{\beta\alpha'} + \Theta_{\alpha',k}\mathcal{A}_{\beta\alpha}\mathcal{B}^*_{\beta\alpha'}\right]\right\} \tag{A.6}$$

and $\mathcal{O}^{\epsilon}_{\alpha,k}$ appearing in Eq. (9.82) reads

$$\mathcal{O}^{\epsilon}_{\alpha,k} = \sum_{\beta,\alpha'\neq\alpha} \frac{\mathcal{Y}_{\alpha'}(a)}{\mathcal{Y}_{\alpha}(a)} \frac{\epsilon^{(\beta)}_{\alpha,k}\epsilon^{(\beta)^*}_{\alpha',k}}{\Omega^{\rm in}_{\beta,k}}. \tag{A.7}$$

A.2 Energy density

In order to calculate the energy density I need to evaluate the expectation value $\langle\dot{\hat{h}}_{ij}(t,\mathbf{x},y_b)\dot{\hat{h}}^{ij}(t,\mathbf{x},y_b)\rangle_{\rm in}$. Using (8.67) and the relation $e^{\bullet}_{ij}(-\mathbf{k}) = (e^{\bullet}_{ij}(\mathbf{k}))^*$ I obtain

$$\begin{aligned}\langle\dot{\hat{h}}_{ij}(t,\mathbf{x},y_b)\dot{\hat{h}}^{ij}(t,\mathbf{x},y_b)\rangle_{\rm in} = \sum_{\bullet\bullet'}\int \frac{d^3k}{(2\pi)^{3/2}}\frac{d^3k'}{(2\pi)^{3/2}}\times \\ \times\langle\dot{\hat{h}}_{\bullet}(t,y_b,\mathbf{k})\dot{\hat{h}}^{\dagger}_{\bullet'}(t,y_b,\mathbf{k}')\rangle_{\rm in} e^{i(\mathbf{k}-\mathbf{k}')\cdot\mathbf{x}} e^{\bullet}_{ij}(\mathbf{k})\ \left(e^{\bullet'\,ij}(\mathbf{k}')\right)^*.\end{aligned} \tag{A.8}$$

By means of the expansion (9.55) the expectation value $\langle\dot{\hat{h}}_{\bullet}(t,y_b,\mathbf{k})\dot{\hat{h}}^{\dagger}_{\bullet'}(t,y_b,\mathbf{k}')\rangle_{\rm in}$ becomes

$$\langle\dot{\hat{h}}_{\bullet}(t,y_b,\mathbf{k})\dot{\hat{h}}^{\dagger}_{\bullet'}(t,y_b,\mathbf{k}')\rangle_{\rm in} = \frac{\kappa_5}{L^3}\sum_{\alpha\alpha'}\langle\hat{p}_{\alpha,\mathbf{k},\bullet}(t)\hat{p}^{\dagger}_{\alpha',\mathbf{k}',\bullet'}(t)\rangle_{\rm in}\phi_{\alpha}(t,y_b)\phi_{\alpha'}(t,y_b). \tag{A.9}$$

From the definition of $\hat{p}_{\alpha,\mathbf{k},\bullet}(t)$ in Eq. (9.56) it is clear that this expectation value will in general contain terms proportional to the coupling matrix and its square when expressed in terms of $\epsilon^{(\beta)}_{\alpha,k}$. However, since I'm interested in the expectation value at late times only when the brane moves very slowly such that the mode couplings go to zero and a physical meaningful particle definition can be given, I can set

$$\langle\hat{p}_{\alpha,\mathbf{k},\bullet}(t)\hat{p}^{\dagger}_{\alpha',\mathbf{k}',\bullet'}(t)\rangle_{\rm in} = \left\langle\dot{\hat{q}}_{\alpha,-\mathbf{k},\bullet}(t)\dot{\hat{q}}^{\dagger}_{\alpha',-\mathbf{k}',\bullet'}(t)\right\rangle_{\rm in}. \tag{A.10}$$

Calculating this expectation value by using Eq. (9.53) leads to an expression which, as for the power spectrum calculation before, has a divergent part related to the zero-point energy of the instantaneous vacuum state (normal ordering problem). I remove this part by a subtraction scheme similar to Eq (A.4). The final result reads

$$\langle\dot{\hat{q}}_{\alpha,\mathbf{k},\bullet}(t)\dot{\hat{q}}^{\dagger}_{\alpha',\mathbf{k}',\bullet'}(t)\rangle_{\rm in,phys} = \frac{1}{2}\left[\sum_{\beta}\frac{\dot{\epsilon}^{(\beta)}_{\alpha,k}(t)\dot{\epsilon}^{(\beta)^*}_{\alpha',k'}(t)}{\sqrt{\Omega^{\rm in}_{\beta,k}\Omega^{\rm in}_{\beta,k'}}} - \Omega_{\alpha,k}(t)\delta_{\alpha\alpha'}\right]\delta_{\bullet\bullet'}\delta^{(3)}(\mathbf{k}-\mathbf{k}'). \tag{A.11}$$

Inserting this result into Eq. (A.9), splitting the summations in sums over $\alpha=\alpha'$ and $\alpha\neq\alpha'$ and neglecting the oscillating $\alpha\neq\alpha'$ contributions having averaging over several oscillations in mind, leads to

$$\langle\dot{\hat{h}}_{\bullet}(t,y_b,\mathbf{k})\dot{\hat{h}}^{\dagger}_{\bullet'}(t,y_b,\mathbf{k}')\rangle_{\rm in} = \frac{1}{a^2}\frac{\kappa_5}{L}\sum_{\alpha}\mathcal{K}_{\alpha,k}(t)\mathcal{Y}^2_{\alpha}(a)\delta_{\bullet\bullet'}\delta^{(3)}(\mathbf{k}-\mathbf{k}') \tag{A.12}$$

where the function $\mathcal{K}_{\alpha,k}(t)$ is formally given by

$$\mathcal{K}_{\alpha,k}(t) = \sum_{\beta}\frac{|\dot{\epsilon}^{(\beta)}_{\alpha,k}(t)|^2}{\Omega^{\rm in}_{\beta,k}} - \Omega_{\alpha,k}(t) = \Omega_{\alpha,k}(t)\mathcal{N}_{\alpha,k}(t) \tag{A.13}$$

and I have made use of Eq. (9.75). The relation between $\sum_{\beta}|\dot{\epsilon}^{(\beta)}_{\alpha,k}(t)|^2/\Omega^{\rm in}_{\beta,k}$ and the number of created particles can easily be established. Using the above expression in Eq. (A.8) leads eventually to

$$\langle 0,{\rm in}|\dot{\hat{h}}_{ij}(t,\mathbf{x},y_b)\dot{\hat{h}}^{ij}(t,\mathbf{x},y_b)|0,{\rm in}\rangle = \frac{1}{a^2}\frac{\kappa_5}{L}\sum_{\alpha}\int\frac{d^3k}{(2\pi)^3}\mathcal{K}_{\alpha,k}(t)\mathcal{Y}^2_{\alpha}(a) \tag{A.14}$$

where I have used that

$$\sum_{\bullet} e^{\bullet}_{ij}(\mathbf{k})\ \left(e^{\bullet\,ij}(\mathbf{k})\right)^* = 2. \tag{A.15}$$

The final expression for the energy density Eq. (9.90) is then obtained by exploiting that $\kappa_5/L = \kappa_4$.

Appendix B

Numerics

B.1 Generalities

To solve the system of differential equations formed by Eqs. (3.76) and (3.77) numerically I decompose $\xi_n^{(m)}(t)$ and $\eta_n^{(m)}(t)$ in their real and imaginary parts:

$$\xi_n^{(m)} = u_n^{(m)} + iv_n^{(m)}\,,\ \eta_n^{(m)} = x_n^{(m)} + iy_n^{(m)}. \tag{B.1}$$

The resulting coupled system of first-order differential equations can then be written in the form

$$\dot{\mathbf{X}}^{(m)}(t) = \mathbf{W}(t)\mathbf{X}^{(m)}(t) \tag{B.2}$$

with real vectors $\mathbf{X}^{(m)}(t)$ and matrix $\mathbf{W}(t)$. Choosing the representation

$$\mathbf{X}^{(m)} = (u_1^{(m)}...u_{n_{\max}}^{(m)}x_1^{(m)}...x_{n_{\max}}^{(m)}v_1^{(m)}...v_{n_{\max}}^{(m)}y_1^{(m)}...y_{n_{\max}}^{(m)})^T, \tag{B.3}$$

where I have truncated the infinite system via introducing the cut-off parameter $n_{\max}$, the $4\,n_{\max} \times 4\,n_{\max}$ - matrix $\mathbf{W}(t)$ becomes

$$\mathbf{W}(t) = -\begin{bmatrix} \mathbf{C}^-(t) & \mathbf{C}^+(t) & -\mathbf{A}^+(t) & \mathbf{A}^-(t) \\ \mathbf{C}^+(t) & \mathbf{C}^-(t) & -\mathbf{A}^-(t) & \mathbf{A}^+(t) \\ \mathbf{A}^+(t) & -\mathbf{A}^-(t) & \mathbf{C}^-(t) & \mathbf{C}^+(t) \\ \mathbf{A}^-(t) & -\mathbf{A}^+(t) & \mathbf{C}^+(t) & \mathbf{C}^-(t) \end{bmatrix} \tag{B.4}$$

with the $n_{\max} \times n_{\max}$ - matrices $\mathbf{C}^{\pm}(t) = \left[c_{kn}^{\pm}(t)\right]$, $1 \le k, n \le n_{\max}$ and diagonal matrices $\mathbf{A}^{\pm}(t) = [a_{nn}^{\pm}(t)]$ where $a_{nn}^{\pm}(t)$ and $c_{nk}^{\pm}(t)$ are defined in Eq. (3.78) and Eq. (3.79), respectively. The number of particles (3.56) created in a mode n at $t = t_{\text{out}}$ may now be expressed in terms of the real functions:

$$\begin{aligned} \mathcal{N}_n^{\text{out}} &= \frac{1}{4}\sum_{m=1}^{n_{\max}} \frac{\Omega_n^{\text{out}}}{\Omega_m^{\text{in}}}\Big\{ \left[\Delta_n^-(t_{\text{out}})u_n^{(m)}(t_{\text{out}}) + \Delta_n^+(t_{\text{out}})x_n^{(m)}(t_{\text{out}})\right]^2 \\ &+ \left[\Delta_n^-(t_{\text{out}})v_n^{(m)}(t_{\text{out}}) + \Delta_n^+(t_{\text{out}})y_n^{(m)}(t_{\text{out}})\right]^2 \Big\} \end{aligned} \tag{B.5}$$

which in the particular case $\Omega_n^{\text{in}} = \Omega_n^{\text{out}}\ \forall n$ reduces to

$$\mathcal{N}_n^{\text{out}} = \frac{1}{4}\sum_{m=1}^{n_{\max}} \left[\left(x_n^{(m)}(t_{\text{out}})\right)^2 + \left(y_n^{(m)}(t_{\text{out}})\right)^2\right]. \tag{B.6}$$

In order to calculate (B.5) the system (B.2) has to be evolved numerically $n_{\max}$-times (m running from 1 to $n_{\max}$) up to $t = t_{\text{out}}$ with initial conditions

$$v_n^{(m)}(t_{\text{in}}) = x_n^{(m)}(t_{\text{in}}) = y_n^{(m)}(t_{\text{in}}) = 0 \quad \text{and} \quad u_n^{(m)}(t_{\text{in}}) = 2\delta_{nm}. \tag{B.7}$$

This shows that the numerical effort can become quite time and memory intensive if the cut-off parameter is large and the integration times are long. If $n_{\max} = 100$, for instance, a typical cut-off parameter used in the

simulations, the matrix $\mathbf{W}(t)$ has size 400×400 and the system (B.2) has to be solved 100 times, each time with different initial conditions. Fortunately, these runs with varying initial conditions are independent of each other such that the code is easy to parallelize. I have done this using MPI and the simulations for the tensor perturbations were performed on the Myrinet cluster of the University of Geneva. The results presented for the scalar and electromagnetic field were obtained by using standard PC's without parallelization. The code has been written in C++ and I have used integration routines based on different standard solvers. Mainly employed were the Runge-Kutta-Fehlberg 4th-5th order method (`rkf45`) and the Runge-Kutta Prince-Dormand method (`rk8pd`). Source codes provided by the GNU Scientific Library (GSL) [222] as well as the MATPACK - Library [223] (some of the scalar field results) were used.
Besides investigating the stability of the numerical solutions in dependence on the cut-off $n_{\max}$ the quality of the numerical solutions can be assessed by checking the validity of the Bogoliubov relations

$$\sum_m \left[\mathcal{A}_{mn}(t_1)\mathcal{A}^*_{mk}(t_1) - \mathcal{B}^*_{mn}(t_1)\mathcal{B}_{mk}(t_1)\right] = \delta_{nk} \tag{B.8}$$

$$\sum_m \left[\mathcal{A}_{mn}(t_1)\mathcal{B}^*_{mk}(t_1) - \mathcal{B}^*_{mn}(t_1)\mathcal{A}_{mk}(t_1)\right] = 0. \tag{B.9}$$

In the next two sections I restrict myself to show to which accuracy the diagonal part of (B.8) is satisfied, i.e. I consider the quantity

$$d_n = 1 - \sum_m \left[|\mathcal{A}_{mn}|^2 - |\mathcal{B}_{mn}|^2\right] \tag{B.10}$$

which, analytically, has to be zero. In the following two sections I show and discuss representative examples demonstrating the high accuracy of the numerical simulations.

B.2 Accuracy examples: TE-mode simulations

In Fig. B.1 I show $d_n(t)$, i.e. Eq. (B.10) evaluated as a continuous function of time corresponding to two numerical results discussed in section 5.4.
Panels (a) and (b) correspond to the exact coupling case $M = \sqrt{2}\pi$ (cf. Fig. 5.7) with the absolute and relative errors (err) for the Runge-Kutta Prince-Dormand method (`rk8pd`) [222] preset to 10^{-8} (a) and 10^{-12} (b). Thereby two "bands" are shown. The upper one correspond to $n = 1$ to 5 whereas the lower one correspond to $n = 16$ to $n_{\max} = 20$. The deviation from zero is larger for higher n because these modes are more affected by the truncation of the infinite system through the cut-off $n_{\max}$. Comparing the absolute value of the maximal deviation of $d_n(t = 8000)$ from zero which is $\approx 3.5 \times 10^{-4}$ for err=10^{-8} and $\approx 1.5 \times 10^{-8}$ for err=10^{-12} with the number of particles created in the resonantly excited modes $N_1(t = 8000) \approx 350$ and $N_5(t = 8000) \approx 400$ demonstrates that the numerical simulations guarantee a good accuracy. In panel (c) and (d) I show $d_n(t)$ for the case $M = 0.4$ (cf. Fig. 5.5) for the cut-off values $n_{\max} = 30$ (c) and $n_{\max} = 50$ (d). The numerical simulations have been performed with err=10^{-8} and again two bands are shown corresponding to the first five (upper band) and last five (lower band) values of n. For $n_{\max} = 50$ the deviation of the absolute value of d_n from zero for the last values $n = 46, ..., 50$ [panel (d)] is slightly larger compared to the deviation for the last five modes for $n_{\max} = 30$. But the deviation of $d_n(t)$ from zero for the first modes $n = 1, ..., 5$ is smaller for $n_{\max} = 50$ than for $n_{\max} = 30$, i.e. the accuracy for the first modes improves when increasing $n_{\max}$ as it is expected. Comparing $|d_n(t = 2000)| \approx 3 \times 10^{-4}$ for $n_{\max} = 50$ with the number of created particles $\mathcal{N}_1(t = 2000) \approx 124$ demonstrates again the good accuracy of the numerical simulations.

B.3 Accuracy examples: tensor mode simulations

For any value of the three-momentum k, the system of differential equations (9.70) and (9.71) is, using the same parameterization as in B.1, also of the form (B.2).
However, in the braneworld case additional complications arise which make the numerical simulations more involved. The main difficulty is that most of the entries of the matrix $\mathbf{W}(t)$ are not known analytically. This is due to the fact that Eq. (9.13) which determines the time-dependent KK-masses $m_i(t)$ does not have an (exact) analytical solution. Hence, except for the 00-component, the coupling matrix $M_{\alpha\beta}$ is not known analytically. I therefore have to determine the time-dependent KK-spectrum $\{m_n(t)\}_{n=1}^{n_{\max}}$ by solving Eq. (9.13) numerically. In addition, also the part M^N_{ij} [Eq. (9.31)] has to be calculated numerically since the integral over the particular

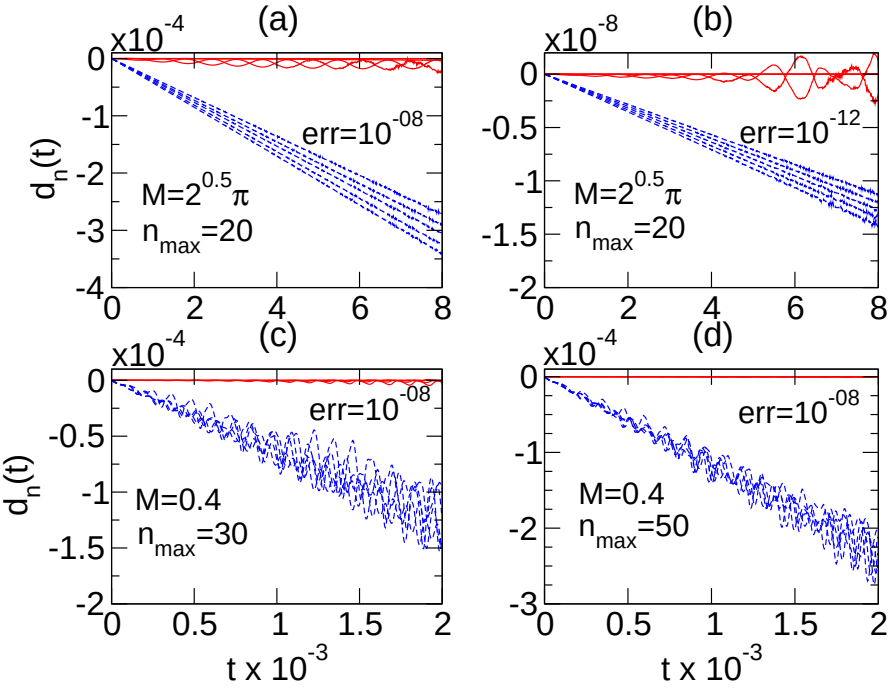

Figure B.1: The function $d_n(t)$ for $\omega_{\rm cav} = 2\Omega_1^{\rm in}$ and $M = \sqrt{2}\pi$ [panel (a) and (b)] and $M = 0.4$ [panel (c) and (d)]. In any case $d_n(t)$ is shown for $n = 1, ..., 5$ (upper bands) and the last five values $n = n_{\rm max} - 4, ..., n_{\rm max}$ (lower bands). With "err" I denote the presetted values for the relative and absolute error used in the numerical simulations performed with, in these cases, the Runge-Kutta Prince-Dormand method.

combination of Bessel functions could not be found analytically.
I numerically evaluate the KK-spectrum and the integral M_{ij}^N for discrete time-values t_i and use spline routines to assemble $\mathbf{W}_k(t)$. The system (B.2) can then be solved with the standard routines already used for the case of the electromagnetic field. I chose the separation of the t_i's in a non-uniform way. A more dense mesh close to the bounce and a less dense mesh at early and late times. The independence of the numerical results on the particular separation is checked. In order to implement the bounce as realistic as possible I do not spline the KK-spectrum very close to the bounce but re-calculate it numerically at any time t it is needed in the differential equation solver. This minimizes possible artificial effects caused by using a spline in the direct vicinity of the bounce. The same has been done for M_{ij}^N and I have found that splining M_{ij}^N when propagating through the bounce does not affect the numerical results.
Again, entirely routines provided by the GNU Scientific Library (GSL) have been employed. Different routines for root finding, and integration and several differential equation solvers have been compared. The code has been parallelized (MPI) in order to deal with the intensive numerical computations.
In Fig. B.2 I compare final KK-graviton spectra $\mathcal{N}_{n,k,\bullet}^{\rm out}$ with the expression $d_n(t_{\rm out})$ for two different cases corresponding to numerical results shown in Figs. 10.20 and 10.21. One observes that also for this, much more complicated numerical problem, the accuracy of the numerical simulations is very good. Even if the particle number is only of order 10^{-7} to 10^{-6}, the deviation of $d_n(t_{\rm out})$ from zero is at least one order of magnitude smaller. This demonstrates the reliability of our numerical simulations and that we can trust the numerical results presented in this work.

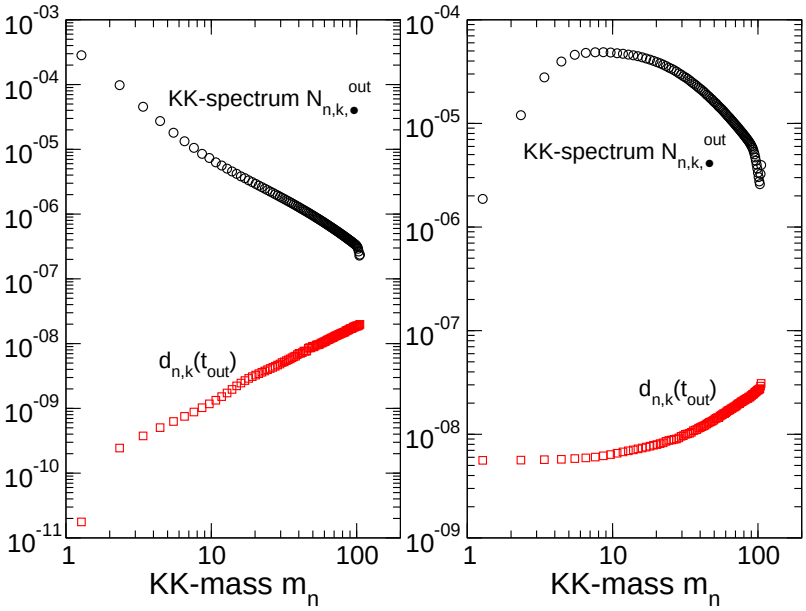

Figure B.2: Comparison of the final KK-graviton spectrum $\mathcal{N}^{\rm out}_{n,k,\bullet}$ with the expression $d_n(t_{\rm out})$. Left panel: $y_s = 3$, $k = 0.1$, $v_b = 0.03$ and $n_{\rm max} = 100$ [cf. Fig. 10.20]. Right panel: $y_s = 3$, $k = 30$, $v_b = 0.1$ and $n_{\rm max} = 100$ [cf. Fig. 10.21]. In both cases, the preset accuracy for root finding, integration and the differential equation solver is 10^{-12}.

Bibliography

[1] M. Abramowitz and I. A. Stegun, *Handbook of mathematical functions with formulas, graphs, and mathematical tables*, National Bureau of Standards, 1970.

[2] M. A. Andreata and V. V. Dodonov, *Energy density and packet formation in a vibrating cavity*, J. Phys. A **33**, 3209 (2000).

[3] I. Antoniadis, N. Arkani-Hamed, S. Dimopoulos and G. Dvali, *New dimensions at a millimeter to a Fermi and superstrings at a TeV*, Phys. Lett. B **436** 257 (1998), [arXiv:hep-ph/9804398].

[4] N. D. Antunes, *Numerical simulation of vacuum particle production: applications to cosmology, dynamical Casimir effect and time-dependent non-homogeneous dielectrics*, (2003) [arXiv:hep-ph/0310131].

[5] E. Arbel-Segev et al, *Prospects of employing superconductiong stripline resonators for studying the dynamical Casimir effect experimentally* (2006), [arXiv:quant-ph/0606099].

[6] N. Arkani-Hamed, S. Dimopoulos and G. R. Dvali, *The hierarchy problem and new dimensions at a millimeter*, Phys. Lett. **B429**, 263 (1998), [arXiv:hep-ph/9803315].

[7] N. Arkani-Hamed, S. Dimopoulos and G. R. Dvali, *Phenomenology, astrophysics and cosmology of theories with sub-millimeter dimensions and TeV scale quantum gravity*, Phys. Rev. **D59**, 086004 (1999), [arXiv:hep-ph/9807344].

[8] C. P. Bachas, *Lectures on D-branes* (1998), [arXiv:hep-th/9806199].

[9] G. Barton and C. Eberlein, *On quantum radiation from a moving body with finite refractive index*, Ann. Phys. (N.Y.) **227**, 222 (1993).

[10] R. A. Battye, C. van de Bruck, and A. Mennim, *Cosmological tensor perturbations in the Randall-Sundrum model: Evolution in the near-brane limit*, Phys. Rev. D **69**, 064040 (2004), [arXiv:hep-th/0308134].

[11] R. A. Battye and A. Mennim, *Multiple-scales analysis of cosmological perturbations in brane-worlds*, Phys. Rev. D **70**, 124008 (2004), [arXiv:hep-th/0408101].

[12] E. Bertschinger, *Cosmological perturbation theory and structure formation* (2000), [arXiv:astro-ph/0101009].

[13] P. Binétruy, C. Deffayet, U. Ellwanger, and D. Langlois, *Brane cosmological evolution in a bulk with cosmological constant*, Phys. Lett. B **477**, 285 (2000), [arXiv:hep-th/9910219].

[14] P. Binétruy, C. Deffayet and D. Langlois, *Non-conventional cosmology from a brane-universe*, Nucl. Phys. B **565**, 269 (2000), [arXiv:hep-th/9905012].

[15] N. D. Birrell and P. C. W. Davis, *Quantum fields in curved space*, Cambridge University Press, Cambridge, 1984.

[16] T. Boehm, *Cosmology of Brane Universes and Brane Gases*, PhD Thesis, University of Geneva (2004).

[17] M. Bordag (ed), *Quantum Field Theory under the Influence of External Conditions*, Proceedings, 3rd Workshop, Leipzig, Germany, September 18-22, 1995. Teubner, Stuttgart, 1996.

[18] M. Bordag (ed.), *Quantum Field Theory under the Influence of External Conditions*, Proceedings, 5th Workshop, Leipzig, Germany, September 10-14, 2001, Int. J. Mod. Phys. A **17** (2002).

[19] M. Bordag, U. Mohideen, and V. M. Mostepanenko, *New developments in the Casimir effect*, Phys. Rept. **353**, 1 (2001), [arXiv:quant-ph/0106045].

[20] D. Boyanovsky, H. J. de Vega, R. Holman, and J. F. J. Salgado, *Analytical and numerical study of preheating dynamics*, Phys. Rev. D **54**, 7570 (1996), [arXiv:hep-ph/9608205].

[21] T. H. Boyer, *Quantum electromagnetic zero point energy of a conducting spherical shell and the Casimir model for a charged particle*, Phys. Rev. **174**, 1764 (1968).

[22] C. Braggio et al, *A novel experimental approach for the detection of the dynamical Casimir effect* Europhys. Lett. **70**, 754 (2005), [arXiv:quant-ph/0411085].

[23] J. D. Bratt, A. C. Gault, R. J. Scherrer and T. P. Walker, *Big Bang nucleosynthesis constraints on brane cosmologies*, Phys. Lett. B **546**, 19-22 (2002), [arXiv:astro-ph/0208133].

[24] G. Bressi, G. Carugno, R. Onofrio, and G. Ruoso, *Measurement of the Casimir force between parallel metallic surfaces*, Phys. Rev. Lett **88**, 041804 (2002), [arXiv:quant-ph/0203002].

[25] J. Broeze and E. F. G. van Daalen, *Radiation boundary conditions for the two-dimensional wave equation from a variational principle*, Math. Comp. **58**, 73 (1992).

[26] M. Brown-Hayes et al, *Thermal and dissipative effects in Casimir physics*, J. Phys. A: Math. Gen. **39**, 6195 (2006), [arXiv:quant-ph/0611118].

[27] R. Brustein, M. Gasperini, M. Giovannini, and G. Veneziano, *Relic gravitational waves from string cosmology*, Phys. Lett. B **361**, 45 (1995), [arXiv:hep-th/9507017].

[28] A. Buonanno, T. Damour, and G. Veneziano, *Pre - big bang bubbles from the gravitational instability of generic string vacua*, Nucl. Phys. **B543**, 275 (1999), [arXiv:hep-th/9806230].

[29] A. Campos and C. F. Sopuerta, *Evolution of cosmological models in the brane-world scenario*, Phys. Rev. D **63**, 104012 (2001), [arXiv:hep-th/0101060].

[30] A. Campos and C. F. Sopuerta, *Bulk effects in the cosmological dynamics of brane-world scenarios*, Phys. Rev. D **64**, 104011 (2001), [arXiv:hep-th/0105100].

[31] C. Cartier and R. Durrer, *Tachyonic perturbations in AdS(5) orbifolds*, Phys. Rev. D **71**, 064022 (2005), [arXiv:hep-th/0409287].

[32] C. Cartier, R. Durrer, and E. Copeland, *Cosmological perturbations and the transition from contraction to expansion*, Phys. Rev. D **67**, 103517 (2003), [arXiv:hep-th/0301198].

[33] H. B. G. Casimir, *On the Attraction Between Two Perfectly Conducting Plates*, Proc. K. Ned. Akad. Wet. **51**, 793 (1948).

[34] H. B. G. Casimir, *Introductory remarks on quantum electrodynamics*, Physica, **19**, 846 (1953).

[35] H. B. G. Casimir, *The Casimir effect 50 years later*, Proceedings of the Fourth Workshop on Quantum Field Theory Under the Influence of External Conditions Leipzig, 1998, ed M. Bordag, World Scientific, Singapore (1999).

[36] M. Castagnino and R. Ferraro, *The Radiation From Moving Mirrors: The Creation And Absorption Of Particles*, Ann. Phys. (N.Y.) **154**, 1 (1984).

[37] A. V. Chizhov, G. Schrade and M. S. Zubairy, *Quantum statistics of vacuum in a cavity with a moving mirror*, Phys. Lett. A **230**, 269 (1997).

[38] J. Chiaverini, S. J. Smullin, A. A. Geraci, D. M. Weld, and A. Kapitulnik, *New Experimental Constraints on Non-Newtonian Forces below 100 μm*, Phys. Rev. Lett. **90**, 151101 (2003), [arXiv:hep-ph/0209325].

[39] C. K. Cole and W. C. Schieve, *Radiation modes of a cavity with a moving boundary*, Phys. Rev. A. **52**, 4405 (1995).

[40] C. K. Cole and W. C. Schieve, *Resonant energy exchange between a moving boundary and radiation modes of a cavity*, Phys. Rev. A. **64**, 023813 (2001).

[41] M. Crocce, D. A. R. Dalvit, and F. D. Mazzitelli, *Resonant photon creation in a three-dimensional oscillating cavity*, Phys. Rev. A. **64**, 013808 (2001), [arXiv:quant-ph/0012040].

[42] M. Crocce, D. A. R. Dalvit and F. D. Mazzitelli, *Quantum electromagnetic field in a three-dimensional oscillating cavity*, Phys. Rev. A. **66**, 033811 (2002), [arXiv:quant-ph/0205104].

[43] M. Crocce, D. A. R. Dalvit, F. C. Lombardo, and F. D. Mazzitelli, *Model for resonant photon creation in a cavity with time-dependent conductivity*, Phys. Rev. A **70**, 033811 (2004), [arXiv:quant-ph/0404135].

[44] M. Crocce, D. A. R. Dalvit, F. C. Lombardo, and F. D. Mazzitelli, *Hertz potentials approach to the dynamical Casimir effect in cylindrical cavities of arbitrary section*, J. Opt. B: Quantum Semiclass. Opt. **7**, S32 (2005), [arXiv:quant-ph/0411106].

[45] E. F. G. Van Daalen, J. Broeze, and E. van Groesen, *Variational principles and conservation laws in the derivation of radiation boundary conditions for wave equations*, Math. Comp. **58**, 55 (1992).

[46] D. A. R. Dalvit and F. D. Mazzitelli, *Creation of photons in an oscillating cavity with two moving mirrors*, Phys. Rev. A. **59**, 3049 (1999), [arXiv:quant-ph/9810092].

[47] D. A. R. Dalvit and F. D. Mazzitelli, *Renormalization-group approach to the dynamical Casimir effect*, Phys. Rev. A. **57**, 2113 (1998), [arXiv:quant-ph/9710048].

[48] D. A. R. Dalvit, F. D. Mazzitelli, and X. Orsi Millán, *The dynamical Casimir effect for different geometries*, J.Phys.A: Math. Gen. **39** 6261 (2006).

[49] D. A. R. Dalvit, private communication.

[50] G. Darmois, Mémorial des sciences mathématiques, fascicule 25 chap. 5, Gauthier-Villars, 1927.

[51] P. C. W. Davis and S. A. Fulling, *Radiation from Moving Mirrors and from Black Holes*, Proc. R. Soc. London, **A356**, 237 (1977).

[52] N. Deruelle, T. Dolezel and J. Katz, *Perturbations of brane worlds*, Phys. Rev. **D63**, 083513 (2001) [arXiv:heo-th/0010215].

[53] S. Dodelson, *Modern Cosmology*, Academic Press, San Diego, 2003.

[54] A. V. Dodonov, S. S. Mizrahi and V. V. Dodonov, *Continuous photodetection model: quantum jump engineering and hints for experimental verification* (2006), [arXiv:quant-ph/0612067].

[55] Dodonov V V, Klimov A B and Nikonov D E 1993, *Quantum phenomena in nonstationary media*, Phys. Rev. A **47**, 4422 (1993).

[56] V. V. Dodonov and A. B. Klimov, and D. E. Nikonov, *Quantum phenomena in resonators with moving walls*, J. Math. Phys. **34**, 2742 (1993).

[57] V. V. Dodonov and A. B. Klimov, *Generation and detection of photons in a cavity with a resonantly oscillating boundary*, Phys. Rev. A. **53**, 2664 (1996).

[58] V. V. Dodonov, *Resonance excitation and cooling of electromagnetic modes in a cavity with an oscillating wall*, Phys. Lett. A **213**, 219 (1996).

[59] V. V. Dodonov, *Resonance photon generation in a vibrating cavity*, J. Phys. A: Math. Gen. **31**, 9835 (1998), [arXiv:quant-ph/9810077].

[60] V. V. Dodonov, *Photon creation and excitation of a detector in a cavity with a resonantly vibrating wall*, Phys. Lett. A **207**, 126 (1995).

[61] A. V. Dodonov, E. V. Dodonov, and V. V. Dodonov, *Photon generation from vacuum in nondegenerate cavities with regular and random periodic displacements of boundaries* (2003), [arXiv:quant-ph/0308144].

[62] A. V. Dodonov and V. V. Dodonov, *Nonstationary Casimir effect in cavities with two resonantly coupled modes*, Phys. Lett. A **289**, 291 (2001), [arXiv:quant-ph/0109019].

[63] V. V. Dodonov, *Generation of photons in a lossy and detuned cavity with an oscillating boundary*, Phy. Lett. A **244**, 517 (1998).

[64] V. V. Dodonov, *Dynamical Casimir effect in a nondegenerate cavity with losses and detuning*, Phy. Rev. A **58**, 4147 (1998).

[65] V. V. Dodonov, *Nonstationary Casimir effect and analytical solutions for quantum fields in cavities with moving boundaries*, Adv. Chem. Phys. **119**, 309 (2001), [arXiv:quant-ph/0106081].

[66] R. Durrer and F. Vernizzi, *Adiabatic perturbations in pre-big bang models: Matching conditions and scale invariance*, Phys. Rev. D **66**, 083503 (2002), [arXiv:hep-ph/0203275].

[67] R. Durrer and P. Kocian, *Testing extra dimensions with the binary pulsar*, Class. Quantum Grav. **21**, 2127 (2004), [arXiv:hep-th/0305181].

[68] R. Durrer, *Cosmological Perturbation Theory*, Lect.Notes Phys.653:31-70 (2004), [arXiv:astro-ph/0402129].

[69] R. Durrer, *Braneworlds*, AIP Conf.Proc.782:202-240 (2005), [arXiv:hep-th/0507006].

[70] R. Easther, D. Langlois, R. Maartens, and D. Wands, *Evolution of gravitational waves in Randall-Sundrum cosmology*, J. Cosmol. Astropart. Phys. **0310**, 014 (2003), [arXiv:hep-th/0308078].

[71] E. Elizalde, S. D. Odintsov, A. Romeo, A. A. Bytsenko, S. Zerbini, *Zeta Regularization Techniques with Applications*, World Scientific, Singapore, 1994.

[72] A. Fedotov, N. Narozhny, and Y. Lozovik, *Instantaneous approximation for the dynamical Casimir effect*, J. Opt. B: Quantum Semiclass. Opt. **7**, S64 (2005).

[73] F. Finkel, A. Gonzales-Lopes, A. L. Maroto, and M. A. Rodriguez, *The Lamé equation in parametric resonance after inflation*, Phys. Rev. D **62**, 103515 (2000), [arXiv:hep-ph/0006117].

[74] E. G. Floratos and G. K. Leontaris, *Low scale unification, Newton's law and extra dimensions*, Phys. Lett. B**465**, 95 (1999), [arXiv:hep-ph/9906238].

[75] L. H. Ford and A. Vilenkin, *Quantum radiation by moving mirrors*, Phys. Rev. D **25**, 2569 (1982).

[76] L. H. Ford, *Quantum Field Theory in Curved Spacetime* (1997), [arXiv:gr-qc/9707062].

[77] L.-P. Fu, C. K. Duan, and G.-C. Guo, *Created photon distribution in a cavity with a moving wall*, Phys. Lett. A **234**, 163 (1997).

[78] S. A. Fulling and P. C. W. Davis, *Radiation from a Moving Mirror in Two Dimensional Space-Time: Conformal Anomaly*, Proc. R. Soc. London, **A348** 393 (1976).

[79] S. A. Fulling, *Nonuniqueness of canonical field quantization in riemannian space-time*, Phys. Rev. D **7**, 2850 (1973).

[80] S. A. Fulling, *Aspects of Quantum Field Theory in Curved Space-Time*, Cambridge University Press, 1996.

[81] M. Gasperini and G. Veneziano, *Pre - big bang in string cosmology*, Astropart. Phys. **1**, 317 (1993), [arXiv:hep-th/9211021].

[82] G. F. Giudice, R. Rattazzi, and J. D. Wells, *Quantum gravity and extra dimensions at high-energy colliders*, Nucl. Phys. B**544**, 3 (1999), [arXiv:hep-ph/9811291].

[83] W. Goldberger and M. B. Wise, *Modulus Stabilization with Bulk Fields*, Phys. Rev. Lett. **83**, 4922 (1999), [arXiv:hep-ph/9907447].

[84] R. Golestanian and M. Kardar, *Mechanical Response of Vacuum*, Phys. Rev. Lett. **78**, 3421 (1997), [arXiv:quant-ph/9701005].

[85] D. S. Gorbunov, V. A. Rubakov and S. M. Sibiryakov, *Gravity waves from inflating brane or mirrors moving in AdS(5)*, JHEP **10**, 015 (2001), [arXiv:hep-th/0108017].

[86] I. S. Gradshteyn and I. M .Ryzhik, *Tables of Integrals, Series and Products* Academic, New York, 1994.

[87] A. A. Grib, S. G. Mamayev and V. M. Mostepanenko, *Vacuum Quantum Effects in Strong Fields*, Friedmann Laboratory Publishing, St. Petersburg, 1994.

[88] A. H. Guth, *Inflationary universe: A possible solution to the horizon and flatness problems*, Phys. Rev. D **23**, 347 (1981).

[89] S. W. Hawking, T. Hertog, and H. S. Reall, *Brane new world*, Phys. Rev. D **62**, 043501 (2000), [arXiv:hep-th/0003052].

[90] S. W. Hawking, T. Hertog, and H. S. Reall, *Trace anomaly driven inflation*, Phys. Rev. D **63**, 083504 (2001) [arXiv:hep-th/0010232].

[91] T. Hiramatsu, K. Koyama, and A. Taruya, *Evolution of gravitational waves from inflationary brane world : numerical study of high-energy effects*, Phys. Lett. B **578**, 269 (2004), [arXiv:hep-th/0308072].

[92] T. Hiramatsu, K. Koyama, and A. Taruya, *Evolution of gravitational waves in the high-energy regime of braneworld cosmology*, Phys. Lett. B **609**, 133 (2005), [arXiv:hep-th/0410247].

[93] T. Hiramatsu, *High-energy effects on the spetctrum of the inflationary gravitational wave background in braneworld cosmology*, Phys. Rev. D **73**, 084008 (2006), [arXiv:hep-th/0601105].

[94] P. Horava and E. Witten, *Heterotic and type I string dynamics from eleven-dimensions*, Nucl. Phys. **B460**, 506 (1996), [arXiv:hep-th/9510209].

[95] P. Horava and E. Witten, *Eleven-dimensional supergravity on a manifold with boundary*, Nucl. Phys. **B475**, 94 (1996), [arXiv:hep-th/9603142].

[96] J. K. Hoskins, R. D. Newman, R. Spero, and J. Schultz, *Experimental tests of the gravitational inverse-square law for mass separations from 2 to 105 cm*, Phys. Rev. D **32**, 3084 (1985).

[97] C. D. Hoyle et al., *Submillimeter test of the gravitational inverse-square law*, Phys. Rev. D **70**, 042004 (2004), [arXiv:hep-ph/0405262].

[98] C. D. Hoyle et al., *Submillimeter Test of the Gravitational Inverse-Square Law: A Search for "Large" Extra Dimensions*, Phys. Rev. Lett. **86**, 1418 (2001), [arXiv:hep-ph/0011014].

[99] K. Ichiki and K. Nakamura, *Causal structure and gravitational waves in brane world cosmology*, Phys. Rev. D **70**, 064017 (2004), [arXiv:hep-th/0310282].

[100] K. Ichiki and K. Nakamura, *Stochastic gravitational wave background in brane world cosmology* (2004), [arXiv:astro-ph/0406606].

[101] D. Ida, *Brane-world cosmology*, JHEP **0009**, 014 (2000), [arXiv:gr-qc/9912002].

[102] W. Israel, *Singular hypersurfaces and thin shells in general relativity*, Nuovo Cim. B **44S10**, 1 (1966) [Erratum-ibid. B **48** (1967 NUCIA,B44,1.1966) 463].

[103] T. Jacobson, *Introduction to Quantum Fields in Curved Spacetime and the Hawking Effect* (2004), [arXiv:gr-qc/0308048].

[104] J.-Y. Ji, H.-H. Jung, J.-W. Park, and K.-S. Soh, *Production of photons by the parametric resonance in the dynamical Casimir effect*, Phys. Rev. A. **56**, 4440 (1997), [arXiv:quant-ph/9706007].

[105] J.-Y. Ji, H.-H. Jung, and K.-S. Soh, *Interference phenomena in the photon production between two oscillating walls*, Phys. Rev. A. **57**, 4952 (1998), [arXiv:quant-ph/9709046].

[106] H. Jing, Q.-Y. Shi, and J.-S. Wu, *Dynamical Casimir effect at finite temperature*, Phys. Lett. A **268**, 174 (2000).

[107] H. Johnston and S. Sarkar, *Moving mirrors and time-varying dielectrics*, Phys. Rev. A **51**, 4109 (1995).

[108] Z. Kakushadze and S. H. H. Tye, *Brane world*, Nucl.Phys. **B548**, 180 (1999), [arXiv:hep-th/9809147].

[109] R. Kallosh, L. Kovman and A. Linde, *Pyrotechnic universe*, Phys. Rev. D **64** 123523 (2001), [arXiv:hep-th/0104073].

[110] T. Kaluza, *On the Problem of Unity in Physics*, Sitzungsber. Preuss. Akad. Wiss. Berlin, 966 (1921).

[111] D. J. Kapner et al., *Tests of the Gravitational Inverse-Square Law below the Dark-Energy Length Scale*, Phys. Rev. Lett. **98**, 021101 (2007), [arXiv:hep-ph/0611184].

[112] J. Khoury, B. A. Ovrut, P.J. Steinhardt, and N. Turok, *Ekpyrotic universe: Colliding branes and the origin of the hot big bang*, Phys. Rev. D **64** 123522 (2001), [arXiv:hep-th/0103239].

[113] J. Khoury, B. A. Ovrut, N. Seiberg, P.J. Steinhardt and N. Turok, *From big crunch to big bang*, Phys. Rev. D **65** 086007 (2002), [arXiv:hep-th/0108187].

[114] J. Khoury, B. A. Ovrut, P.J. Steinhardt and N. Turok, *Density perturbations in the ekpyrotic scenario*, Phys. Rev. D **66** 046005 (2002), [arXiv:hep-th/0109050].

[115] J. Khoury, P.J. Steinhardt and N. Turok, *Inflation versus Cyclic Predictions for Spectral Tilt*, Phys. Rev. Lett. **91** 161301 (2003), [arXiv:astro-ph/0302012].

[116] J. Khoury, P.J. Steinhardt and N. Turok, *Designing Cyclic Universe Models*, Phys. Rev. Lett. **92** 031302 (2004), [arXiv:hep-th/0307132].

[117] W. J. Kim, J. H. Brownell, and R. Onofrio, *Detectability of Dissipative Motion in Quantum Vacuum via Superradiance*, Phys. Rev. Lett **96**, 200402 (2006).

[118] W. J. Kim, J. H. Brownell, and R. Onofrio, *Erratum: Detectability of Dissipative Motion in Quantum Vacuum via Superradiance*, Phys. Rev. Lett **97**, 089902 (2006).

[119] O. Klein, *Quantum Theory and Five-Dimensional Theory of Relativity*, Z. Phys. **37**, 895 (1926).

[120] A. B. Klimov and V. Altuzar, *Spectrum of photons generated in a one-dimensional cavity with oscillating boundary*, Phys. Lett. A **226**, 41 (1997).

[121] T. Kobayashi and T. Tanaka, *Quantum-mechanical generation of gravitational waves in a braneworld*, Phys. Rev. D **71**, 124028 (2005), [arXiv:hep-th/0505065].

[122] T. Kobayashi and T. Tanaka, *Spectrum of gravitational waves in Randall-Sundrum braneworld cosmology*, Phys. Rev. D **73**, 044005 (2006), [arXiv:hep-th/0511186].

[123] T. Kobayashi and T. Tanaka, *Initial Kaluza-Klein fluctuations and inflationary gravitational waves in braneworld cosmology*, Phys. Rev. D **73**, 124031 (2006), [arXiv:hep-th/0602168].

[124] T. Kobayashi, H. Kudoh, and T. Tanaka, *Primordial gravitational waves in an inflationary braneworld*, Phys. Rev. D **68**, 044025 (2003), [arXiv:gr-qc/0305006].

[125] T. Kobayashi and T. Tanaka, *Leading order corrections to the cosmological evolution of tensor perturbations in braneworld*, J. Cosmol. Astropart. Phys. **0410**, 015 (2004), [arXiv:gr-qc/0408021].

[126] H. Kodama and M. Sasaki, *Cosmological Perturbation Theory* Prog.Theor.Phys.Suppl.**78**, 1 (1984).

[127] L. Kofman, A. D. Linde, and A. A. Starobinsky, *Reheating after inflation*, Phys. Rev. Lett. **73**, 3195 (1994), [arXiv:hep-th/9405187].

[128] L. Kofman, A. D. Linde, and A. A. Starobinsky, *Towards the theory of reheating after inflation*, Phys. Rev. D **56**, 3258 (1997), [hep-ph/9704452].

[129] E. W. Kolb and M. S. Turner, *The Early Universe*, Westview Press, 1994.

[130] K. Koyama, *Late time behavior of cosmological perturbations in a single brane model*, J. Cosmol. Astropart. Phys. **09**, 10 (2004), [arXiv:astro-ph/0407263].

[131] P. Kraus, *Dynamics of anti-de Sitter domain walls*, J. High Energy Phys. **9912**, 011 (1999), [arXiv:hep-th/9910149].

[132] A. Lambrecht, M.-T. Jaekel, and S. Reynaud, *Motion Induced Radiation from a Vibrating Cavity*, Phys. Rev. Lett. **77**, 615 (1996), [arXiv:quant-ph/9606029].

[133] S. K. Lamoreaux, *Demonstration of the Casimir Force in the 0.6 to 6 μm Range*, Phys. Rev. Lett **78**, 5 (1997).

[134] S. K. Lamoreaux, *Erratum: Demonstration of the Casimir Force in the 0.6 to 6 μm Range [Phys. Rev. Lett. 78, 5 (1997)]*, Phys. Rev. Lett **81**, 5475 (1997).

[135] S. K. Lamoreaux, *The Casimir force: background, experiments, and applications*, Rep. Prog. Phys. **68**, 201 (2005).

[136] D. Langlois, *Gravitation and cosmology in brane-world*, Troisieme Cycle de la Physique en Suisse Romande, 2007.

[137] D. Langlois, K. Maeda and D. Wands, *Conservation Laws for Collisions of Branes and Shells in General Relativity*, Phys. Rev. Lett. **88** 181301 (2002), [arXiv:gr-qc/0111013].

[138] D. Langlois, R. Maartens, and D. Wands, *Gravitational waves from inflation on the brane*, Phys. Lett. B **489**, 259 (2000), [arXiv:hep-th/0006007].

[139] C. Lanczos, Ann. Phys. (Leipzig) **74**, 518 (1924).

[140] C. K. Law, *Resonance Response of the Quantum Vacuum to an Oscillating Boundary*, Phys. Rev. Lett. **73**, 1931 (1994).

[141] C. K. Law, *Effective Hamiltonian for the radiation in a cavity with a moving mirror and a time-varying dielectric medium*, Phys. Rev. A **49**, 433 (1994).

[142] C. K. Law, *Interaction between a moving mirror and radiation pressure: A Hamiltonian formulation*, Phys. Rev. A **51**, 2537 (1995).

[143] G. Lazarides, *Introduction to Cosmology*, Proceedings, Corfu Summer Institute on Elementary Particle Physics, 1998, [arXiv:hep-ph/9904502].

[144] J. Lesgourgues, *Inflationary Cosmology*, Troisieme Cycle de la Physique en Suisse Romande, 2006.

[145] L. Li and B. Z. Li, *Numerical solutions of the generalized Moore's equations for a one-dimensional cavity with two moving mirrors*, Phys. Lett. A, **300**, 27 (2002).

[146] A. D. Linde, *Particle Physics and Inflationary Cosmology* Harwood Academic Publishers, London, 1990.

[147] R. de la Llave and N. P. Petrov, *Theory of circle maps and the problem of one-dimensional optical resonator with a periodically moving wall*, Phys. Rev. E **59**, 6637 (1999).

[148] A. Lukas, B. A. Ovrut, and D. Waldram, *On the four-dimensional effective action of strongly coupled heterotic string theory*, Nucl. Phys. **B532**, 43 (1998), [arXiv:hep-th/9710208].

[149] A. Lukas, B. A. Ovrut, and D. Waldram, *Gaugino condensation in M theory on* S^1/Z_2, Phys. Rev. D **57**, 7529 (1998), [arXiv:hep-th/9711197].

[150] A. Lukas, B. A. Ovrut, K. S. Stelle, and D. Waldram, *The Universe as a domain wall*, Phys. Rev. D **59**, 086001 (1999), [arXiv:hep-th/9803235].

[151] D. H. Lyth, *Introduction to Cosmology*, Lectures given at the Summer School in High Energy Physics and Cosmology, ICTP (Trieste) 1993, [arXiv:astro-ph/9312022].

[152] R. Maartens, *Brane world gravity*, Living Rev. Relativity **7**, 7 (2004).

[153] R. Maartens, D. Wands, B. A. Bassett, and I. P. C. Heard, *Chaotic inflation on the brane*, Phys. Rev. D **62**, 041301 (2000), [arXiv:hep-ph/9912464].

[154] M. Maggiore, *Gravitational wave experiments and early universe cosmology*, Phys. Rept. **331**, 283 (2000), [arXiv:gr-qc/9909001].

[155] P. A. Maia Neto, *Vacuum radiation pressure on moving mirrors*, J. Phys. A: Math. Gen. **27**, 2167 (1994).

[156] P. A. Maia Neto and L. A. S. Machado, *Quantum radiation generated by a moving mirror in free space*, Phys. Rev. A **54**, 3420 (1996).

[157] O. Méplan and C. Gignoux, *Exponential Growth of the Energy of a Wave in a 1D Vibrating Cavity: Application to the Quantum Vacuum*, Phys. Rev. Lett. **76**, 408 (1996).

[158] P. W.Milonni, *The Quantum Vacuum - An Introduction To Quantum Electrodynamics*, Academic Press, Boston, 1994.

[159] C. W. Misner, K. S. Thorne and J. A. Wheeler, *Gravitation*, W.H. Freeman and Company, San Francisco, USA, 1973.

[160] K. A. Milton, *The Casimir effect: recent controversies and progress*, J. Phys. A:Math. Gen. **37**, R209 (2004), [arXiv:hep-th/0406024].

[161] H. Mizuta, C. Goodings, M. Wagner and S. Ho, *Three-dimensional numerical analysis of multi-mode quantum transport in zero-dimensional resonant tunnelling diodes*, J. Phys.: Condens. Matter **4**, 8783 (1992).

[162] U. Mohideen and A. Roy, *Precision Measurement of the Casimir Force from 0.1 to 0.9* μm , Phys. Rev. Lett **81**, 4549 (1998), [arXiv:physics/9805038].

[163] G. T. Moore, *Quantum Theory of the Electromagnetic Field in a Variable-Length One-Dimensional Cavity*, J. Math. Phys. **11**, 2679 (1970).

[164] V. M. Mostepanenko and N. N. Trunov, *The Casimir Effect and its Applications*, Clarendon Press, Oxford, 1997.

[165] V. F. Mukhanov, H. A. Feldman, and R. H. Brandenberger, *Theory of cosmological perturbations. Part 1. Classical perturbations, Part 2. Quantum theory of perturbations, Part 3. Extensions*, Phys. Rept.**215**, 203 (1992).

[166] S. Mukohyama, *Brane-world solutions, standard cosmology, and dark radiation*, Phys. Lett. B **473**, 241 (2000), [arXiv:hep-th/9911165].

[167] S. Mukohyama, T. Shiromizu and K. i. Maeda, *Global structure of exact cosmological solutions in the brane world*, Phys. Rev. D **62**, 024028 (2000) [Erratum-ibid. D **63**, 029901 (2001)], [arXiv:hep-th/9912287].

[168] S. Mukohyama, *Integro-differential equation for brane-world cosmological perturbations*, Phys. Rev. **D64**, 064006 (2001), [arXiv:hep-th/0104185].

[169] D. F. Mundarain and P. A. Maia Neto, *Quantum radiation in a plane cavity with moving mirrors*, Phys. Rev. A **57**, 1379 (1998), [arXiv:quant-ph/9808064].

[170] K. Nakazato and R. J. Blaikie, *The effect of mode coupling on ballistic electron transport in quantum wires*, J. Phys.: Condens. Matter **3**, 5729 (1991).

[171] A. Neronov, *Brane collisions in anti-de Sitter space*, J. High Energy Phys. **0111**, 007 (2001), [arXiv:hep-th/0109090].

[172] P. J. E. Peebles, *The large scale structure of the universe*, Princton University Press, Princeton, 1980.

[173] A. Pérez-Lorenzana, *An Introduction to Extra Dimensions* (2005), [arXiv:hep-ph/0503177].

[174] M. A. Pinsky, *Partial Differential Equations and Boundary-Value Problems with Applications*, McGraw-Hill, New York, 1991.

[175] G. Plunien, B. Müller, and W. Greiner, *The Casimir Effect*, Phys. Rept. **134**, 87 (1986).

[176] G. Plunien, R. Schützhold, and G. Soff, *Dynamical Casimir Effect at Finite Temperature* , Phys. Rev. Lett. **84**, 1882 (2000), [arXiv:quant-ph/9906122].

[177] J. Polchinski, *String theory. An introduction to the bosonic string, Vol.I*, Cambridge University Press, Cambridge, UK, 1998.

[178] J. Polchinski, *String theory. Superstring theory and beyond, Vol.II*, Cambridge University Press, Cambridge, UK, 1998.

[179] J. Polchinski, *Dirichlet-Branes and Ramond-Ramond Charges*, Phys. Rev. Lett. **75**, 4724 (1995), [arXiv:hep-th/9510017].

[180] J. Polchinski, *Tasi Lectures on D-branes* (1996), [arXiv:hep-th/9611050].

[181] L. Randall and R. Sundrum, *Large Mass Hierarchy from a Small Extra Dimension*, Phys. Rev. Lett. **83**, 3370 (1999), [arXiv:hep-ph/9905221].

[182] L. Randall and R. Sundrum, *An Alternative to Compactification*, Phys. Rev. Lett. **83**, 4690 (1999), [arXiv:hep-th/9906064].

[183] M. Razavy, *2nd Quantization in a Box with a Moving Wall*, Lett. Nuovo Cimento **37**, 449 (1983).

[184] M. Razavy and J. Terning, *Quantum radiation in a one-dimensional cavity with moving boundaries* , Phys. Rev. D **31**, 307 (1985).

[185] T. G. Rizzo, *Pedagogical Introduction to Extra Dimensions* (2004), [arXiv:hep-ph/0409309].

[186] P. Wegrzyn, T. Rog, *Vacuum energy of a cavity with a moving boundary*, Act. Phys. Pol. **B32**, 129 (2001).

[187] A. Roy, C. Y. Lin, and U. Mohideen, *Improved precision measurement of the Casimir force* , Phys. Rev. D **60**, 111101 (1999), [arXiv:quant-ph/9906062].

[188] A. Roy and U. Mohideen, *Demonstration of the Nontrivial Boundary Dependence of the Casimir Force*, Phys. Rev. Lett **82**, 4380 (1999).

[189] V. A. Rubakov and M. E. Shaposhnikov, *Do we live inside a domain wall?* Phys. Lett. B**152**, 136 (1983).

[190] V. A. Rubakov, *Large and infinite extra dimensions*, Phys.Usp.**44**, 871 (2001), [arXiv:hep-th/0104152].

[191] H. Saito and H. Hyuga, *The Dynamical Casimir Effect for an Oscillating Dielectric Model*, J. Phys. Soc. Jpn. **56**, 3513 (1996).

[192] E. Sassaroli, Y. N. Srivastava, and A. Widom, *Photon production by the dynamical Casimir effect*, Phys. Rev. A **50**, 1027 (1994).

[193] G. Schaller, R. Schützhold, G. Plunien and G. Soff, *Dynamical Casimir effect in a designed leaky cavity*, Phys. Lett. A **297**, 81 (2002), [arXiv:quant-ph/0203068].

[194] G. Schaller, R. Schützhold, G. Plunien and G. Soff, *Dynamical Casimir effect in a leaky cavity at finite temperature*, Phy. Rev. A **66**, 023812 (2002), [arXiv:quant-ph/0203139].

[195] R. Schützhold, G. Plunien and G. Soff, *Trembling cavities in the canonical approach*, Phys. Rev. A **57**, 2311 (1998), [arXiv:quant-ph/9709008].

[196] R. Schützhold and M. Tiersch, *Decoherence versus dynamical Casimir effect*, J. Opt. B: Quantum Semiclass. Opt. **7**, S120 (2005), [arXiv:quant-ph/0408087].

[197] R. Schützhold, *Aspects of Quantum radiation*, Dissertation, Technische Universität Dresden, 2001.

[198] R. Schützhold, G. Plunien, and G. Soff, *Motion-induced particle creation from a finite-temperature state*, Phys. Rev. A **65**, 043820 (2002).

[199] S. Seahra, *Gravitational waves and cosmological braneworlds: A characteristic evolution scheme*, Phys. Rev. D **74**, 044010 (2006), [arXiv:hep-th/0602194].

[200] N. Sen, *Limit conditions of gravity fields in discontinuity surfaces*, Ann. Phys. (Leipzig) **73**, 365 (1924).

[201] G. Shiu and S. H. H. Tye, *TeV scale superstring and extra dimensions*, Phys. Rev. D **58**, 106007 (1998), [arXiv:hep-th/9805157].

[202] Y. Shtanov, J. Traschen, and R. H. Brandenberger, *Universe reheating after inflation*, Phys. Rev. D **56**, 3258 (1997), [arXiv:hep-ph/9407247].

[203] M. J. Sparnaay, *Measurements of Attractive Forces Between Flat Plates*, Physica (Utrecht) **24**, 751 (1958).

[204] R. Spero, J. K. Hoskins, R. D. Newman, J. Pellam, and J. Schultz, *Test of the Gravitational Inverse-Square Law at Laboratory Distances*, Phys. Rev. Lett. **44**, 1645 (1980).

[205] P.J. Steinhardt, and N. Turok, *Cosmic evolution in a cyclic universe*, Phys. Rev. D **65** 126003 (2002), [arXiv:hep-th/0111098].

[206] H. Stephani, *General Relativity*, Cambridge University Press, Cambridge, 1996.

[207] N. Straumann, *From Primordial Quantum Fluctuations to the Anisotropies of the Cosmic Microwave Background Radiation*, Annalen Phys. (Leipzig) **15**, 701 (2006), [arXiv:hep-ph/0505249].

[208] S. Takagi, *Vacuum Noise and Stress Induced by Uniform Acceleration*, Prog. Theor. Phys. Suppl. **88**, 1 (1986).

[209] T. Tanaka and X. Montes, *Gravity in the brane-world for two-branes model with stabilized modulus*, Nucl. Phys. B **582**, 259 (2000), [arXiv:hep-th/0001092].

[210] A. Tolley, N. Turok, and P.J. Steinhardt, *Cosmological perturbations in a big crunch / big bang space-time*, Phys. Rev. D **69** 106005 (2004), [arXiv:hep-th/0306109].

[211] M. Uhlmann, G. Plunien, R. Schützhold, and G. Soff, *Resonant Cavity Photon Creation via the Dynamical Casimir Effect*, Phys. Rev. Lett. **93**, 193601 (2004), [arXiv:quant-ph/0404157].

[212] W. G. Unruh, *Notes on black-hole evaporation*, Phys. Rev. D **14**, 870 (1976).

[213] W. G. Unruh and R. M. Wald, *Acceleration radiation and the generalized second law of thermodynamics*, Phys. Rev. D **25**, 942 (1982).

[214] G. Veneziano, *Scale factor duality for classical and quantum strings*, Phys. Lett. B **265**, 287 (1991).

[215] H. Verlinde, *Holography and compactification*, Nucl. Phys. B**580**, 264 (2000), [arXiv:hep-th/9906182].

[216] D. N. Vollick, *Cosmology on a three-brane*, Class. Quant. Grav. **18**, 1 (2001), [arXiv:hep-th/9911181].

[217] R. M. Wald, *General Relativity*, The University of Chicago Press, Chicago, 1984.

[218] R. M. Wald, *Quantum Field Theory in Curved Spacetime and Black Hole Thermodynamics*, Chicago Lectures in Physics, The University of Chicago Press, Chicago, 1994.

[219] P. Wegrzyn, *Exact closed-form analytical solutions for vibrating cavities*, J. Phys. B: At. Mol. Opt. Phys. **40**, 2621 (2007), [arXiv:0706.4078].

[220] A. Wipf, *Quantum Fields near Black Holes* (1998), [arXiv:hep-th/9801025].

[221] E. Witten, *Strong coupling expansion of Calabi-Yau compactification*, Nucl. Phys. **B471**, 135 (1996), [arXiv:hep-th/9602070].

[222] www.gnu.org/software/gsl/

[223] www.matpack.de